INTERIM REPORT

Accession No.
ORNL/NUREG/TM-322

Contract Program or Project Title: MULTIROD BURST TESTS

Subject of this Document: BUNDLE B-1 TEST DATA

Type of Document: DATA REPORT

Authors: R. H. Chapman, D. O. Hobson, J. L. Crowley, A. W. Longest

Date of Document: May 23, 1979

Date Published: June 1979

Responsible NRC Individual and NRC Office or Division: M. L. Picklesimer, Fuel Behavior Branch, Division of Reactor Safety Research, Office of Nuclear Regulatory Research

Prepared for the
U.S. Nuclear Regulatory Commission
Office of Nuclear Regulatory Research
Under Interagency Agreements DOE 40-551-75 and 40-552-75

NRC FIN No. B0120

Prepared by the
OAK RIDGE NATIONAL LABORATORY
Oak Ridge, Tennessee 37830
operated by
UNION CARBIDE CORPORATION
for the
DEPARTMENT OF ENERGY

INTERIM REPORT

INTERIM REPORT ORNL/NUREG/TM-322

Burdle B-1 Test Data

Multirod Burst Test Program

R. H. Chapman
D. O. Hobson
J. L. Crowley
A. W. Longest

Prepared for the U.S. Nuclear Regulatory Commission
Office of Nuclear Regulatory Research
Under Interagency Agreements DOE 40-551-75 and 40-552-75

OAK RIDGE NATIONAL LABORATORY
OPERATED BY UNION CARBIDE CORPORATION · FOR THE DEPARTMENT OF ENERGY

Printed in the United States of America. Available from
National Technical Information Service
U.S. Department of Commerce
5285 Port Royal Road, Springfield, Virginia 22161

INTERIM REPORT

Accession No.
ORNL/NUREG/TM-322

Contract Program or Project Title: MULTIROD BURST TESTS

Subject of this Document: BUNDLE B-1 TEST DATA

Type of Document: DATA REPORT

Authors: R. H. Chapman, D. O. Hobson, J. L. Crowley, A. W. Longest

Date of Document: May 23, 1979

Date Published: June 1979

Responsible NRC Individual and NRC Office or Division: M. L. Picklesimer, Fuel Behavior Branch, Division of Reactor Safety Research, Office of Nuclear Regulatory Research

Prepared for the
U.S. Nuclear Regulatory Commission
Office of Nuclear Regulatory Research
Under Interagency Agreements DOE 40-551-75 and 40-552-75

NRC FIN No. B0120

Prepared by the
OAK RIDGE NATIONAL LABORATORY
Oak Ridge, Tennessee 37830
operated by
UNION CARBIDE CORPORATION
for the
DEPARTMENT OF ENERGY

INTERIM REPORT

CONTENTS

LIST OF TABLES

LIST OF TABLES (continued)

LIST OF FIGURES

LIST OF FIGURES (continued)

LIST OF FIGURES (continued)

LIST OF FIGURES (continued)

LIST OF FIGURES (continued)

LIST OF FIGURES (continued)

FOREWORD

Examination, analysis, and interpretation of a bundle test take place over a long period of time, and it is our practice to report progress and results as they become available. Dissemination of the information in this manner results in its being disjointed and scattered throughout several publications. This presents some problems to the users in that one is never sure if the information at hand is the most recent. It is our intention to alleviate some of these problems by (1) publication (with limited distribution) of a data report on each bundle test and (2) publication of interpretative reports when sufficient information has been developed to warrant such action.

Consistent with this intention, the objective of this report is to provide a reference source of information and results obtained during the test and from pretest and posttest examination of the test array. We believe the data presented herein, consisting of plots, tabulations, and photographs, are both necessary and sufficient for interpretation of the test. In deciding what (and how much) information should be included, we had to anticipate to a certain extent the potential uses of the data. As a result, certain data have been excluded, but these contain information that can be characterized as "second generation" data, such as computer-drawn cross sections.

Also, it was decided that the data should be presented in this reference source with a minimum of interpretation. We will continue to publish interpretations in our progress reports, and, finally, we plan to publish an interpretative report on all the bundle tests. This final report will be based on data reported in the individual test data reports, such as this one, and information reported in the progress reports.

This report is derived from research performed by the Multirod Burst Test (MRBT) Program at Oak Ridge National Laboratory (ORNL). This research is sponsored by the Division of Reactor Safety Research of the Nuclear Regulatory Commission, and the results are published routinely in a series of progress reports, topical reports, quick-look reports, and data reports. This particular report is in the last category.

Progress reports published by the MRBT Program include:

NUREG Report No.	ORNL Report No.	Period covered
	ORNL/TM-4729	July–September 1974
	ORNL/TM-4805	October–December 1974
	ORNL/TM-4914	January–March 1975
	ORNL/TM-5021	April–June 1975
	ORNL/TM-5154	July–September 1975
	ORNL/NUREG/TM-10	October–December 1975
	ORNL/NUREG/TM-36	January–March 1976
	ORNL/NUREG/TM-74	April–June 1976
	ORNL/NUREG/TM-77	July–September 1976
	ORNL/NUREG/TM-95	October–December 1976
	ORNL/NUREG/TM-108	January–March 1977
	ORNL/NUREG/TM-135	April–June 1977
NUREG/CR-0103	ORNL/NUREG/TM-200	July–December 1977
NUREG/CR-0225	ORNL/NUREG/TM-217	January–March 1978
NUREG/CR-0398	ORNL/NUREG/TM-243	April–June 1978
NUREG/CR-0655	ORNL/NUREG/TM-297	July–December 1978

Topical reports pertaining to research and elopment carried out by this program are:

1. R. H. Chapman (comp.), *Characterization of Zircaloy-4 Tubing Procured for Fuel Cladding Research Programs*, ORNL/NUREG/TM-29 (July 1976).
2. W. E. Baucum and R. E. Dial, *An Apparatus for Spot Welding Sheathed Thermocouples to the Inside of Small-Diameter Tubes at Precise Locations*, ORNL/NUREG/TM-33 (August 1976).
3. W. A. Simpson, Jr., et al., *Infrared Inspection and Characterization of Fuel-Pin Simulators*, ORNL/NUREG/TM-55 (November 1976).
4. R. H. Chapman et al., *Effect of Creep Time and Heating Rate on Deformation of Zircaloy-4 Tubes Tested in Steam with Internal Heaters*, NUREG/CR-0343 (ORNL/NUREG/TM-245) (October 1978).

The following limited-distribution quick-look reports have been issued by this program:

1. R. H. Chapman (comp.), *Quick-look Report on MRBT No. 1 4 × 4 Bundle Burst Test*, Internal Report ORNL/MRBT-2 (September 1977).
2. R. H. Chapman (comp.), *Quick-look Report on MRBT No. 2 4 × 4 Bundle Burst Test*, Internal Report ORNL/MRBT-3 (November 1977).
3. R. H. Chapman, *Quick-look Report on MRBT No. 3 4 × 4 Bundle Burst Test*, Internal Report ORNL/MRBT-4 (August 1978).

ABSTRACT

A compilation of B-1 test data is presented. These data were obtained during the test and from pretest and posttest examination of the test array. They are presented in considerable detail with minimum interpretation, which will be the subject of a future report.

The B-1 test is the first of a series of 4 x 4 bundle tests performed by the Multirod Burst Test (MRBT) Program at Oak Ridge National Laboratory (ORNL). This research is sponsored by the Nuclear Regulatory Commission (NRC).

A brief description of the experiment and a summary of bundle performance are also included with the results of the B-1 test. Both graphical and tabular formats are used to show temperature, pressure, and tube rupture data as functions of test time; strain data for the cladding in each of the fuel rod simulators; and flow test results obtained after the bundle test. Photographic documentation is provided for both the overall bundle, before and after testing, and the 55 cross sections cut from the tested bundle for strain measurements.

The purpose of this report is to provide a background document for interpretative reports published previously and to be published in the future.

1. INTRODUCTION

This report presents, in detail, the experimental data for the first 4 × 4 multirod burst test (B-1), conducted within the framework of the Multirod Burst Test (MRBT) Program at Oak Ridge National Laboratory (ORNL). This work is sponsored by the Division of Reactor Safety Research of the Nuclear Regulatory Commission (NRC). The report is intended primarily as a source document for B-1 test results, with a minimum amount of interpretation of the data. Because of this, it should be read in conjunction with the published[1-6] results and interpretations.

No inferences should be drawn from the tabular data in this report concerning their precision. In most instances, the tabulations were generated by computer routines from data tapes, and the values are given to more significant figures than the data warrant. The appropriately referenced reports should be consulted for insight into both the precision and the accuracy of the data contained herein.

A brief description of the B-1 test design and procedures will be given, followed by the test results.

2. TEST DESCRIPTION

The first bundle burst test (B-1) was performed successfully July 22, 1977. The test consisted of an electrically heated 4 × 4 bundle and shroud.

Figure 1 is a simplified drawing of the test assembly. Table 1 and Fig. 2 give pertinent details of the fuel pin simulators. The fuel simulators (internal heaters) used in the test were the best available for use at the time the fuel pin simulators were assembled. As a result, the axial temperature distribution (as determined from pretest infrared characterization scans) of the individual fuel simulators was not as uniform as desired. Detailed study of the pretest characterization scans confirmed that the lack of uniformity contributed to the observed failure locations.

The Zircaloy-4 tubes (10.9 mm OD × 0.635 mm wall thickness) used to fabricate the test assemblies came from the master lot of tubing purchased[7] for use in all the NRC-sponsored cladding research programs. Serial numbers of the tubes are given in Table 1.

Each fuel pin simulator was instrumented with a fast-response, strain-gage-type pressure transducer and four Inconel-sheathed (0.71-mm-OD) type K thermocouples with ungrounded junctions. The thermocouples were spot welded (using an apparatus developed[8] specifically for this purpose) at axial and azimuthal positions (see Figs. 3 and 4) selected to provide an overall indication of the temperature distribution within the test array. One of the simulator thermocouples (TE 12-4) was inoperative during the test; four thermocouples (TE 9-1, TE 9-3, TE 14-2, TE 14-3) became detached from the tube wall during assembly and probably indicated temperatures higher than existed on the Zircaloy. (Thermocouples are identified in the plots and text by the nomenclature TE 12-4, where 12 is the rod number and 4 is the thermocouple number in that fuel pin simulator as identified in Fig. 3.) Six bare-wire (0.25-mm-diam) type S thermocouples were spot welded to the thin (0.25-mm-thick Inconel) resistance-heated shroud surrounding the rod array at locations indicated in Fig. 3. The nomenclature for these thermocouples includes the number 90 to indicate shroud application. Three of these thermocouples

experienced electrical interference and gave erratic signals during the time power was on the bundle. Millivolt signals from the pressure transducers, thermocouples, and electrical power measuring instruments were recorded on magnetic tape by a computer-controlled data acquisition system (CCDAS) for subsequent analysis.

The test could be terminated by any of four actions: (1) a signal generated by the CCDAS that all 16 simulators had burst, (2) a signal generated by the CCDAS that 10 thermocouples had exceeded the upper temperature limit (100°C above the expected burst temperature), (3) a signal generated by a timer that limited the transient to a predetermined time period, and (4) operator override.

Preparations for the test began early on July 21 with heatup of the test vessel and checkout of the instrumentation. Thermal equilibrium of the assembly was achieved in about 6 hr; pressure leak rates of the fuel pin simulators were acceptably low (i.e., less than 15 kPa/min). A short powered run (4-sec transient) was conducted at that time to ensure that the data acquisition system and all the instrumentation were functioning properly and that the performance of the test assembly was as expected. Examination of the quick-look data from this short transient showed that the indicated performance of the heated shroud was not correct. Considerable time was expended in checkout and evaluation of the anomalous indications. During this time the test assembly was maintained at about 350°C, and either the No. 3 fuel pin simulator or the associated pressure measuring system developed a severe leak (about 1000 kPa pressure loss/min). Although the location of the leak was never ascertained, the copper gasket in the lower end seal (see Fig. 2) was the suspected cause of the leak.

A second short powered run (4-sec) was conducted late on July 22 to determine if the heated shroud anomalies had been corrected. Evaluation of the quick-look data indicated that the shroud heating rate was approximately half that anticipated and that at least three of the shroud thermocouples were giving erratic temperature indications when power was on. Since other, more reliable measurements indicated that the specified current and voltage conditions indeed existed, it was decided to proceed

with the burst test as soon as the bundle temperature could be stabilized at the desired initial conditions.

A separate problem (unrelated to the test) developed during the holding time between the two short powered runs. This problem was associated with the insulation resistance of the dc generator, and, for several hours further continuation of the test was in doubt. Finally, a method was devised to switch the test load to another dc generator for the remainder of the test.

As mentioned earlier, one of the simulators (No. 3) developed a severe leak during the long (~36 hr) holding time at ~350°C, and other simulators gave indications of deterioration. Following stabilization of the bundle temperature at about 355°C after the second short powered run, all the fuel pin simulators (except No. 3) were pressurized simultaneously with helium to approximately 8700 kPa (pressure differential above the steam pressure) and isolated from the pressure supply system. Simulator 3 was pressurized slightly higher in an attempt to offset the effect of the severe leak. This measure was not totally successful, but it was adequate to cause moderate deformation and failure of the cladding on this simulator.

During the transient, steam pressure in the test vessel was 275 kPa, bundle steam inlet temperature was ~350°C, and flow was ~4.2 kg/hr; the Reynolds number (≈250) also remained constant. When power was terminated, valves opened automatically to increase the steam flow to about 30 kg/hr to facilitate cooling of the test assembly. The test vessel was vented to atmospheric pressure simultaneously with the increase in steam flow.

Following the burst test, the fuel simulators were removed and the deformed bundle was placed in the flow shroud of a water loop to measure the axial pressure loss profile. These losses were compared with those of an undeformed reference bundle.

3. SUMMARY OF BUNDLE PERFORMANCE

3.1 Fuel Rod Simulators

Table 2 summarizes pertinent pressure and temperature data from the B-1 test; these data have been revised from those included in the quick-look report.[1] Initial conditions for the test were essentially the same as those used[5] for SR-28 and SR-29, which were conducted to obtain single-rod burst test data for comparison with the B-1 bundle test data. As is apparent in the table, the initial temperature distribution (at 0.5 sec before power-on) throughout the bundle was fairly uniform. The six shroud thermocouples indicated temperatures between 358 and 360°C, and the inlet steam temperature was 349°C. The sensor that provided the steam temperature was improperly located (very close to the wall of the steam pipe) and probably indicated a temperature somewhat lower than actually existed.

Table 2 also lists the temperature indicated by each of the thermocouples at the time of burst for the respective simulators. The burst temperatures (underlined in the table) were selected in accord with our practice of using the highest measured value as the burst temperature. As noted earlier, four thermocouples were known to be detached from the wall and probably indicated temperatures somewhat higher than actual wall temperatures. The spread in temperatures in a given simulator is not unusual, considering the location of the thermocouples (Figs. 3 and 4) and the power distribution of the fuel simulators as determined from the pretest infrared characterization scans.

Table 3 lists some of the volume-related data for the B-1 tubes. It can be seen that the initial gas volumes were quite uniform among the tubes — ranging from 49.0 to 51.5 cm^3 — but these bore little relation to either the fractional pressure decreases or the fractional volume increases. Although the gas volume is reasonably typical, the distribution of the volume is not typical of a full-length fuel rod. Of the total initial volume (at room temperature), about 13% is in the heated portion of the annulus between the fuel simulator and the inside diameter of the Zircaloy tube, 10% is in the unheated portion of the annulus, 33%

is in the pressure transducer and connecting tube, and 44% is distributed in the end regions (mostly at the upper end) of the fuel pin simulator. At any given time during the test, all these volumes have different temperatures (the major volumes remain at or near room temperature), ranging from room temperature to cladding temperature, and one cannot calculate the fractional volume increase from the pressure decrease in a straightforward manner. Instead, we calculated the volume increase from the tube deformation profiles (assuming circular cross sections).

Table 4 shows the conditions existing at the time of maximum pressure (corresponding approximately to the beginning of plastic deformation) of each simulator. Tables giving pressure and temperature conditions throughout the bundle at the time of each burst are presented later in the report.

The performance of all the simulators was about the same with the exception of No. 3, which reflected the loss in pressure discussed earlier. Power was on the bundle 20.85 sec; the average heating rate over the time interval of 3 to 15 sec was about 30°C/sec. The first burst (No. 12) occurred 17.00 sec after the start of the transient, and the fifteenth burst (No. 5) occurred after 17.65 sec of heating. The sixteenth burst (No. 3) occurred 2.05 sec after power to the bundle was terminated. (Power was terminated by the high-temperature limit criteria.) Table 5 gives the time distribution of the bursts; resolution of time by the CCDAS clock is to the nearest 0.05 sec. A histogram of the bursts is given in Fig. 5, which shows that most (14) of the bursts occurred within a 0.5-sec interval.

The burst temperature—burst pressure data for the B-1 test (data for simulator 3 are not included) and the two single-rod tests (SR-28 and SR-29), which were conducted for comparison with the bundle tests, are plotted in Fig. 6. We have assumed the burst temperatures (see Table 2) for the individual bundle simulators to be the highest temperatures measured at the time of failure; this is consistent with the definition used for single-rod tests. In simulator 9, the highest temperature was measured on a detached thermocouple, so the burst temperature was taken to be the highest value measured by an attached thermocouple. The solid line in

the figure is our single-rod correlation;[5] the dashed line is a linear least-squares fit to the B-1 data set. At first glance, it appears that the B-1 data indicate higher burst temperatures than would be predicted from the single-rod correlation; however, it should be noted that the correlation is based on external bare-wire thermocouple measurements, whereas the bundle temperature measurements were obtained from internal sheathed thermocouples.

Our experience with single-rod tests indicates that internal thermocouples give considerably higher temperatures (under certain conditions) compared with the external bare-wire thermocouples, which we believe provide a much more accurate measurement of the true Zircaloy temperature. Part of the differential is due to the fact that the indicated temperature is at the thermocouple junction and not at the point where the sheath is welded to the tube. For comparison, the differences in internal and external thermocouple measurements are included in Fig. 6 for SR-28 and SR-29. (These are the only single-rod tests with internal thermocouples conducted to date in this pressure range.) The plotted single-rod temperature data points (i.e., the internal and external thermocouple measurements) were not obtained at the same location; they are the maximum values measured by either type thermocouple at the time of burst without regard to location, which is consistent with our definition of burst temperature. Based on the external thermocouple measurements, both of the single-rod tests are in agreement with the single-rod correlation, whereas the internal thermocouple measurements indicate considerable error. Assuming similar errors exist in the bundle tests, one must conclude that the bundle data are in good agreement with the single-rod correlation, if the differences in measuring techniques are taken into account. This is supported by the fact that the least-squares fit of the bundle data set is displaced from single-rod correlation by an almost constant value (13 to 17°C) over the range of burst pressures and that the displacement is consistent with single-rod test (i.e., SR-28 and SR-29) observations.

3.2 Heated Shroud Performance

As described earlier, bare-wire type S thermocouples (0.25 mm diam) were spot welded to the outside surface of the thin (0.25-mm-thick), resistance-heated Inconel shroud surrounding the test array (see Fig. 1). Three thermocouples were attached to the north side, and one thermocouple was attached to each of the other three sides (see Fig. 3 for locations and identifications). Figure 7 compares the temperatures measured on the north side to that measured on the No. 3 simulator at a point opposite TE 90-2. Although the north side shroud temperatures were about 150°C lower than the simulator temperature (after about 17 sec of heating), they were very stable and did not indicate electrical interference. To the contrary, the shroud thermocouples on the other three sides indicated severe electrical interference from the heating current and provided erroneous information. As evident in Fig. 7, shroud thermocouple TE 90-2 (elevation of 38.9 cm) gave the highest reading, TE 90-3 (elevation of 13.9 cm) the next highest, and TE 90-1 (elevation of 62.5 cm) the lowest. Both the indicated shroud temperatures and the high-to-low ranking were unexpected and raised questions as to the validity of the measurements. Also, it was speculated in the B-1 quick-look report[1] that discoloration of the shroud in the vicinity of some of the tube bursts was evidence of shroud overheating. These questions were resolved subsequently by some shroud heating tests in which the shroud from the B-2 test assembly was instrumented with 12 thermocouples, installed in the test facility (without the bundle), and tested at power and steam conditions that duplicated as nearly as possible those that were used in the B-1 test. The same thermocouples were used for TE 90-1 through TE 90-6 in both tests, so that the same errors should be present. The thermal insulation between the outside of the shroud and the shroud box was revised for the shroud tests (to agree with the concept to be used in subsequent bundle tests) to replace the insulation board with a combination of gas gap and reflective-type insulation (see Ref. 2 for details).

Figure 8 shows the temperature increase (~20°C/sec) measured by TE 90-2 in both the B-1 and the shroud heating tests. As shown, excellent agreement was obtained until the time the bursts began to occur (~17 sec)

in the B-1 test, and the agreement is independent of temperature level; this implies that either heating the shroud by energy transfer from the bundle and cooling the shroud by the steam flow had negligible effects on the shroud temperature during the B-1 test or else the two effects balanced each other throughout the transient. The latter does not appear reasonable since the transfer mechanisms are not the same (convection vs radiation) and have different functional dependencies on the temperature differences.

Similar comparisons are shown in Figs. 9 and 10 for TE 90-1 and TE 90-3, respectively. As shown in the figures, the temperatures at these points diverged after 6 to 8 sec of heating, with the temperatures measured in the B-1 test being lower than in the shroud heating test.

This behavior is attributed to localized cooling of the shroud in the B-1 test by contact with the Al_2O_3 pads used to isolate (electrically) the bundle grids from the shroud, by contact with the insulation board outside the shroud, or by a combination of the two. (The thermocouples were attached to the shroud about 3.5 cm away from the centerline of the grid.) Figure 11 compares the axial temperature distribution as measured in the B-1 and the shroud heating tests (the line is a least-squares fit to the open-circle data points from two different tests). The axial gradient (~40°C over the heated length of the bundle) is due to heat transfer to the steam (inlet temperature constant at ~350°C) as it passes downward through the test assembly. Although electrical noise interfered with the thermocouples on the east, south, and west sides of the shroud in the B-1 test and produced erroneous information, the shroud heating tests provided evidence that the temperature uniformity around the shroud was very good at elevation 38.2 cm, as shown in Fig. 12.

Based on the shroud heating tests, we concluded that TE 90-2 provided an accurate indication of the shroud temperature during the B-1 test. Thermocouples TE 90-1 and TE 90-3 probably indicated accurate temperatures, and the shroud was probably cooled at these points by the grid isolating pads. It was suggested in the B-1 quick-look report[1] that discoloration of the shroud in the vicinity of the bursts (in particular at the four bursts at an elevation of approximately 76 cm) might be evidence of shroud overheating, and this might have influenced the location

of the bursts. To [illegible]ty, the shroud heating tests showed no evidence (see Fig. 11) of shroud overheating, particularly near the upper group of bursts. We believe the discoloration occurred after the bursts and was caused by the hot gas escaping from the simulators at the time of failure. The shroud tests also indicated negligible energy transfer from the bundle to the shroud when the temperature difference was less than about 100°C.

4. BUNDLE TEST RESULTS

This section presents, in a number of subsections, the detailed results of the B-1 test. The purpose of this presentation is to provide a fairly complete reference source of uninterpreted data.

Part of the following presentation will be in the form of data plots to provide an overall picture of the progress of the test. Much of this graphical information is backed up by exhaustive computer-acquired data listings which are stored on magnetic data tapes. For example, the temperature-time and pressure-time curves are plotted from readings taken at 0.05-sec intervals during the temperature transient. Tabular data will be presented where detail is deemed important, for example, the conditions of the bundle at the time of each tube rupture.

4.1 Transient Results

4.1.1 Bundle average behavior

The information contained in this section was obtained during the course of the B-1 test transient. The data were recorded by the data acquisition system in the continuous scan mode (i.e., 10,000 samples/sec; ~100 sensors) over a period of about 12 min. Each rod was instrumented with four thermocouples attached to the interior surface at various elevations above the bottom of the heated zone. In addition, the heated shroud was monitored by six thermocouples attached to its outer surface. These locations were shown in Figs. 3 and 4, previously. Average bundle and shroud temperatures and heating rates were obtained by averaging the thermocouple measurements in various combinations.

Figure 13 shows the average bundle and shroud temperatures and the bundle-shroud temperature difference as a function of heating time; Fig. 14 shows the average bundle and shroud heating rates as a function of heating time.

The radial distribution was obtained by averaging certain thermocouples, as shown in Fig. 15. The axial distribution was obtained by averaging thermocouples at various elevations in the bundle. The axial

and radial distributions are shown in Figs. 16 and 17, respectively. The number of measurements averaged to obtain the plotted data points are indicated in each of the figures.

The axial distribution of the tube bursts is noted on the right side of Fig. 17; information on burst times and temperatures is not available from this figure. Figure 18 continues (until the end of the continuous data scan) the axial temperature distribution plot during the posttest cooldown. The dashed lines indicate the distribution at the time of the first tube burst (17.0 sec) and the time power was terminated (20.85 sec).

4.1.2 Pressure and temperature plots as a function of time

Individual pressure and temperature curves for the simulators are shown in Figs. 19 through 34. These curves were computer-plotted at 0.05-sec intervals from the magnetic data storage tapes. Each of the figures is comprised of four temperature plots (corresponding to the four thermocouples attached to the individual simulator) and one pressure curve. Thermocouple identification in the figures follows the numbering scheme shown in Figs. 3 and 4.

In general, the burst time for each simulator can be detected by the sudden drop in the pressure curve. This is also reflected in the temperature curves as sudden changes in their slopes. The time of maximum pressure (see Table 4) is also the time at which the major expansion of the rod began. Subsequent plastic deformation caused a continuing decrease in pressure until rupture occurred. The behavior of simulator 3 was different due to a leak that developed prior to the transient.

4.1.3 Bundle conditions at the time of rupture

The preceding section showed graphically the progress of the B-1 bundle through the test transient. Qualitative information on burst-time, temperature, etc., can be obtained from the various figures, but more quantitative information is given in Tables 6 through 21 on the bundle conditions at the individual burst times. These tables (computer printouts from the data tape) list the times from power-on and power-off for which the tabulation was made, the simulator differential pressure,

simulator temperatures (with minimum, maximum, and average values), and times from the other tube bursts (relative to that for which the table pertains). Pertinent miscellaneous data are also printed out. These include shroud temperatures (TE 90-1 through TE 90-6), steam inlet (TE-304) and exit (TE-305) temperatures, vessel pressure (PE-301), shroud current (EIE-10), bundle current (difference between EIE-10 and EIE-20), bundle voltage (EEE-20) and shroud voltage (difference between EEE-10 and EEE-20).

The vessel pressure sensor (PE-301) gave erroneous readings and should be ignored. The correct pressure was obtained (and used to calculate the tabulated differential pressures) from a direct reading pressure indicator. The thermocouples for measuring steam temperature (TE-304 and TE-305) were positioned such that they did provide true values. Also, as mentioned earlier, four simulator thermocouples (TE 9-1, TE 9-3, TE 14-2, and TE 14-3) became detached from the wall during assembly and probably indicated temperatures higher than existed on the Zircaloy surface. The values given in the tables for these thermocouples are the actual measured values and do not take this possible error into account. Readings given in the tables for TE 12-4 should be ignored, since it was inoperative during the test. In comparing the various simulators, it should be noted that the No. 3 simulator behaved abnormally due to partial depressurization.

4.2 Pretest and Posttest Results

The information contained in this section was obtained from the pretest and posttest examinations of the B-1 test array. Some information, such as the simulator infrared scans, resulted from quality assurance efforts made to characterize the test components. Other information, such as bundle cross-section photographs, were obtained as a step in the posttest examination of the bundle. The results are presented in considerable detail, since we believe these data are extremely important to the interpretation of the test in terms of deformation behavior and distribution.

4.2.1 Pretest bundle photographs

Although not directly applicable to the interpretation of the B-1 test, selected photographs of the bundle assembly are included in this section for general interest. Various details of the grid spacers, pressure lines, and monitoring instrumentation may be seen.

Figure 35 shows the test array prior to installation of the shroud. The upper end, to the left, is flanged for attachment to the test vessel (see Fig. 1). Above the flange is the thermocouple connector ring. One face of the thin (0.25-mm thick) electrically heated shroud and backup thermal insulation is shown beneath the test array. The electrically isolated seal glands and flexible power leads that connect the lower end of the individual simulators to the bundle current collector are shown in Fig. 36. The flexible leads allow free (downward) expansion of the simulators during the test.

Figure 37 shows the completed test assembly, including the shroud and its support structure.

Figure 38 is a close-up view of the top of the assembly showing the thermocouple connector ring and the power and pressure connections to each of the fuel pin simulators.

Figure 39 is a close-up of the lower end, with the shroud power leads including the unconnected shroud trim current leads (see Fig. 1). The lowest of the four bundle grids can be seen on the rods, and close inspection shows the end of the shroud as a thin sheet of metal that lines the cavity around the bundle. The flexible connectors between the shroud and the current collector allow free expansion (downward) of the bundle during heatup.

Figure 40 is an overall view of the test assembly as installed in the insulated test vessel. Services to the bundle, such as gas (helium) and steam supplies, electrical power, thermocouple leads, etc., can be seen.

4.2.2 Posttest bundle photographs

After the test was completed, B-1 was removed from the test vessel for examination. Figure 41 is an overall view of the bundle (above) and the shroud (below) after partial disassembly. The four grid spacers can be

seen, as well as the heated length which appears as the shiny black region of the bundle.

The following photographs show all four faces of B-1 immediately after removal from the test vessel. A meter scale is provided to indicate distance along the bundle relative to the bottom of the original heated length. The faces are identified as N, E, S, and W, a nomenclature that was retained throughout all subsequent analysis of the test. Figures 42-A, 42-B, and 42-C show the North (N) face of B-1 and of the shroud. Several test effects are noticeable: (1) bursts and relatively large expansions occurred in three different regions of the bundle, (2) the shroud was dented by several of the bursts, (3) the heated zone produced a shiny black surface, and (4) the rods in the bundle changed lengths by different amounts. The latter effect can be seen both in the surface discoloration at the lower end and in the different positions of the lower end fittings. (These were aligned prior to the test.) Figures 43, 44, and 45 show similar views of the east, south, and west faces, respectively, of the bundle and shroud. Comments about Fig. 42 apply equally to these photographs.

Figure 46 is a close-up of the lower end of the bundle and illustrates the different length changes among the rods. All rods were originally of equal length. This phenomenon is caused by the preferred orientation or texture of the Zircaloy combined with burst temperatures in the α-phase, and it is discussed in Ref. 9.

Following preliminary examination, photography, and flow testing (to be described later), the bundle was encapsulated in epoxy for sectioning. Figure 47 shows the as-cast bundle before sectioning, and Fig. 48 shows a marked bundle (actually test B-2) and a sectioned bundle (B-1). The scribed lines across the face of the bundle indicate the positions at which the sections were subsequently cut. The longitudinal line and the angled longitudinal line aided in positioning the cut sections relative to the heated length. Four typical cut sections are shown at the bottom of the photograph.

4.2.3 Bundle cross section photographs

The encapsulated bundle was sectioned at 55 axial positions, and each of the sections was photographed for strain determinations. Figures 49

through 103 present photographs (~1×) of all of the cross sections. The series starts at a section 13.5 cm below the start of the heated length (i.e., in the undeformed region) and continues to a section 92.5 cm above the start of that length, or approximately 1.0 cm above the top of the heated length.

Starting with Fig. 51, all the figures have white arrow points in the upper left corner. The distance along the edge of the epoxy matrix between the arrow points is proportional to the elevation of the section and can be used to calculate the height (above the bottom of the heated zone) at which the actual cut was made.

Figure 49, taken 13.6 cm below the bottom of the heated zone, is representative of the undeformed bundle. All the tubes had moderate strain peaks [a minimum of 7.7% on No. 3 (the leaking tube) and a maximum of 26.8% on No. 15] about halfway between the start of the heated zone and the lower grid; Fig. 54 shows a section in this region at an elevation of 5.2 cm. A section through the lower grid (at elevation 11.8 cm) is shown in Fig. 56; the restraining influence of the grid (due to lateral grid forces and/or local cooling of the tube by the grid) is clearly evident by the range of strains (4.1 to 7.0%) observed in this section. Note the tendency of the grids to deform the tubes into square cross sections (e.g., tube 7 in the figure) at the points where the lateral forces are applied. Figure 61, the section at elevation 20.1 cm, shows the lateral displacement and large strain of No. 11 (52.5%) and No. 15 (41.6%). Barely evident in the figure is the pinhole burst in No. 15; an enlarged view of the tube (Fig. 104) shows the burst more clearly. This burst, the lowest one in the bundle and one of the two pinhole bursts observed in the test, may be at the thermocouple (TE 15-1) attachment; however, it is not certain at this time that this is the case. The elevation is in agreement, but the angular orientation disagrees by about 10° of rotation. As shown in Fig. 104, the wall is thinned more in the vicinity of tube No. 14 than near the burst; this appears to be evidence that failure was initiated by a defect of some kind.

Figure 63, the section taken at elevation 22.3 cm, shows the bursts in tubes 11 and 16. Apparently the burst in No. 11 deformed the No. 10 tube, which had previously burst (see Table 5 for the time sequence of the

bursts). In this figure, the strain in tube 11 is 48.9%, whereas in Fig. 61, it is 52.5%. These values were confirmed by an independent check using dividers to measure the perimeters.

The bursts in tubes 10 and 16 are shown in Fig. 64, the section taken at elevation 23.9 cm. One gets the impression that the flare-out of the left side of the No. 16 tube burst wrapped around the adjacent tube (No. 15) and then recoiled to the final position. This section is also interesting because total tube expansion (all tubes) in this section is one of the four maxima observed in the axial profile of the coolant channel flow area restriction. (This will be discussed in more detail later.)

Figures 66 and 67, the sections at elevations 26.5 and 28.1 cm, respectively, are interesting because they show considerable lateral displacement of the tubes while retaining space for coolant crossflow. The oval shape of tube 6 in Fig. 67 is interesting since this is just below the burst, as shown in Fig 68 (at elevation 29.7 cm).

Figure 71, the section at elevation 34.5 cm, is interesting because it is at one of the three minima observed in the axial profile of the coolant channel flow area restriction. The burst in tube 13 is shown in Fig. 75 (elevation 40.8 cm); this burst experienced the maximum strain (58.9%) observed in this test. The burst in tube 8 (elevation 44.7 cm) is shown in Fig. 77, and the bursts (elevation 46.7 cm) in tubes 9 and 14 are shown in Fig. 78. Although the bursts in these two tubes occurred only 0.05 sec apart (see Table 5), the directions of the bursts do not suggest interaction.

The section containing the maximum total deformation (all tubes) is shown in Fig. 79 (elevation 47.5 cm), which also shows the second of the two pinhole bursts observed in the test; this burst, in tube 5, is shown more clearly in Fig. 105. Since it was easier to locate this burst from the bottom side of the next higher section, the photograph was made looking up from the bottom of the bundle. It is printed in reverse so that the tubes and the burst appear in their proper orientation (relative to all the other photographs) when viewed from the top. This burst appears to have been initiated by a defect (slightly greater strains were observed at other positions on the tube) and is also in the vicinity of a

thermocouple (TE 5-4) attachment. The angle of the burst is definitely rotated about 13° from the thermocouple attachment, and the elevation is approximately 6 mm below the as-built position of the thermocouple. However, when the axial shrinkage (during the test) is taken into account, the elevations are in close agreement.

It appears in Fig. 79 that tube 10 was in contact with No. 9 at some time to produce the slight concavity in No. 9 evident in the figure. The burst in tube 12 is shown in both Figs. 79 and 80 (elevations 47.5 and 48.6 cm, respectively); the strains in the respective sections are 35.4 and 37.4%.

It will be recalled that tube 3 developed a severe leak prior to the test and continued to depressurize (see Fig. 21) during the test; however, the tube deformed a fair amount and burst 2.05 sec after power to the bundle was terminated. The burst is shown in Fig. 81 (elevation 50.4 cm).

A section through the spring clips of the upper grid is shown in Fig. 89 (elevation 66.9 cm). As was observed in Fig. 56, strong restraint of the grid on tube deformation is evident. Figure 93 (elevation 74.2 cm) shows the lower end of the burst in tube 7; the burst is shown at elevation 76.5 cm in Fig. 94. This figure also shows the bursts in tube Nos. 1, 2, and 4; these bursts appear again in the next higher section (Fig. 95), which is for elevation 77.3 cm. The sequence of these bursts (to the nearest 0.05 sec) was tube 4, 1, and then 2 (see Table 5).

Table 22 summarizes the burst data. The precise location of the burst midpoint was difficult to establish in most cases. The axial position of the bursts in tubes 1, 2, 4, 13, and 14 were determined accurately before the bundle was cast in the epoxy matrix; locations of the others were determined from the elevations of the sections in which they appear. (An attempt was made to cut the section at the midpoint of the burst, but this point was difficult to observe for the bursts facing inward.) Definition of the orientation was even more difficult due to the lateral displacement of the tubes and the shape of the burst flare-out; thus, the orientations and elevations given in the table are our best estimate of the points at which the bursts occurred. The orientations are shown in the plan view of the bundle in Fig. 106, and the elevations are indicated in Fig. 107.

4.2.4 Strain data and tube strain profiles

Following posttest flow characterization of the B-1 test array (discussed in Sect. 4.2.6), the bundle was cast into an epoxy matrix and sectioned at 5 axial positions for determining the circumferential strain in each tube in each of the sections.

The strain measurements were obtained from enlarged (~5×) photographs of the sections (see Figs. 49 through 103 for ~1× photographs) by digitizing and recording on magnetic tape the coordinates of a number (20-40, depending on shape and deformation) of points on the inside and outside perimeters of the tubes. The accuracy of the digitizer, referred to the actual size of the tubes, is about 0.025 mm. The data were fitted to smooth curves, using a cubic spline fitting routine, and were then used to calculate inner and outer perimeters, enclosed (tube-wall) area, and the centroid of the area. Straight lines were used to joint the ends of the tube openings (at the burst points) to define the calculational boundaries; however, the lengths of the straight lines were excluded from the perimeter calculations. The strain (the total circumferential elongation expressed as a percent of the original circumference) was computed on the basis of the outside perimeter. Figure 108 compares the actual section to the graphical output of the curve fitting routine for the section made at elevation 77.3 cm. Strain measurements (the average of five measurements on the 5× photograph) are given in the photograph, and these are considered accurate. The upper number in each tube shape in the computer simulation is the tube identification; the lower figure is the strain in percent. The cross is the centroid of the area enclosed by the outside perimeter. The coordinate grid is relative to the sides of the epoxy matrix. Comparison of the photograph and the computer simulation shows that the data processing methodology calculates the strain and reconstructs the shapes and areas quite well. Although tube wall thinning (see tubes 5 and 7) is reproduced, these data were insufficient to provide accurate wall thickness reduction; other (available) measuring techniques would be required to obtain this type of data.

Table 23 gives the strain in each tube at each of the sections. Figures 109 through 124 give the axial distribution of the circumferential strain for tubes 1 through 16, respectively; the burst location is noted.

Before the fuel simulators were assembled, the axial temperature distribution of each of the fuel simulators (internal heaters) was characterized by an infrared scanning technique.[10] The respective characterization scans are shown with the deformation profiles for reference purposes; the axial locations of the thermocouples are noted on the characterization scans.

In general, the strain decreases sharply at each end of the heated length, reflecting the strength associated with the sharp axial temperature gradients in these regions. The upper ends reflect the short thermal entrance region required to heat the incoming steam (~350°C) to near the tube surface temperature. The Reynolds modulus of the steam, based on inlet conditions and original tube dimensions, was 250; this is compared to a range of 600 to 800 used in earlier single-rod tests. The higher steam flow in the single-rod tests suppressed deformation and bursts in the thermal entrance region in comparison to the B-1 test observations.

The restraint of the interior grids (centered at the 10- and 66-cm elevations) is clearly evident in all the profiles. A striking feature of the profiles is the unusually good correlation between the deformation and the infrared characterization scans. Considering the facts that (1) the grids had a strong restraining effect, (2) circumferential temperature gradients are known to exist in the fuel simulators, and (3) the characterization scans are for a single angular orientation, there is generally good agreement in the scans and the burst locations. The burst in tube 5 apparently was initiated by a defect at a point that was not in agreement with the characterization scan (see Fig. 113). The burst in tube 15 was also apparently caused by a defect, but the burst location is in very good agreement with the characterization scan (see Fig. 123). In general, the burst strains were all greater than those observed in our (unheated shroud) single-rod tests for comparable test temperatures, as shown in Fig. 125.

Axial shrinkage over the heated zone of the individual tubes showed considerable scatter but was in general agreement with earlier single-rod test results as shown in Fig. 126.

For the tubes and spacing (10.92 mm OD on a 14.43-mm-square pitch; 1.32 pitch-to-diameter ratio) used in the B-1 test, adjacent tubes should

touch after 32% uniform expansion. Figure 127 plots those portions of each tube over which the strain exceeded 32%; maximum deformation in tube 3, which leaked prior to the transient, was less than this value, as indicated in Fig. 111. In tubes 9 and 11, greater than 32% expansion occurred over lengths equal to 10 (original) tube diameters, and these lengths were not overlapping.

4.2.5 Coolant channel flow area restriction

As evident from the deformation profiles for the individual tubes, significant deformation was observed at a number of points. However, the total expansion for all the tubes at any cross section is much more important, since it determines the coolant channel flow area restriction.

One method for calculating the restriction is to consider unit cells centered about the open space between fuel rods; an alternative method considers unit cells centered about the fuel rods. Obviously, both methods give the same results for infinite arrays, but, for small test arrays, different results will be obtained. The percentage coolant channel flow area restriction was calculated with the rod-centered unit cell method, using the equation

$$B = 100 \left[\frac{\sum^{n=16} (A_{d,n} - A_o)}{16\ (p^2 - A_o)} \right],$$

where

B = percentage restriction in coolant channel flow area,
$A_{d,n}$ = outside area of deformed tube (mm^2),
A_o = outside area of original tube (mm^2),
p = tube-to-tube pitch in square array (mm).

With this definition, B is zero for no deformation and is 100 if all the tubes deform into a square whose sides are of length p (completely filling the open area). For the case of uniform ballooning such that the tubes just come into contact (i.e., 32% strain for the dimensions appropriate to this test), B is 61%.

In summing the deformed tube areas in the above equation for those sections that contain bursts, one must decide how to treat the burst tube flare-out. Two definitions were used that appear to be reasonable upper and lower limits of the coolant channel flow area restriction. The first definition, which is believed to be representative of the upper limit, consists of drawing straight lines between the ends of the tube flare-outs to establish a burst tube area, as illustrated in Fig. 128. Special consideration was given to those flare-outs that enclosed adjacent tubes to exclude overlapping areas, as noted by tube 4 in the figure. The second definition, which is believed to be representative of the lower limit, considered the burst tube cross section as a circle (see tube 7 in the figure) with a perimeter equal to that of the tube. The latter definition is considered a reasonable approximation of the tube just before burst.

For the nonburst cross sections, the actual area (regardless of shape) enclosed by the outside perimeter was used in the summation; these areas and the ones based on the first definition for burst tubes were calculated from the fitted curves of the digitized coordinates of the enlarged photographs. The deformed tube areas $A_{d,n}$ are tabulated in Table 24 for each tube at each section based on the first definition of the burst tube area and in Table 25 based on the second definition. The last column (on the right side) gives the summation of the individual $A_{d,n}$. The summed areas were used in the above equation to calculate the coolant channel flow area restriction at each section; the results are given in Table 26 and plotted in Fig. 129 as a function of heated length. The flow channel restriction differs only in the sections where tube bursts occurred. The cross-sectional area occupied by the grids was not included in the calculation; including this area (~47 mm^2) would slightly increase the restriction at the grid locations (centered about elevations 10 and 66 cm). The maximum restriction (at elevation 46.7 cm) was 58 or 49%, depending on which method for handling the tube flare-out was used.

It is evident from viewing the photographs of the transverse sections (Figs. 49 through 103) that the tubes have undergone significant lateral displacement. In fact, it was speculated earlier that tube contact may have existed during the transient to cause most bursts to be

directed toward open spaces. To obtain an idea of the extent of tube centerline relocation, a least-squares fitting routine was used to fit the original grid layout at each of the sections to the centroids determined for the tube areas. A typical graphical output of the fitting routine is shown in Fig. 130, which corresponds to the sections shown in Figs. 95 and 107. The coordinate system used in Fig. 130, like that in Fig. 128, is referenced to the epoxy matrix. The crosses in Fig. 130 represent the locations of the centroid of the posttest tube area, and the dots represent the pretest centerline locations of the tubes. There appears to be an outward movement of the tubes; this probably reflects the lack of restraint in this small test array that would not be present in a very large array.

4.2.6 Flow test results

Flow tests were conducted on the deformed B-1 test array and on a geometrically identical reference bundle to characterize the pressure losses for flows in the range $10^4 \lesssim Re \lesssim 10$. A flow shroud that had a net coolant flow area with the reference bundle of 28.8 cm^2 was used to enclose the bundle. (This shroud is identified in other MRBT reports as shroud No. 1.) The shroud-bundle assembly was oriented vertically and the flow directed upward.

The B-1 tube bursts required a thick gasket and reliefs cut in the walls of the shroud flow channel (see Fig. 131 for orientation of B-1 in the shroud) to accommodate the bundle. Axial locations of the three relief grooves fell (1) on the right side of the flow channel at 76.6 cm above the bottom of the heated zone, ending 5.1 cm below the wall top with a 4.9-cm width; (2) on the left side of the channel at 46.3 cm above the bottom of the heated zone, ending 2.8 cm below the wall top with a 3.5-cm width; and (3) on the left side at 40.3 cm above the bottom of the heated zone, ending 1.9 cm below the wall top with a 3.0-cm width. The effect of these modifications on the pressure measurements was not significant.

The pressure taps for the flow tests were positioned as shown in Table 27. The spacings are given relative to the average position of the lower end of the heated zone of B-1.

Flow test data are presented below in the form of graphs and tables. The interpretative report[6] of the flow tests should be consulted for a detailed description of the test procedures and, more importantly, a discussion of the accuracy and precision of the test data.

A total of ten flow tests were performed — six on the reference bundle and four on the B-1 bundle. Figures 132 through 135 show comparisons of the average differential pressure loss profiles for the B-1 and reference bundles at four different nominal flow rates. Figures 136 and 137 show the results of two additional flow tests of the reference bundle.

Tabulated data for the ten flow tests are shown in Tables 28 through 37 relative to the bottom taps on each side of the flow shroud. These data were averaged, for each flow test, to produce the graphs in Figs. 132 through 135 and were used directly in Figs. 136 and 137.

Finally, the results of all of the flow tests are given in Fig. 138, together with the equations to which the data were fitted.

Observations and mathematical analysis of the data (reported elsewhere[6]) show that two conclusions may be reached: (1) the relief grooves cut into the shroud walls did not detrimentally affect the pressure loss measurements to a significant degree and (2) the agreement between measurements and mathematical predictions indicates that the burst bundle measurements should also be of good quality, barring adverse flow deflection effects induced by the bundle distortion. For the burst and reference bundles, the error for each pressure measurement (which is also dependent on the measured flow velocity) is estimated to be less than 15%.

5. ACKNOWLEDGMENTS

Data presented in this report reflect the combined effort of a number of people over an extended period of time, spanning fabrication, testing, and pretest and posttest examination of the test array.

We wish to acknowledge the contribution of K. R. Carr for his careful attention to all the instrumentation and control aspects of the test; E. L. Biddle, J. N. Money, and C. Cross for assembly of the test array and for the many other necessary support tasks; F. R. Gibson for programming and operation of the computer-controlled data acquisition system; J. F. Mincey for conducting the flow tests; N. M. Atchley for sectioning and photographing the bundle cross sections; E. G. Sewell for programming and processing the strain data; the Fuel Pin Simulator Development Group, under the leadership of K. W. McCulloch, for development and procurement of the fuel simulators; and the many other groups and individuals who had a part in the successful fulfillment of the test objectives.

6. REFERENCES

1. R. H. Chapman, compiler, *Quick-look Report on MRBT No. 1 4 × 4 Bundle Burst Test*, Internal Report ORNL/MRBT-2 (September 1977).
2. R. H. Chapman, *Multirod Burst Test Program Progress Report for July–December 1977*, NUREG/CR-0103 (ORNL/NUREG/TM-200).
3. R. H. Chapman, *Multirod Burst Test Program Progress Report for January–March 1978*, NUREG/CR-0225 (ORNL/NUREG/TM-217).
4. R. H. Chapman, *Multirod Burst Test Program Progress Report for July–December 1978*, NUREG/CR-0655 (ORNL/NUREG/TM-297).
5. R. H. Chapman, *Multirod Burst Test Program Progress Report for April–June 1977*, ORNL/NUREG/TM-135.
6. J. F. Mincey, *Steady-State Axial Pressure Losses Along the Exterior of Deformed Multirod Burst Test (MRBT) Bundles B-1 and B-2*, ORNL/NUREG/TM report (in preparation).
7. R. H. Chapman, compiler, *Characterization of Zircaloy-4 Tubing Procured for Fuel Cladding Research Programs*, ORNL/NUREG/TM-29 (July 1976).
8. W. E. Baucum and R. E. Dial, *An Apparatus for Spot Welding Sheathed Thermocouples to the Inside of Small-Diameter Tubes at Precise Locations*, ORNL/NUREG/TM-33 (August 1976).
9. R. H. Chapman, *Multirod Burst Test Program Quarterly Progress Report for January–March 1977*, ORNL/NUREG/TM-108.
10. W. A. Simpson, Jr., et al., *Infrared Inspection and Characterization of Fuel-Pin Simulators*, ORNL/NUREG/TM-55 (November 1976).

Table 1. As-built data for fuel pin simulators used in B-1 test

Bundle position No.	Zircaloy tube serial No.	Internal heater[a]		Fuel pin simulator gas volume[b] (cm^3)
		Serial No.	Element resistance (Ω)	
1	0024	2828052	4.13	49.2
2	0675	2828046	4.06	51.5
3	0018	2828051	4.18	49.7
4	0676	2828057	4.15	49.8
5	0686	2828061	4.08	50.4
6	0014	2828048	4.15	50.3
7	0678	2828047	4.07	49.6
8	0025	2828045	4.07	50.0
9	0016	2828058	4.01	49.0
10	0687	2828044	4.08	50.7
11	0017	2828049	4.18	49.2
12	0683	2828060	4.09	50.5
13	0684	2828062	4.01	50.2
14	0022	2828050	4.17	50.1
15	0685	2828055	4.04	49.5
16	0026	2828035	4.03	50.2

[a] All 16 internal heaters were fabricated by SEMCO.

[b] The fuel pin simulator volume, measured at room temperature before assembly of the bundle, includes a pressure transducer and connecting tube identical to the test facility hookup for each simulator.

Table 2. Summary of burst test results

RCE NO.	INITIAL CONDITIONS: DIFFERENTIAL PRESSURE (KPA)	INITIAL CONDITIONS: TEMPERATURES (DEG C) TE-1	TE-2	TE-3	TE-4	MAXIMUM PRESSURE DIFFERENTIAL (KPA)	APPROXIMATE BURST CONDITIONS: DIFFERENTIAL PRESSURE (KPA)	APPROXIMATE BURST CONDITIONS: TEMPERATURES (DEG C)[a] TE-1	TE-2	TE-3	TE-4	BURST TIME (SEC)
1	8697.2	355.2	356.1	356.1	356.1	9104.4	7749..	851.6	851.6	820.8	843.9	17.15
2	8696.3	358.9	356.1	358.1	354.2	9086.5	7412.6	864.2	847.8	815.1	867.1	17.20
3[b]	6628.0[b]	355.2	356.1	357.0	354.2	6494.2[b]	3680.4[b]	924.4[b]	937.1[b]	936.1[b]	910.8[b]	22.90[b]
4	8687.5	358.9	356.1	356.1	354.2	9087.8	7946.7	816.1	854.5	860.3	810.3	17.05
5	8716.3	355.2	356.1	355.2	355.2	9117.4	6930.1	859.4	840.1	864.2	871.9	17.65
6	8691.6	354.2	357.0	356.1	355.2	9148.6	7614.0	866.1	871.9	861.3	825.6	17.10
7	8693.4	356.1	356.1	356.1	355.2	9085.7	7255.8	869.0	826.6	863.2	833.3	17.30
8	8683.2	355.4	357.3	357.3	356.4	9101.9	7406.5	872.0	840.1	831.4	856.5	17.20
9	8703.5	355.2	357.0	357.0	357.9	9133.3	7097.2	855.5[c]	870.0	894.2[c]	822.8	17.35
10	8680.6	355.4	356.4	359.1	356.4	9090.1	7299.1	873.0	870.1	825.6	820.8	17.20
11	8616.2	355.2	357.0	356.1	354.2	9037.3	7267.9	843.9	846.8	838.1	842.0	17.45
12	8647.3	353.3	357.0	356.1	[d]	9065.3	7684.1	856.5	863.2	844.9	[d]	17.00
13	8653.5	358.9	357.6	356.1	353.3	9115.9	7522.9	832.4	861.3	877.7	872.9	17.05
14	8685.2	353.3	357.0	356.1	355..	9135.9	7355.1	818.0	843.0[c]	873.9[c]	874.8	17.40
15	8651.0	357.0	356.1	356.1	358.9	9092.4	7326.5	865.1	820.8	845.8	844.9	17.40
16	8675.0	355.4	357.3	356.4	358.2	9096.8	7530.4	824.6	845.8	807.4	847.8	17.20

[a] Underscored values selected as burst temperatures.

[b] Rod 3 developed a severe leak prior to the test, and its behavior is abnormal; burst occurred 2.05 sec after power cutoff.

[c] Thermocouple became detached from wall during assembly; indicated temperature is probably higher than existed on wall.

[d] Thermocouple was inoperative during test.

Table 3. Summary of B-1 test results related to volume changes

Rod No.	Initial gas volume[a] (cm^3)	Strain at burst (%)	Fractional[b] pressure decrease	Fractional[c] volume increase	Volume increase[d] of tube over heated length (%)	Average[e] strain (%)
1	49.2	36	1.12	1.50	28.9	14
2	51.5	32	1.17	1.66	39.4	18
3[f]	49.7	23[f]	1.72[f]	1.29[f]	16.6[f]	8[f]
4	49.8	36	1.09	1.46	26.7	13
5	50.4	43	1.26	1.93	55.0	24
6	50.3	43	1.14	1.53	31.3	15
7	49.6	36	1.20	1.75	43.6	10
8	50.0	42	1.17	1.65	38.2	18
9	49.0	44	1.23	1.86	49.3	22
10	50.7	45	1.19	1.73	43.2	20
11	49.1	49	1.19	1.77	44.5	20
12	50.5	37	1.12	1.56	32.9	15
13	50.2	59	1.16	1.70	40.8	19
14	50.1	42	1.18	1.73	42.5	19
15	49.5	42	1.19	1.75	43.5	20
[illegible]	50.2	39	1.15	1.62	36.6	17

[a] Measured at room temperature; includes fuel pin simulator (FPS), pressure transducer, and connecting tube.

[b] Ratio of initial pressure to burst pressure.

[c] Ratio of final to initial gas volume; includes FPS, pressure transducer, and connecting tube.

[d] Obtained from deformation profiles assuming circular cross sections.

[e] Assumes volume increase is uniformly distributed over heated length.

[f] Tube developed severe leak prior to transient; deformation behavior is abnormal.

Table 4. Summary of maximum pressures

ROD NO.	INITIAL CONDITIONS					CONDITIONS AT TIME OF MAXIMUM PRESSURES					
	DIFFERENTIAL PRESSURE (KPA)	TEMPERATURES (DEG C) TE-1	TE-2	TE-3	TE-4	DIFFERENTIAL PRESSURE (KPA)	TEMPERATURES (DEG C) TE-1	TE-2	TE-3	TE-4	TIME (SEC)
1	8657.2	355.2	356.1	356.1	356.1	9104.4	674.1	674.1	672.2	685.3	10.95
2	8696.3	356.9	356.1	356.1	354.2	9086.5	705.0	699.4	691.9	697.5	11.40
3[a]	6628.0[a]	355.2	356.1	357.0	354.2	6494.2[a]	355.2	357.0	357.0	354.2	0.15
4	8687.5	356.9	356.1	356.1	354.2	9087.8	690.0	695.6	700.3	687.2	11.75
5	8716.3	355.2	356.1	355.2	355.2	9117.4	702.2	698.5	698.5	705.0	11.75
6	8691.6	354.2	357.0	356.1	355.2	9148.6	706.0	719.1	710.7	701.3	11.95
7	8693.4	356.1	356.1	356.1	355.2	9085.7	684.4	679.7	680.6	685.3	11.10
8	8683.2	355.4	357.3	357.3	356.4	9101.9	706.3	693.2	699.7	702.5	11.40
9	8703.5	355.2	357.0	357.0	357.9	9133.3	694.7	690.0	700.3	663.8	11.15
10	8680.6	355.4	356.4	359.1	356.4	9090.1	713.8	706.3	697.9	694.2	11.80
11	8616.2	355.2	357.0	356.1	354.2	9037.3	711.6	697.5	697.5	697.5	11.75
12	8647.3	353.3	357.0	356.1	[b]	9065.3	711.6	707.9	710.7	[b]	11.65
13	8693.5	356.9	357.0	356.1	353.3	9115.9	695.6	708.8	727.6	712.6	11.80
14	8685.2	353.3	357.0	356.1	355.2	9135.9	689.1	707.9	703.2	702.2	11.75
15	8651.0	357.0	356.1	356.1	358.9	9092.4	693.8	679.7	697.5	698.5	11.25
16	8675.0	355.4	357.3	356.4	358.2	9096.8	699.7	696.0	692.3	685.8	11.75

[a] Rod 3 developed a severe leak prior to test, and its behavior is abnormal.

[b] Thermocouple inoperative during test.

Table 5. Distribution of bursts with time in B-i test

Time (sec)	No. of bursts	Simulator No.
17.00	1	12
17.05	2	4,13
17.10	1	6
17.15	1	1
17.20	4	2,8,10,16
17.25	0	
17.30	1	7
17.35	1	9
17.40	2	14,15
17.45	1	11
17.50	0	
17.55	0	
17.60	0	
17.65	1	5
22.90	1	3

[a]Power was terminated at 20.85 sec.

Table 6. Test conditions summary at rod 1 burst time

TIME FROM POWER-ON 17.15 SEC. TIME FROM POWER-OFF -3.70 SEC.

ROD NO.	DIFFERENTIAL PRESSURE (KPA)	TEMPERATURES (DEG C)							TIME FROM BURST (SEC)
		TE-1	TE-2	TE-3	TE-4	MINIMUM	MAXIMUM	AVERAGE	
1	7749.8	851.6	851.6	820.8	843.9	820.8	851.6	842.0	0.00
2	7450.6	863.2	846.8	814.1	865.1	814.1	865.1	847.3	-0.05
3	4411.4	845.8	855.5	848.7	825.6	825.6	855.5	843.9	-5.75
4	5174.3	806.5	853.6	858.4	810.3	806.5	858.4	832.2	0.10
5	7689.3	857.4	832.4	846.8	874.8	832.4	874.8	852.9	-0.50
6	5656.7	864.2	868.1	844.9	825.6	825.6	868.1	850.7	0.05
7	7488.1	869.0	823.7	871.0	831.4	823.7	871.0	848.8	-0.15
8	7493.0	872.0	840.1	831.4	855.5	831.4	872.0	849.7	-0.05
9	7414.2	852.6	857.4	889.4	810.3	810.3	889.4	852.4	-0.20
10	7386.8	871.1	868.1	824.6	820.8	820.8	871.1	846.2	-0.05
11	7695.8	833.3	844.9	839.1	837.2	833.3	844.9	838.6	-0.30
12	2940.2	857.4	860.3	843.0	109.7	109.7	860.3	667.6	0.15
13	5270.7	822.8	850.7	874.8	871.0	822.8	874.8	854.8	0.10
14	7691.1	812.2	838.1	871.9	869.0	812.2	871.9	847.8	-0.25
15	7684.0	864.2	816.1	844.9	844.9	816.1	864.2	842.5	-0.25
16	7605.7	822.7	844.9	806.4	846.8	806.4	846.8	830.2	-0.05

MISCELLANEOUS INSTRUMENTS

50	TE-90-1	682.3 DEG C	51	TE-90-2	720.8 DEG C	52	TE-90-3	701.6 DEG C
53	TE-90-4	684.7 DEG C	54	TE-90-5	720.8 DEG C	55	TE-90-6	634.7 DEG C
58	TE-305	341.1 DEG C	408	PE-301	205.8 KPA	472	EIE-10	863.1 AMPS
473	EEE-10	208.4 VOLTS	474	EIE-20	131.5 AMPS	475	EEE-20	190.6 VOLTS
478	TE-304	349.3 DEG C						

Table 7. Test conditions summary at rod 2 burst time

TIME FROM POWER-ON 17.20 SEC. TIME FROM POWER-OFF -3.65 SEC.

ROD NO.	DIFFERENTIAL PRESSURE (KPA)	TEMPERATURES (DEG C)							TIME FROM BURST (SEC)
		TE-1	TE-2	TE-3	TE-4	MINIMUM	MAXIMUM	AVERAGE	
1	6760.8	845.8	850.7	817.0	842.0	817.0	850.7	838.9	0.05
2	7412.6	864.7	847.8	815.1	867.1	815.1	867.1	848.5	0.00
3	4411.4	84[illegible].8	857.4	850.7	826.6	826.6	857.4	845.6	-5.70
4	3681.7	807.4	853.6	860.3	812.2	807.4	860.3	833.4	0.15
5	7626.0	855.5	832.4	848.7	873.9	832.4	873.9	852.6	-0.45
6	4059.9	864.2	868.1	837.2	829.5	829.5	868.1	849.7	0.10
7	7415.5	869.0	824.7	868.1	832.4	824.7	869.0	848.5	-0.10
8	7406.5	872.0	840.1	831.4	856.5	831.4	872.0	850.0	0.00
9	7336.7	853.6	863.2	891.3	812.2	812.2	891.3	855.1	-0.15
10	7299.1	873.0	870.1	825.6	820.8	820.8	873.0	847.4	0.00
11	7631.7	835.3	844.9	840.1	837.2	835.3	844.9	839.3	-0.25
12	2057.9	860.3	862.2	845.8	108.8	108.8	862.2	669.3	0.20
13	3543.8	819.9	847.8	873.9	871.0	819.9	873.9	853.1	0.15
14	7619.6	813.2	837.2	872.9	871.0	813.2	872.9	848.6	-0.20
15	7618.4	865.1	817.0	845.8	844.9	817.0	865.1	843.2	-0.20
16	7530.4	824.6	845.8	807.4	847.8	807.4	847.8	831.4	0.00

MISCELLANEOUS INSTRUMENTS

50	TE-90-1	682.3 DEG C	51	TE-90-2	719.6 DEG C	52	TE-90-3	700.4 DEG C
53	TE-90-4	690.8 DEG C	54	TE-90-5	720.8 DEG C	55	TE-90-6	629.7 DEG C
58	TE-305	341.1 DEG C	403	PE-301	205.8 KPA	472	EIE-10	863.1 AMPS
473	EEE-10	208.5 VOLTS	474	EIE-20	131.5 AMPS	475	EEE-20	190.6 VOLTS
476	TE-304	349.3 DEG C						

Table 8. Test conditions summary at rod 3 burst time

TIME FROM POWER-ON 22.90 SEC. TIME FROM POWER-OFF 2.05 SEC.

ROD NO.	DIFFERENTIAL PRESSURE (KPA)	TEMPERATURES (DEG C)							TIME FROM BURST (SEC)
		TE-1	TE-2	TE-3	TE-4	MINIMUM	MAXIMUM	AVERAGE	
1	-105.4	925.4	924.4	911.7	926.4	911.7	926.4	922.0	5.75
2	-57.5	947.9	932.2	898.1	949.8	898.1	949.8	932.0	5.70
3	3680.4	924.4	937.1	936.1	910.8	910.8	937.1	927.1	0.00
4	-100.2	901.0	960.6	958.6	897.1	897.1	960.6	929.3	5.85
5	-56.5	930.3	907.8	953.7	938.1	907.8	953.7	932.5	5.25
6	-100.0	940.0	968.4	931.2	918.6	918.6	968.4	939.6	5.80
7	-80.5	935.1	910.8	916.6	911.7	910.8	935.1	918.6	5.60
8	-106.6	979.6	926.9	915.1	892.5	892.5	979.6	928.5	5.70
9	-104.4	976.3	963.5	971.4	918.6	918.6	976.3	957.4	5.55
10	-101.9	979.6	953.7	909.2	915.1	909.2	979.6	939.4	5.70
11	-133.1	933.2	917.6	976.3	939.1	917.6	976.3	941.5	5.45
12	-114.2	961.6	936.1	938.1	117.1	117.1	961.6	738.2	5.90
13	-59.7	909.8	907.8	943.0	969.4	907.8	969.4	932.5	5.85
14	-105.3	915.6	930.3	964.5	912.7	912.7	964.5	930.8	5.50
15	-102.1	944.9	911.7	906.9	913.7	906.9	944.9	919.3	5.50
16	-110.3	930.9	948.7	879.8	916.1	879.8	948.7	918.9	5.70

MISCELLANEOUS INSTRUMENTS

50	TE-90-1	716.0 DEG C	51	TE-90-2	783.6 DEG C	52	TE-90-3	704.0 DEG C
53	TE-90-4	741.1 DEG C	54	TE-90-5	769.5 DEG C	55	TE-90-6	742.3 DEG C
58	TE-305	341.5 DEG C	408	PE-301	205.8 KPA	472	EIE-10	0.6 AMPS
473	EEE-10	0.1 VOLTS	474	EIE-20	0.1 AMPS	475	EEE-20	0.1 VOLTS
478	TE-304	348.9 DEG C						

Table 9. Test conditions summary at rod 4 burst time

TIME FROM POWER-ON 17.05 SEC. TIME FROM POWER-OFF -3.80 SEC.

ROD NO.	DIFFERENTIAL PRESSURE (KPA)	TEMPERATURES (DEG C)							TIME FROM BURST (SEC)
		TE-1	TE-2	TE-3	TE-4	MINIMUM	MAXIMUM	AVERAGE	
1	7876.1	852.6	847.8	818.9	842.0	818.9	852.6	840.3	-0.10
2	7632.4	861.3	843.9	812.2	863.2	812.2	863.2	845.2	-0.15
3	4418.4	843.9	852.6	846.8	823.7	823.7	852.6	841.8	-5.85
4	7946.7	816.1	854.5	860.3	810.3	810.3	860.3	835.3	0.00
5	7815.9	858.4	830.4	843.0	872.9	830.4	872.9	851.2	-0.60
6	7820.9	868.1	871.0	863.2	825.6	825.6	871.0	857.0	-0.05
7	7626.0	869.0	820.8	870.0	829.5	820.8	870.0	847.3	-0.25
8	7637.2	872.0	838.1	831.4	855.5	831.4	872.0	849.3	-0.15
9	7555.1	851.6	849.7	886.5	805.5	805.5	886.5	848.3	-0.30
10	7540.3	867.2	865.2	822.7	818.9	818.9	867.2	843.5	-0.15
11	7810.0	828.5	843.9	840.1	835.3	828.5	843.9	836.9	-0.40
12	6367.8	854.5	859.4	837.2	108.8	108.8	859.4	665.0	0.05
13	7522.9	832.4	861.3	877.7	872.9	832.4	877.7	861.1	0.00
14	7805.5	809.3	837.2	870.0	867.1	809.3	870.0	845.9	-0.35
15	7793.5	861.3	815.1	844.9	843.9	815.1	861.3	841.3	-0.35
16	7733.7	818.9	842.9	805.5	844.9	805.5	844.9	828.0	-0.15

MISCELLANEOUS INSTRUMENTS

50	TE-90-1	687.1 DEG C	51	TE-90-2	723.2 DEG C	52	TE-90-3	706.4 DEG C
53	TE-90-4	696.8 DEG C	54	TE-90-5	723.2 DEG C	55	TE-90-6	637.1 DEG C
58	TE-305	341.1 DEG C	408	PE-301	205.8 KPA	472	EIE-10	863.1 AMPS
473	EEE-10	208.4 VOLTS	474	EIE-20	131.5 AMPS	475	EEE-20	190.6 VOLTS
478	TE-304	349.3 DEG C						

Table 10. Test conditions summary at rod 5 burst time

TIME FROM POWER-ON 17.65 SEC. TIME FROM POWER-OFF -3.20 SEC.

ROD NO.	DIFFERENTIAL PRESSURE (KPA)	TEMPERATURES (DEG C)							TIME FROM BURST (SEC)
		TE-1	TE-2	TE-3	TE-4	MINIMUM	MAXIMUM	AVERAGE	
1	188.0	843.0	857.4	829.5	845.8	829.5	857.4	843.9	0.50
2	357.2	833.3	850.7	815.1	864.2	815.1	864.2	840.8	0.45
3	4376.2	857.4	867.1	863.2	835.3	835.3	867.1	855.7	-5.25
4	195.9	815.1	867.1	872.9	818.0	815.1	872.9	843.3	0.60
5	6530.1	859.4	840.1	864.2	871.9	840.1	871.9	858.9	0.00
6	233.1	862.2	884.5	844.9	845.8	844.9	884.5	859.4	0.55
7	743.6	850.7	825.6	841.0	832.4	825.6	850.7	837.4	0.35
8	666.6	885.7	843.9	836.2	830.4	830.4	885.7	849.1	0.45
9	1049.5	871.0	875.8	885.5	834.3	834.3	885.5	866.6	0.30
10	429.4	882.7	865.2	830.4	832.3	830.4	882.7	852.7	0.45
11	3214.9	842.0	841.0	850.7	843.0	841.0	850.7	844.2	0.20
12	83.2	876.8	867.1	863.2	110.6	110.6	876.8	679.4	0.65
13	146.3	824.7	840.1	873.9	882.6	824.7	882.6	855.3	0.60
14	1525.1	834.3	841.0	861.3	858.4	834.3	861.3	848.7	0.25
15	1738.4	853.6	842.0	841.0	836.2	836.2	853.6	843.2	0.25
16	1014.8	834.3	858.4	818.9	834.3	818.9	858.4	836.5	0.45

MISCELLANEOUS INSTRUMENTS

50	TE-90-1	679.9 DEG C	51	TE-90-2	717.2 DEG C	52	TE-90-3	699.2 DEG C
53	TE-90-4	688.3 DEG C	54	TE-90-5	718.4 DEG C	55	TE-90-6	619.8 DEG C
58	TE-305	341.1 DEG C	408	PE-301	205.8 KPA	472	EIE-10	862.5 AMPS
473	EEF-10	208.5 VOLTS	474	EIE-20	131.4 AMPS	475	EEE-20	190.6 VOLTS
478	TE-304	348.9 DEG C						

Table 11. Test conditions summary at rod 6 burst time

TIME FROM POWER-ON 17.10 SEC. TIME FROM POWER-OFF -3.75 SEC.

ROD NO.	DIFFERENTIAL PRESSURE (KPA)	TEMPERATURES (DEG C)							TIME FROM BURST (SEC)
		TE-1	TE-2	TE-3	TE-4	MINIMUM	MAXIMUM	AVERAGE	
1	7820.0	852.6	849.7	819.9	843.0	819.9	852.6	841.3	-0.05
2	7561.5	863.2	844.9	813.2	864.2	813.2	864.2	846.4	-0.10
3	4418.4	845.8	854.5	847.8	823.7	823.7	854.5	843.0	-5.80
4	7205.8	811.3	853.6	858.4	808.4	808.4	858.4	832.9	0.05
5	7759.6	859.4	831.4	844.9	874.8	831.4	874.8	852.6	-0.55
6	7614.0	866.1	871.9	861.3	825.6	825.6	871.9	856.2	0.00
7	7560.7	868.1	822.8	870.0	830.4	822.8	870.0	847.8	-0.20
8	7565.1	872.0	839.1	831.4	854.6	831.4	872.0	849.3	-0.10
9	7484.6	852.6	850.7	888.4	807.4	807.4	888.4	849.8	-0.25
10	7459.9	869.1	865.2	823.7	819.8	819.8	869.1	844.5	-0.10
11	7752.9	831.4	843.9	840.1	836.2	831.4	843.9	837.9	-0.35
12	4256.3	856.5	859.4	839.1	108.8	108.8	859.4	665.9	0.10
13	7341.2	832.4	859.4	877.7	872.9	832.4	877.7	860.6	0.05
14	7748.3	810.3	837.2	871.9	868.1	810.3	871.9	846.9	-0.30
15	7742.4	863.2	816.1	844.9	843.9	816.1	863.2	842.0	-0.30
16	7665.9	821.8	843.9	806.4	844.9	806.4	844.9	829.2	-0.10

MISCELLANEOUS INSTRUMENTS

50	TE-90-1	681.1 DEG C	51	TE-90-2	720.8 DEG C	52	TE-90-3	702.8 DEG C
53	TE-90-4	706.4 DEG C	54	TE-90-5	722.0 DEG C	55	TE-90-6	634.7 DEG C
58	TE-305	340.8 DEG C	408	PE-301	205.8 KPA	472	EIE-10	863.1 AMPS
473	EEE-10	208.4 VOLTS	474	EIE-20	131.5 AMPS	475	EEE-20	190.6 VOLTS
478	TE-304	349.3 DEG C						

Table 12. Test conditions summary at rod 7 burst time

TIME FROM POWER-ON 17.30 SEC. TIME FROM POWER-OFF -3.55 SEC.

ROD NO.	DIFFERENTIAL PRESSURE (KPA)	TEMPERATURES (DEG C) TE-1	TE-2	TE-3	TE-4	MINIMUM	MAXIMUM	AVERAGE	TIME FROM BURST (SEC)
1	2810.2	837.2	850.7	817.0	840.1	817.0	850.7	836.2	0.15
2	4712.9	814.1	841.0	805.5	859.4	805.5	859.4	830.0	0.10
3	4404.3	849.7	859.4	853.6	828.5	828.5	859.4	847.8	-5.60
4	1537.6	810.3	856.5	862.2	814.1	810.3	862.2	835.8	0.25
5	7459.5	853.6	834.3	852.6	872.9	834.3	872.9	853.3	-0.35
6	2134.3	862.2	871.9	837.2	836.2	836.2	871.9	851.9	0.20
7	7255.8	869.0	826.6	863.2	833.3	826.6	869.0	848.0	0.00
8	4440.7	865.2	835.2	826.6	844.9	826.6	865.2	843.0	0.10
9	7181.7	854.5	868.1	893.3	819.9	819.9	893.3	858.9	-0.05
10	4130.9	870.1	863.3	822.7	820.8	820.8	870.1	844.2	0.10
11	7503.3	840.1	844.9	839.1	840.1	839.1	844.9	841.0	-0.15
12	1042.0	864.2	865.1	849.7	109.7	109.7	865.1	672.2	0.30
13	1655.6	819.9	844.9	871.9	872.9	819.9	872.9	852.4	0.25
14	7458.0	816.1	838.1	871.9	872.9	816.1	872.9	849.8	-0.10
15	7454.4	866.1	818.0	845.8	844.9	818.0	866.1	843.7	-0.10
16	5649.5	825.6	841.0	810.3	829.5	810.3	841.0	826.6	0.10

MISCELLANEOUS INSTRUMENTS

50	TE-90-1	681.1 DEG C	51	TE-90-2	716.0 DEG C	52	TE-90-3	696.8 DEG C
53	TE-90-4	678.6 DEG C	54	TE-90-5	719.6 DEG C	55	TE-90-6	624.8 DEG C
56	TE-305	341.1 DEG C	408	PE-301	205.8 KPA	472	EIE-10	863.1 AMPS
473	EEE-10	208.4 VOLTS	474	EIE-20	131.4 AMPS	475	EEE-20	190.6 VOLTS
478	TE-304	349.3 DEG C						

Table 13. Test conditions summary at rod 8 burst time

TIME FROM POWER-ON 17.20 SEC. TIME FROM POWER-OFF -3.65 SEC.

ROD NO.	DIFFERENTIAL PRESSURE (KPA)	TEMPERATURES (DEG C)							TIME FROM BURST (SEC)
		TE-1	TE-2	TE-3	TE-4	MINIMUM	MAXIMUM	AVERAGE	
1	6760.8	845.8	850.7	817.0	842.0	817.0	850.7	838.9	0.05
2	7412.6	864.2	847.8	815.1	867.1	815.1	867.1	848.5	0.00
3	4411.4	847.8	857.4	850.7	826.6	826.6	857.4	845.6	-5.70
4	3681.7	807.4	853.6	860.3	812.2	807.4	860.3	833.4	0.15
5	7626.0	855.5	832.4	848.7	873.9	832.4	873.9	852.6	-0.45
6	4059.9	864.2	868.1	837.2	829.5	829.5	868.1	849.7	0.10
7	7415.5	869.0	824.7	868.1	832.4	824.7	869.0	848.5	-0.10
8	7406.5	872.0	840.1	831.4	856.5	831.4	872.0	850.0	0.00
9	7336.7	853.6	863.2	891.3	812.2	812.2	891.3	855.1	-0.15
10	7299.1	873.0	870.1	825.6	820.8	820.8	873.0	847.4	0.00
11	7631.7	835.3	844.9	840.1	837.2	835.3	844.9	839.3	-0.25
12	2057.9	860.3	862.2	845.8	108.8	108.8	862.2	669.3	0.20
13	3543.8	819.9	847.8	873.9	871.0	819.9	873.9	853.1	0.15
14	7619.6	813.2	837.2	872.9	871.0	813.2	872.9	848.6	-0.20
15	7618.4	865.1	817.0	845.8	844.9	817.0	865.1	843.2	-0.20
16	7530.4	824.6	845.8	807.4	847.8	807.4	847.8	831.4	0.00

MISCELLANEOUS INSTRUMENTS

50	TE-90-1	682.3 DEG C	51	TE-90-2	719.6 DEG C	52	TE-90-3	700.4 DEG C
53	TE-90-4	650.8 DEG C	54	TE-90-5	720.8 DEG C	55	TE-90-6	629.7 DEG C
58	TE-305	341.1 DEG C	408	PE-301	205.8 KPA	472	EIE-10	863.1 AMPS
473	EEE-10	208.5 VOLTS	474	EIE-20	131.5 AMPS	475	EEE-20	190.6 VOLTS
47E	TE-304	349.3 DEG C						

Table 14. Test conditions summary at rod 9 burst time

TIME FROM POWER-ON 17.35 SEC. TIME FROM POWER-OFF -3.50 SEC.

ROD NO.	DIFFERENTIAL PRESSURE (KPA)	TEMPERATURES (DEG C)							TIME FROM BURST (SEC)
		TE-1	TE-2	TE-3	TE-4	MINIMUM	MAXIMUM	AVERAGE	
1	1875.8	838.1	851.6	818.9	841.0	818.9	851.6	837.4	0.20
2	3205.0	806.5	841.0	805.5	859.4	805.5	859.4	828.1	0.15
3	4397.3	850.7	860.3	855.5	829.5	829.5	860.3	849.0	-5.55
4	1424.2	811.3	857.4	864.2	814.1	811.3	864.2	836.8	0.30
5	7429.1	855.5	834.3	853.6	871.9	834.3	871.9	853.8	-0.30
6	1566.4	861.3	873.9	837.2	839.1	837.2	873.9	852.9	0.25
7	6414.7	864.2	825.6	858.4	827.6	825.6	864.2	843.9	0.05
8	3205.6	868.1	837.2	827.5	842.0	827.5	868.1	843.7	0.15
9	7097.2	855.5	870.0	894.2	822.8	822.8	894.2	860.6	0.00
10	2813.3	872.0	861.3	824.6	822.7	822.7	872.0	845.2	0.15
11	7432.0	841.0	845.8	839.1	840.1	839.1	845.8	841.5	-0.10
12	745.9	867.1	864.2	852.6	109.7	109.7	867.1	673.4	0.35
13	1203.1	820.8	843.9	871.9	874.8	820.8	874.8	852.9	0.30
14	7426.6	817.0	841.0	872.9	873.9	817.0	873.9	851.2	-0.05
15	7428.7	866.1	818.9	845.8	845.8	818.9	866.1	844.2	-0.05
16	4326.3	827.5	842.9	813.1	828.5	813.1	842.9	828.0	0.15

MISCELLANEOUS INSTRUMENTS

50	TE-90-1	681.1 DEG C	51	TE-90-2	717.2 DEG C	52	TE-90-3	698.0 DEG C
53	TE-90-4	699.2 DEG C	54	TE-90-5	719.6 DEG C	55	TE-90-6	621.1 DEG C
58	TE-305	341.1 DEG C	408	PE-301	205.8 KPA	472	EIE-10	862.5 AMPS
473	EEE-10	208.5 VOLTS	474	EIE-20	131.5 AMPS	475	EEE-20	190.6 VOLTS
478	TE-304	349.3 DEG C						

Table 15. Test conditions summary at rod 10 burst time

TIME FROM POWER-ON 17.20 SEC. TIME FROM POWER-OFF -3.65 SEC.

ROD NO.	DIFFERENTIAL PRESSURE (KPA)	TEMPERATURES (DEG C)							TIME FROM BURST (SEC)
		TE-1	TE-2	TE-3	TE-4	MINIMUM	MAXIMUM	AVERAGE	
1	6760.8	845.8	850.7	817.0	842.0	817.0	850.7	838.9	0.05
2	7412.6	864.2	847.8	815.1	867.1	815.1	867.1	848.5	0.00
3	4411.4	847.8	857.4	850.7	826.6	826.6	857.4	845.6	-5.70
4	3681.7	807.4	853.6	860.3	812.2	807.4	860.3	833.4	0.15
5	7626.0	855.5	832.4	848.7	873.9	832.4	873.9	852.6	-0.45
6	4059.9	864.2	868.1	837.2	829.5	829.5	868.1	849.7	0.10
7	7415.5	869.0	824.7	868.1	832.4	824.7	869.0	848.5	-0.10
8	7406.5	872.0	840.1	831.4	856.5	831.4	872.0	850.0	0.00
9	7336.7	853.6	863.2	891.3	812.2	812.2	891.3	855.1	-0.15
10	7259.1	873.0	870.1	825.6	820.8	820.8	873.0	847.4	0.00
11	7631.7	835.3	844.9	840.1	837.2	835.3	844.9	839.3	-0.25
12	2057.9	860.3	862.2	845.8	108.8	108.8	862.2	669.3	0.20
13	3543.8	819.9	847.8	873.9	871.0	819.9	873.9	853.1	0.15
14	7619.6	813.2	837.2	872.9	871.0	813.2	872.9	848.6	-0.20
15	7618.4	865.1	817.0	845.8	844.9	817.0	865.1	843.2	-0.20
16	7530.4	824.6	845.8	807.4	847.8	807.4	847.8	831.4	0.00

MISCELLANEOUS INSTRUMENTS

50	TE-90-1	682.3 DEG C	51	TE-90-2	719.6 DEG C	52	TE-90-3	700.4 DEG C
53	TE-90-4	690.8 DEG C	54	TE-90-5	720.8 DEG C	55	TE-90-6	629.7 DEG C
58	TE-305	341.1 DEG C	408	PE-301	205.8 KPA	472	EIE-10	863.1 AMPS
473	EEE-10	208.5 VOLTS	474	EIE-20	131.5 AMPS	475	EEE-20	190.6 VOLTS
476	TE-304	349.3 DEG C						

Table 16. Test conditions summary at rod 11 burst time

TIME FROM POWER-ON 17.45 SEC. TIME FROM POWER-OFF -3.40 SEC.

ROD NO.	DIFFERENTIAL PRESSURE (KPA)	TEMPERATURES (DEG C)							TIME FROM BURST (SEC)
		TE-1	TE-2	TE-3	TE-4	MINIMUM	MAXIMUM	AVERAGE	
1	886.9	839.1	853.6	822.8	842.0	822.8	853.6	839.4	0.30
2	1577.9	814.1	844.9	809.3	860.3	809.3	860.3	832.2	0.25
3	4390.3	853.6	863.2	858.4	831.4	831.4	863.2	851.6	-5.45
4	766.6	813.2	861.3	867.1	816.1	813.2	867.1	839.4	0.40
5	7274.5	856.5	836.2	857.4	871.9	836.2	871.9	855.5	-0.20
6	657.0	859.4	877.7	839.1	842.0	839.1	877.7	854.5	0.35
7	2579.2	858.4	819.9	843.9	825.6	819.9	858.4	837.0	0.15
8	1920.7	874.9	840.1	831.4	837.2	831.4	874.9	845.9	0.25
9	4477.4	853.6	869.0	886.5	816.1	816.1	886.5	856.3	0.10
10	1528.9	874.9	861.3	827.5	826.6	826.6	874.9	841.6	0.25
11	7267.9	843.9	846.8	838.1	842.0	838.1	846.8	842.7	0.00
12	358.1	870.0	864.2	856.5	109.7	109.7	870.0	675.1	0.45
13	6C9.5	821.8	843.0	872.9	877.7	821.8	877.7	853.8	0.40
14	6540.5	817.0	842.0	870.0	871.0	817.0	871.0	850.0	0.05
15	6305.6	860.3	822.8	843.0	842.0	822.8	860.3	842.0	0.05
16	2628.6	830.4	848.7	817.0	828.5	817.0	848.7	831.2	0.25

MISCELLANEOUS INSTRUMENTS

50	TE-90-1	675.0 DEG C	51	TE-90-2	713.6 DEG C	52	TE-90-3	694.4 DEG C
53	TE-90-4	679.9 DEG C	54	TE-90-5	713.6 DEG C	55	TE-90-6	617.4 DEG C
58	TE-305	341.1 DEG C	408	PE-301	205.8 KPA	472	EIE-10	863.1 AMPS
473	EEE-10	208.4 VOLTS	474	EIE-20	131.4 AMPS	475	EEE-20	190.6 VOLTS
478	TE-304	349.3 DEG C						

Table 17. Test conditions summary at rod 12 burst time

TIME FROM POWER-ON 17.00 SEC. TIME FROM POWER-OFF -3.85 SEC.

ROD NO.	DIFFERENTIAL PRESSURE (KPA)	TEMPERATURES (DEG C)							TIME FROM BURST (SEC)
		TE-1	TE-2	TE-3	TE-4	MINIMUM	MAXIMUM	AVERAGE	
1	7932.2	851.6	846.8	818.0	841.0	818.0	851.6	839.4	-0.15
2	7696.2	859.4	843.0	811.3	861.3	811.3	861.3	843.7	-0.20
3	4425.4	843.0	851.6	845.8	821.8	821.8	851.6	840.6	-5.90
4	8004.8	816.1	852.6	858.4	809.3	809.3	858.4	834.1	-0.05
5	7872.1	857.4	829.5	843.0	871.0	829.5	871.0	850.2	-0.65
6	7852.2	867.1	870.0	860.3	825.6	825.6	870.0	855.8	-0.10
7	7651.3	868.1	819.9	868.1	828.5	819.9	868.1	846.1	-0.30
8	7702.1	871.1	837.2	829.5	855.5	829.5	871.1	848.3	-0.20
9	7618.5	850.7	848.7	885.5	804.6	804.6	885.5	847.4	-0.35
10	7558.7	864.3	863.3	821.8	817.9	817.9	864.3	841.8	-0.20
11	7859.9	826.6	842.0	840.1	833.3	826.6	842.0	835.5	-0.45
12	7684.1	856.5	863.2	844.9	108.8	108.8	863.2	668.3	0.00
13	7555.6	831.4	861.3	877.7	871.0	831.4	877.7	860.3	-0.05
14	7862.7	807.4	836.2	868.1	866.1	807.4	868.1	844.5	-0.40
15	7844.5	860.3	815.1	843.9	843.0	815.1	860.3	840.6	-0.40
16	7793.9	817.0	841.0	805.5	842.9	805.5	842.9	826.6	-0.20

MISCELLANEOUS INSTRUMENTS

50	TE-90-1	694.4 DEG C	51	TE-90-2	728.0 DEG C	52	TE-90-3	707.6 DEG C
53	TE-90-4	694.4 DEG C	54	TE-90-5	728.0 DEG C	55	TE-90-6	623.6 DEG C
5E	TE-305	341.1 DEG C	408	PE-301	205.8 KPA	472	EIE-10	863.1 AMPS
473	EEE-10	208.4 VOLTS	474	EIE-20	131.5 AMPS	475	EEE-20	190.6 VOLTS
47E	TE-304	349.3 DEG C						

Table 18. Test conditions summary at rod 13 burst time

TIME FROM POWER-ON 17.05 SEC. TIME FROM POWER-OFF -3.80 SEC.

ROD NO.	DIFFERENTIAL PRESSURE (KPA)	TEMPERATURES (DEG C)							TIME FROM BURST (SEC)
		TE-1	TE-2	TE-3	TE-4	MINIMUM	MAXIMUM	AVERAGE	
1	7876.1	852.6	847.8	818.9	842.0	818.9	852.6	840.3	-0.10
2	7832.4	861.3	843.9	812.2	863.2	812.2	863.2	845.2	-0.15
3	4418.4	843.9	852.6	846.8	823.7	823.7	852.6	841.8	-5.85
4	7546.7	816.1	854.5	860.3	810.3	810.3	860.3	835.3	0.00
5	7815.9	858.4	830.4	843.0	872.9	830.4	872.9	851.2	-0.60
6	7820.9	868.1	871.0	863.2	825.6	825.6	871.0	857.0	-0.05
7	7626.0	869.0	820.8	870.0	829.5	820.8	870.0	847.3	-0.25
8	7637.2	872.0	838.1	831.4	855.5	831.4	872.0	849.3	-0.15
9	7555.1	851.6	849.7	886.5	805.5	805.5	886.5	848.3	-0.30
10	7540.3	867.2	865.2	822.7	818.9	818.9	867.2	843.5	-0.15
11	7810.0	828.5	843.9	840.1	835.3	828.5	843.9	836.9	-0.40
12	6367.8	854.5	859.4	837.2	108.8	108.8	859.4	665.0	0.05
13	7522.9	832.4	861.3	877.7	872.9	832.4	877.7	861.1	0.00
14	7805.5	809.3	837.2	870.0	867.1	809.3	870.0	845.9	-0.35
15	7793.5	861.3	815.1	844.9	843.9	815.1	861.3	841.3	-0.35
16	7733.7	818.9	842.9	805.5	844.9	805.5	844.9	828.0	-0.15

MISCELLANEOUS INSTRUMENTS

50	TE-90-1	687.1 DEG C	51	TE-90-2	723.2 DEG C	52	TE-90-3	706.4 DEG C
53	TE-90-4	696.8 DEG C	54	TE-90-5	723.2 DEG C	55	TE-90-6	637.1 DEG C
58	TE-305	341.1 DEG C	408	PE-301	205.8 KPA	472	EIE-10	863.1 AMPS
473	EFE-10	208.4 VOLTS	474	EIE-20	131.5 AMPS	475	EEE-20	190.6 VOLTS
478	TE-304	349.3 DEG C						

Table 19. Test conditions summary at rod 14 burst time

TIME FROM POWER-ON 17.40 SEC. TIME FROM POWER-OFF -3.45 SEC.

ROD NO.	DIFFERENTIAL PRESSURE (KPA)	TEMPERATURES (DEG C)							TIME FROM BURST (SEC)
		TE-1	TE-2	TE-3	TE-4	MINIMUM	MAXIMUM	AVERAGE	
1	1292.4	838.1	852.6	821.8	841.0	821.8	852.6	838.4	0.25
2	2228.6	809.3	843.0	807.4	859.4	807.4	859.4	829.8	0.20
3	4397.3	852.6	861.3	856.5	830.4	830.4	861.3	850.2	-5.50
4	1048.4	812.2	859.4	865.1	815.1	812.2	865.1	838.0	0.35
5	7351.8	856.5	835.3	855.5	871.9	835.3	871.9	854.8	-0.25
6	1162.0	860.3	875.8	838.1	841.0	838.1	875.8	853.8	0.30
7	4377.0	859.4	820.8	848.7	823.7	820.8	859.4	838.2	0.10
8	2501.7	871.1	838.1	829.5	839.1	829.5	871.1	844.4	0.20
9	6561.8	854.5	870.0	892.3	806.5	806.5	892.3	855.8	0.05
10	2104.4	874.0	861.3	826.6	825.6	825.6	874.0	846.9	0.20
11	7353.5	843.0	845.8	838.1	841.0	838.1	845.8	842.0	-0.05
12	527.3	868.1	864.2	854.5	109.7	109.7	868.1	674.1	0.40
13	855.6	821.8	843.0	871.9	875.8	821.8	875.8	853.1	0.35
14	7355.1	818.0	843.0	873.9	874.8	818.0	874.8	852.4	0.00
15	7326.6	865.1	820.8	845.8	844.9	820.8	865.1	844.2	0.00
16	3357.1	829.5	845.8	816.0	828.5	816.0	845.8	830.0	0.20

MISCELLANEOUS INSTRUMENTS

50	TE-90-1	677.4 DEG C	51	TE-90-2	714.8 DEG C	52	TE-90-3	695.6 DEG C
53	TE-90-4	654.4 DEG C	54	TE-90-5	716.0 DEG C	55	TE-90-6	619.8 DEG C
56	TE-305	341.3 DEG C	408	PE-301	205.8 KPA	472	EIE-10	863.1 AMPS
473	EEE-10	208.4 VOLTS	474	EIE-20	131.4 AMPS	475	EEE-20	190.6 VOLTS
478	TE-304	349.3 DEG C						

Table 20 Test conditions summary at rod 15 burst time

TIME FROM POWER-ON 17.40 SEC. TIME FROM POWER-OFF -3.45 SEC.

ROD NO.	DIFFERENTIAL PRESSURE (KPA)	TEMPERATURES (DEG C)							TIME FROM BURST (SEC)
		TE-1	TE-2	TE-3	TE-4	MINIMUM	MAXIMUM	AVERAGE	
1	1292.4	838.1	852.6	821.8	841.0	821.8	852.6	838.4	0.25
2	2228.6	809.3	843.0	807.4	859.4	807.4	859.4	829.8	0.20
3	4357.3	852.6	861.3	856.5	830.4	830.4	861.3	850.2	-5.50
4	1048.4	812.2	859.4	865.1	815.1	812.2	865.1	838.0	0.35
5	7351.8	856.5	835.3	855.5	871.9	835.3	871.9	854.8	-0.25
6	1162.0	860.3	875.8	838.1	841.0	838.1	875.8	853.8	0.30
7	4377.0	859.4	820.8	848.7	823.7	820.8	859.4	838.2	0.10
8	2501.7	871.1	838.1	829.5	839.1	829.5	871.1	844.4	0.20
9	6561.8	854.5	870.0	892.3	806.5	806.5	892.3	855.8	0.05
10	2104.4	874.0	861.3	826.6	825.6	825.6	874.0	846.9	0.20
11	7353.5	843.0	845.8	838.1	841.0	838.1	845.8	842.0	-0.05
12	527.3	868.1	864.2	854.5	109.7	109.7	868.1	674.1	0.40
13	855.6	821.8	843.0	871.9	875.8	821.8	875.8	853.1	0.35
14	7355.1	818.0	843.0	873.9	874.8	818.0	874.8	852.4	0.00
15	7326.6	865.1	820.8	845.8	844.9	820.8	865.1	844.2	0.00
16	3357.1	829.5	845.8	816.0	828.5	816.0	845.8	830.0	0.20

MISCELLANEOUS INSTRUMENTS

50	TE-90-1	677.4 DEG C	51	TE-90-2	714.8 DEG C	52	TE-90-3	695.6 DEG C
53	TE-90-4	694.4 DEG C	54	TE-90-5	716.0 DEG C	55	TE-90-6	619.8 DEG C
58	TE-305	341.3 DEG C	408	PE-301	205.8 KPA	472	EIE-10	863.1 AMPS
473	EEE-10	208.4 VOLTS	474	EIE-20	131.4 AMPS	475	EEE-20	190.6 VOLTS
478	TE-304	349.3 DEG C						

Table 21. Test conditions summary at rod 16 burst time

TIME FROM POWER-ON 17.20 SEC. TIME FROM POWER-OFF -3.65 SEC.

ROD NO.	DIFFERENTIAL PRESSURE (KPA)	TEMPERATURES (DEG C)							TIME FROM BURST (SEC)
		TE-1	TE-2	TE-3	TE-4	MINIMUM	MAXIMUM	AVERAGE	
1	6760.8	845.8	850.7	817.0	842.0	817.0	850.7	838.9	0.05
2	7412.6	864.2	847.8	815.1	867.1	815.1	867.1	848.5	0.00
3	4411.4	847.8	857.4	850.7	826.6	826.6	857.4	845.6	-5.70
4	3681.7	807.4	853.6	860.3	812.2	807.4	860.3	833.4	0.15
5	7626.0	855.5	832.4	848.7	873.9	832.4	873.9	852.6	-0.45
6	4059.9	864.2	868.1	837.2	829.5	829.5	868.1	849.7	0.10
7	7415.5	869.0	824.7	868.1	832.4	824.7	869.0	848.5	-0.10
8	7406.5	872.0	840.1	831.4	856.5	831.4	872.0	850.0	0.00
9	7336.7	853.6	863.2	891.3	812.2	812.2	891.3	855.1	-0.15
10	7259.1	873.0	870.1	825.6	820.8	820.8	873.0	847.4	0.00
11	7631.7	835.3	844.9	840.1	837.2	835.3	844.9	839.3	-0.25
12	2057.9	860.3	862.2	845.8	108.8	108.8	862.2	669.3	0.20
13	3543.8	819.9	847.8	873.9	871.0	819.9	873.9	853.1	0.15
14	7615.6	813.2	837.2	872.9	871.0	813.2	872.9	848.6	-0.20
15	7618.4	865.1	817.0	845.8	864.9	817.0	865.1	843.2	-0.20
16	7530.4	824.6	845.8	807.4	847.8	807.4	847.8	831.4	0.00

MISCELLANEOUS INSTRUMENTS

50	TE-90-1	682.3 DEG C	51	TE-90-2	719.6 DEG C	52	TE-90-3	700.4 DEG C
53	TE-90-4	690.8 DEG C	54	TE-90-5	720.8 DEG C	55	TE-90-6	629.7 DEG C
58	TE-305	341.1 DEG C	408	PE-301	205.8 KPA	472	EIE-10	863.1 AMPS
473	EEE-10	208.5 VOLTS	474	EIE-20	131.5 AMPS	475	EEE-20	190.6 VOLTS
478	TE-304	349.3 DEG C						

Table 22. Summary of B-1 burst data

Rod No.	Burst characteristics		Approximate position	
	Temperature (°C)	Strain (%)	Elevation[a] (cm)	Angle[b] (deg)
1	852	36	76.5	310
2	867	32	77.3	330
3[c]	937[c]	23[c]	50.4	120
4	860	36	76.8	295
5	872	43	47.5	30
6	872	43	29.7	205
7	869	36	76.5	315
8	872	42	44.7	310
9	870	44	46.7	75
10	873	45	23.9	330
11	847	49	22.3	210
12	863	37	48.6	335
13	878	59	40.8	205
14	875	42	46.4	170
15	865	42	20.1	325
16	848	39	23.9	335

[a]Elevation above bottom of heated zone.

[b]Looking down on bundle and measured clockwise from bundle north.

[c]Tube developed severe leak prior to transient; deformation behavior is abnormal.

Table 23. Percent circumferential strain in the tubes of the B-1 test

Elevation (cm)	Tube No.															
	1	2	3	4	5	6	7	8	9	10	11	12	13	14	15	16
0.0	1.5	0.6	2.7	2.1	1.4	1.5	1.2	1.3	1.7	1.8	1.8	1.7	2.7	1.9	1.7	1.6
1.8	5.6	8.1	7.6	8.4	6.2	10.1	7.4	8.2	8.2	9.2	6.2	8.2	8.9	8.1	8.7	6.4
3.3	7.8	18.3	10.0	10.3	8.4	15.6	13.5	16.0	13.7	20.1	11.1	10.3	10.5	12.1	20.1	12.6
5.2	7.6	17.7	7.7	10.7	8.2	12.9	14.1	16.9	15.0	18.2	13.5	9.3	8.7	12.8	26.8	12.6
8.9	3.5	4.8	4.0	5.0	4.4	6.0	5.5	6.3	5.0	6.5	6.1	4.9	3.8	4.6	5.3	5.2
11.8	4.6	5.6	4.1	6.0	5.2	6.1	6.4	7.3	5.2	6.8	7.0	5.9	4.4	4.7	6.2	5.4
14.1	13.2	16.1	8.7	12.0	17.3	20.3	17.7	16.3	18.4	21.0	20.5	15.8	25.0	16.6	27.3	17.9
15.4	11.8	15.3	10.4	13.0	24.0	21.0	16.9	15.6	20.0	22.6	20.5	15.9	36.9	18.9	36.4	21.9
17.3	12.7	14.7	10.7	13.2	29.7	20.4	18.5	16.4	20.7	22.9	25.0	14.4	24.9	19.2	36.0	25.5
18.8	15.3	17.9	9.6	15.4	26.2	22.3	20.1	18.5	27.9	26.3	44.4	14.0	16.7	25.1	38.5	28.1
20.1	13.8	19.1	7.7	14.9	21.4	23.6	21.4	18.1	30.2	30.3	52.5	13.8	12.7	25.4	41.6	29.5
20.6	13.7	19.1	7.4	14.4	20.9	23.5	21.4	17.3	29.5	30.1	52.0	12.7	11.5	23.4	39.0	28.6
22.3	14.1	18.8	8.3	12.3	25.0	23.7	23.7	17.6	28.2	41.1	48.9	14.2	12.2	21.5	30.8	30.3
23.9	13.3	20.1	8.9	12.0	27.4	22.5	25.2	18.3	28.6	44.5	44.4	16.9	14.1	22.9	28.1	38.6
25.5	11.2	22.5	8.3	12.6	28.9	21.3	28.2	18.0	35.6	38.2	44.9	16.7	15.2	25.4	22.2	32.8
26.5	11.6	24.2	8.5	13.3	35.9	24.3	30.2	16.8	37.8	37.2	42.6	16.3	17.8	26.7	19.2	27.0
28.1	12.0	22.9	8.3	14.2	44.1	36.4	28.8	17.2	28.7	35.4	32.4	16.3	22.6	24.1	16.5	21.6
29.7	11.4	20.5	8.2	12.1	34.8	42.7	25.3	17.5	22.4	28.0	22.9	14.9	25.2	20.4	16.4	19.7
30.7	10.2	20.8	8.7	11.6	28.3	37.3	24.3	18.5	20.8	24.1	20.1	14.2	27.9	19.1	18.8	19.3
33.2	8.2	21.0	7.9	9.7	22.9	24.7	27.6	21.1	17.9	21.1	19.5	17.1	19.5	18.2	22.2	17.3
34.5	8.0	19.8	9.2	10.6	24.6	27.0	26.6	20.8	17.9	22.3	20.0	17.6	16.7	16.5	21.3	17.6
36.6	8.4	18.3	10.4	11.9	25.3	23.6	24.9	23.0	15.6	19.9	20.8	15.7	16.6	17.0	19.3	22.3
38.1	10.1	20.7	10.2	12.2	25.8	20.4	22.8	26.8	15.7	18.8	22.6	15.6	21.7	18.9	20.6	24.0
39.7	15.2	24.1	8.1	12.1	26.2	18.8	23.0	29.1	19.2	19.8	23.2	18.2	54.4	23.9	22.2	22.0
40.8	15.6	23.8	8.0	12.2	27.4	18.2	22.6	29.4	22.9	22.4	22.7	18.2	58.9	26.5	20.4	20.6
42.9	13.2	21.6	9.7	13.6	34.4	15.9	21.5	34.9	32.2	23.8	19.7	20.6	26.6	29.4	19.3	21.3
44.7	14.5	22.3	11.9	14.6	37.7	15.3	24.4	41.9	39.6	21.7	19.5	26.4	23.9	39.1	23.5	23.3
46.7	14.9	21.9	10.3	15.2	41.8	15.4	29.3	35.5	43.7	21.3	20.0	31.7	28.7	41.6	25.7	19.8
47.5	14.4	21.1	9.5	15.2	42.5	17.2	32.0	30.9	47.1	23.0	20.5	35.4	26.7	38.1	25.3	18.3
48.6	12.8	19.3	12.3	15.7	37.5	16.0	27.3	28.0	39.0	22.7	18.1	37.4	24.0	31.4	23.6	18.8
50.4	14.7	17.7	22.8	14.6	33.3	15.4	22.7	24.7	37.5	22.6	18.1	31.2	24.2	27.8	20.4	19.2
52.4	18.3	18.4	10.3	11.7	26.1	15.0	21.3	23.9	36.8	23.1	18.6	23.5	23.9	26.0	20.4	17.3
54.0	17.3	18.8	7.8	11.1	23.6	13.4	20.1	19.5	32.2	21.2	17.4	18.2	21.4	21.9	23.2	15.2
55.6	13.2	15.8	6.9	11.2	24.3	12.1	17.4	18.5	28.2	19.1	16.4	15.3	17.1	17.5	21.2	14.5
57.8	11.4	14.5	6.9	11.5	28.5	9.0	17.0	21.0	21.8	15.5	14.1	14.6	15.4	15.9	17.1	14.8
60.1	14.2	15.0	6.2	14.8	20.2	8.1	22.8	18.0	18.9	14.6	13.8	11.6	16.2	17.7	15.3	10.5
61.7	10.9	11.9	5.2	11.7	15.3	7.0	16.8	13.0	12.8	13.7	11.3	9.9	14.6	13.3	13.3	9.0
64.1	3.8	4.0	2.1	4.4	5.8	2.5	4.5	4.9	4.2	4.6	4.1	4.1	5.2	4.8	5.4	4.9
66.9	4.5	5.0	2.0	4.2	5.7	2.2	5.7	5.4	5.7	4.8	4.8	3.9	5.0	4.6	5.6	3.8
68.8	15.5	12.6	5.0	12.1	20.6	4.9	16.0	12.2	13.8	13.7	13.3	12.2	12.1	12.6	13.5	10.3
70.3	22.6	16.1	7.9	14.4	31.6	5.4	19.4	14.2	16.9	17.2	13.9	14.6	12.9	16.9	13.1	12.7
72.7	25.4	22.0	9.5	16.9	43.2	4.4	26.4	17.3	24.5	17.2	15.2	14.6	13.0	23.4	16.1	13.7
74.2	32.3	27.8	10.3	22.4	45.2	5.3	36.4	17.0	31.0	19.7	17.0	14.1	14.9	28.2	20.1	14.3
76.5	35.6	30.5	10.3	36.1	44.8	5.2	35.7	15.7	25.5	20.4	16.1	18.7	20.8	26.9	21.2	16.5
77.3	29.2	32.4	10.2	28.0	39.7	4.8	33.4	16.2	20.4	17.1	14.8	19.9	19.8	23.0	18.4	15.9
80.2	25.7	31.5	9.0	21.1	26.6	5.6	23.6	18.2	22.7	15.6	17.2	17.7	21.2	23.1	18.2	12.8
81.6	20.5	27.9	8.6	18.3	22.5	6.1	19.7	12.6	17.6	14.4	16.3	15.1	16.6	20.5	19.9	11.9
83.5	19.0	27.6	8.1	13.5	23.5	7.8	17.1	10.7	18.2	14.5	15.1	14.4	17.5	17.5	21.4	13.1
85.1	13.9	25.8	5.1	7.9	19.0	4.9	11.6	9.9	19.5	11.1	12.6	12.4	19.5	14.0	17.2	12.7
86.5	12.6	17.4	4.3	6.3	12.9	4.3	8.8	9.2	19.5	10.4	11.5	10.9	18.8	10.5	12.8	11.3
87.9	9.5	7.7	3.4	5.2	5.9	2.8	5.9	7.0	11.4	7.5	7.8	7.6	11.3	6.3	8.1	9.6
90.0	4.9	2.6	1.3	3.7	2.0	1.5	3.1	2.5	1.5	2.5	2.9	0.7	1.7	2.5	4.0	3.8
92.5	-0.2	-0.2	0.3	0.9	-0.2	-0.1	0.0	0.2	0.2	-0.0	0.4	0.4	0.1	0.4	0.5	0.5

Table 24. Upper limit of deformed B-1 tube areas (mm^2)

Elevation (cm)	Tube No.																Total
	1	2	3	4	5	6	7	8	9	10	11	12	13	14	15	16	
0.0	96	94	98	97	96	96	95	96	96	96	97	96	98	97	96	96	1549
1.8	104	109	108	109	105	113	108	109	109	111	105	109	111	109	110	105	1742
3.3	108	131	113	113	110	125	120	125	121	135	115	113	114	117	135	118	1919
5.2	108	1[illegible]	108	114	109	119	121	128	123	130	120	111	110	119	150	118	1926
8.9	100	10[illegible]	101	103	102	103	104	105	103	106	105	103	100	102	103	103	1651
11.8	102	104	101	104	103	105	105	107	103	106	107	104	101	102	105	103	1671
14.1	115	126	110	117	128	135	129	126	131	137	135	125	144	127	151	130	2080
15.4	117	124	114	119	144	137	128	125	134	140	135	125	175	132	174	139	2167
17.3	119	123	114	115	157	135	131	126	136	141	146	122	146	133	173	147	2175
18.8	124	130	112	124	149	140	135	131	153	149	195	121	127	146	179	153	2273
20.1	121	132	108	123	138	143	138	130	158	157	217	121	118	147	189	156	2303
20.6	121	132	108	122	136	142	137	128	157	156	215	118	116	142	180	154	2274
22.3	121	132	109	118	146	143	143	129	153	176	269	122	117	138	159	227	2409
23.9	120	134	111	117	151	140	146	130	154	209	217	127	121	141	153	283	2464
25.5	115	140	109	118	155	137	153	130	172	177	196	127	124	147	139	165	2312
26.5	116	144	110	120	172	144	158	127	177	175	190	126	129	150	133	151	2330
28.1	117	141	109	122	194	173	155	128	155	172	164	126	140	144	127	138	2311
29.7	116	136	109	117	170	253	146	129	140	153	141	123	146	135	126	133	2281
30.7	113	136	110	116	154	176	144	131	136	144	135	122	153	132	131	133	2173
33.2	109	136	109	112	141	145	152	137	130	137	133	128	133	130	139	128	2107
34.5	109	134	111	114	145	150	149	136	130	139	134	129	127	126	137	129	2108
36.6	110	130	113	117	147	143	145	141	125	134	136	125	127	128	133	140	2100
38.1	113	136	113	118	148	135	141	150	125	132	140	125	138	132	136	143	2131
39.7	124	144	109	117	149	132	141	156	133	134	141	130	221	143	139	139	2259
40.8	125	143	109	117	152	130	140	156	141	140	141	130	281	149	135	136	2333
42.9	119	138	112	120	169	125	138	170	163	143	134	136	150	156	133	137	2251
44.7	122	140	117	122	177	124	144	244	182	138	133	149	143	180	142	142	2409
46.7	123	139	113	124	188	124	156	171	291	137	134	162	155	262	147	134	2568
47.5	122	137	112	124	193	128	158	160	201	141	135	210	150	178	147	130	2433
48.6	119	133	118	125	176	126	151	153	180	140	130	222	143	161	142	132	2359
50.4	123	129	160	122	166	124	140	145	177	140	130	161	144	152	135	133	2289
52.4	130	131	113	116	148	123	137	143	175	141	131	142	143	148	135	128	2195
54.0	128	132	108	115	143	120	134	133	163	137	129	130	138	139	141	124	2121
55.6	120	125	106	115	149	117	129	131	153	132	126	124	128	129	137	122	2052
57.8	116	122	106	116	154	111	128	137	138	124	121	123	124	125	128	123	2004
60.1	122	123	105	123	135	109	141	130	132	123	121	116	126	129	124	114	1979
61.7	115	117	103	116	124	107	127	119	119	121	115	113	122	120	120	111	1875
64.1	100	101	97	101	104	98	102	102	101	102	101	101	103	102	103	102	1630
66.9	102	102	97	101	104	97	104	103	104	102	102	101	103	102	104	100	1636
68.8	124	118	103	117	136	102	126	117	121	120	120	117	117	118	120	113	1898
70.3	140	126	109	122	162	103	133	122	128	128	121	122	119	127	119	118	2006
72.7	147	139	112	127	192	102	149	128	145	128	124	122	119	142	126	120	2129
74.2	163	153	113	140	197	103	177	128	160	134	128	121	123	153	135	122	2257
76.5	243	181	113	258	196	103	225	125	147	135	126	131	136	150	137	127	2540
77.3	215	214	113	230	182	102	166	126	135	128	123	134	134	141	131	125	2406
80.2	147	161	111	137	149	104	143	130	140	125	128	129	137	141	130	119	2140
81.6	136	153	110	131	140	105	134	118	129	122	126	123	127	135	134	117	2047
83.5	132	152	109	120	142	108	128	114	130	122	124	122	129	129	137	119	2026
85.1	120	148	103	109	132	103	116	113	133	115	118	118	133	121	128	119	1935
86.5	118	129	101	105	119	101	110	111	133	114	116	115	132	114	119	115	1860
87.9	112	108	100	103	104	99	104	107	116	108	108	108	116	105	109	112	1726
90.0	102	98	96	100	97	96	99	98	96	98	99	94	96	98	101	100	1576
92.5	93	93	94	95	93	93	93	93	94	93	94	94	93	94	94	94	1503

Table 25. Lower limit of B-1 deformed tube areas (mm^2)

Elevation (cm)	Tube No.																Total
	1	2	3	4	5	6	7	8	9	10	11	12	13	14	15	16	
0.0	96	94	98	97	96	96	95	96	96	96	97	96	98	97	96	96	1549
1.8	104	109	108	109	105	113	108	109	109	111	105	109	111	109	110	105	1742
3.3	108	131	113	113	110	125	120	125	121	135	115	113	114	117	135	118	1919
5.2	108	129	108	114	109	119	121	128	123	130	120	111	110	119	150	118	1926
8.9	100	102	101	103	102	103	104	105	103	106	105	103	100	102	103	103	1651
11.8	102	104	101	104	103	105	105	107	103	106	107	104	101	102	105	103	1671
14.1	119	126	110	117	128	135	129	128	131	137	135	125	146	127	151	130	2080
15.4	117	124	114	119	144	137	128	125	134	140	135	125	175	132	174	149	2167
17.3	119	123	114	119	157	135	131	126	136	141	146	122	146	133	173	147	2175
18.8	124	130	112	124	149	140	135	131	153	149	195	121	127	146	179	153	2273
20.1	121	132	108	123	138	143	138	130	158	157	217	121	118	147	187	156	2301
20.6	121	132	108	122	136	142	137	128	157	156	215	118	116	142	180	154	2274
22.3	121	132	109	118	146	143	143	129	153	176	207	122	117	138	159	159	2279
23.9	120	134	111	117	151	140	146	130	154	195	195	127	121	141	153	179	2324
25.5	119	140	109	118	155	137	153	130	172	177	196	127	124	147	139	165	2312
26.5	116	144	110	120	172	144	158	127	177	175	190	128	129	150	133	151	2330
28.1	117	141	109	122	194	173	155	128	155	172	164	126	140	144	127	138	2311
29.7	116	136	109	117	170	190	146	129	140	153	141	123	146	135	126	133	2218
30.7	113	136	110	116	154	176	144	131	136	144	135	122	153	132	131	133	2173
33.2	109	136	109	112	141	145	152	137	130	137	133	128	133	130	139	128	2107
34.5	109	134	111	114	145	150	149	136	130	139	134	129	127	126	137	129	2108
36.6	110	130	113	117	147	143	145	141	125	134	136	125	127	128	133	140	2100
38.1	113	136	113	118	148	135	141	150	125	132	140	125	138	132	136	143	2131
39.7	124	144	109	117	149	132	141	156	133	134	141	130	221	143	139	139	2259
40.8	125	143	109	117	152	130	140	156	141	140	141	130	236	149	135	136	2288
42.9	119	138	112	120	169	125	138	170	163	143	134	136	150	156	133	137	2251
44.7	122	140	117	122	177	124	144	188	182	138	133	149	143	180	142	142	2352
46.7	123	139	113	124	188	124	156	171	193	137	134	162	155	187	147	134	2395
47.5	122	137	112	124	190	128	158	160	201	141	135	171	150	178	147	130	2391
48.6	119	133	118	125	176	126	151	153	180	140	130	176	143	161	142	132	2314
50.4	123	129	141	122	166	124	140	145	177	140	130	161	144	152	135	133	2270
52.4	130	131	113	116	148	93	137	143	175	141	131	142	143	148	135	128	2195
54.0	128	132	108	115	143	1[illegible]	134	133	163	137	129	130	138	139	141	124	2121
55.6	120	125	106	115	149	111	129	131	153	132	126	124	128	129	137	122	2052
57.8	116	122	106	116	154	111	128	137	138	124	121	123	124	125	128	123	2004
60.1	122	123	105	123	135	109	141	130	132	123	121	116	126	129	124	114	1979
61.7	115	117	103	116	124	107	127	119	119	121	115	113	122	120	120	111	1875
64.1	100	101	97	101	104	98	102	102	101	102	101	101	103	102	103	102	1630
66.9	102	102	97	101	104	97	104	103	104	102	102	101	103	102	104	100	1636
68.8	124	118	103	117	136	102	126	117	121	120	120	117	117	118	120	113	1898
70.3	140	126	109	122	162	103	133	122	128	128	121	122	119	127	119	118	2006
72.7	147	139	112	127	192	102	149	128	145	128	124	122	119	142	126	120	2129
74.2	163	153	113	140	197	103	174	128	160	134	128	121	123	153	135	122	2254
76.5	172	159	113	173	196	103	172	125	147	135	126	131	136	150	137	127	2309
77.3	156	164	113	153	182	102	166	126	135	128	123	134	134	141	131	125	2221
80.2	147	161	111	137	149	104	143	130	140	125	128	129	137	141	130	119	2140
81.6	136	153	110	131	140	105	134	118	129	122	126	123	127	135	134	117	2047
83.5	132	152	109	120	142	108	128	114	130	122	124	122	129	129	137	119	2026
85.1	120	148	103	109	132	103	116	113	133	115	118	118	133	121	126	119	1935
86.5	118	129	101	105	119	101	110	111	133	114	116	115	132	114	119	115	1860
87.9	112	108	100	103	104	99	104	107	116	108	108	108	116	105	109	112	1726
90.0	102	98	96	100	97	96	99	98	96	98	99	94	96	98	101	100	1576
92.5	93	93	94	95	93	93	93	93	94	93	94	94	93	94	94	94	1503

Table 26. B-1 coolant channel restriction

Elevation (cm)	Upper limit (%)	Lower limit (%)
0.0	2.7	2.7
1.8	13.3	13.3
3.3	23.0	23.0
5.2	23.3	23.3
8.9	8.3	8.3
11.8	9.4	9.4
14.1	31.7	31.7
15.4	36.5	36.5
17.3	36.9	36.9
18.8	42.3	42.3
20.1	43.9	43.8
20.6	42.4	42.4
22.3	49.7	42.6
23.9	52.7	45.1
25.5	44.4	44.4
26.5	45.4	45.4
28.1	44.3	44.3
29.7	42.7	39.3
30.7	36.8	36.8
33.2	33.2	33.2
34.5	33.3	33.3
36.6	32.8	32.8
38.1	34.5	34.5
39.7	41.5	41.5
40.8	45.8	43.2
42.9	41.1	41.1
44.7	49.7	46.6
46.7	58.4	48.9
47.5	51.0	48.7
48.6	47.0	44.5
50.4	43.1	42.1
52.4	38.0	38.0
54.0	34.0	34.0
55.6	30.2	30.2
57.8	27.6	27.6
60.1	26.2	26.2
61.7	20.5	20.5
64.1	7.2	7.2
66.9	7.5	7.5
68.8	21.8	21.8
70.3	27.7	27.7
72.7	34.4	34.4
74.2	41.4	41.2
76.5	56.9	44.3
77.3	49.6	39.4
80.2	35.0	35.0
81.6	29.9	29.9
83.5	28.8	28.8
85.1	23.8	23.8
86.5	19.7	19.7
87.9	12.4	12.4
90.0	4.2	4.2
92.5	0.3	0.3

Table 27. Pressure tap positions relative to the bottom of the heated zone of bundle B-1

Tap No.	Distance above bottom of heated zone (cm)	Tap No.	Distance above bottom of heated zone (cm)
1-2	96.16	41-42	37.74
3-4	91.08	43-44	35.20
5-6	86.00	45-46	32.66
7-8	83.46	47-48	30.12
9-10	80.92	49-50	27.58
11-12	78.38	51-52	25.04
13-14	75.84	53-54	22.50
15-16	73.30	55-56	19.96
17-18	70.76	57-58	17.42
19-20	68.22	59-60	14.88
21-22	63.14	61-62	12.34
23-24	60.60	63-64	7.26
25-26	58.06	65-66	5.72
27-28	55.52	67-68	2.18
29-30	52.98	69-70	-2.90
31-32	50.44	71-72	-7.98
33-34	47.90	73-74	-13.06
35-36	45.36	75-76	-18.14
37-38	42.82	77-78	-37.35
39-40	40.28	79-80	-47.51

Table 28. Differential pressure drops for the reference bundle at a flow rate of 0.0068 m^3/sec

Tap No.	Pressure (kPa)	Tap No.	Pressure (kPa)
1	11.92	2	11.79
3	11.78	4	11.55
5	10.94	6	11.34
7	10.90	8	11.35
9	10.58	10	10.97
11	10.62	12	10.96
13	10.27	14	1 .01
15	10.40	16	10.65
17	10.25	18	10.69
19	10.23	20	10.57
21	8.70	22	8.84
23	8.32	24	8.45
25	8.10	26	8.80
27	8.21	28	8.41
29	8.07	30	8.39
31	7.80	32	8.25
33	7.71	34	8.03
35	7.67	36	7.98
37	7.46	38	7.86
39	7.49	40	8.01
41	7.38	42	7.22
43	7.25	44	7.26
45	6.85	46	6.84
47	7.02	48	7.46
49	6.34	50	7.25
51	6.71	52	7.24
53	6.66	54	6.90
55	6.29	56	6.88
57	6.26	58	6.79
59	6.30	60	6.70
61	6.77	62	6.91
63	4.24	64	4.66
65	4.22	66	5.05
67	3.76	68	4.24
69	3.69	70	4.28
71	3.70	72	4.02
73	3.18	74	3.88
75	3.41	76	3.31
77	0.64	78	1.26
79	0.0	80	0.0

Table 29. Differential pressure drops for the reference bundle at a flow rate of 0.0092 m^3/sec

Tap No.	Pressure (kPa)	Tap No.	Pressure (kPa)
1	21.51	2	21.85
3	20.67	4	20.60
5	20.34	6	20.35
7	20.32	8	20.01
9	19.65	10	19.84
11	19.43	12	19.70
13	19.23	14	19.32
15	19.13	16	19.10
17	18.85	18	18.96
19	18.92	20	18.87
21	15.84	22	16.50
23	15.48	24	15.32
25	15.32	26	15.25
27	15.00	28	14.83
29	14.87	30	14.77
31	14.65	32	14.61
33	14.24	34	14.20
35	14.15	36	13.98
37	13.81	38	13.80
39	13.45	40	13.59
41	13.46	42	13.57
43	13.40	44	13.24
45	13.04	46	13.12
47	12.79	48	12.84
49	12.54	50	12.62
51	12.51	52	12.47
53	12.14	54	12.13
55	11.81	56	11.89
57	11.81	58	11.94
59	11.46	60	11.56
61	11.78	62	11.62
63	8.30	64	7.79
65	7.79	66	7.67
67	7.44	68	7.54
69	7.00	70	7.20
71	6.49	72	6.71
73	6.10	74	6.36
75	6.75	76	5.41
77	1.63	78	2.27
79	0.0	80	0.0

Table 30. Differential pressure drops for the reference bundle at a flow rate of 0.0125 m^3/sec

Tap No.	Pressure (kPa)	Tap No.	Pressure (kPa)
1	36.18	2	37.10
3	35.13	4	36.40
5	34.60	6	35.32
7	34.51	8	34.75
9	33.91	10	34.41
11	32.98	12	34.06
13	32.84	14	33.45
15	32.66	16	33.23
17	32.46	18	32.93
19	32.48	20	32.33
21	26.60	22	28.38
23	26.24	24	26.38
25	25.73	26	25.74
27	25.49	28	25.41
29	25.05	30	25.51
31	24.64	32	25.15
33	24.35	34	24.50
35	23.68	36	23.99
37	23.36	38	23.65
39	23.10	40	23.08
41	22.82	42	23.13
43	22.40	44	22.78
45	22.01	46	22.75
47	21.87	48	22.43
49	21.33	50	21.72
51	21.08	52	21.51
53	20.77	54	21.11
55	20.06	56	20.64
57	19.83	58	20.48
59	19.72	60	20.00
61	19.92	62	20.14
63	13.80	64	13.35
65	13.14	66	13.19
67	12.58	68	13.26
69	11.84	70	12.24
71	11.04	72	11.56
73	10.20	74	10.97
75	11.53	76	9.67
77	2.71	78	4.13
79	0.0	80	0.0

Table 31. Differential pressure drops for the reference bundle at a flow rate of 0.019 m^3/sec

Tap No.	Pressure (kPa)	Tap No.	Pressure (kPa)
1	77.90	2	80.53
3	76.29	4	77.24
5	75.09	6	75.84
7	74.33	8	74.72
9	72.47	10	73.63
11	71.18	12	72.23
13	70.47	14	71.45
15	70.28	16	71.29
17	69.00	18	70.55
19	69.87	20	70.11
21	56.79	22	62.21
23	55.96	24	56.42
25	55.06	26	55.79
27	53.93	28	55.27
29	53.84	30	54.30
31	53.17	32	54.08
33	51.90	34	52.66
35	50.80	36	52.15
37	50.57	38	51.37
39	49.70	40	50.66
41	48.42	42	50.56
43	48.46	44	49.17
45	47.52	46	48.18
47	47.09	48	48.11
49	46.35	50	46.69
51	44.84		45.92
53	44.56	54	44.98
55	43.74	56	43.85
57	42.72	58	43.86
59	42.38	60	42.94
61	43.15	62	43.21
63	29.34	64	28.91
65	28.08	66	23.26
67	26.99	68	27.99
69	25.34	70	25.76
71	23.63	72	24.52
73	21.65	74	23.57
75	25.56	76	21.71
77	5.91	78	8.77
79	0.0	80	0.0

Table 32. Differential pressure drops for the reference bundle at a flow rate of 0.022 m^3/sec

Tap No.	Pressure (kPa)	Tap No.	Pressure (kPa)
1	103.19	2	104.22
3	101.97	4	101.05
5	97.97	6	99.07
7	96.95	8	97.45
9	95.23	10	95.84
11	93.83	12	94.04
13	92.02	14	93.19
15	92.31	16	90.68
17	90.99	18	91.69
19	91.17	20	91.05
21	73.93	22	80.28
23	72.48	24	73.26
25	71.58	26	72.23
27	70.45	28	71.18
29	69.89	30	69.76
31	68.89	32	69.09
33	67.49	34	68.12
35	66.75	36	67.48
37	65.93	38	66.06
39	64.21	40	65.23
41	63.22	42	65.22
43	62.64	44	63.77
45	61.51	46	62.03
47	61.04	48	61.77
49	59.74	50	60.09
51	58.87	52	58.80
53	58.11	54	57.65
55	56.66	56	56.38
57	55.43	58	56.67
59	54.78	60	54.76
61	55.75	62	55.92
63	37.72	64	37.64
65	35.98	66	35.82
67	34.59	68	36.63
69	32.74	70	33.11
71	30.25	72	31.64
73	27.90	74	30.73
75	33.65	76	29.67
77	7.71	78	10.45
79	0.0	80	0.0

Table 33. Differential pressure drops for the reference bundle at a flow rate of 0.024 m^3/sec

Tap No.	Pressure (kPa)	Tap No.	Pressure (kPa)
1	116.43	2	118.57
3	112.33	4	114.43
5	110.37	6	112.36
7	109.86	8	110.08
9	107.26	10	107.81
11	105.06	12	106.95
13	104.77	14	106.17
15	104.28	16	104.66
17	102.63	18	104.01
19	102.80	20	103.26
21	83.82	22	90.79
23	81.67	24	83.20
25	80.82	26	81.61
27	79.10	28	81.04
29	78.71	30	78.50
31	77.71	32	79.25
33	75.63	34	76.51
35	74.22	36	76.09
37	73.46	38	74.58
39	72.29	40	72.91
41	71.23	42	73.54
43	70.73	44	71.59
45	69.05	46	70.71
47	67.96	48	70.12
49	67.25	50	68.23
51	65.94	52	66.98
53	64.84	54	65.52
55	63.34	56	63.35
57	62.21	58	63.40
59	61.67	60	62.41
61	62.81	62	63.91
63	42.30	64	42.53
65	40.46	66	40.55
67	39.08	68	41.25
69	36.86	70	37.45
71	34.07	72	36.01
73	31.61	74	34.83
75	38.12	76	33.57
77	8.70	78	11.77
79	0.0	80	0.0

Table 34. Differential pressure drops for bundle B-1 at a flow rate of 0.0063 m^3/sec

Tap No.	Pressure (kPa)	Tap No.	Pressure (kPa)
1	17.56	2	16.97
3	17.41	4	16.95
5	17.82	6	17.37
7	17.86	8	17.41
9	17.70	10	17.60
11	17.62	12	17.71
13	17.91	14	17.33
15	17.19	16	16.53
17	16.27	18	15.90
19	15.66	20	15.21
21	13.83	22	13.42
23	14.12	24	13.57
25	14.10	26	13.66
27	14.04	28	13.55
29	14.10	30	13.59
31	14.17	32	14.03
33	14.71	34	14.19
35	14.86	36	13.67
37	12.85	38	12.38
39	11.96	40	11.72
41	11.26	42	11.39
43	11.03	44	11.04
45	11.23	46	10.87
47	11.46	48	10.73
49	12.42	50	10.78
51	10.85	52	11.28
53	10.18	54	10.52
55	9.32	56	8.98
57	9.05	58	8.50
59	8.48	60	7.89
61	7.68	62	7.48
63	5.58	64	5.02
65	5.22	66	4.83
67	4.78	68	4.34
69	4.00	70	3.86
71	3.80	72	3.66
73	3.33	74	3.52
75	3.19	76	3.32
77	0.50	78	0.41
79	0.0	80	0.0

Table 35. Differential pressure drops for bundle B-1 at flow rate of 0.013 m^3/sec

Tap No.	Pressure (kPa)	Tap No.	Pressure (kPa)
1	61.86	2	57.55
3	61.32	4	57.55
5	61.86	6	61.86
7	63.47	8	61.32
9	61.86	10	62.40
11	64.01	12	62.40
13	64.01	14	60.24
15	61.32	16	57.55
17	56.48	18	55.40
19	57.55	20	52.17
21	49.48	22	47.33
23	50.56	24	48.95
25	50.02	26	46.80
27	50.02	28	48.95
29	48.95	30	47.33
31	52.71	32	50.02
33	52.71	34	49.48
35	51.64	36	48.95
37	45.18	38	41.42
39	44.64	40	40.88
41	41.42	42	40.88
43	40.34	44	38.19
45	40.34	46	39.80
47	40.88	48	35.50
49	44.11	50	37.65
51	40.34	52	40.34
53	38.19	54	38.73
55	33.88	56	31.73
57	33.88	58	28.51
59	32.81	60	27.97
61	29.58	62	26.35
63	20.44	64	18.82
65	18.28	66	16.67
67	16.13	68	16.67
69	15.60	70	13.98
71	15.06	72	13.44
73	14.52	74	13.98
75	12.91	76	12.37
77	4.30	78	2.15
79	0.0	80	0.0

Table 36. Differential pressure drops for bundle B-1 at a flow rate of 0.019 m^3/sec

Tap No.	Pressure (kPa)	Tap No.	Pressure (kPa)
1	121.57	2	117.26
3	119.95	4	118.88
5	123.72	6	121.57
7	122.11	8	122.11
9	122.64	10	124.80
11	124.26	12	125.87
13	124.80	14	121.57
15	121.03	16	115.65
17	113.50	18	109.73
19	107.04	20	104.89
21	95.75	22	94.13
23	97.36	24	96.28
25	96.82	26	97.90
27	96.28	28	95.75
29	96.82	30	95.75
31	100.05	32	101.13
33	106.51	34	103.82
35	105.97	36	96.82
37	90.37	38	88.22
39	83.91	40	83.91
41	82.30	42	80.15
43	77.46	44	78.00
45	78.53	46	78.53
47	80.15	48	75.31
49	89.29	50	75.84
51	79.07	52	82.30
53	74.23	54	77.46
55	65.62	56	64.55
57	61.86	58	62.40
59	69.39	60	55.94
61	52.71	62	50.56
63	36.04	64	34.96
65	33.88	66	33.35
67	34.96	68	33.88
69	27.97	70	26.89
71	26.89	72	24.74
73	25.82	74	24.74
75	24.20	76	24.20
77	0.0	78	1.61
79	0.0	80	0.0

Table 37. Differential pressure drops for the bundle B-1 at a flow rate of 0.024 m^3/sec

Tap No.	Pressure (kPa)	Tap No.	Pressure (kPa)
1	179.66	2	187.20
3	177.51	4	184.51
5	184.51	6	191.50
7	183.97	8	192.57
9	182.89	10	195.80
11	183.97	12	194.73
13	188.27	14	180.74
15	178.05	16	169.98
17	167.29	18	162.45
19	160.84	20	154.38
21	142.55	22	135.02
23	144.70	24	138.78
25	144.16	26	140.40
27	143.62	28	138.78
29	146.31	30	140.40
31	147.93	32	138.78
33	157.07	34	143.08
35	156.53	36	150.08
37	132.86	38	150.62
39	124.80	40	146.85
41	118.34	42	129.64
43	116.73	44	122.64
45	117.26	46	117.26
47	123.18	48	111.88
49	131.25	50	114.57
51	114.57	52	118.34
53	107.58	54	111.88
55	97.36	56	95.75
57	96.28	58	89.29
59	86.06	60	80.68
61	77.46	62	73.69
63	56.48	64	51.10
65	51.64	66	47.87
67	48.95	68	50.56
69	39.26	70	40.88
71	39.26	72	35.50
73	38.73	74	37.65
75	39.26	76	36.57
77	4.84	78	1.61
79	0.0	80	0.0

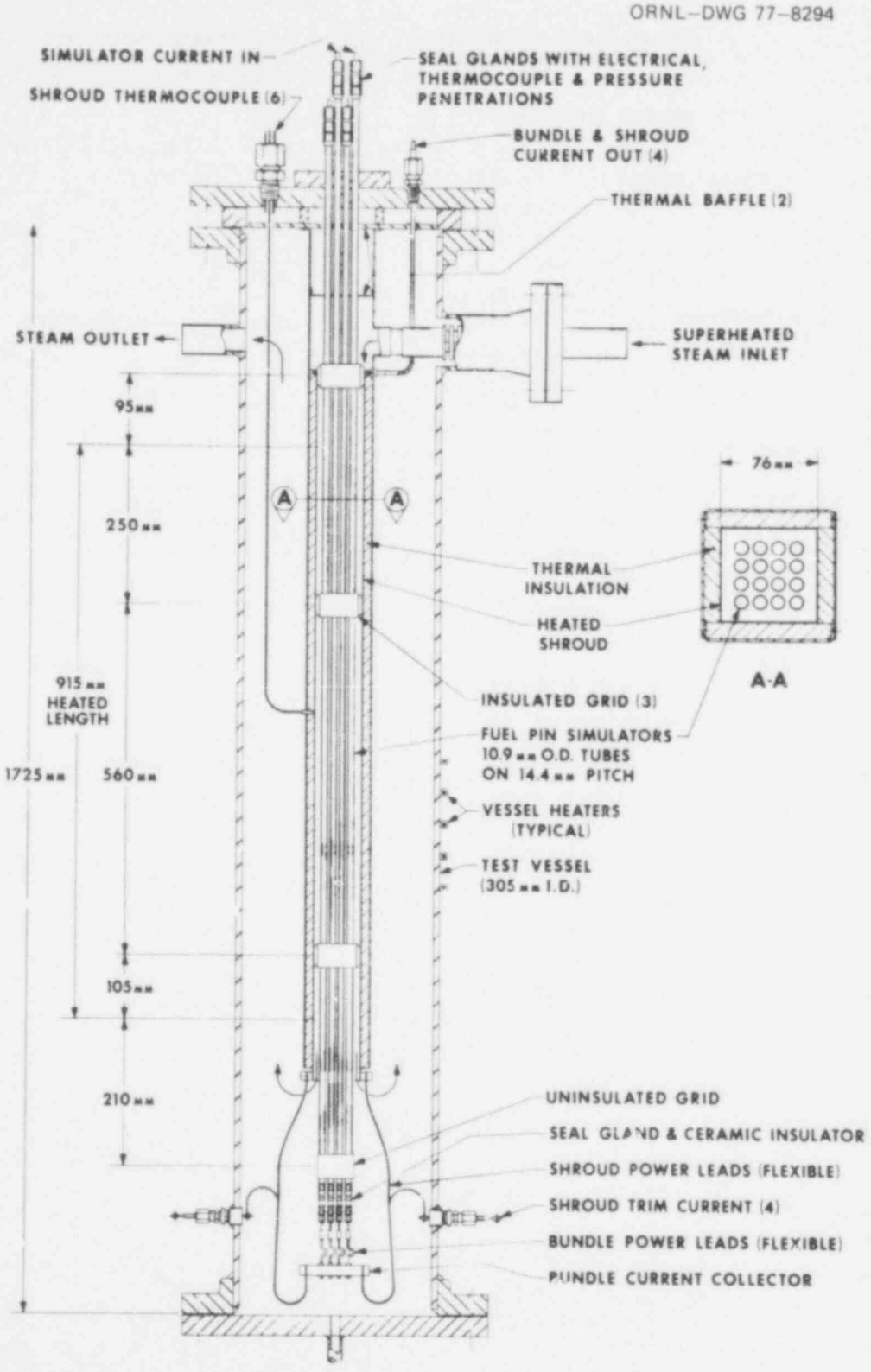

Fig. 1. Schematic of B-1 test assembly.

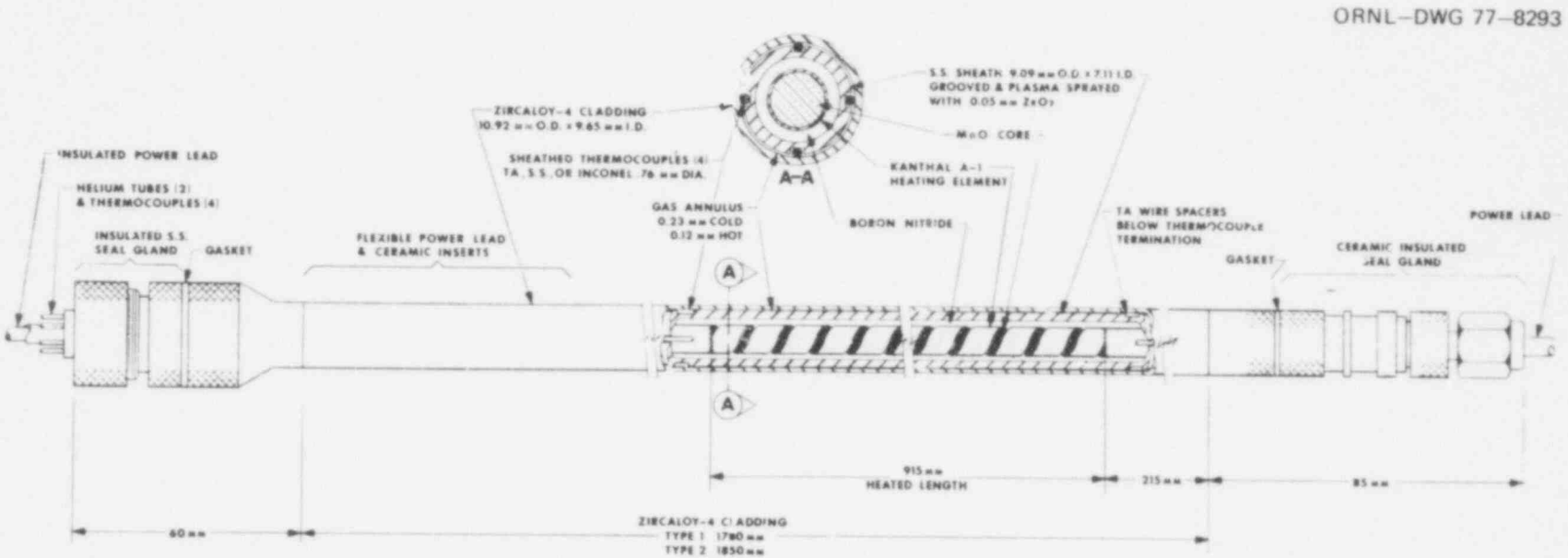

Fig. 2. Typical fuel pin simulator.

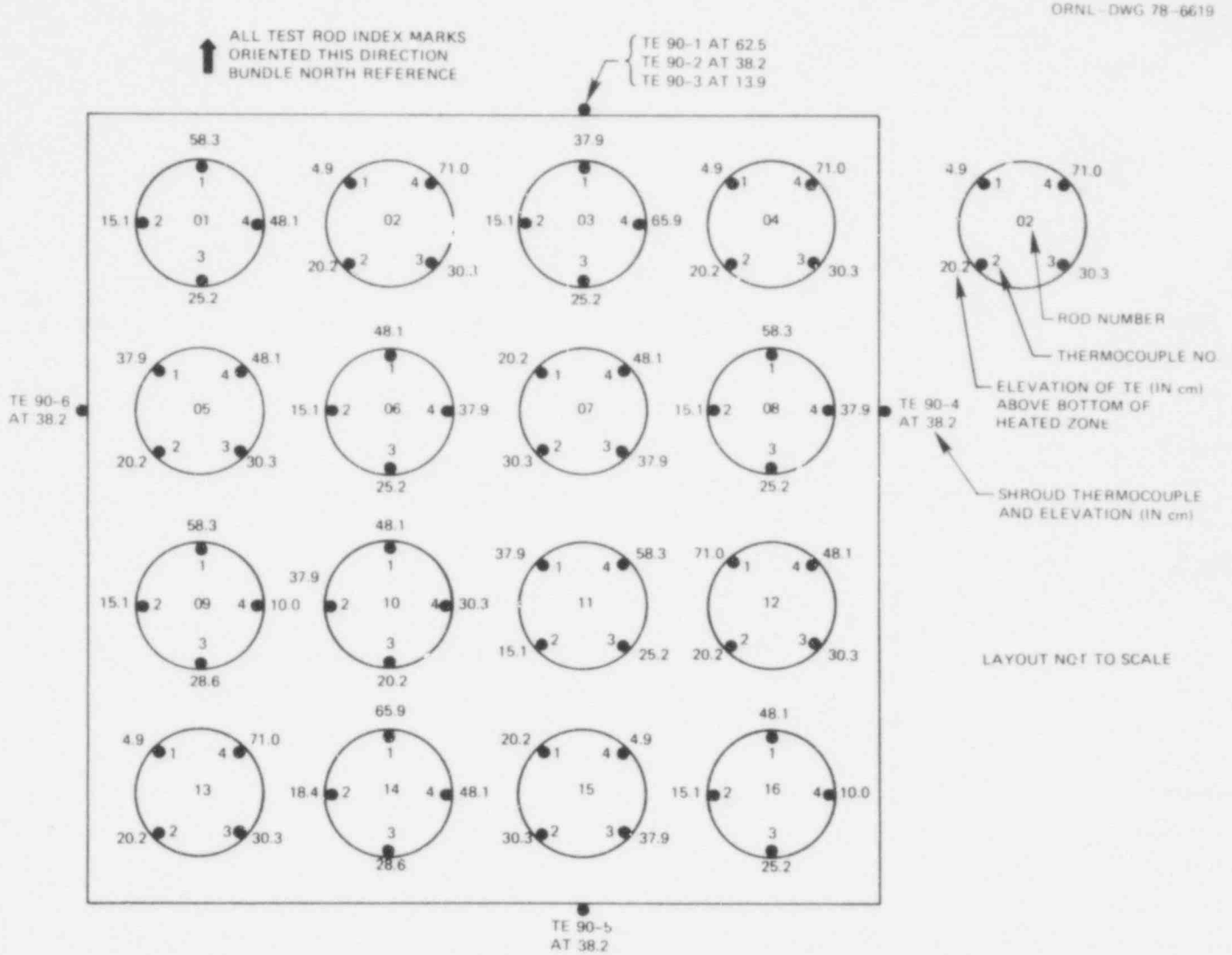

Fig. 3. As-built thermocouple locations in B-1 test (plan view).

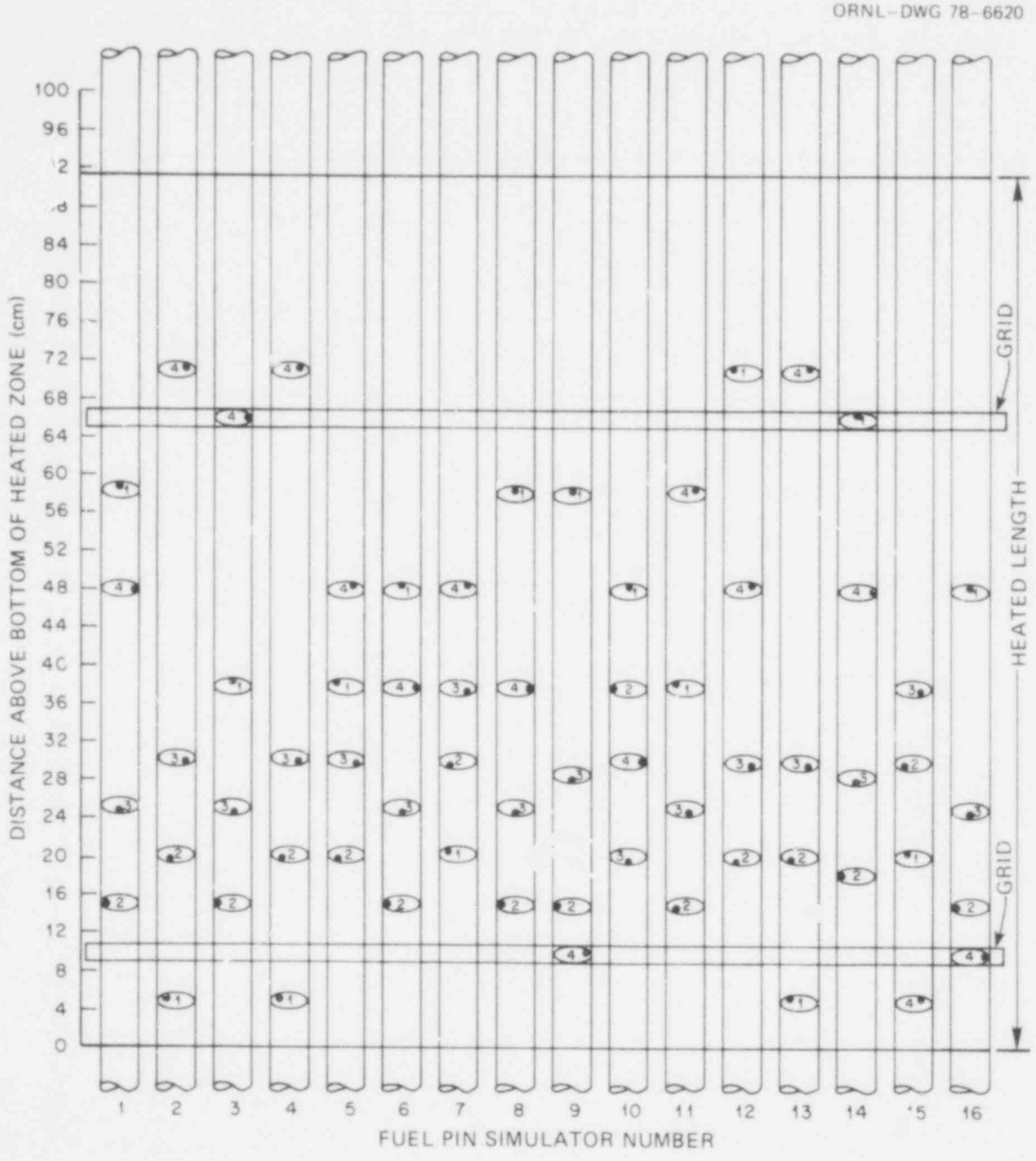

Fig. 4. As-built thermocouple locations in B-1 test (elevation).

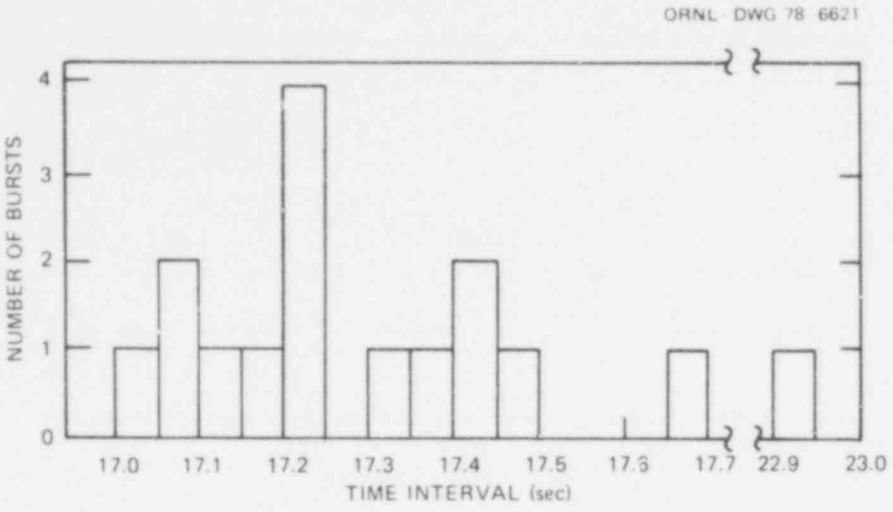

Fig. 5. Burst frequency distribution in B-1 test.

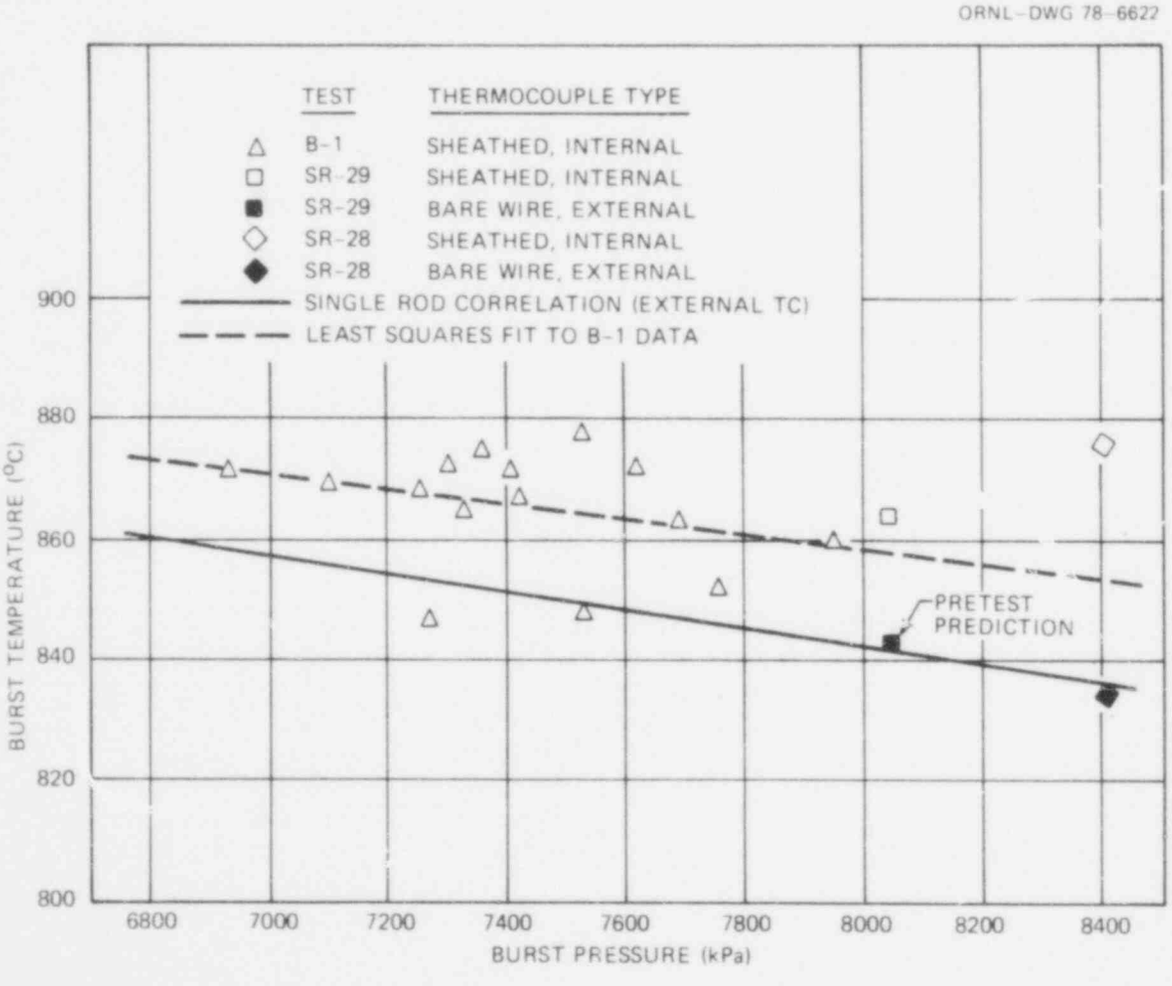

Fig. 6. B-1 burst temperatures compared with single-rod test data.

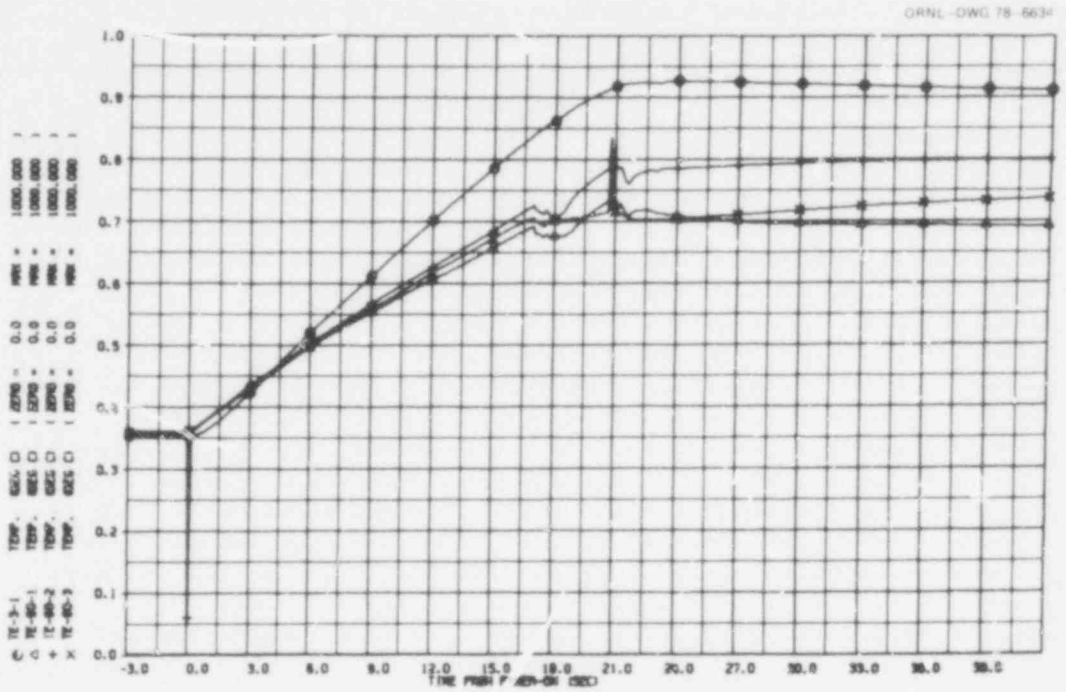

Fig. 7. Temperatures measured on north side of heated shroud in B-1 test.

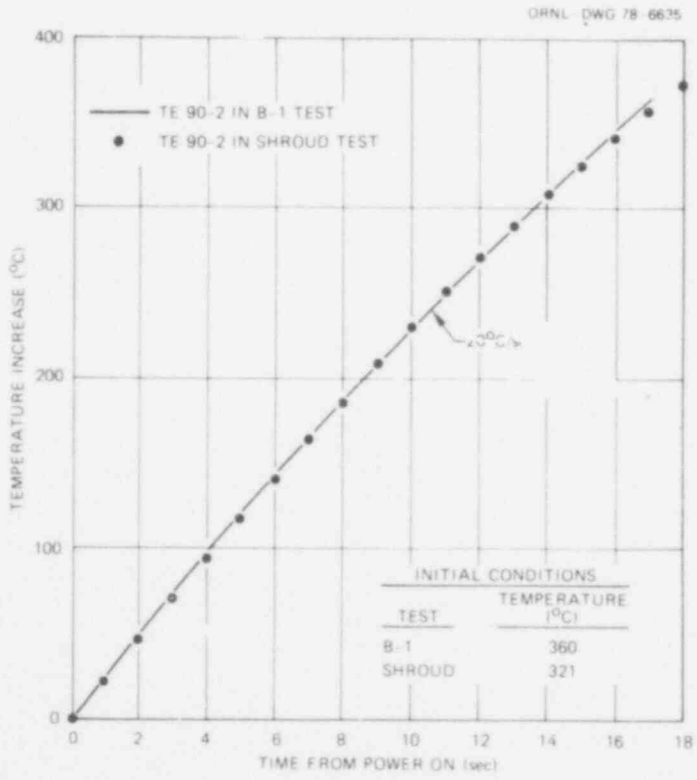

Fig. 8. Comparison of TE 90-2 in B-1 and shroud tests.

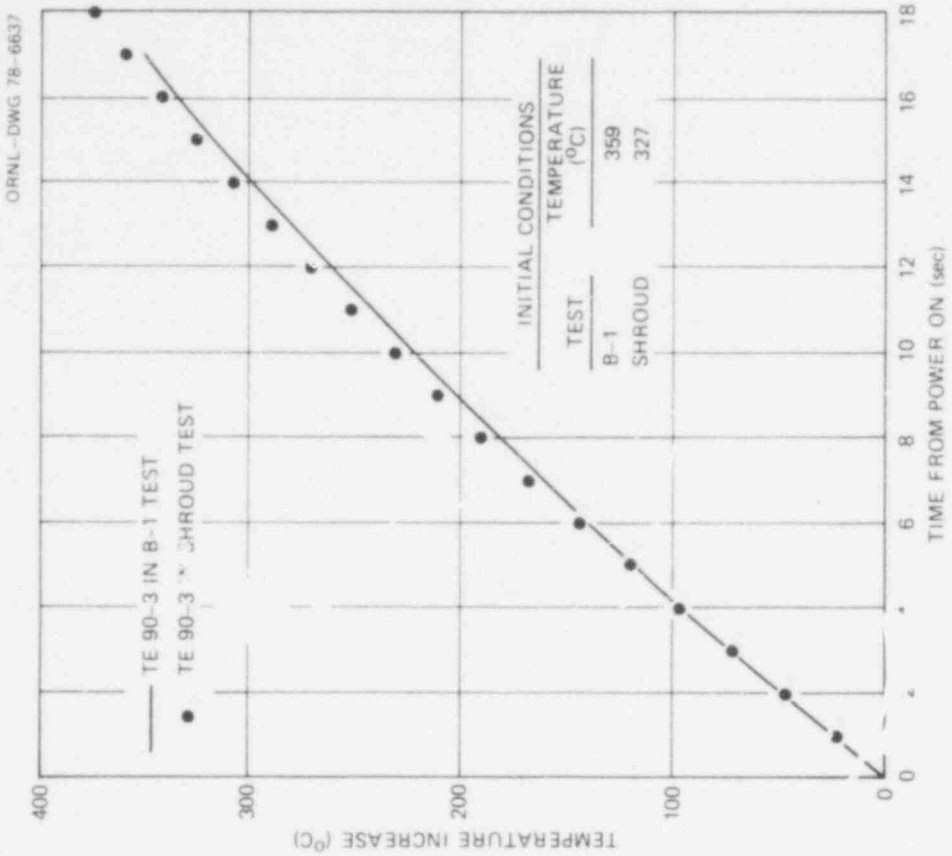

Fig. 10. Comparison of TE 90-3 in B-1 and shroud tests.

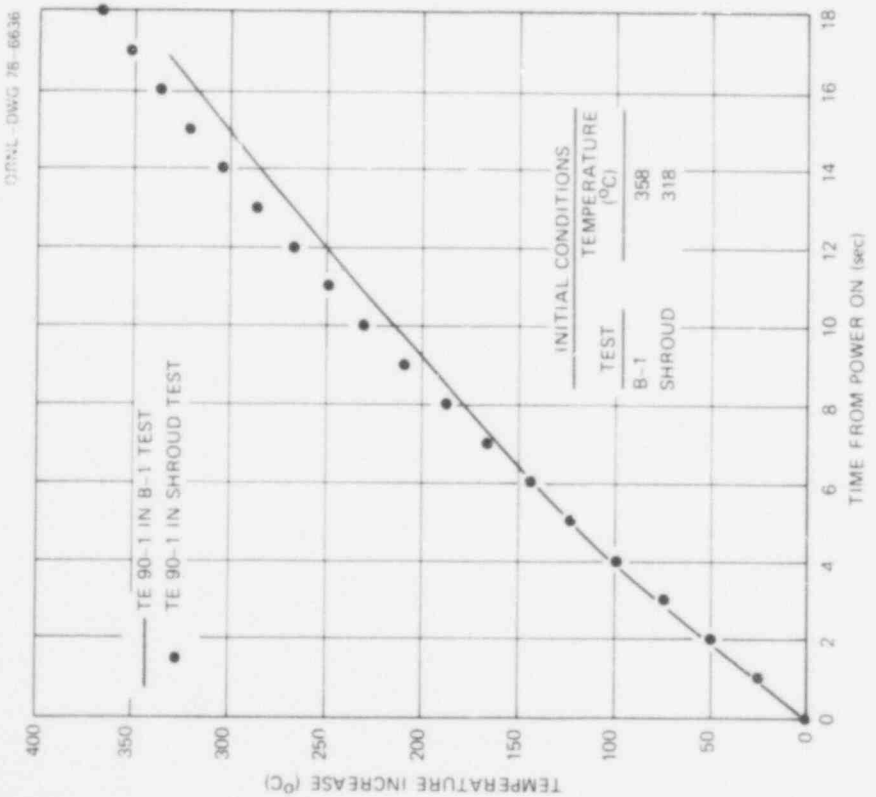

Fig. 9. Comparison of TE 90-1 in B-1 and shroud tests.

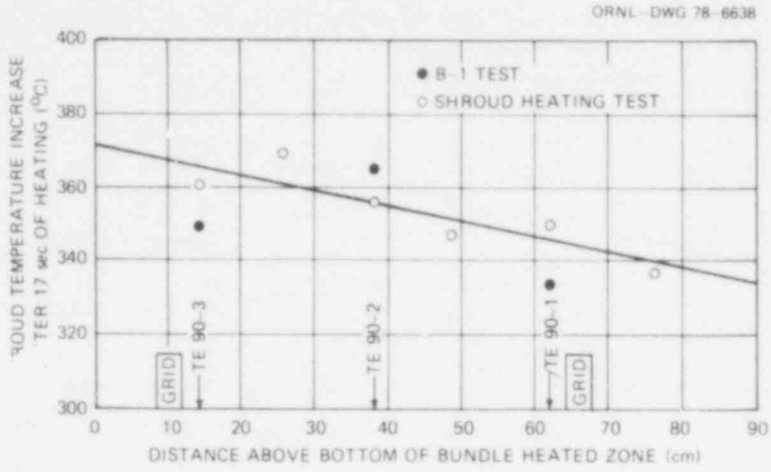

Fig. 11. Comparison of shroud axial temperature distribution in B-1 and shroud tests.

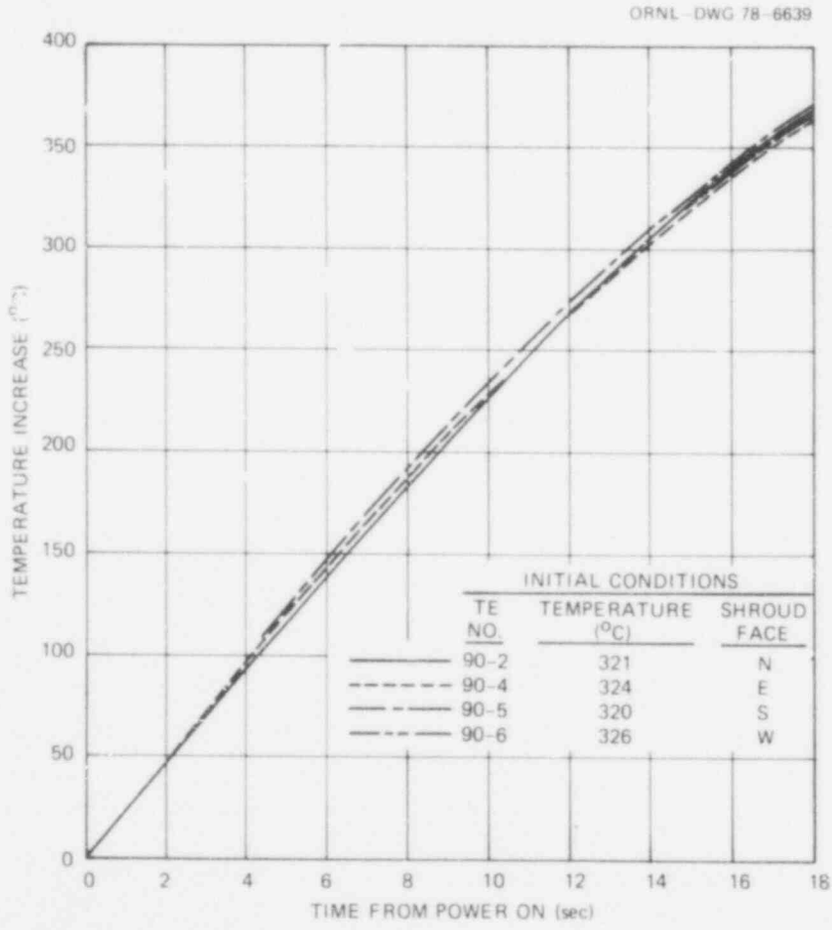

Fig. 12. Circumferential temperature distribution in shroud test for same heating current as used in B-1 test.

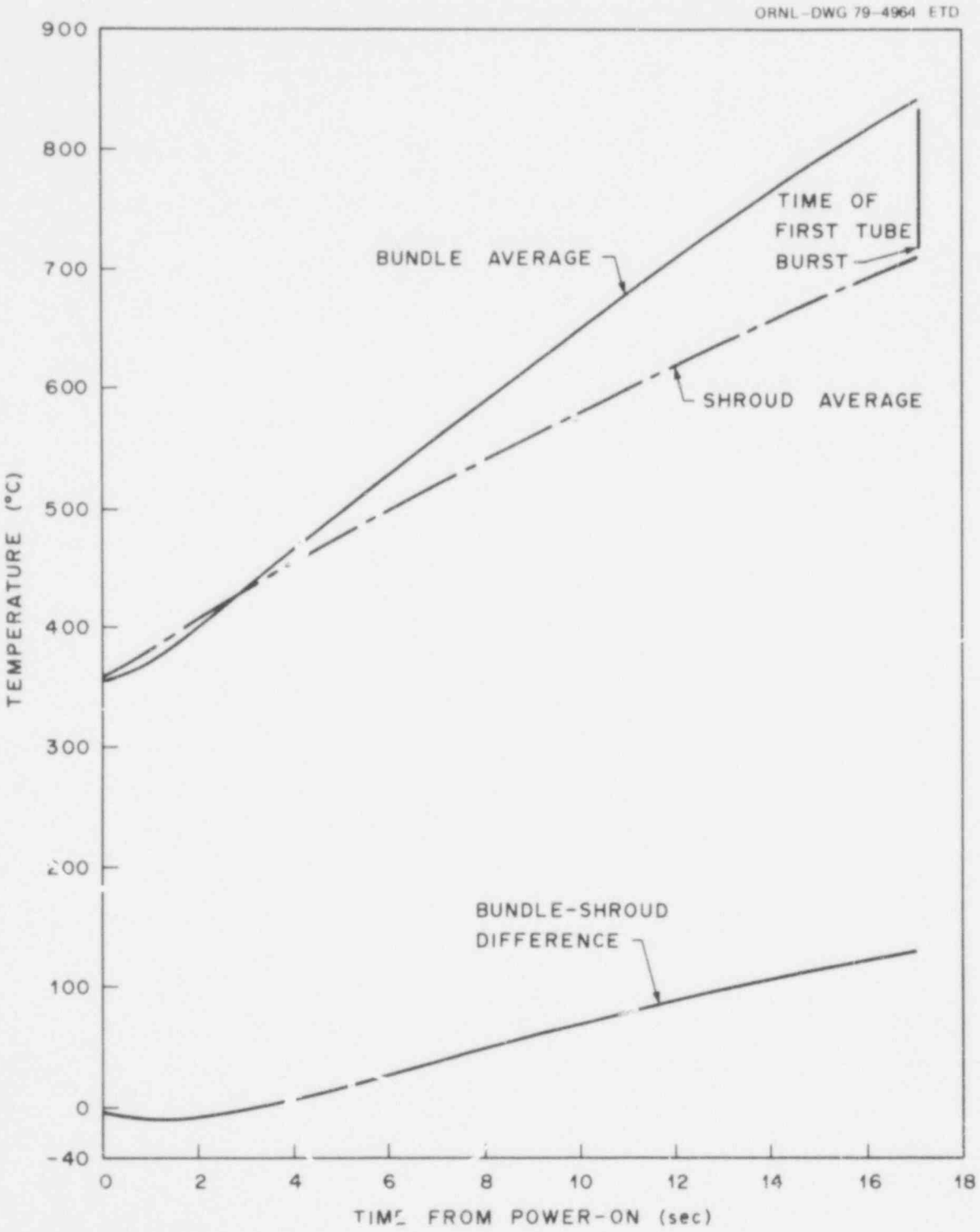

Fig. 13. Average temperatures in B-1 test from power-on until the time of the first tube burst.

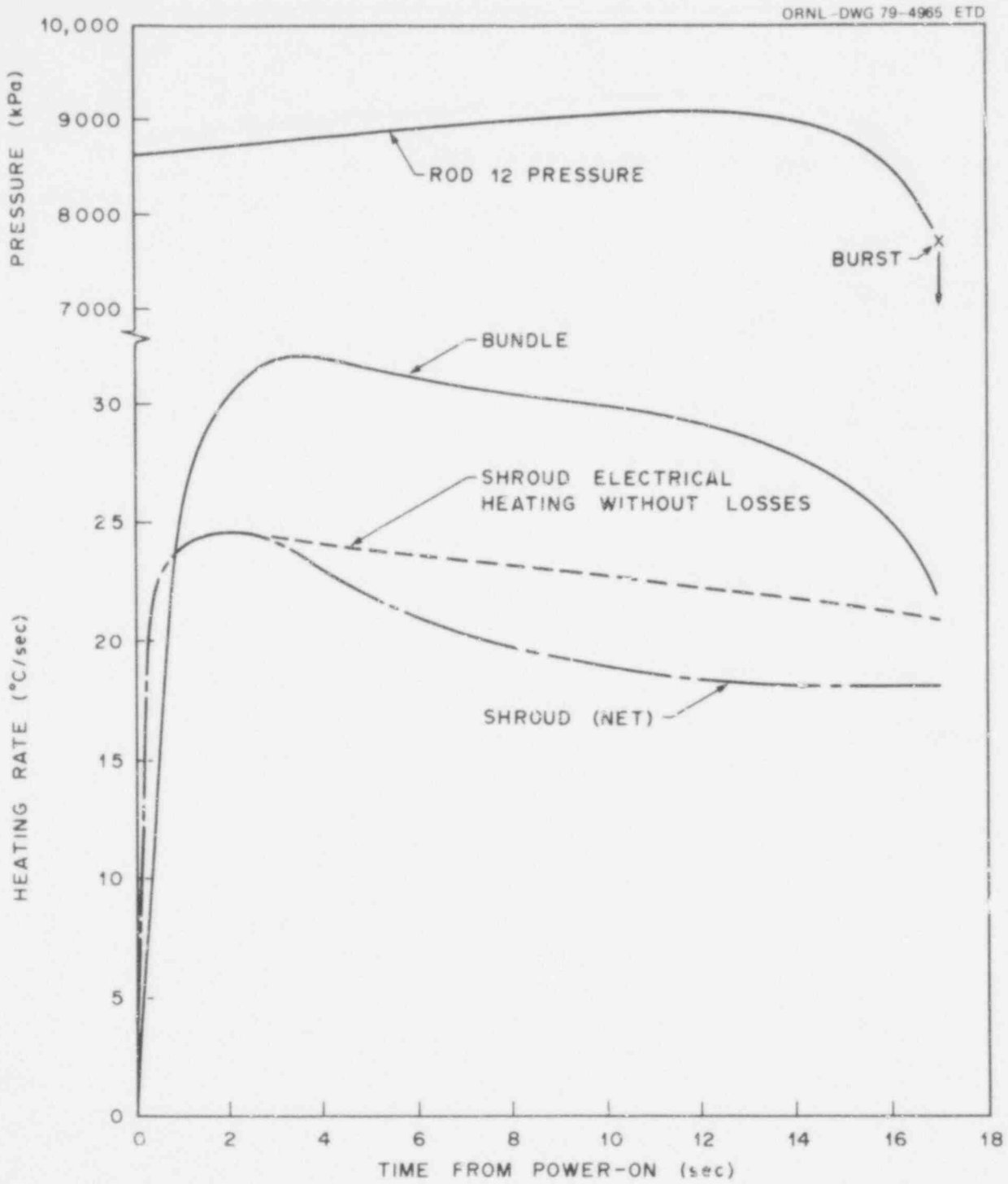

Fig. 14. B-1 bundle and shroud heating rates.

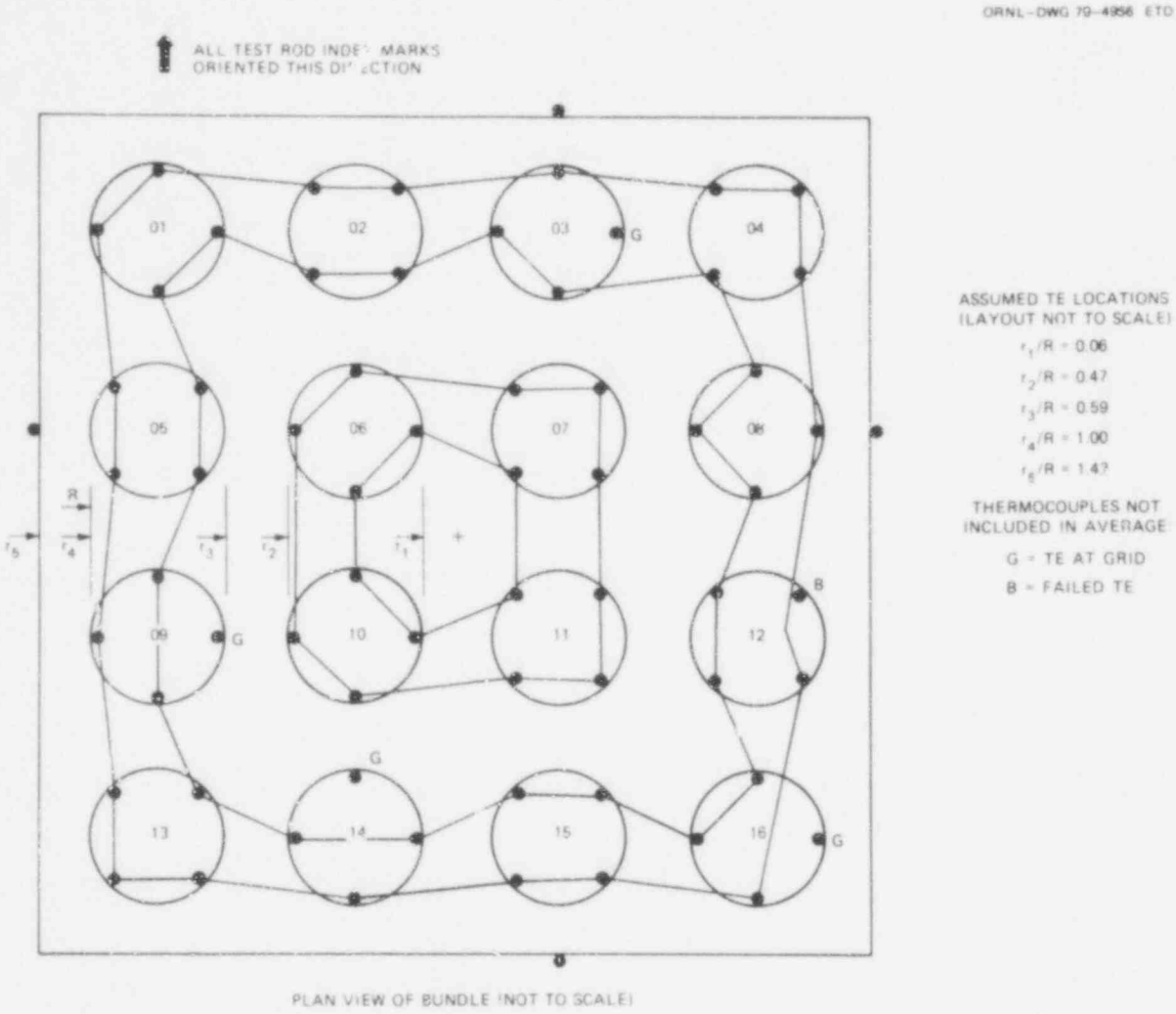

Fig. 15. Thermocouple assignments for calculation of radial temperature profile in B-1 test.

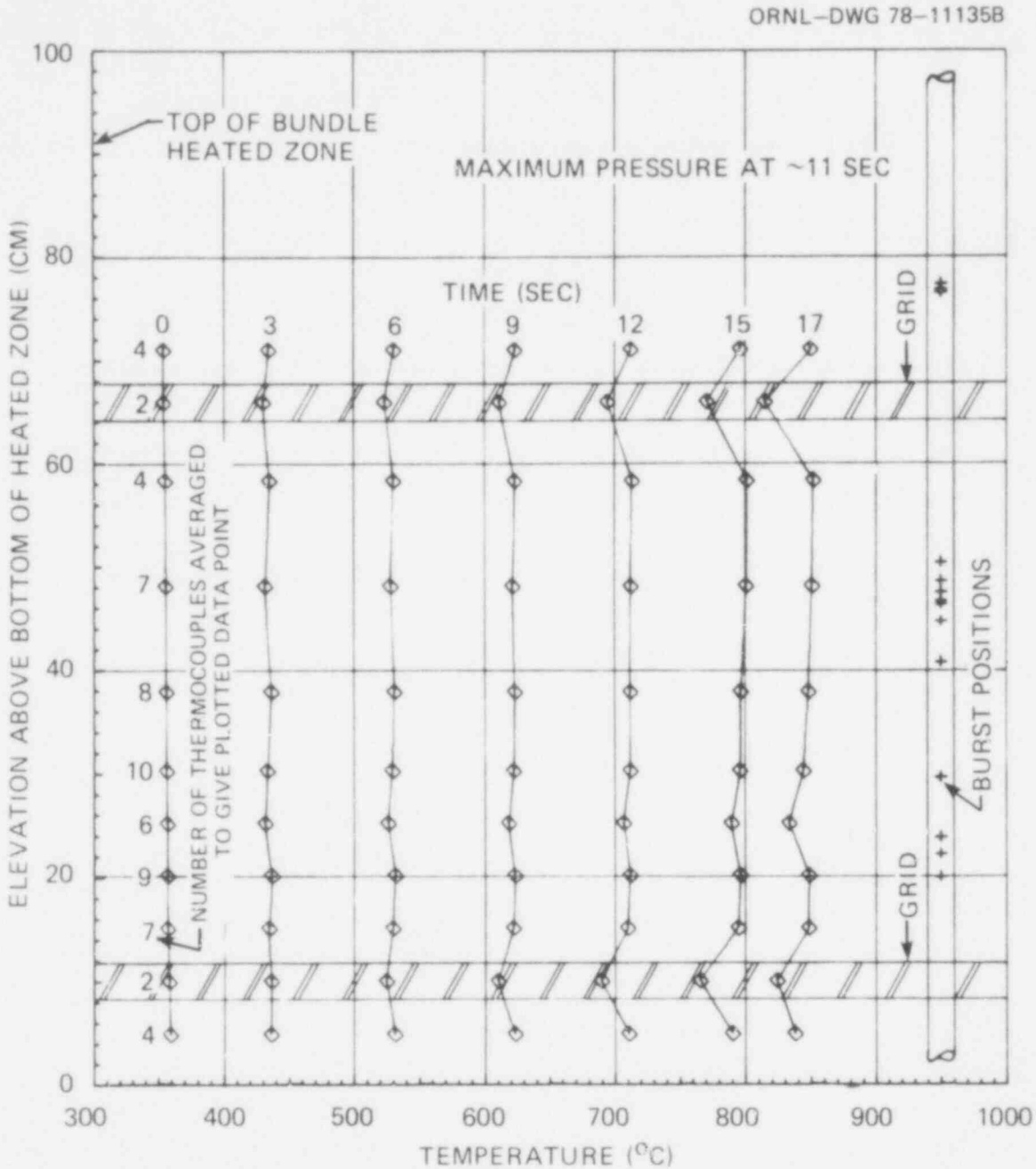

Fig. 16. Time-temperature plot of the axial temperature distribution of the B-1 bundle from power-on until time of first tube burst.

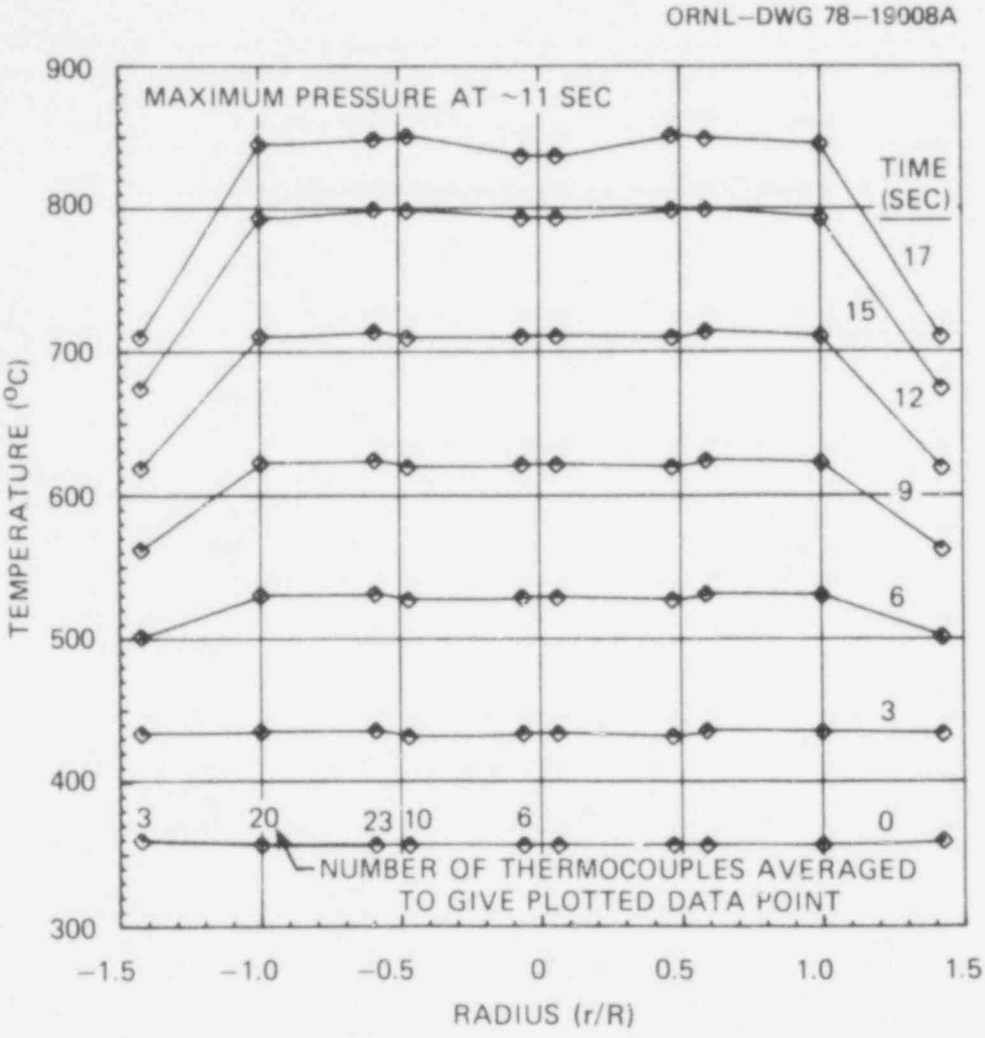

Fig. 17. Time-temperature plot of the radial temperature distribution of the B-1 bundle from power-on until time of first tube burst.

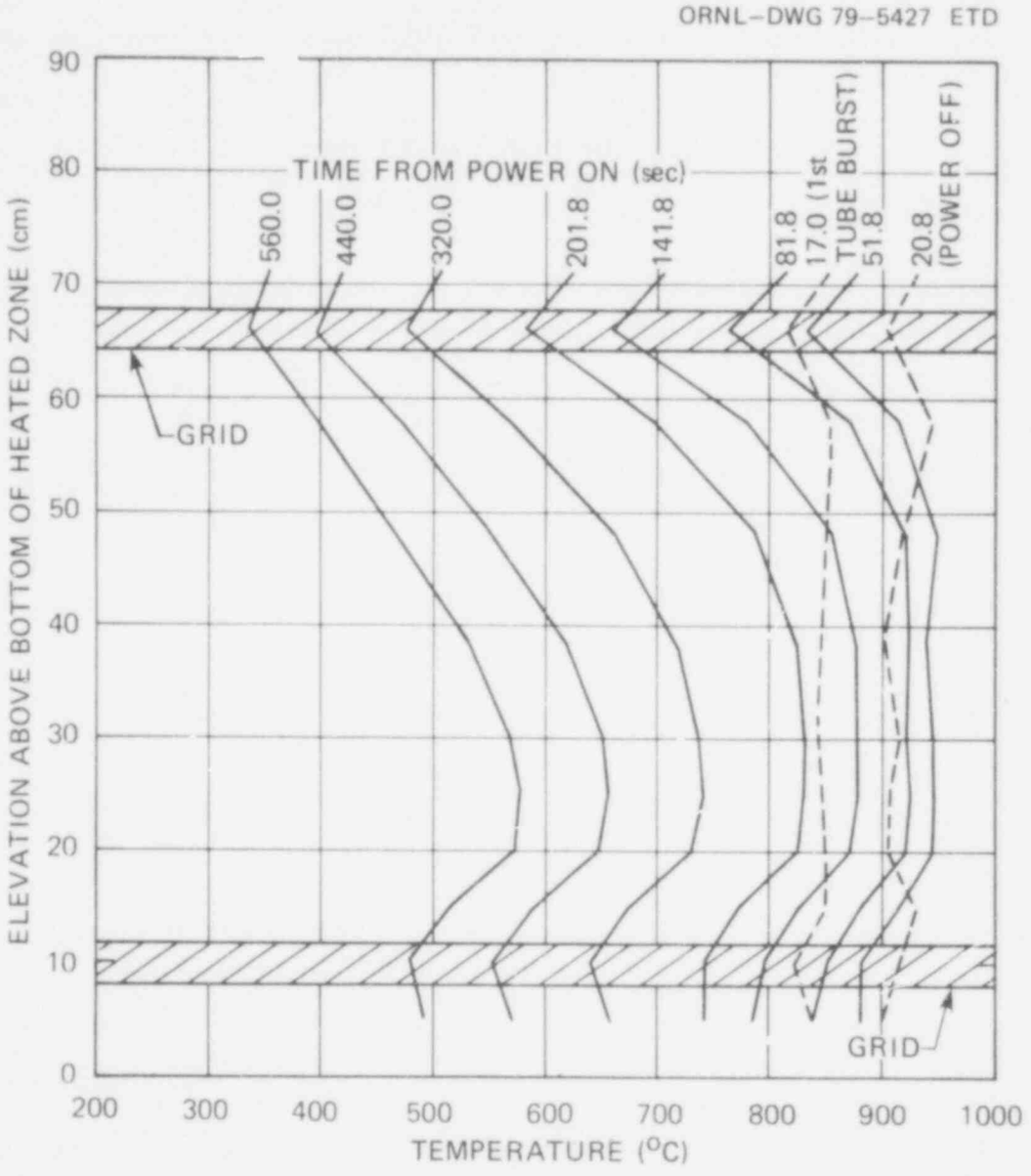

Fig. 18. Axial temperature distribution in B-1 after power termination to bundle.

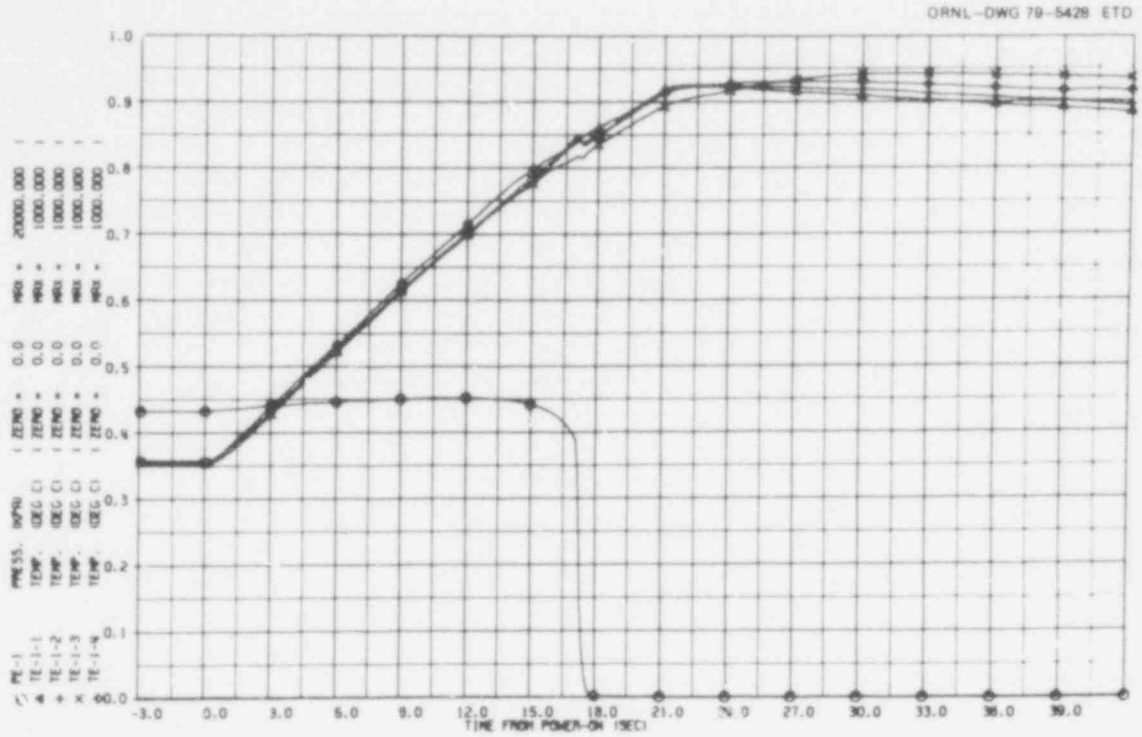

Fig. 19. Temperature and pressure transients for rod No. 1.

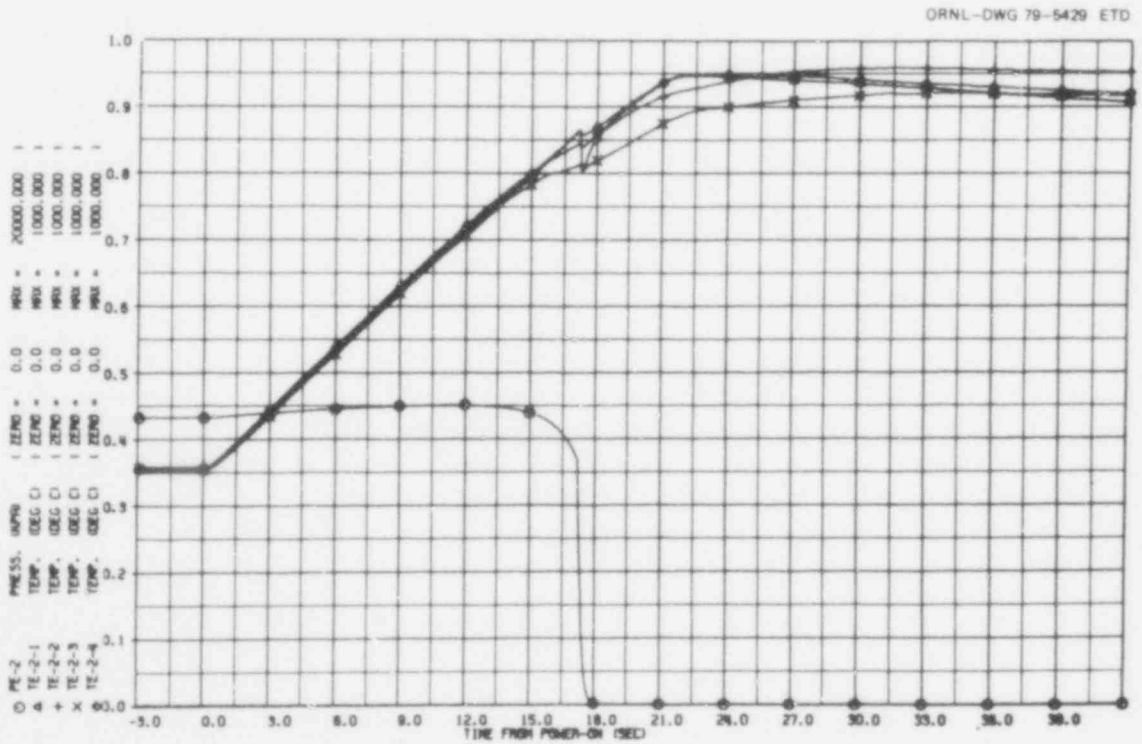

Fig. 20. Temperature and pressure transients for rod No. 2.

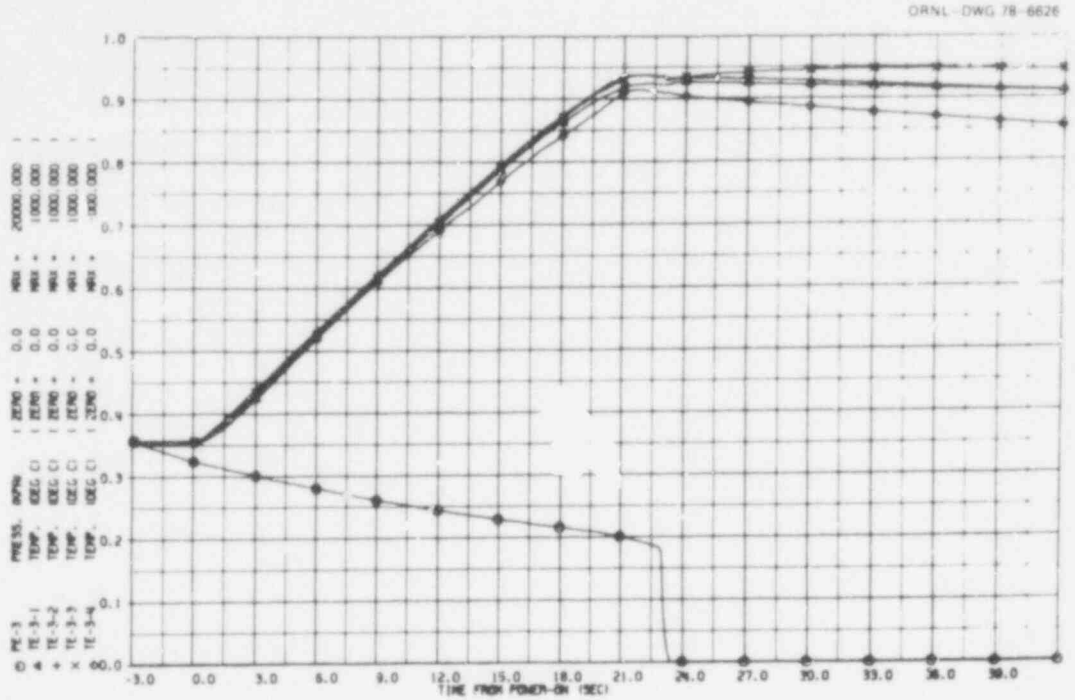

Fig. 21. Temperature and pressure transients for rod No. 3.

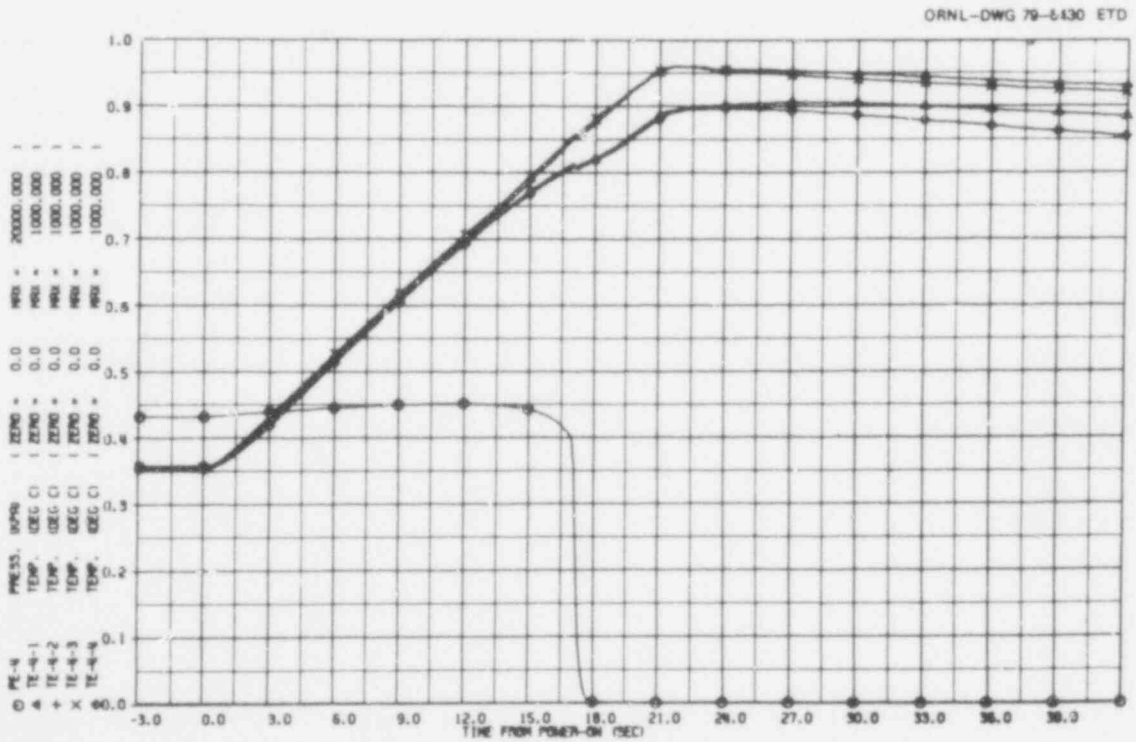

Fig. 22. Temperature and pressure transients for rod No. 4.

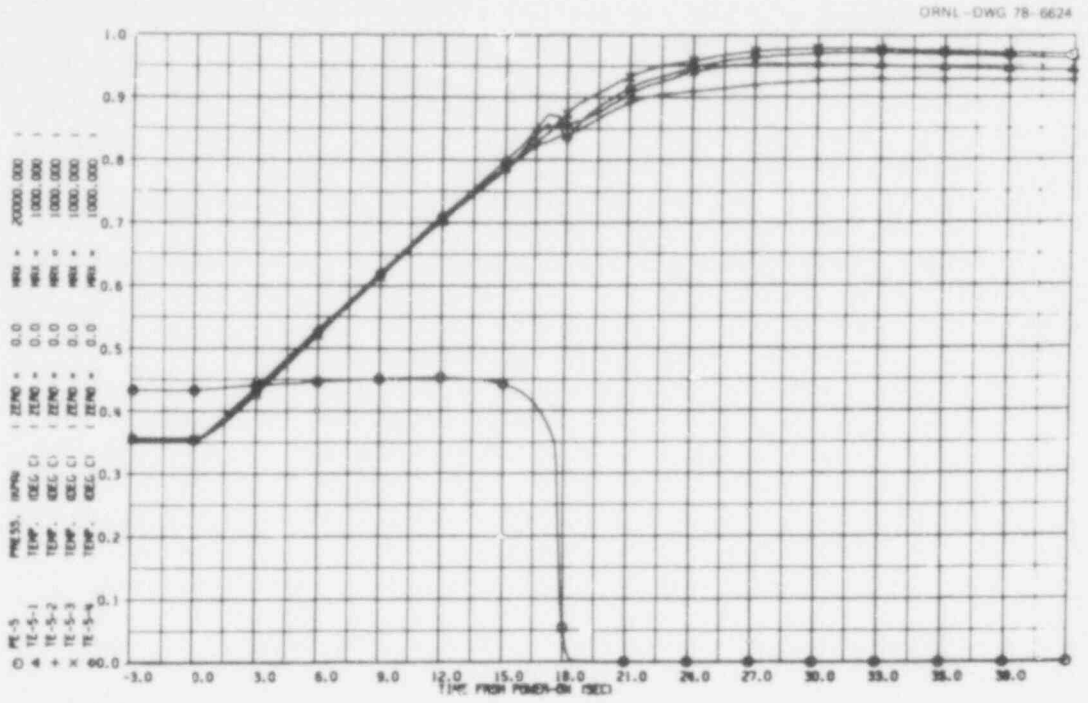

Fig. 23. Temperature and pressure transients for rod No. 5.

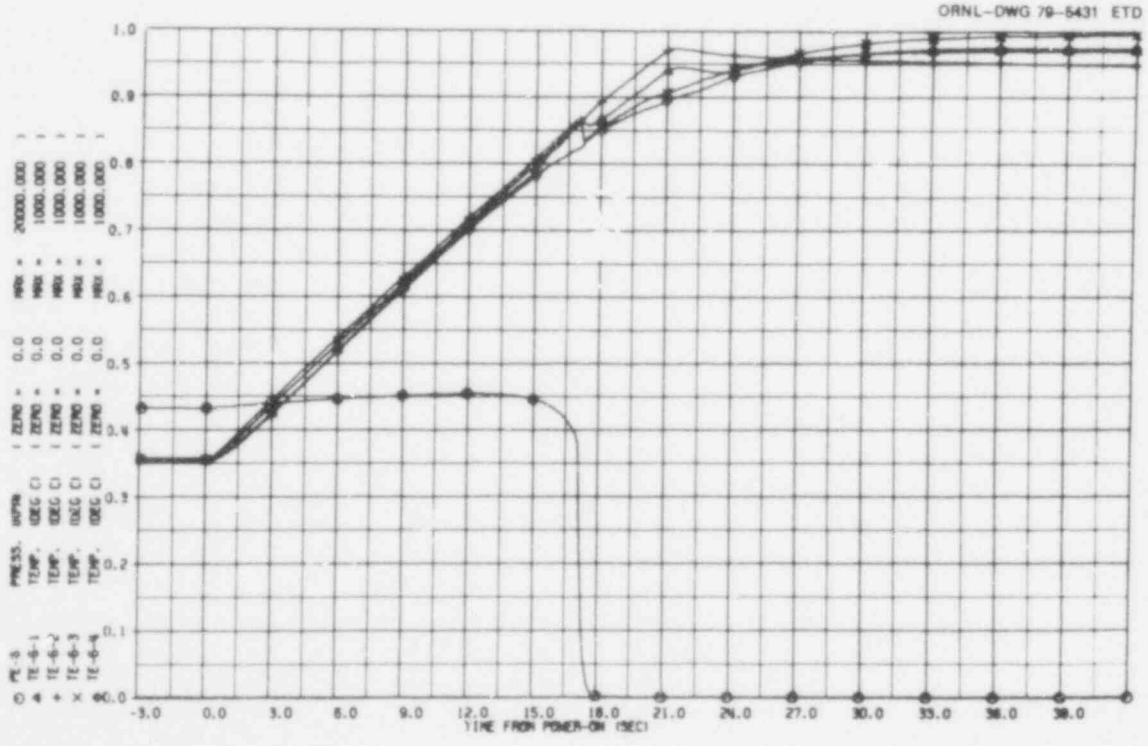

Fig. 24. Temperature and pressure transients for rod No. 6.

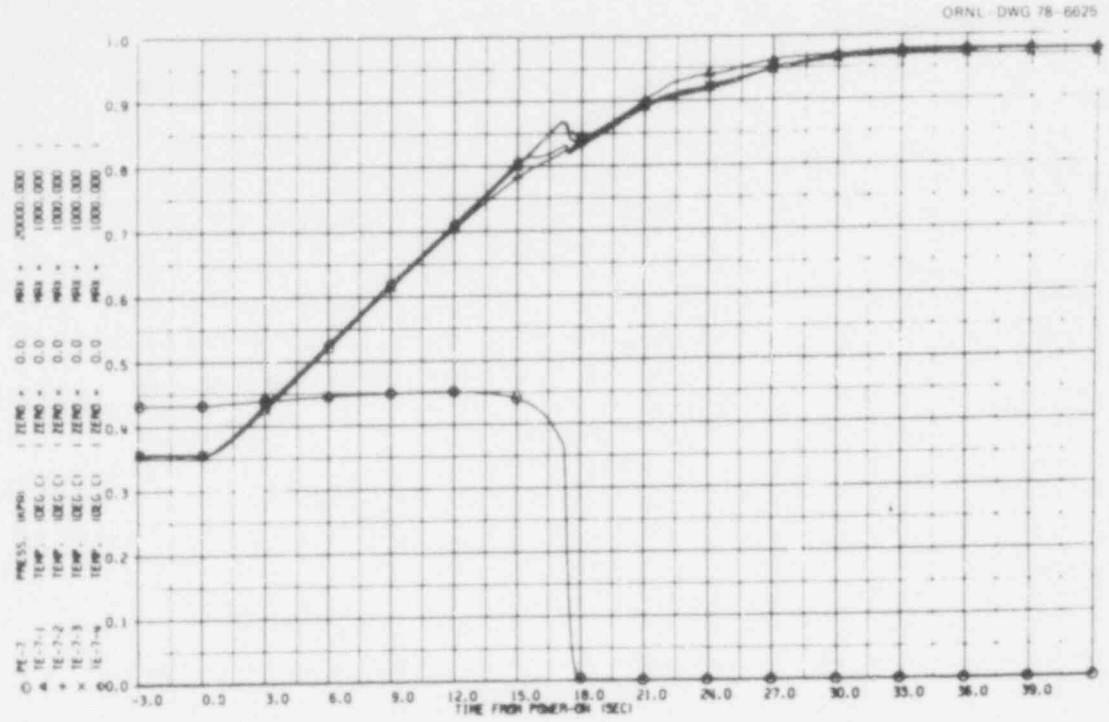

Fig. 25. Temperature and pressure transients for rod No. 7.

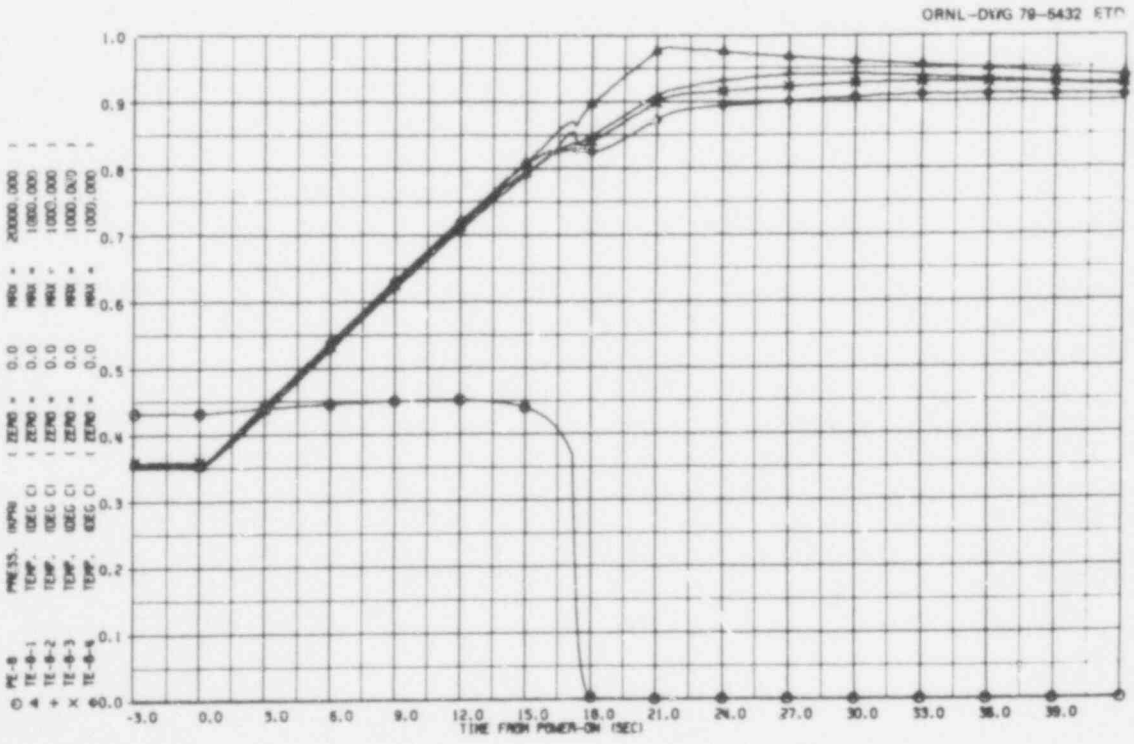

Fig. 26. Temperature and pressure transients for rod No. 8.

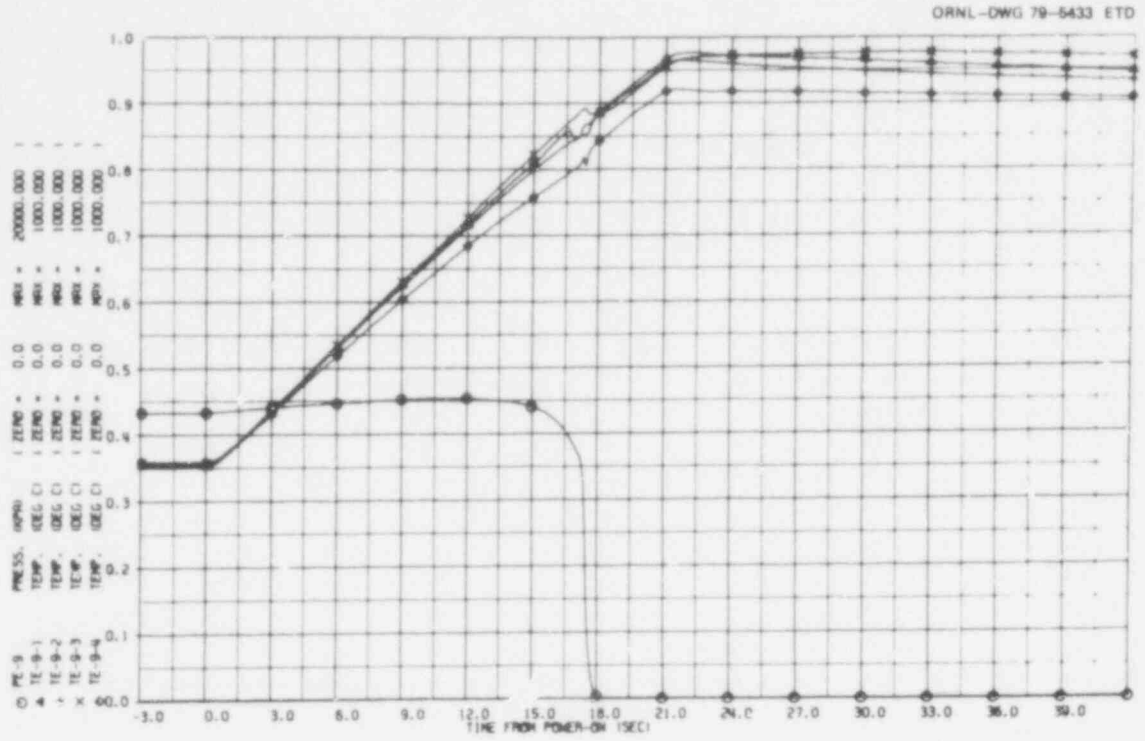

Fig. 27. Temperature and pressure transients for rod No. 9.

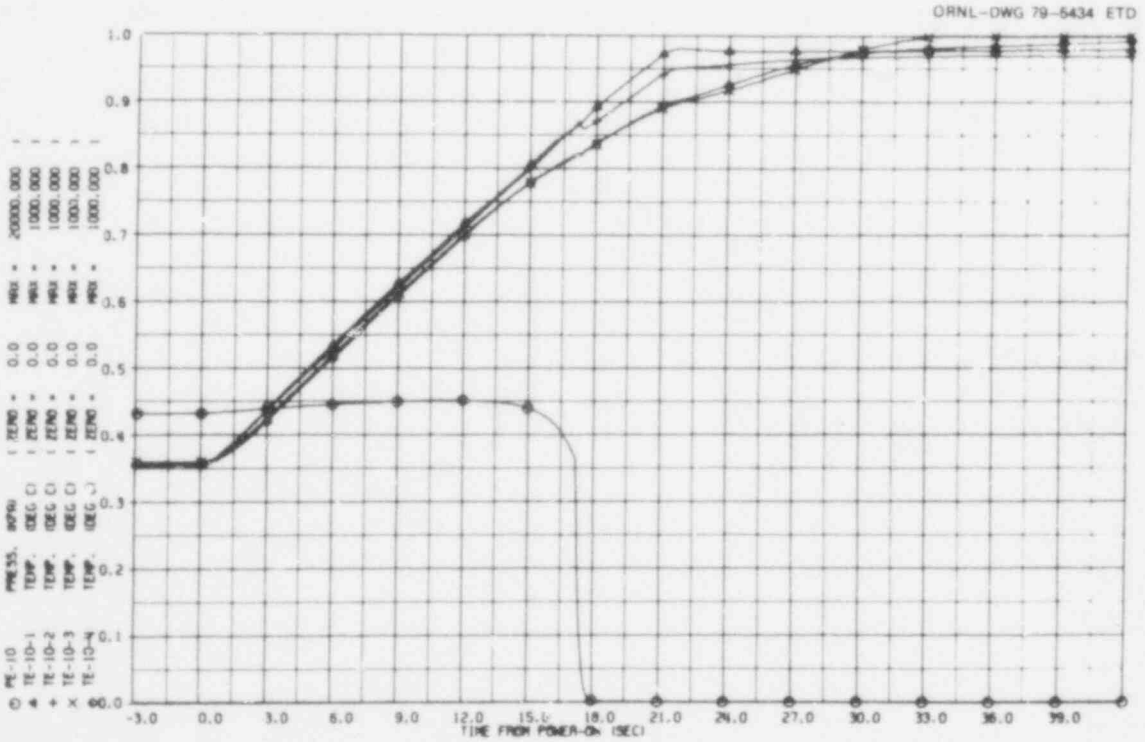

Fig. 28. Temperature and pressure transients for rod No. 10.

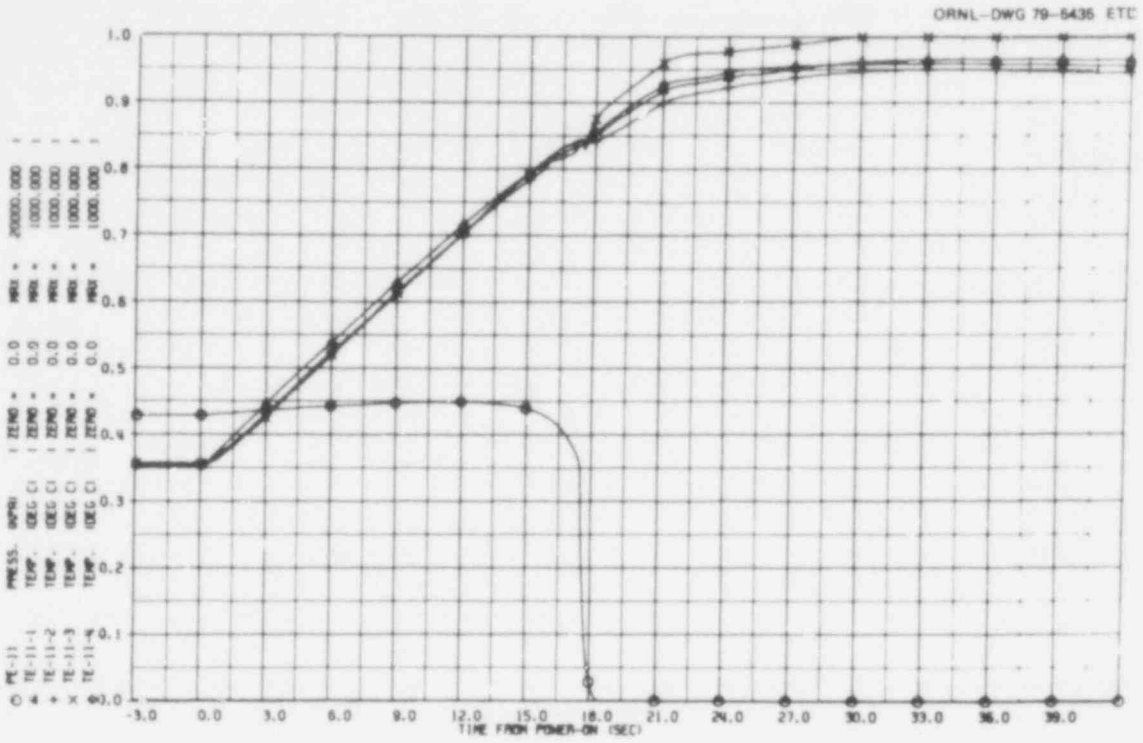

Fig. 29. Temperature and pressure transients for rod No. 11.

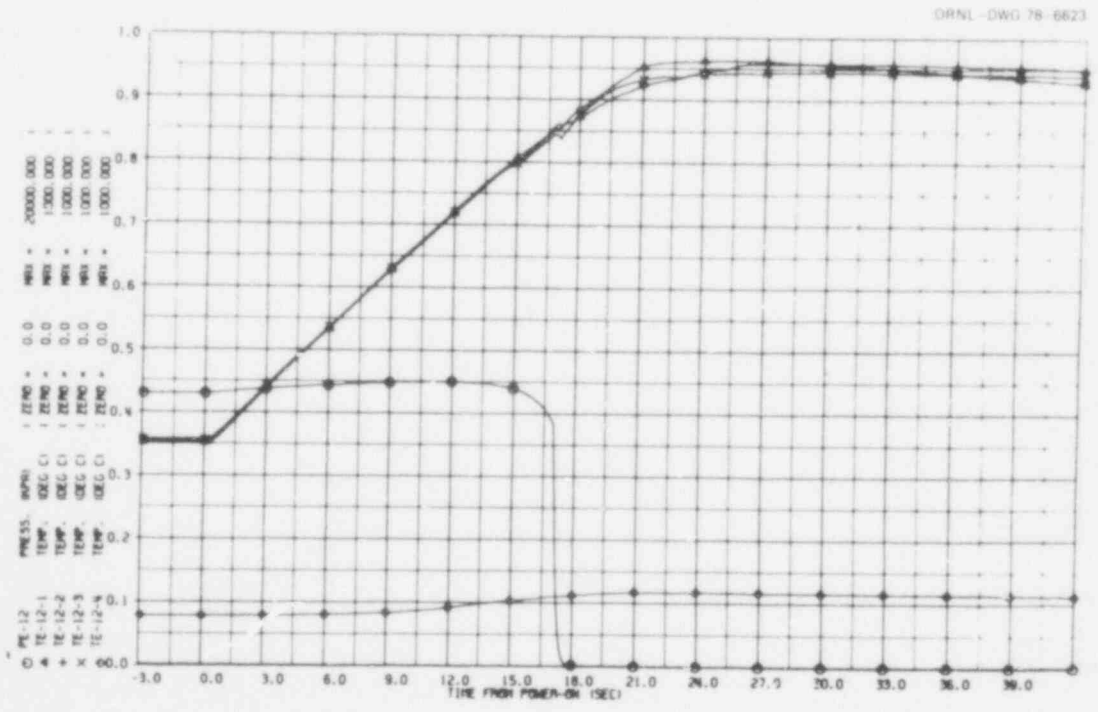

Fig. 30. Temperature and pressure transients for rod No. 12.

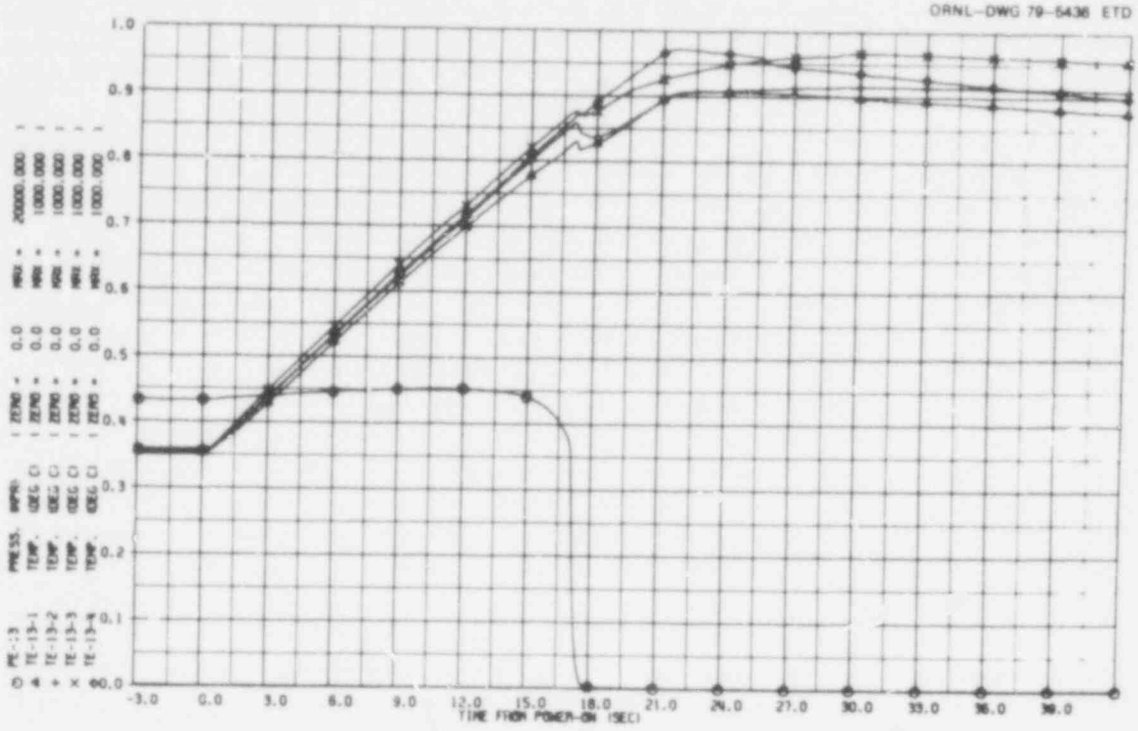

Fig. 31. Temperature and pressure transients for rod No. 13.

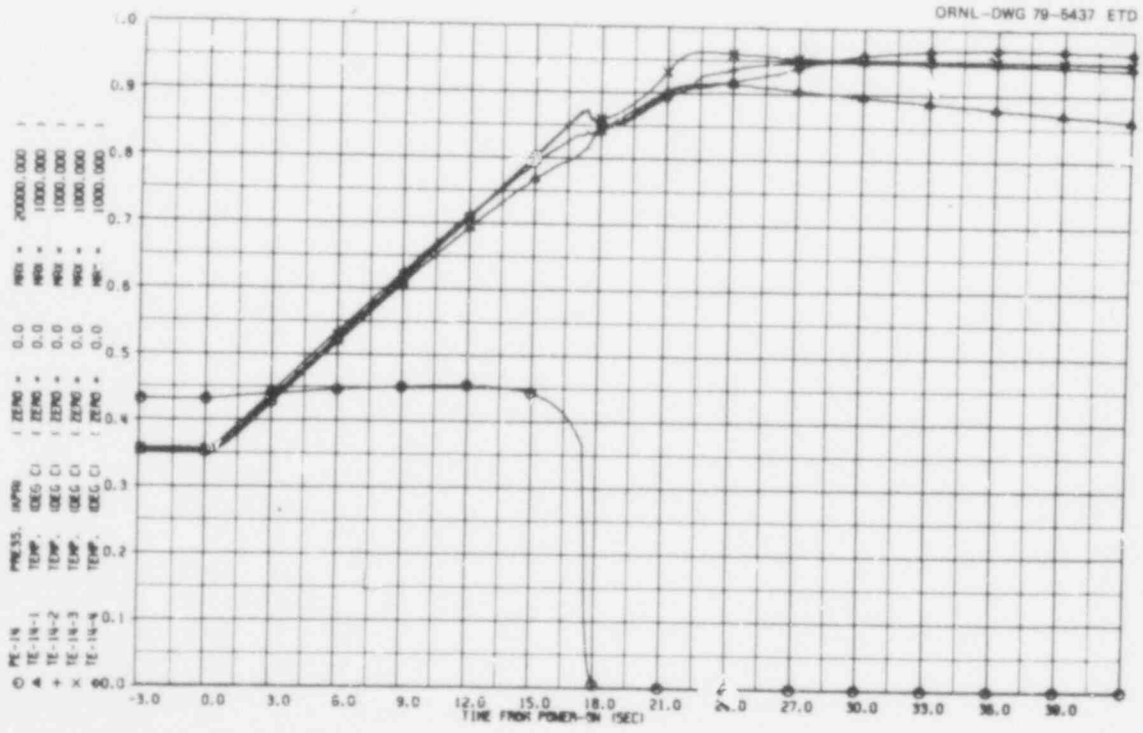

Fig. 32. Temperature and pressure transients for rod No. 14.

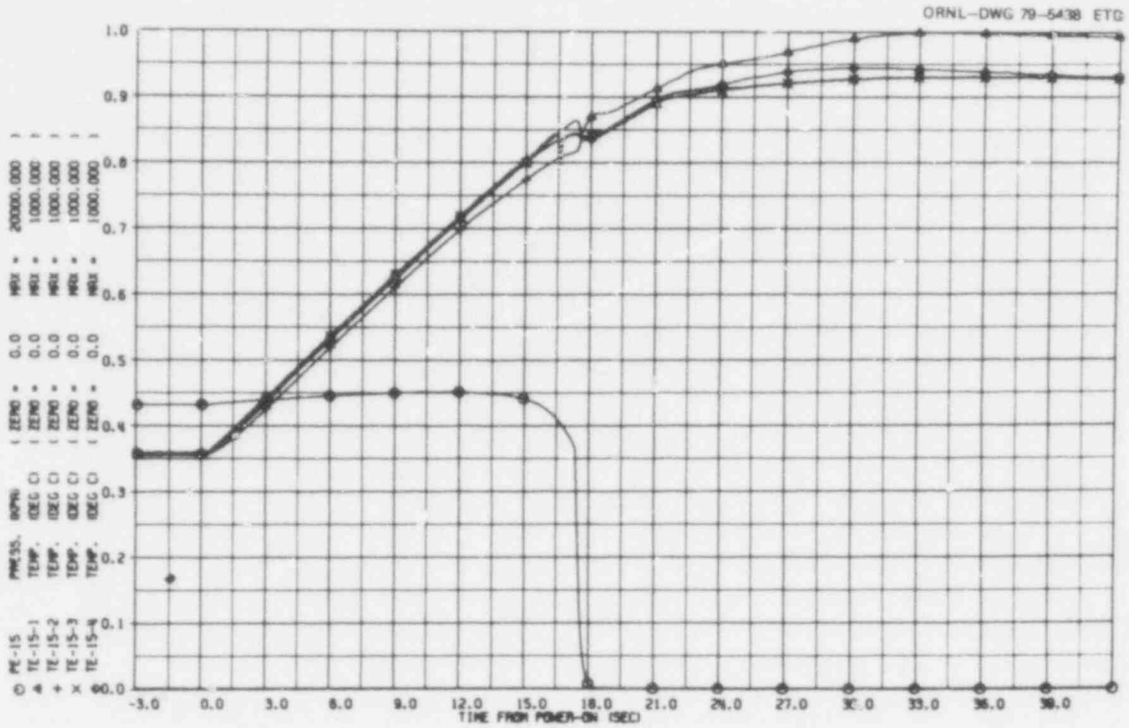

Fig. 33. Temperature and pressure transients for rod No. 15.

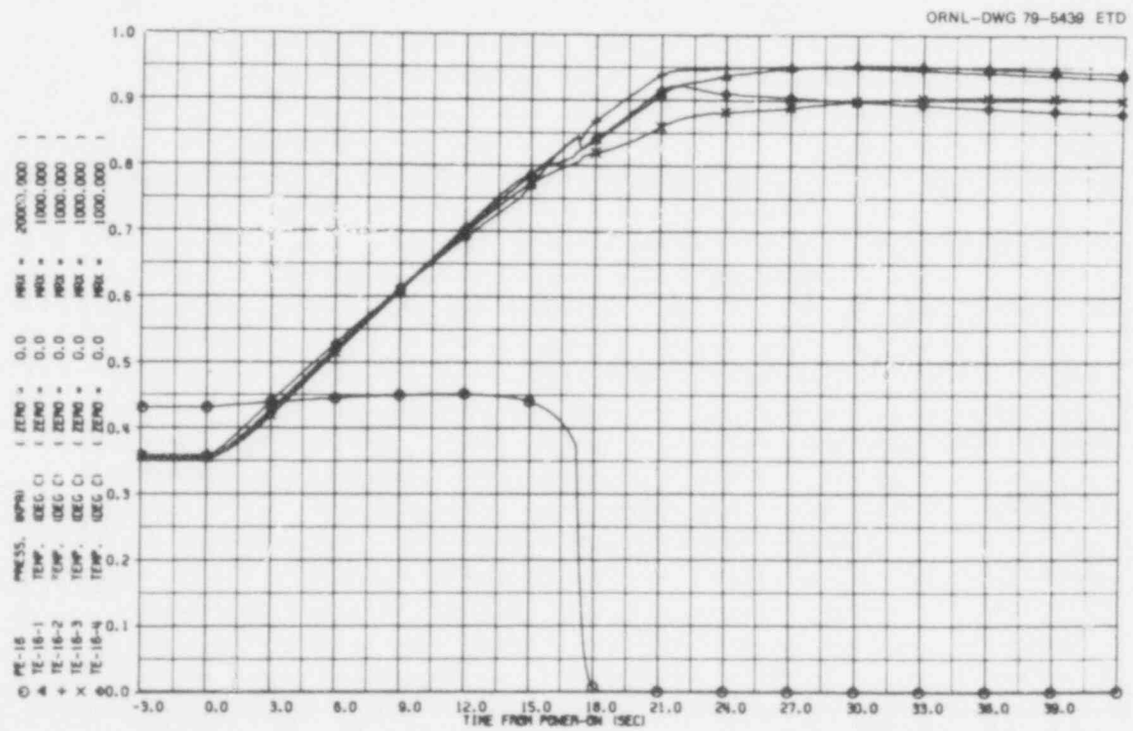

Fig. 34. Temperature and pressure transients for rod No. 16.

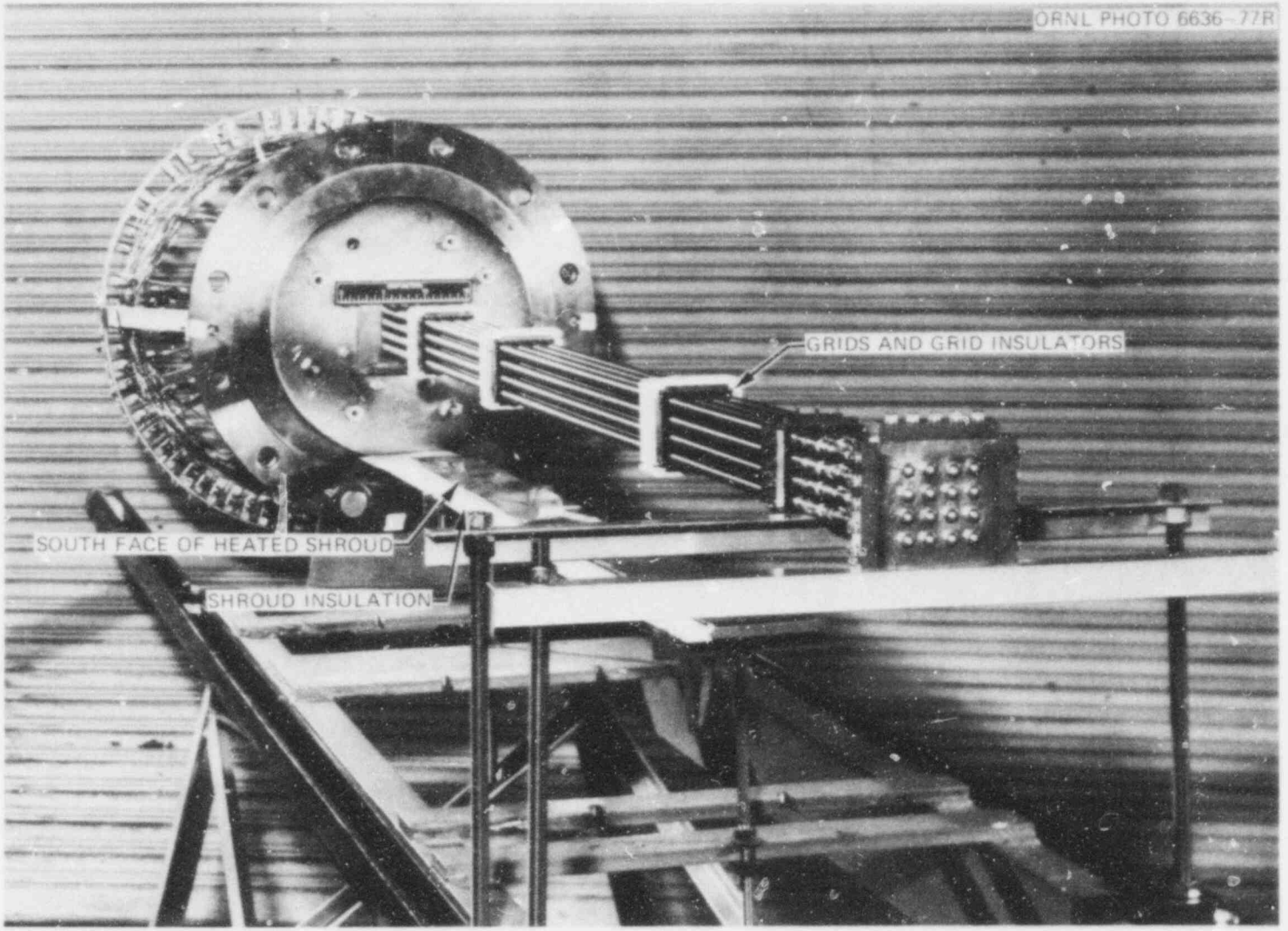

Fig. 35. Partially assembled B-1 test bundle.

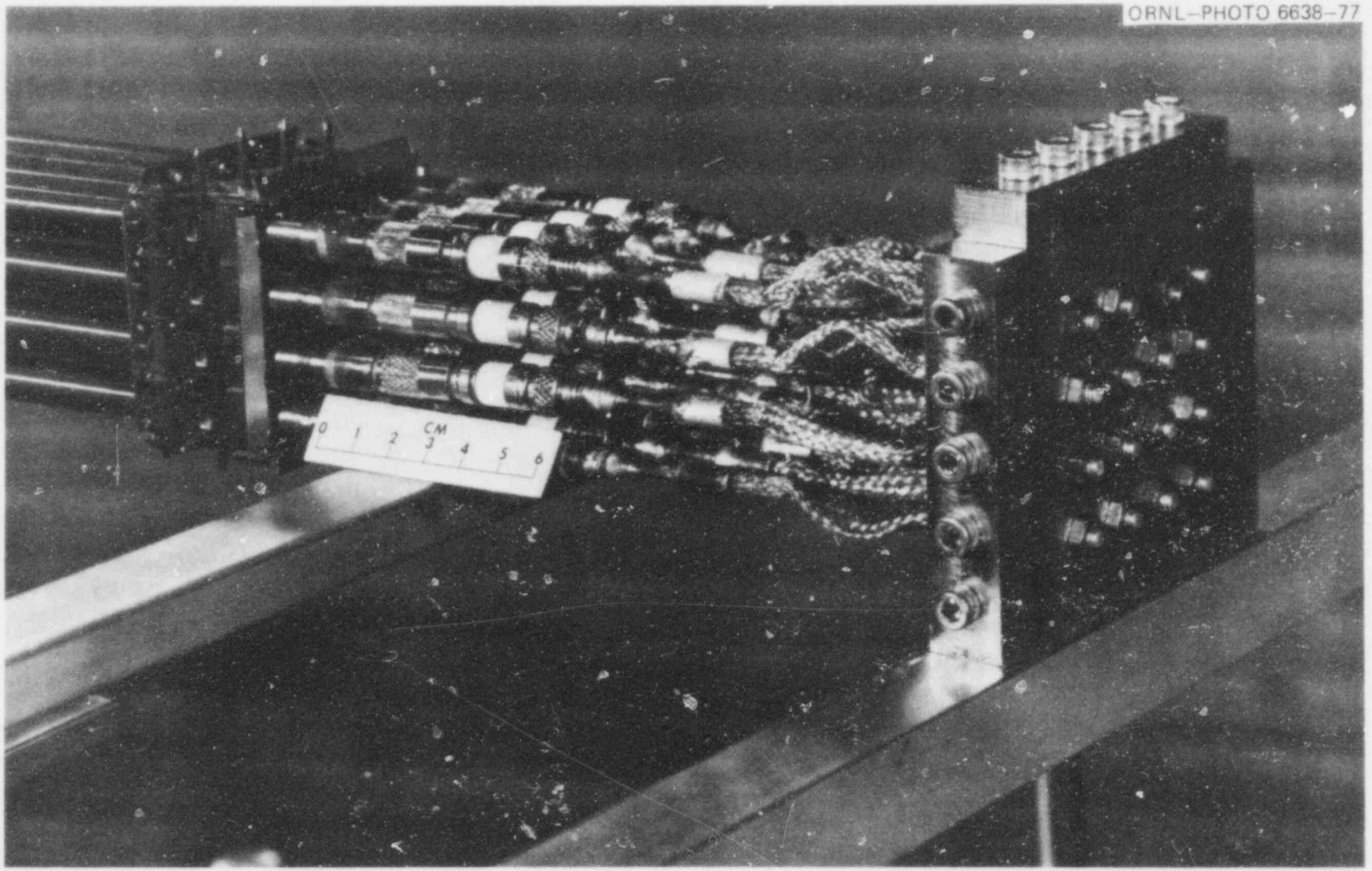

Fig. 36. Lower end of B-1 showing lower grid, seal glands, flexible power leads, and terminal block.

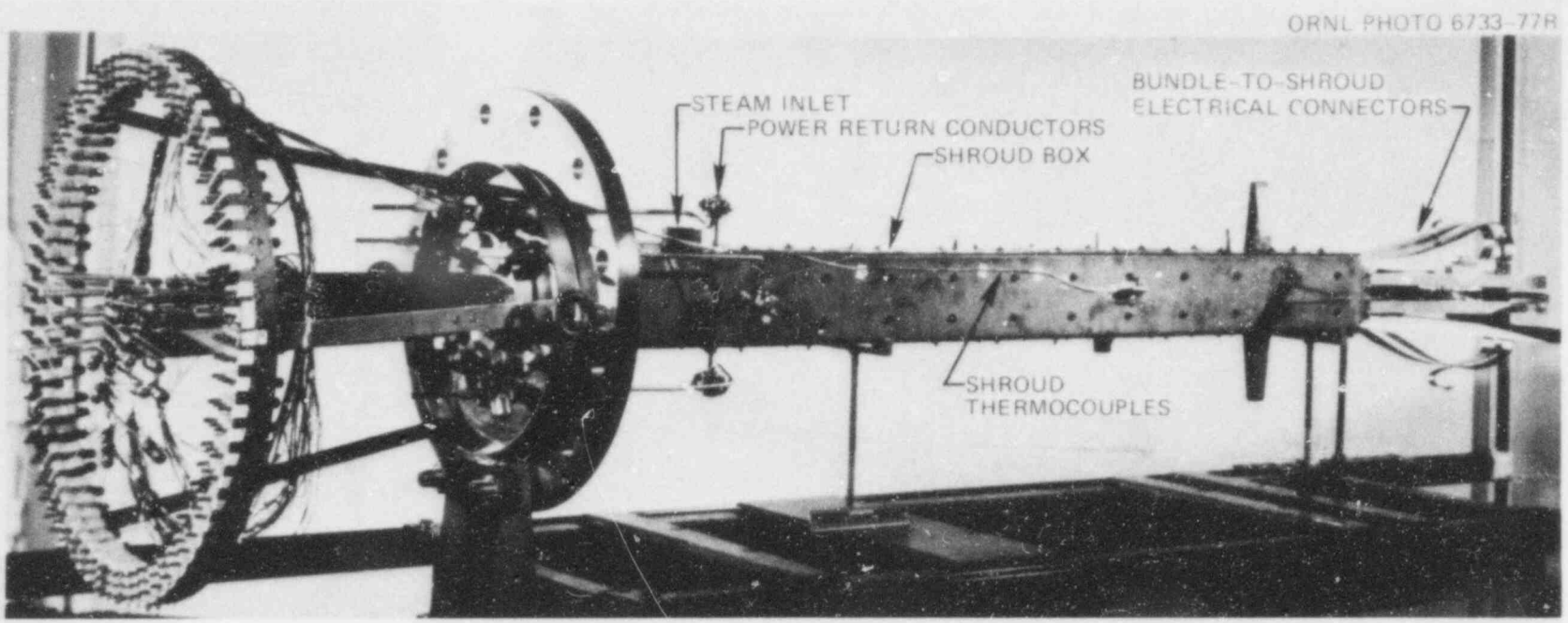

Fig. 37. Completely assembled B-1 test array.

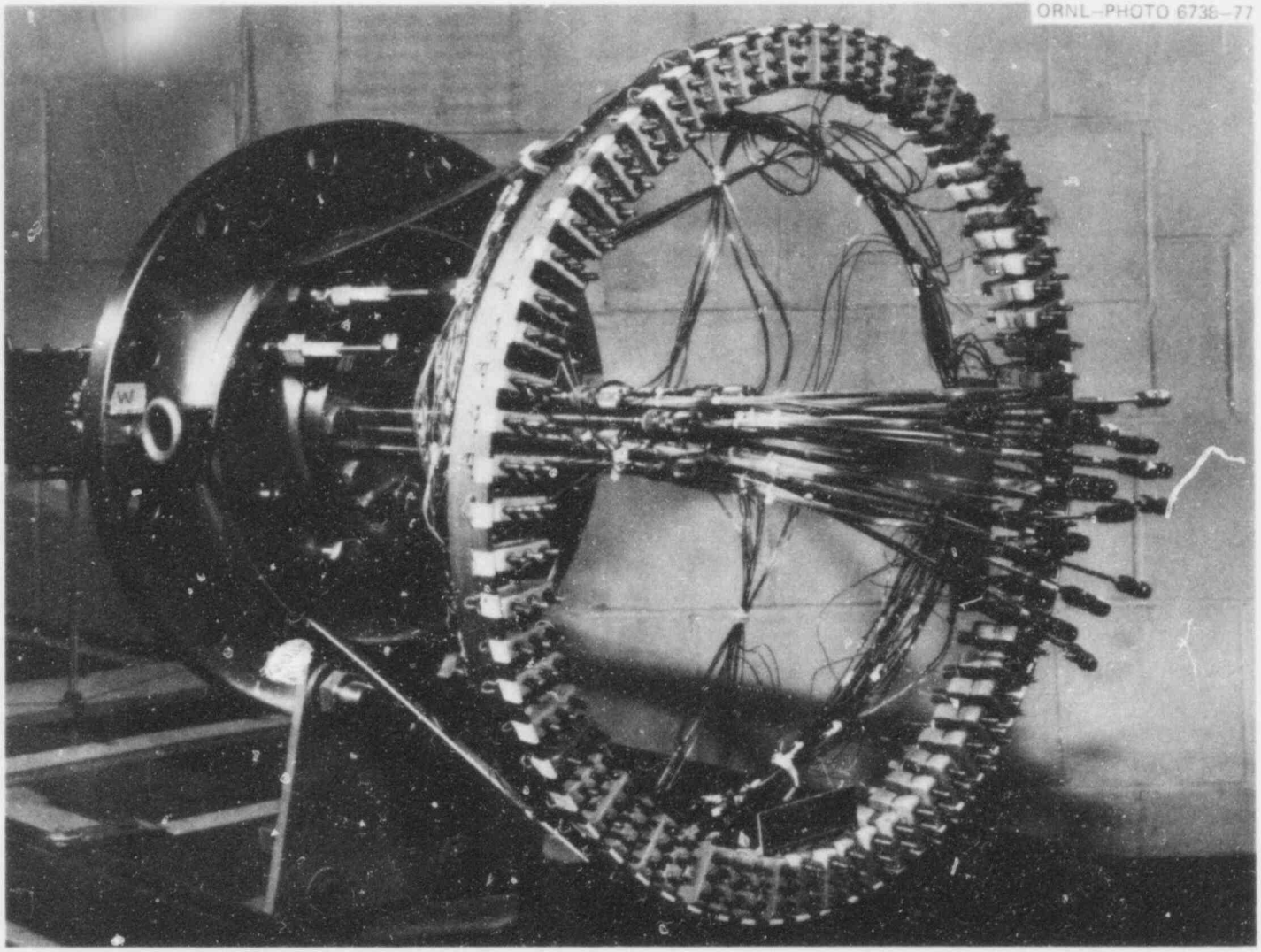

Fig. 38. Top end of B-1 test bundle showing thermocouple connectors, pressure tubes, and power leads.

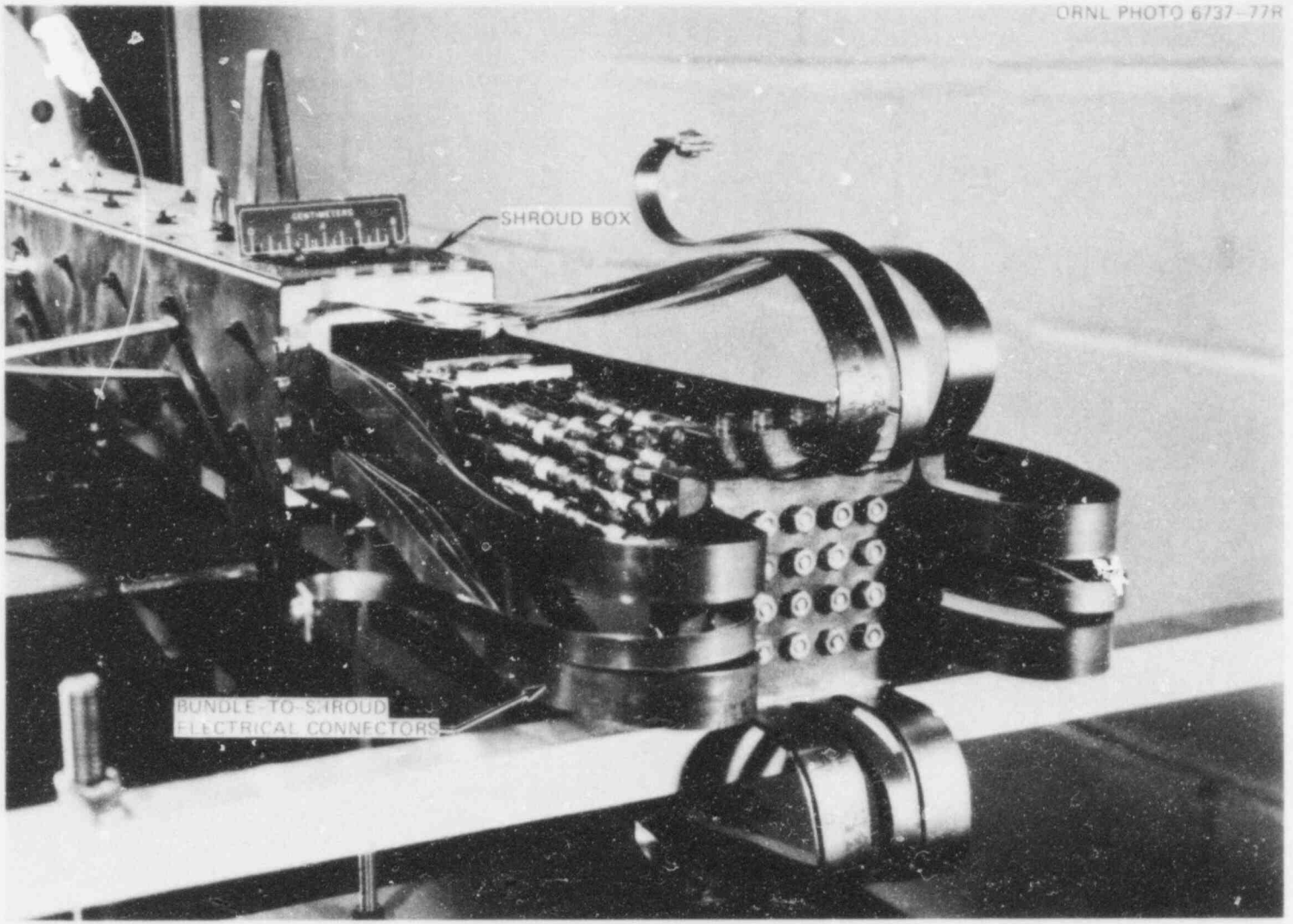

Fig. 39. Lower end of B-1 after installation of heated shroud, shroud box, and electrical connectors.

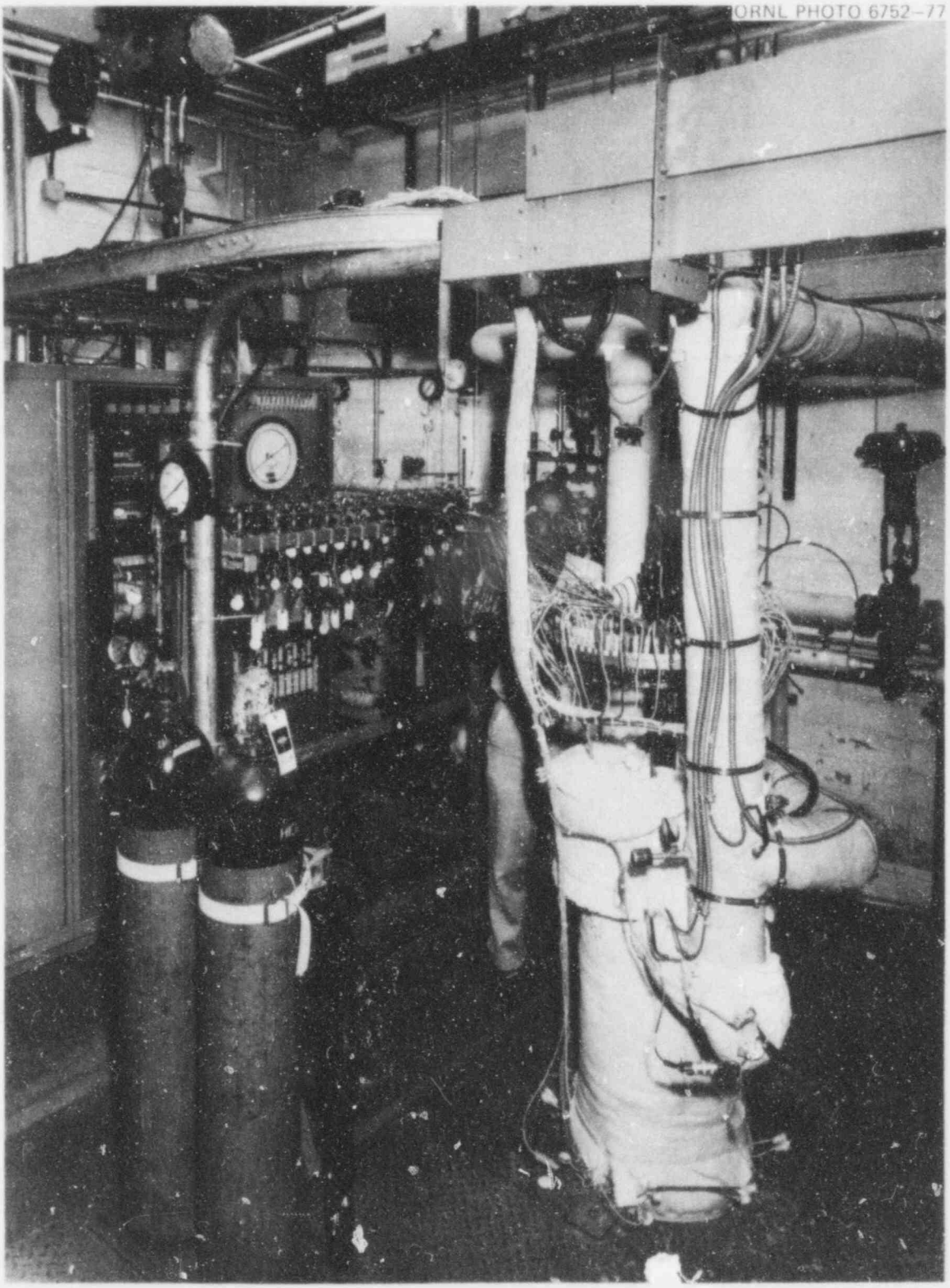

Fig. 40. Overall view of the B-1 test assembly installed in the test facility.

Fig. 41. Overall view of the tested bundle.

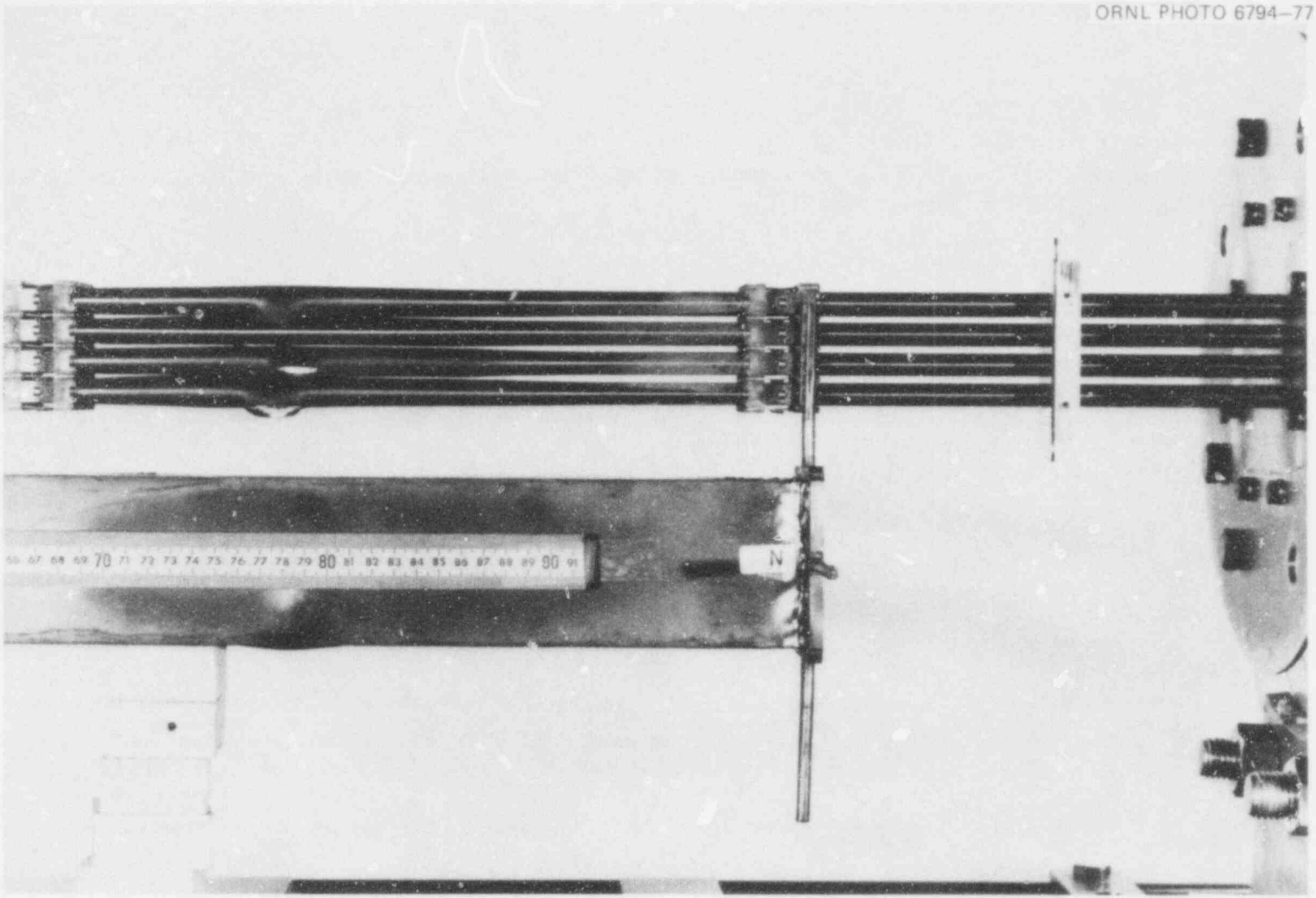

Fig. 42-A. View of north side of tested bundle and shroud (upper end).

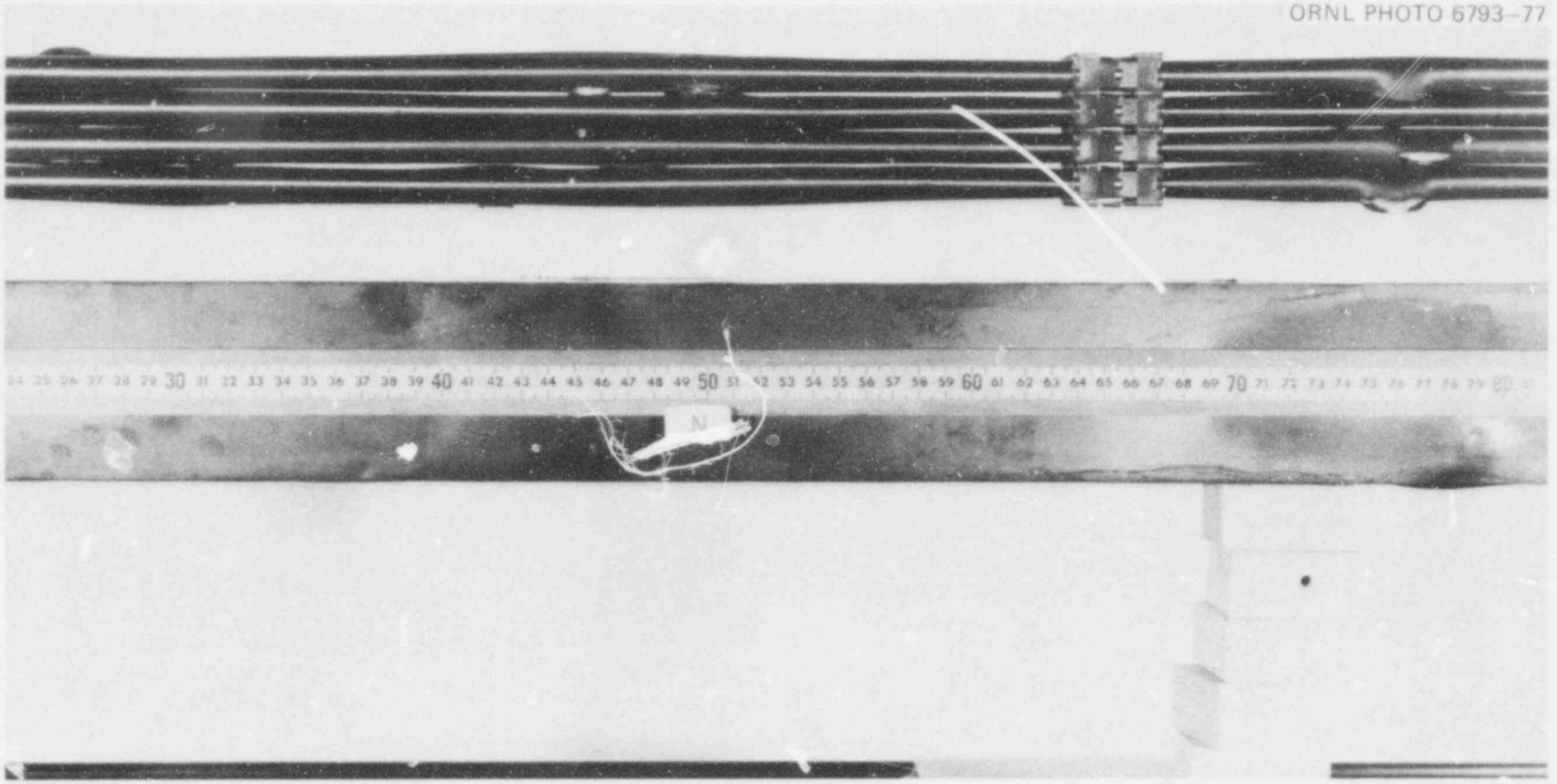

Fig. 42-B. View of north side of tested bundle and shroud (middle region).

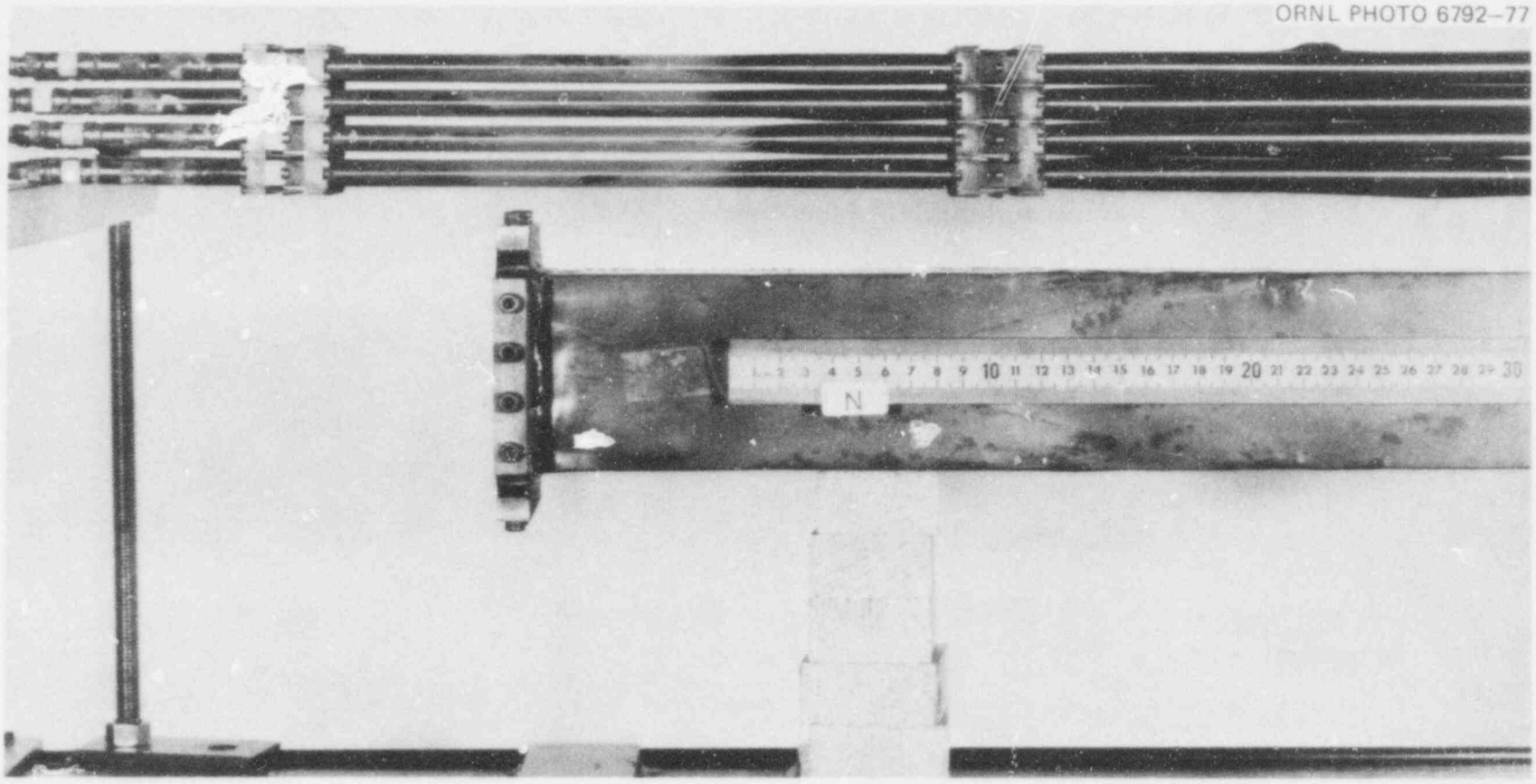

Fig. 42-C. View of north side of tested bundle and shroud (bottom end).

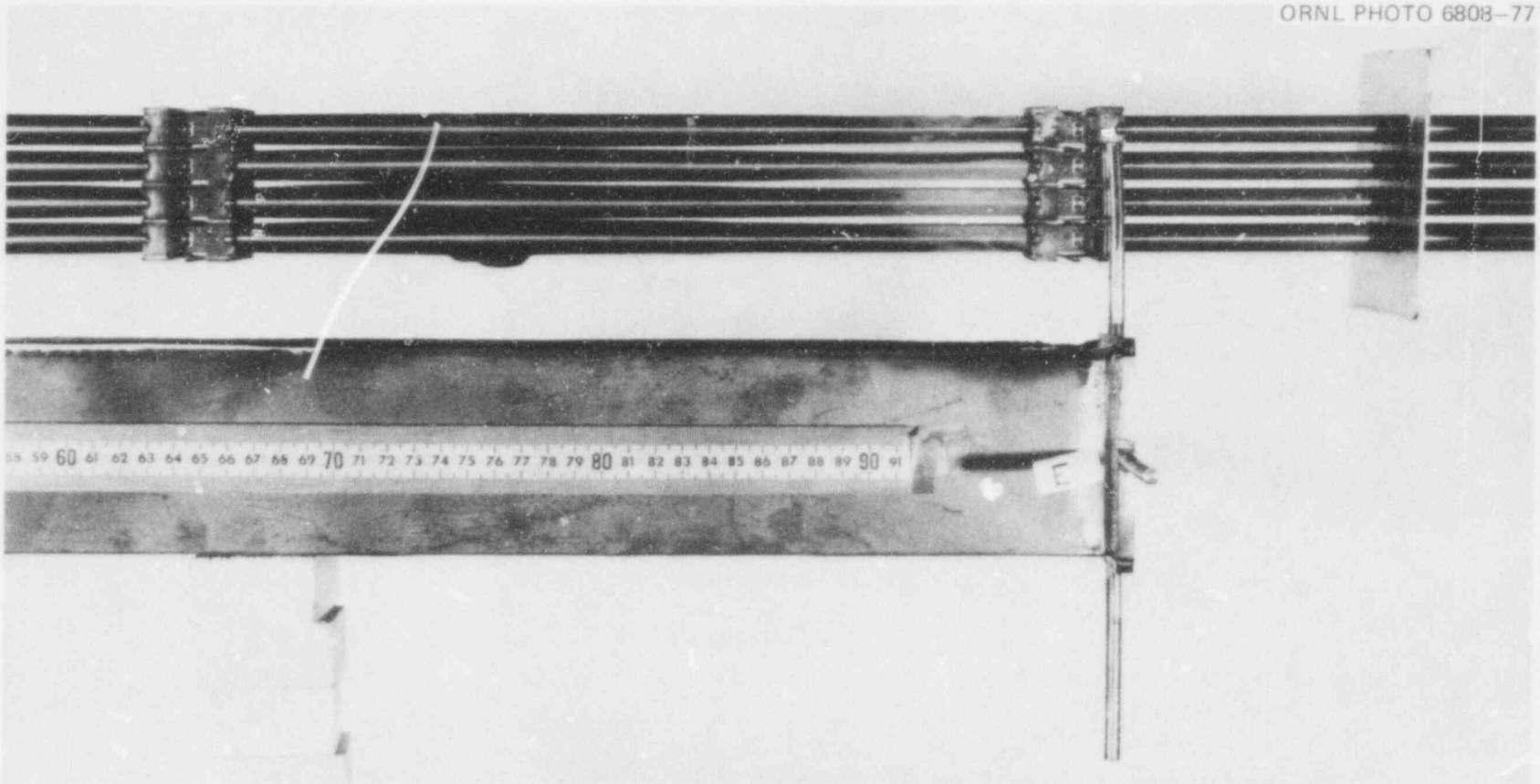

Fig. 43-A. View of east side of tested bundle and shroud (upper end).

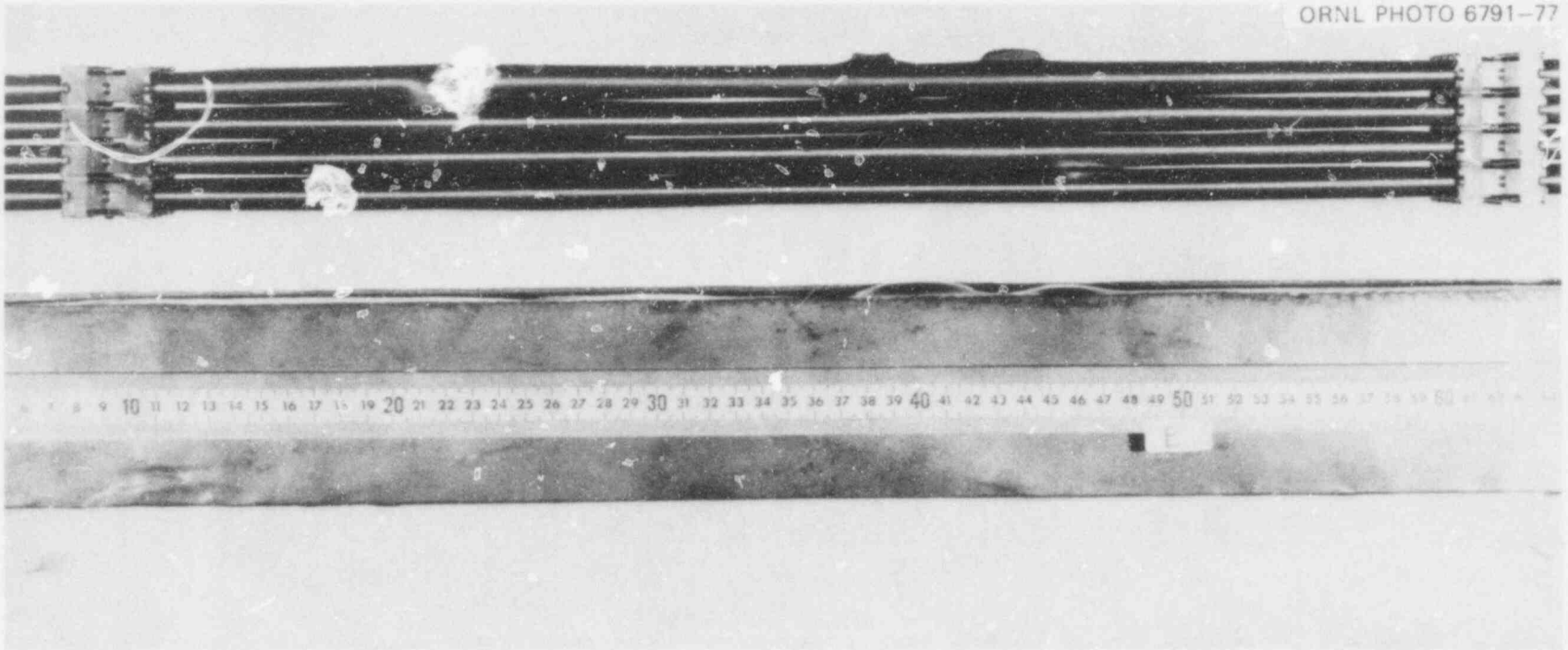

Fig. 43-B. View of east side of tested bundle and shroud (middle region).

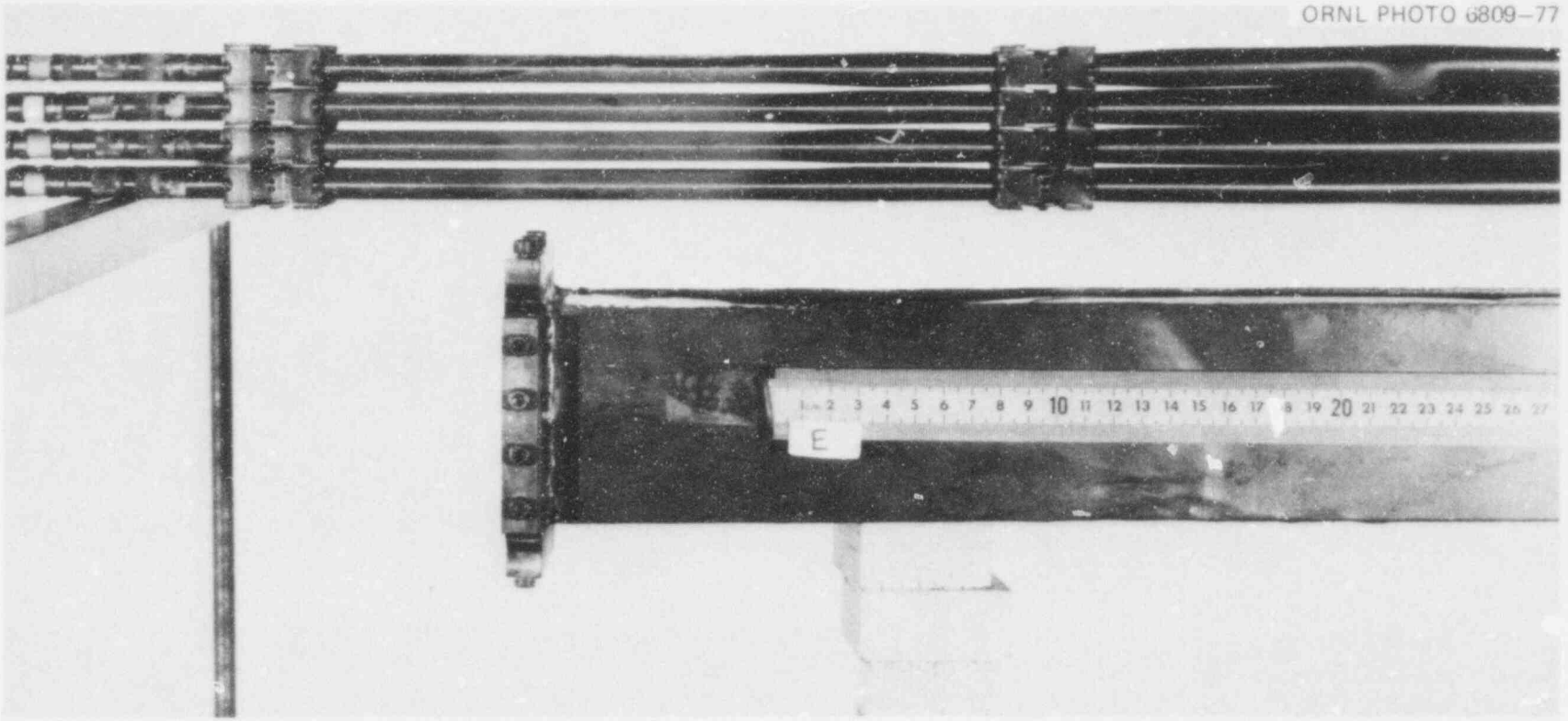

Fig. 43-C. View of east side of tested bundle and shroud (bottom end).

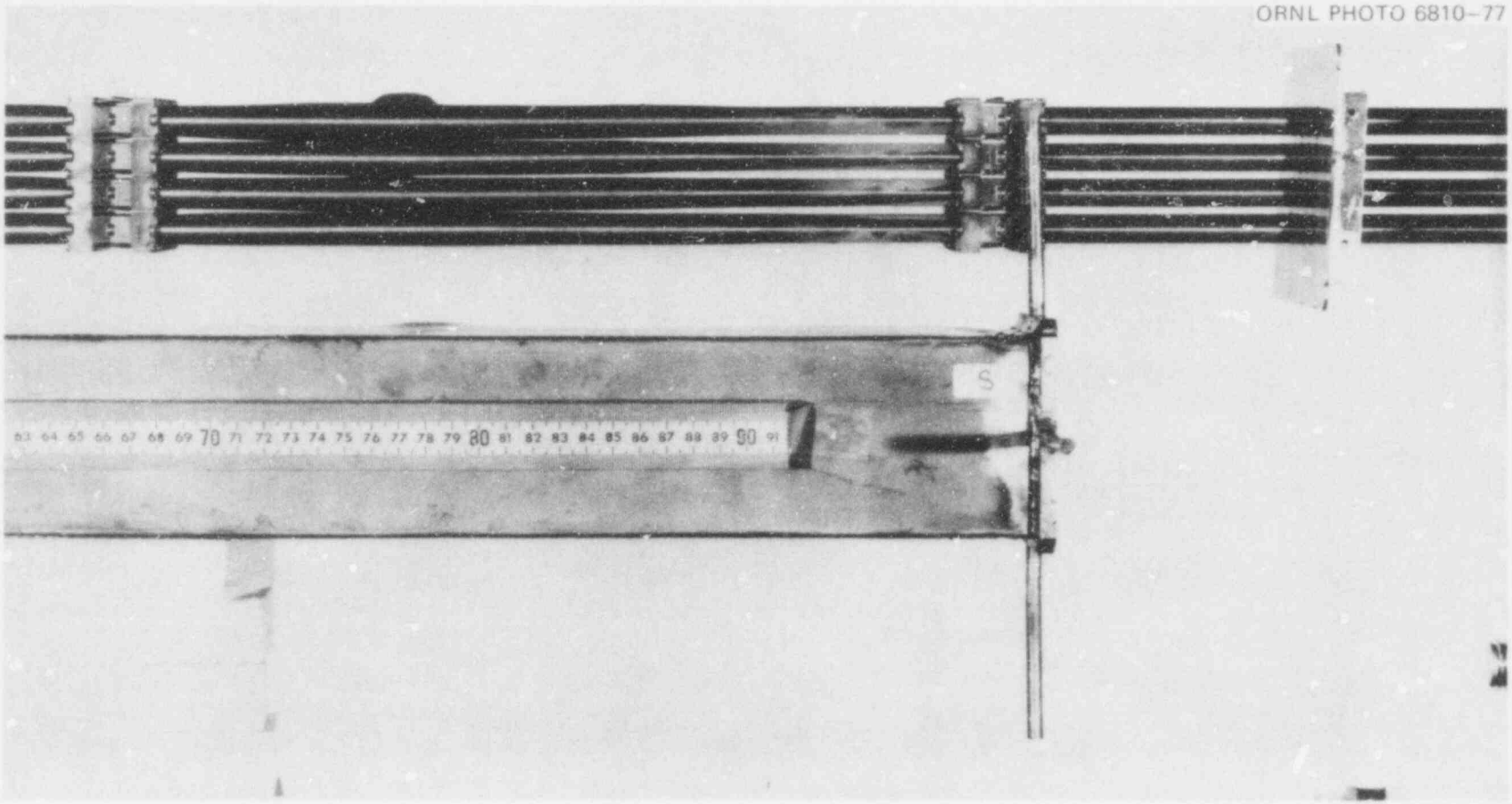

Fig. 44-A. View of south side of tested bundle and shroud (upper end).

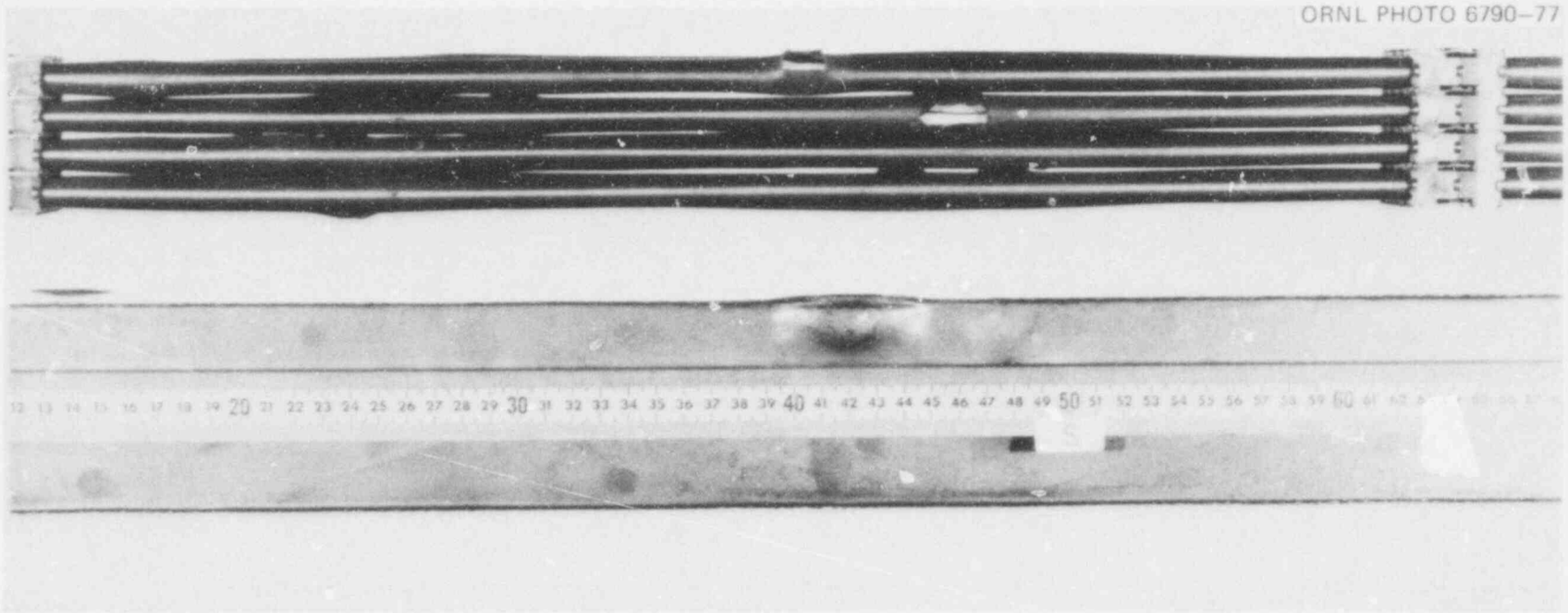

Fig. 44-B. View of south side of tested bundle and shroud (middle region).

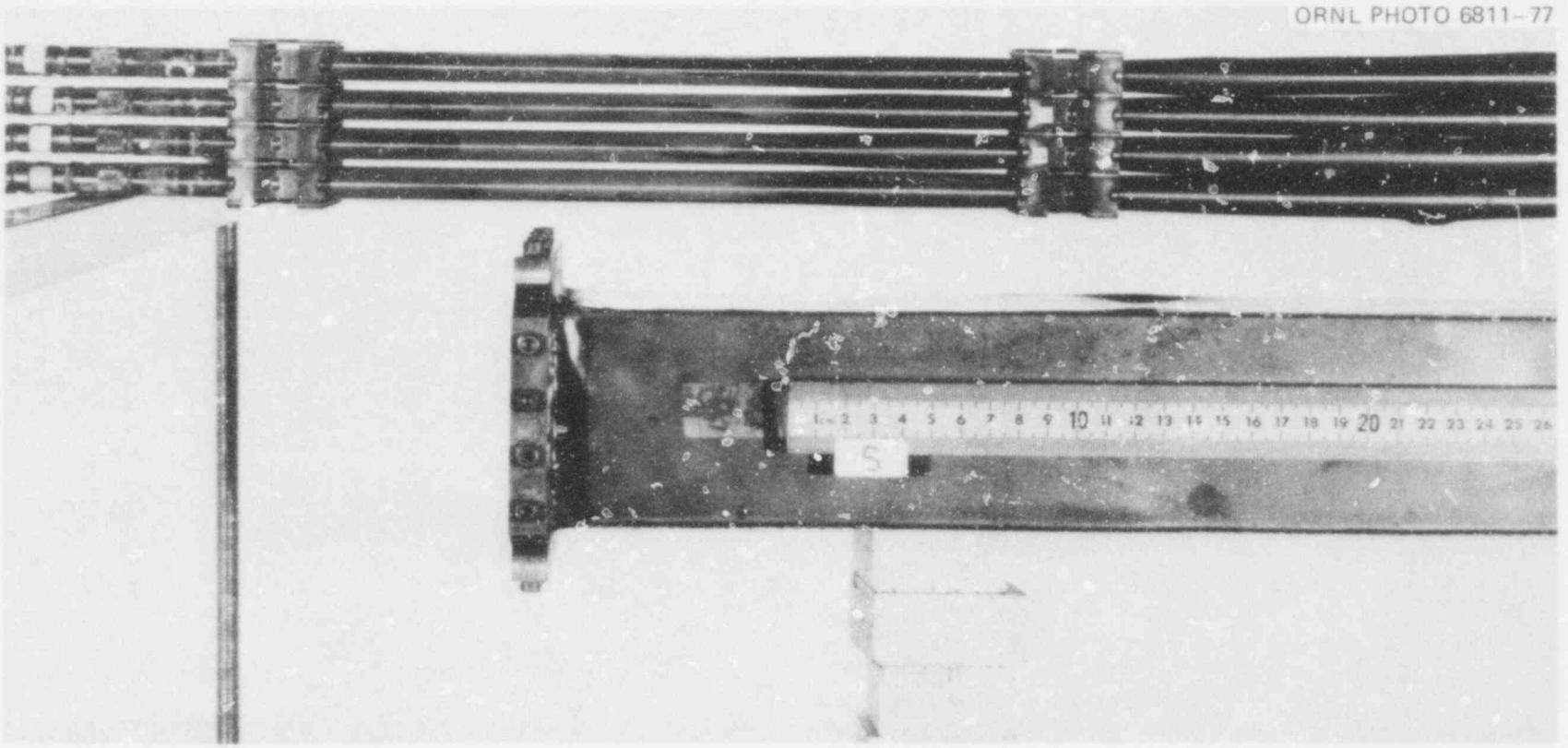

Fig. 44-C. View of south side of tested bundle and shroud (bottom end).

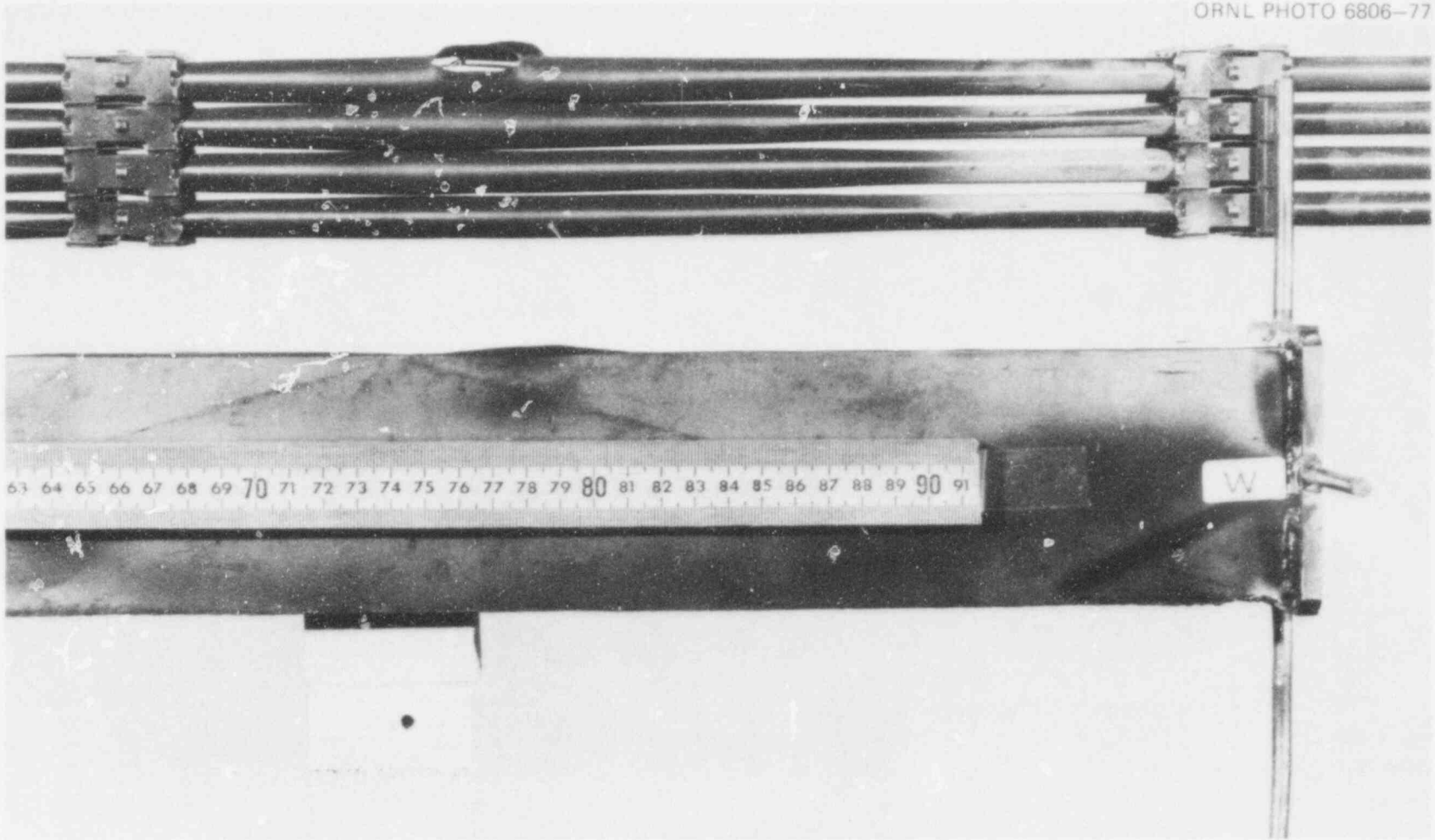

Fig. 45-A. View of west side of tested bundle and shroud (upper end).

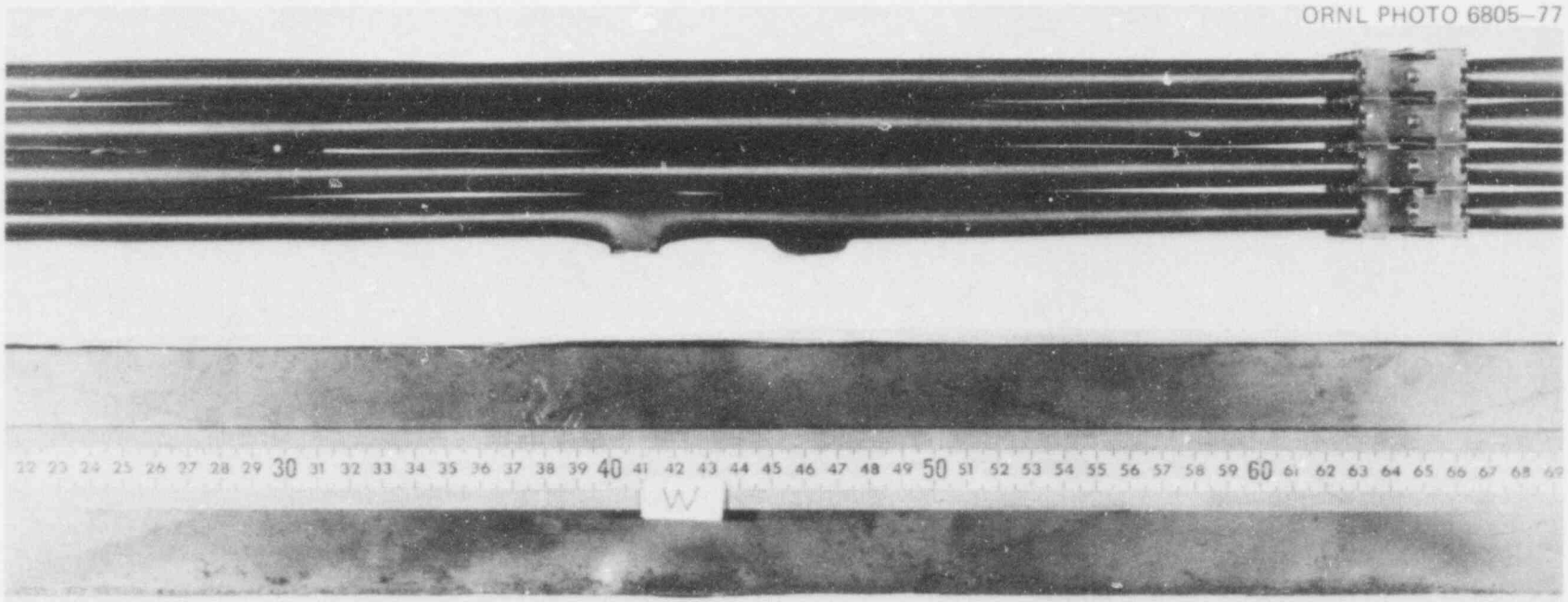

Fig. 45-B. View of west side of tested bundle and shroud (middle region).

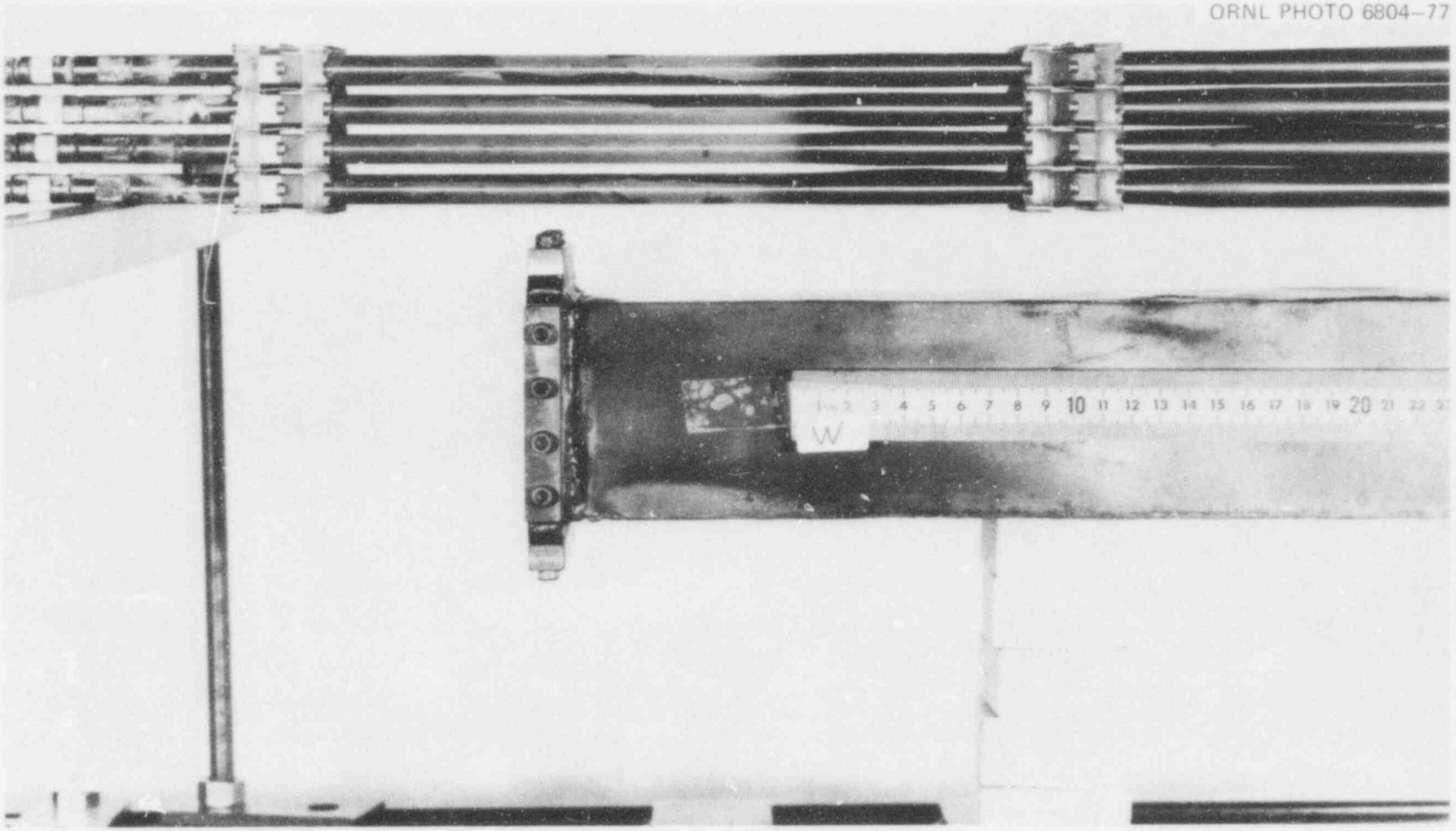

Fig. 45-C. View of west side of tested bundle and shroud (bottom end).

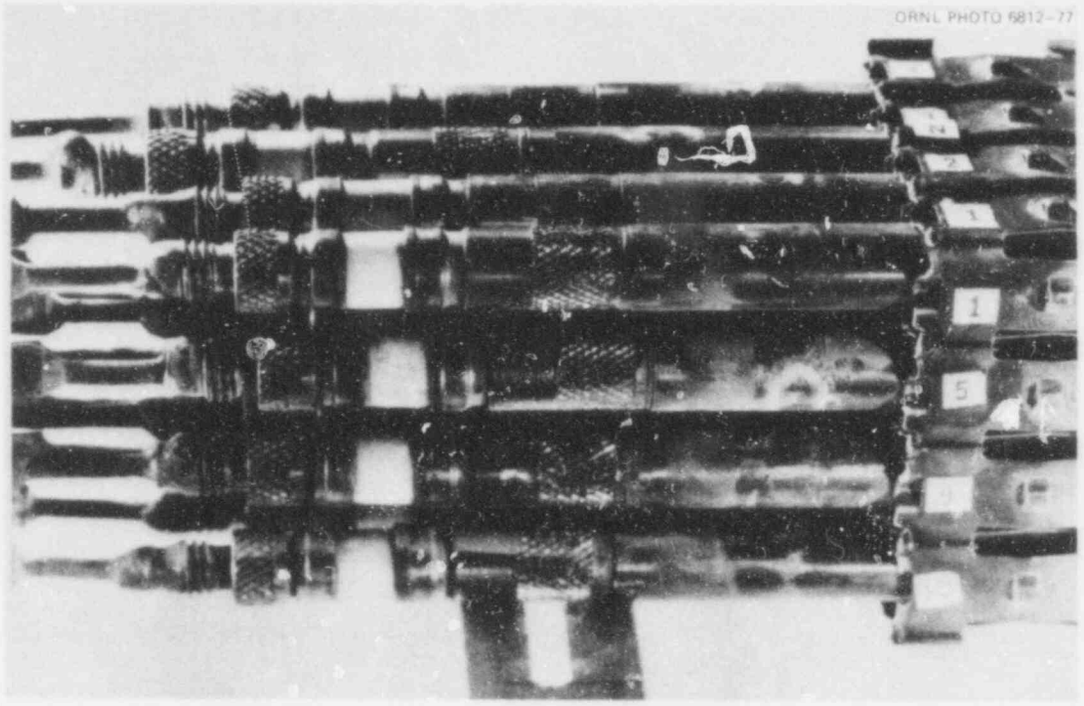

Fig. 46. Close-up of lower end of bundle showing rod length changes.

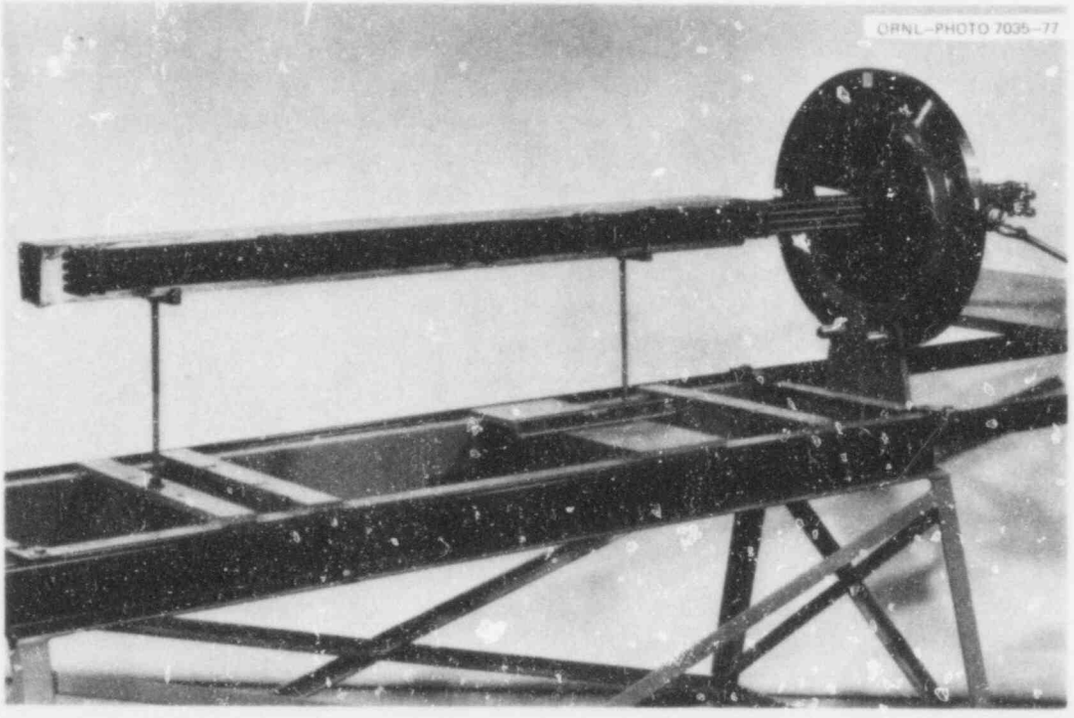

Fig. 47. Tested bundle encapsulated in epoxy.

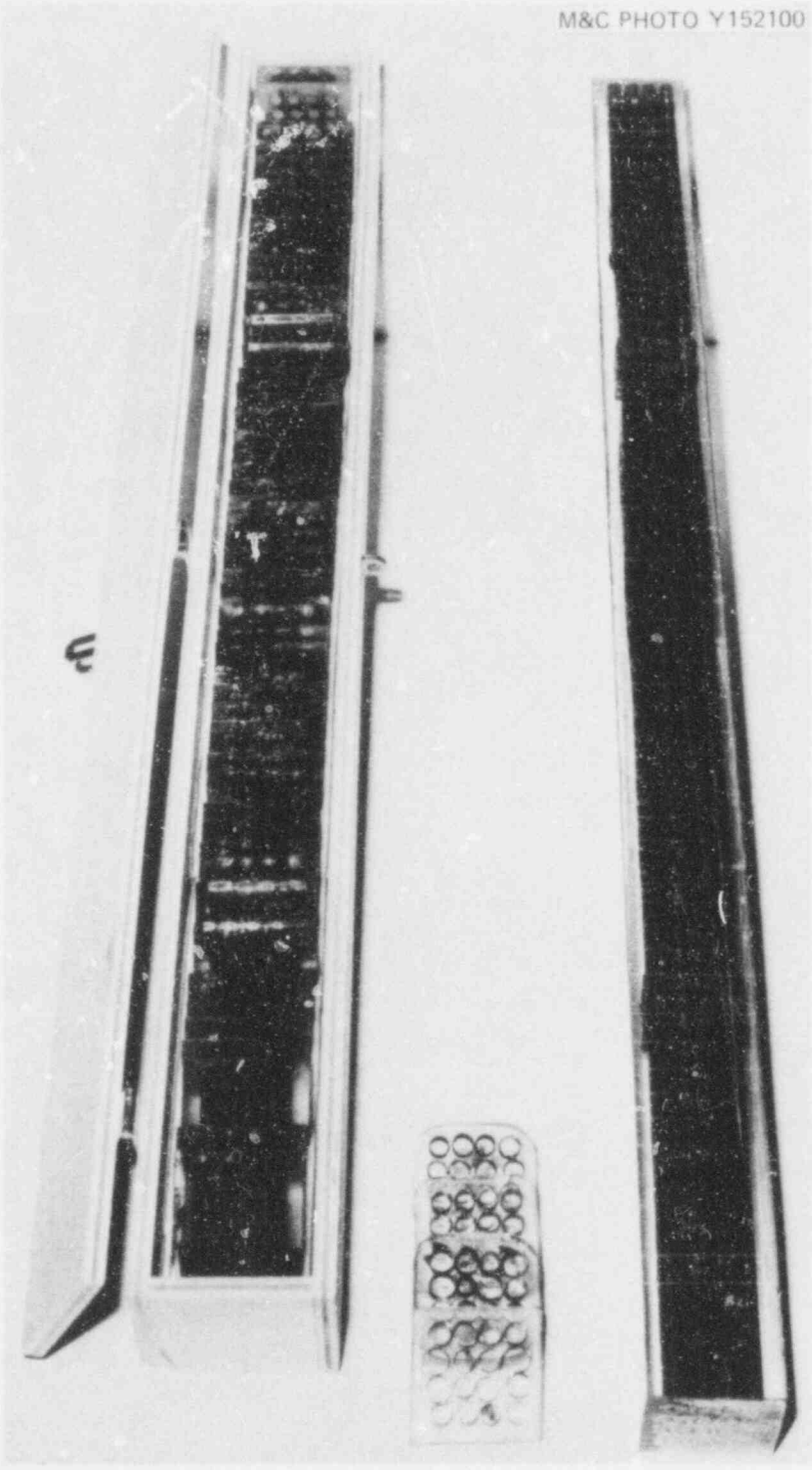

Fig. 48. Two encapsulated test bundles (B-1 and B-2). Bundle B-2 (on right) has been marked for sectioning. Bundle B-1 (on left) has been sectioned. Representative cross sections of B-1 are shown in the center.

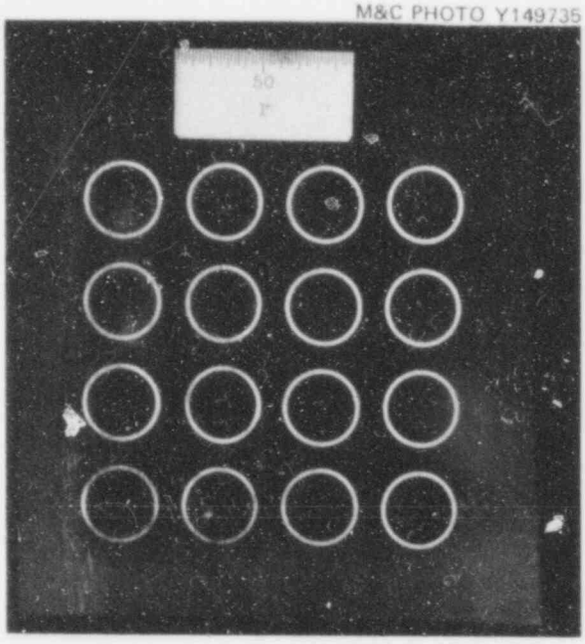

Fig. 49. Section of undeformed region of B-1 at −13.5-cm elevation.

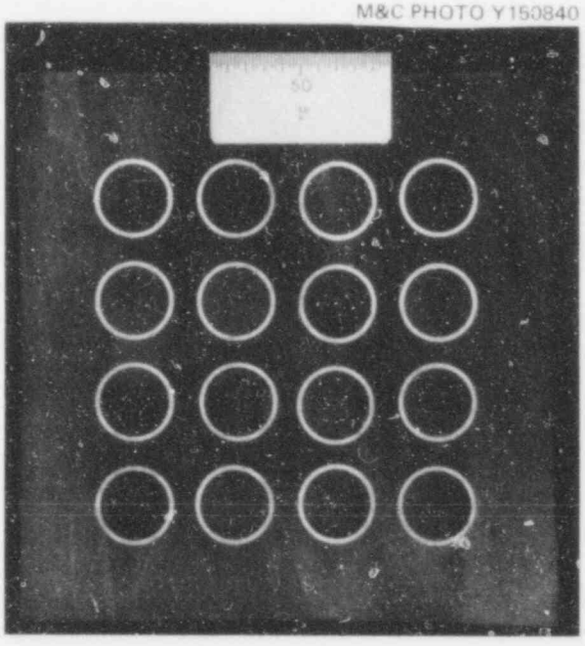

Fig. 50. Section of undeformed region of B-1 at −6.0-cm elevation.

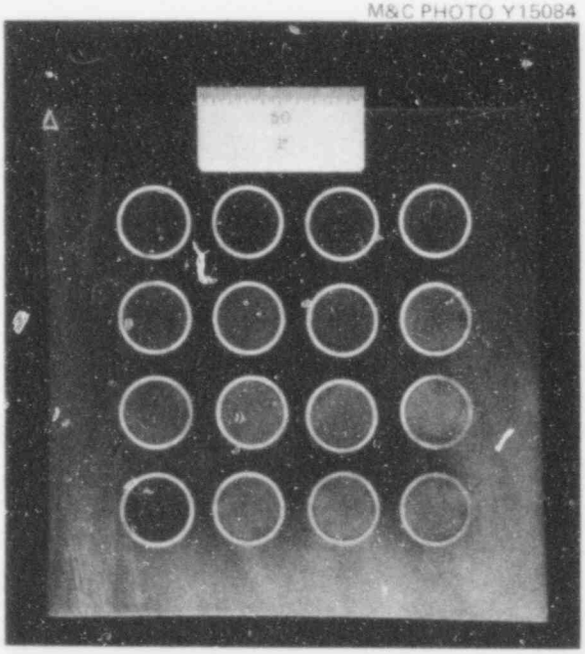

Fig. 51. Section of B-1 at 0.0-cm elevation — the bottom of the heated length.

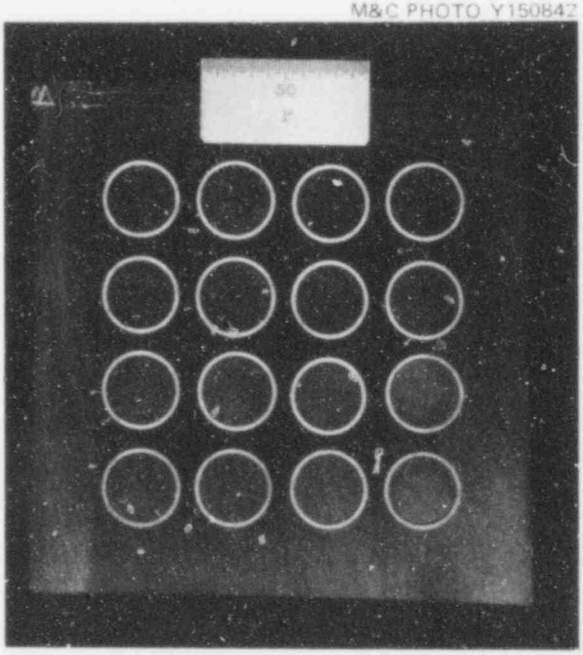

Fig. 52. Section of B-1 at 1.8-cm elevation.

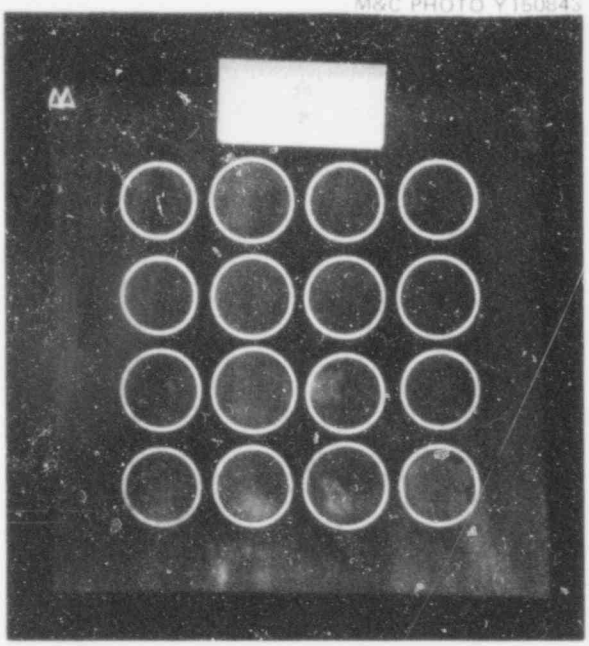

Fig. 53. Section of B-1 at 3.3-cm elevation.

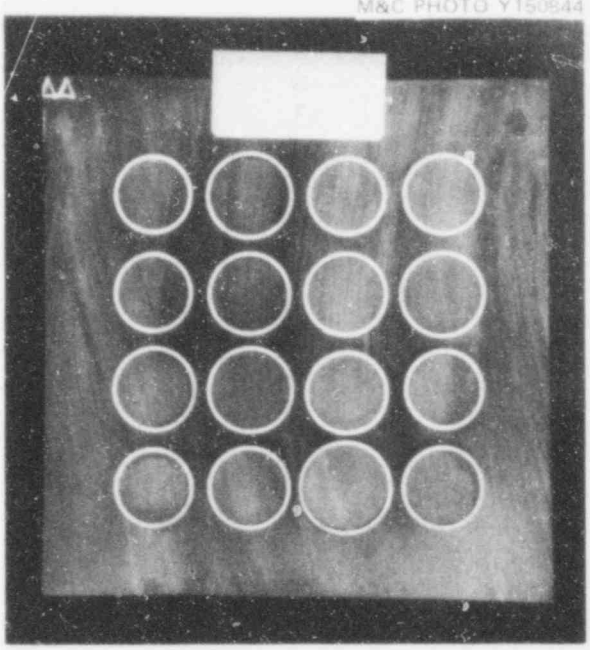

Fig. 54. Section of B-1 at 5.2-cm elevation.

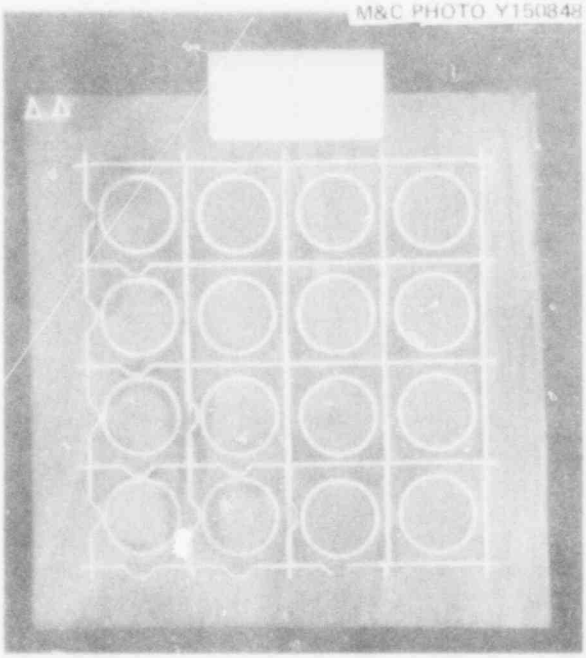

Fig. 55. Section through lower grid of B-1 at 8.9-cm elevation.

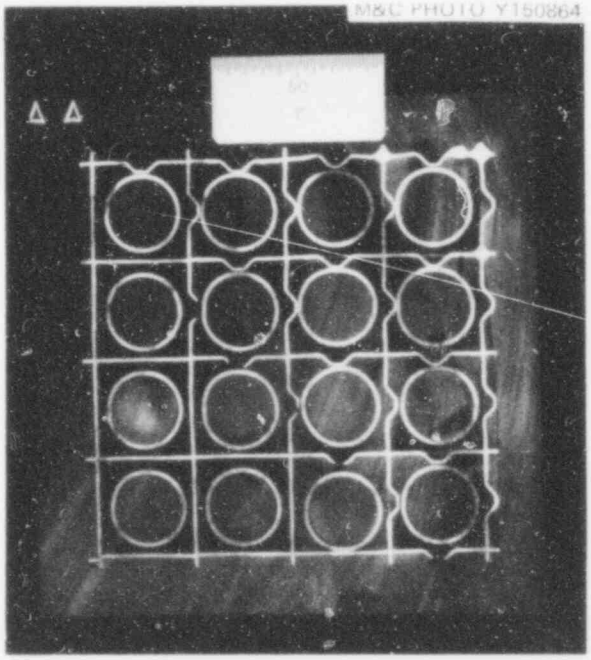

Fig. 56. Section through lower grid of B-1 at 11.8-cm elevation.

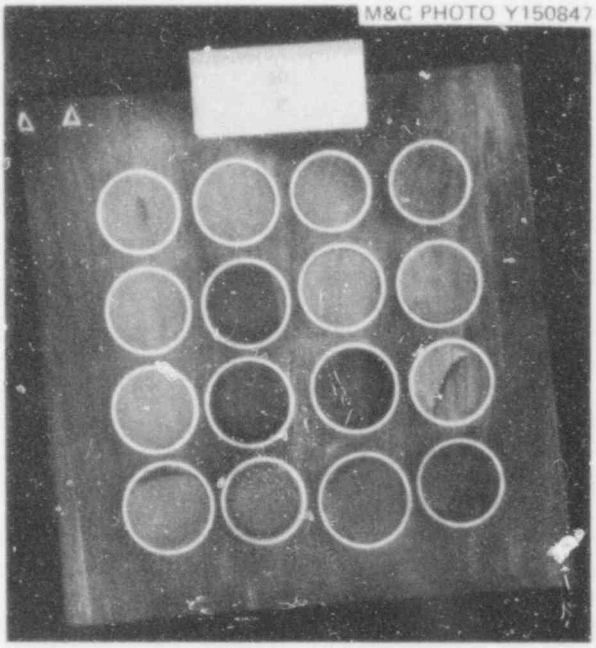

Fig. 57. Section of B-1 at 14.1-cm elevation.

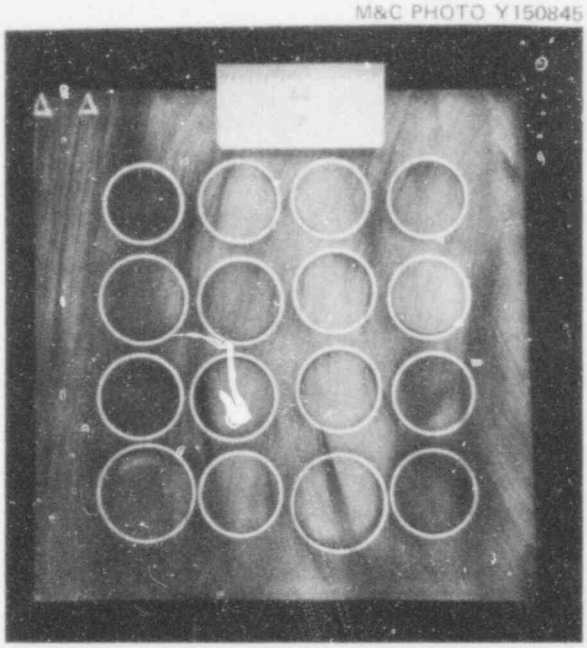

Fig. 58. Section of B-1 at 15.4-cm elevation.

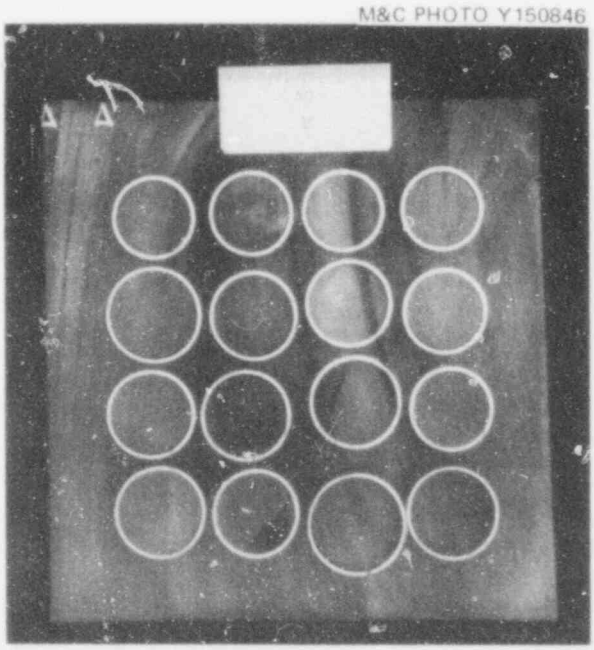

Fig. 59. Section of B-1 at 17.3-cm elevation.

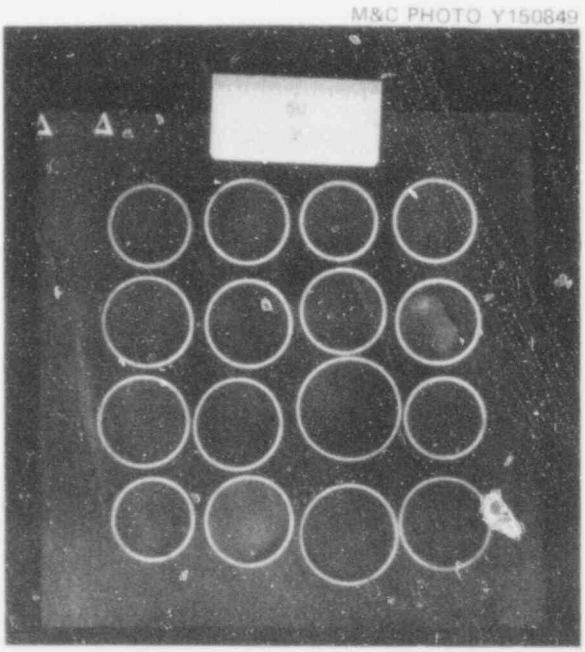

Fig. 60. Section of B-1 at 18.8-cm elevation.

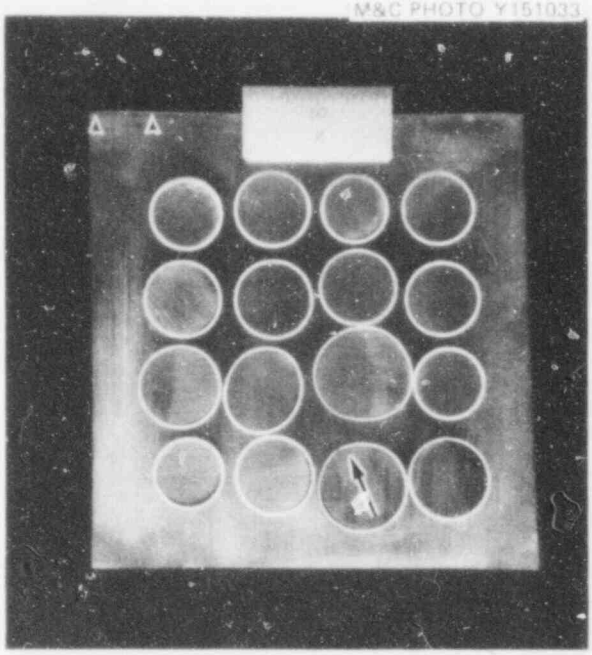

Fig. 61. Section of B-1 at 20.1-cm elevation.

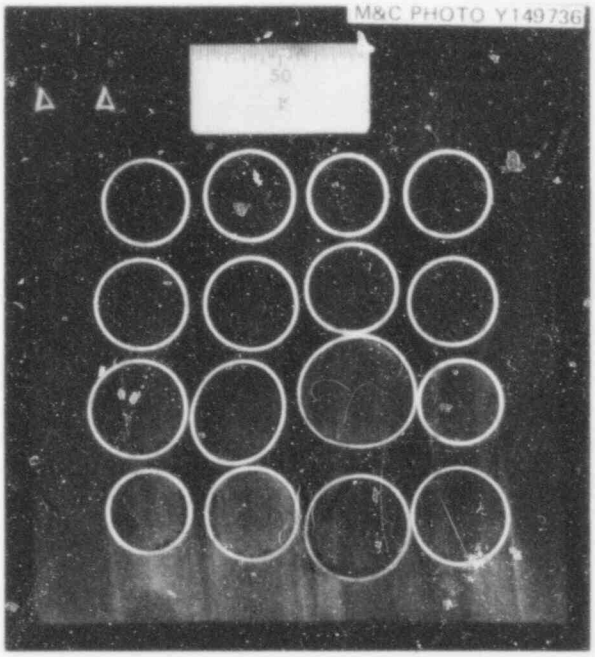

Fig. 62. Section of B-1 at 20.6-cm elevation.

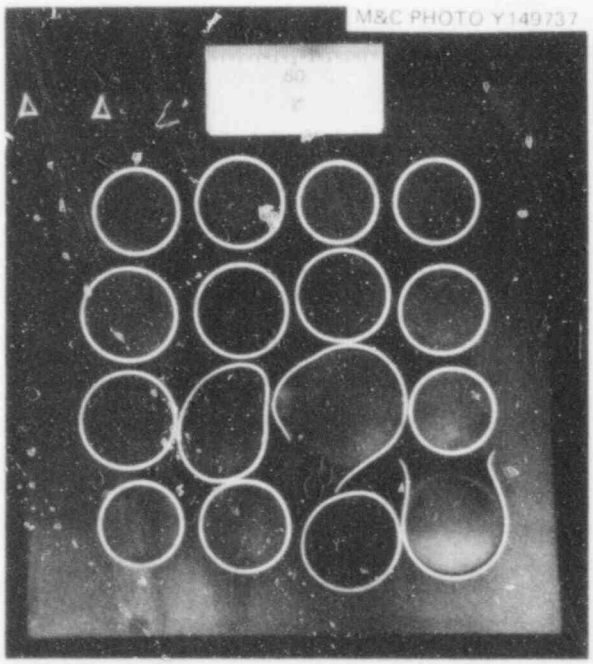

Fig. 63. Section of B-1 at 22.3-cm elevation.

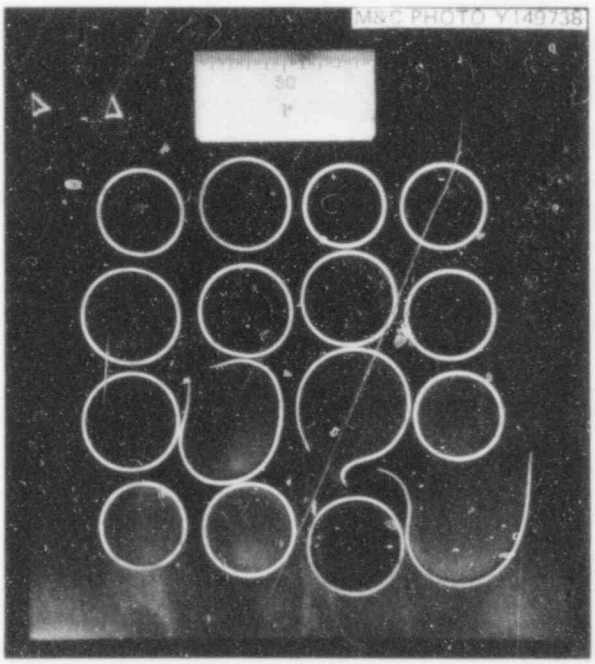

Fig. 64. Section of B-1 at 23.9-cm elevation.

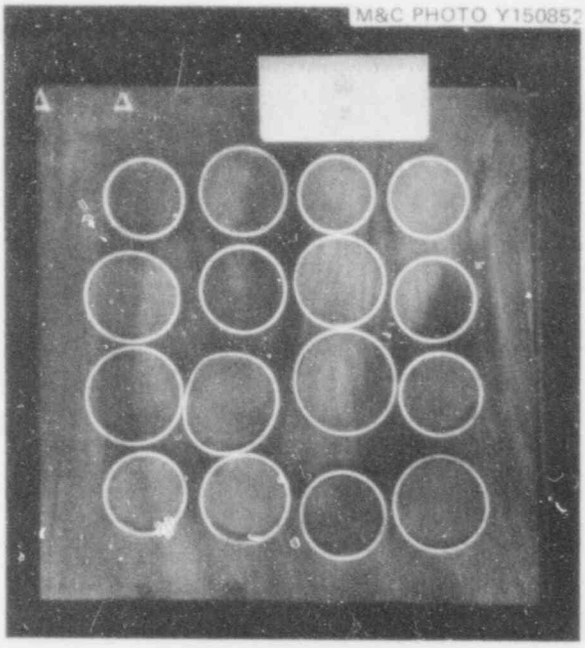

Fig. 65. Section of B-1 at 25.5-cm elevation.

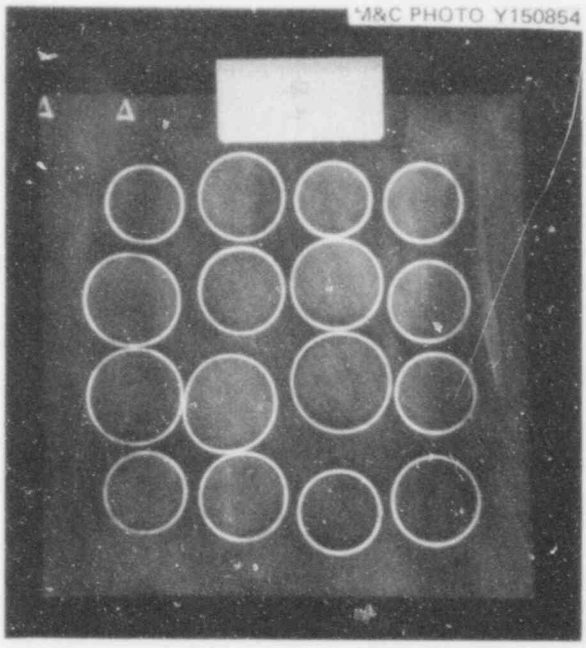

Fig. 66. Section of B-1 at 26.5-cm elevation.

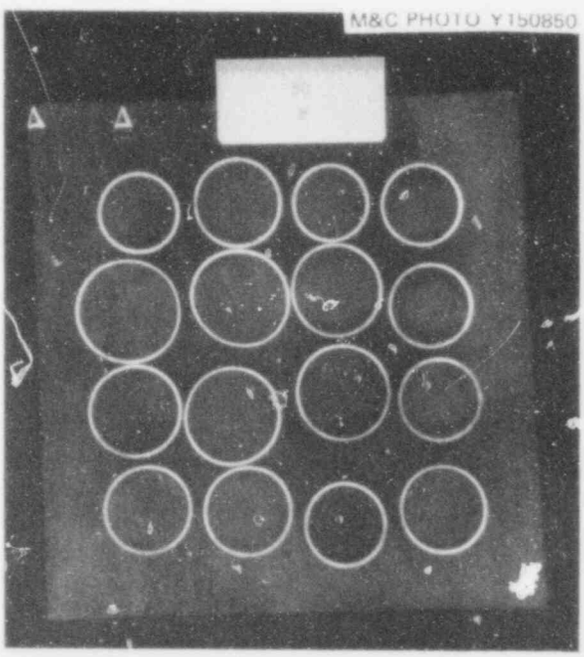

Fig. 67. Section of B-1 at 28.1-cm elevation.

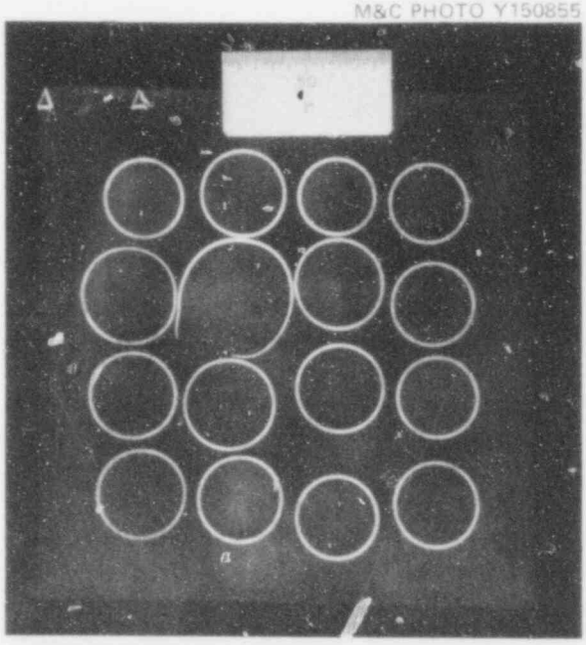

Fig. 68. Section of B-1 at 29.7-cm elevation.

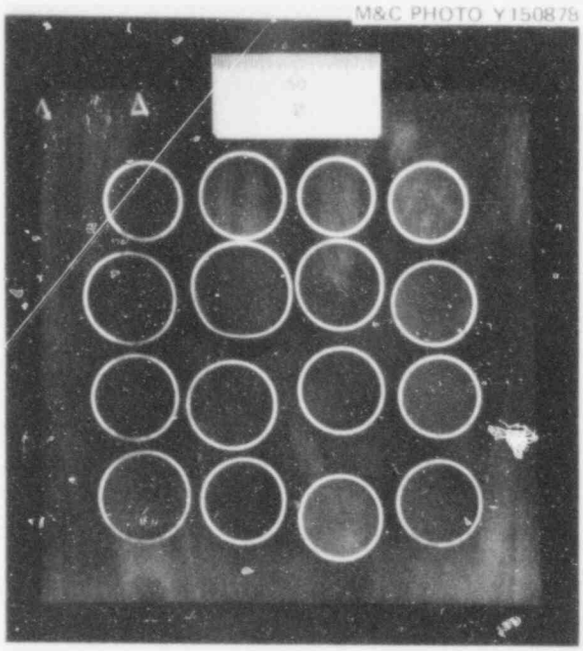

Fig. 69. Section of B-1 at 30.7-cm elevation.

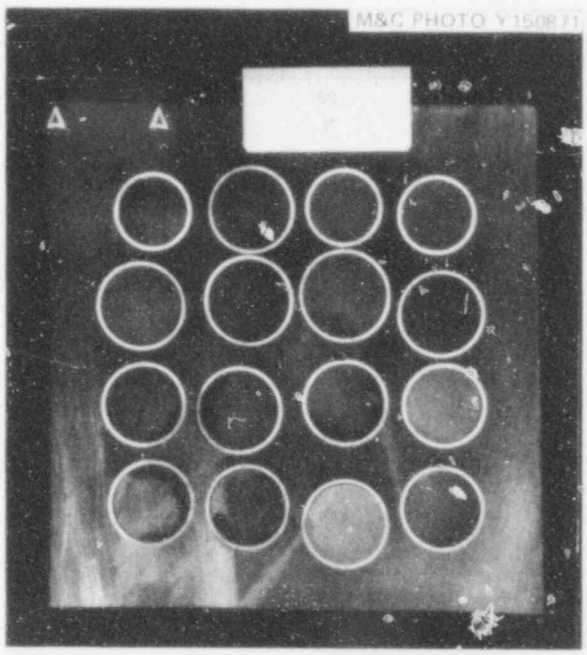

Fig. 70. Section of B-1 at 33.2-cm elevation.

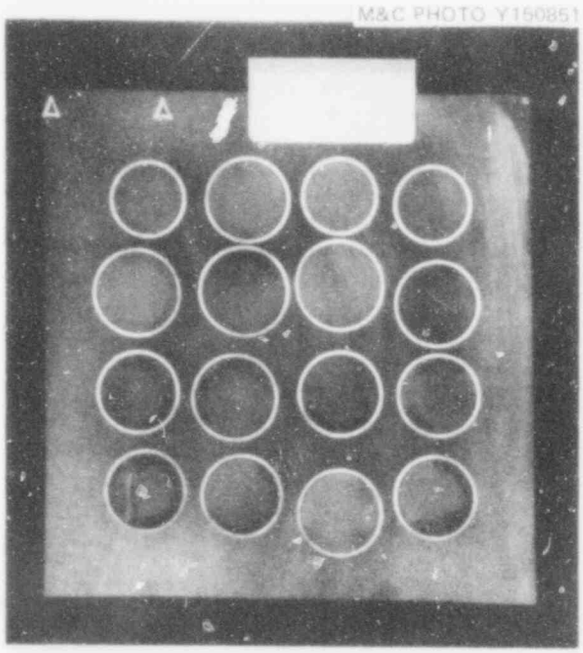

Fig. 71. Section of B-1 at 34.5-cm elevation.

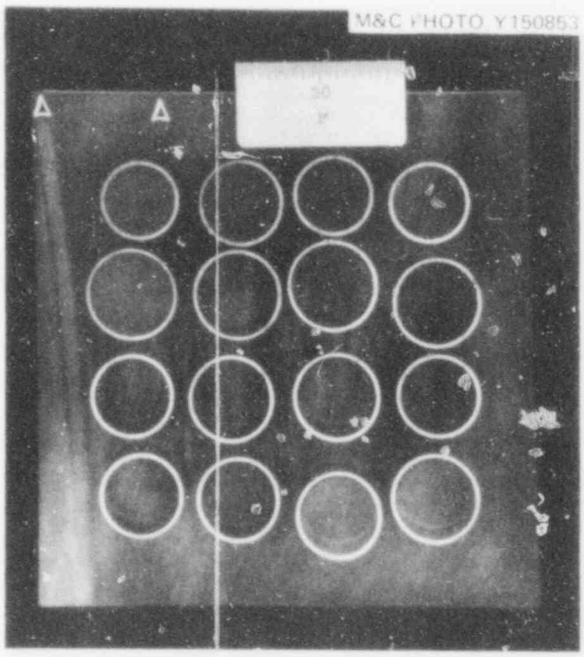

Fig. 72. Section of B-1 at 36.6-cm elevation.

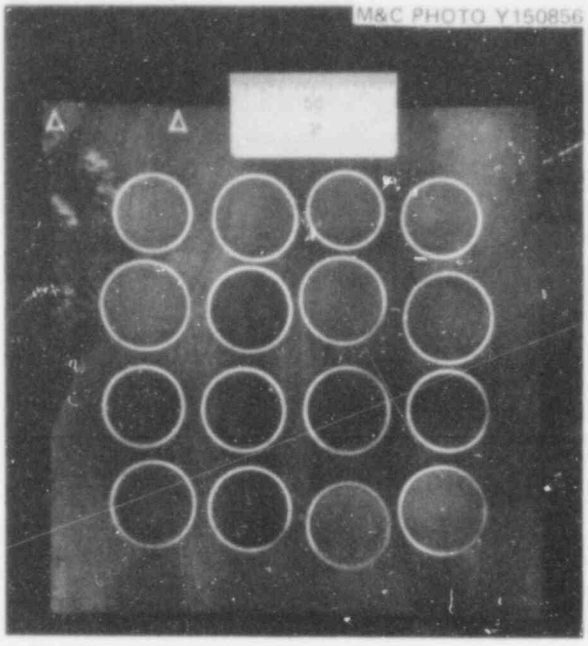

Fig. 73. Section of B-1 at 38.1-cm elevation.

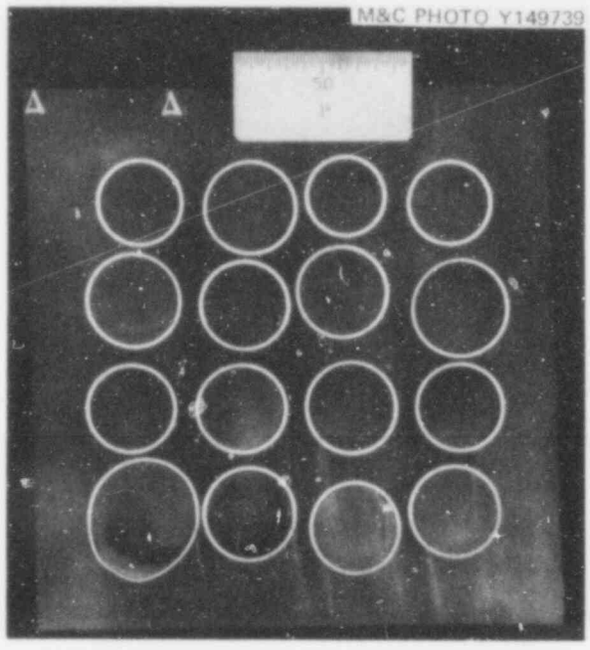

Fig. 74. Section of B-1 at 39.7-cm elevation.

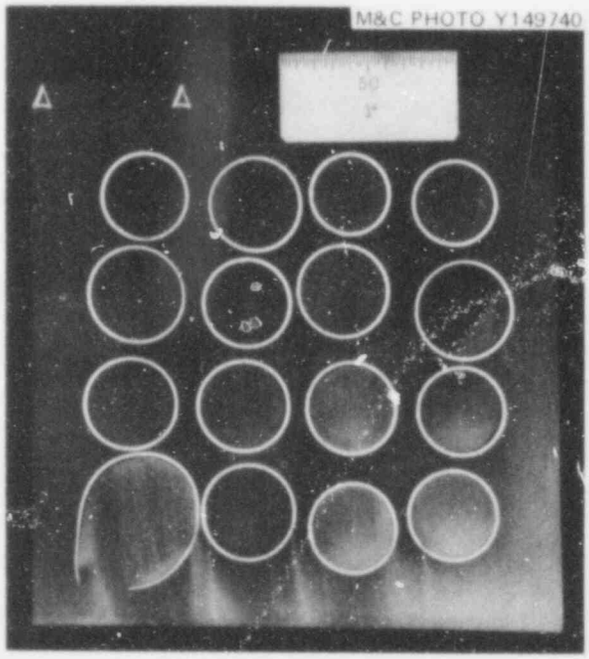

Fig. 75. Section of B-1 at 40.8-cm elevation.

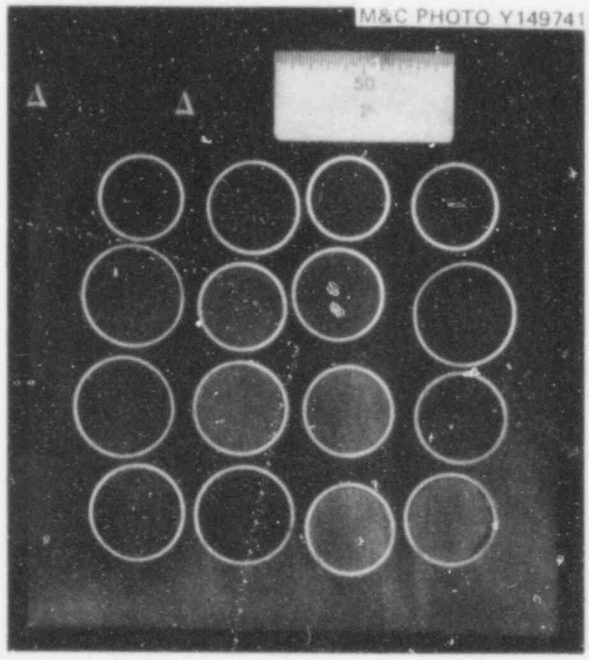

Fig. 76. Section of B-1 at 42.9-cm elevation.

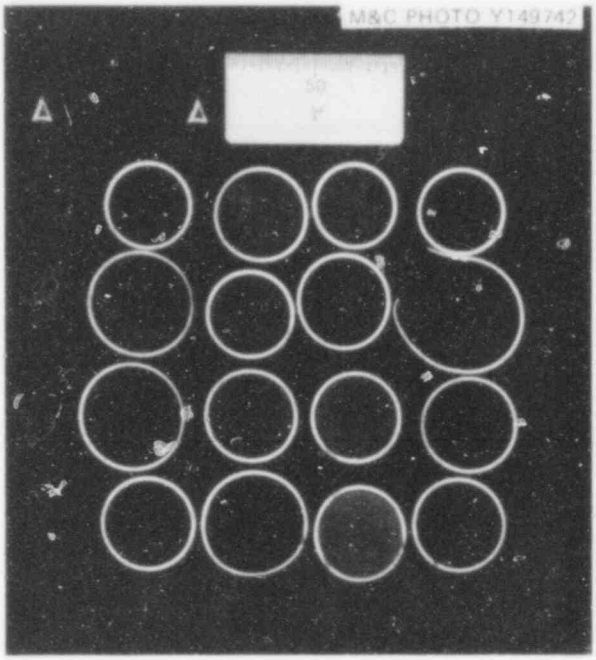

Fig. 77. Section of B-1 at 44.7-cm elevation.

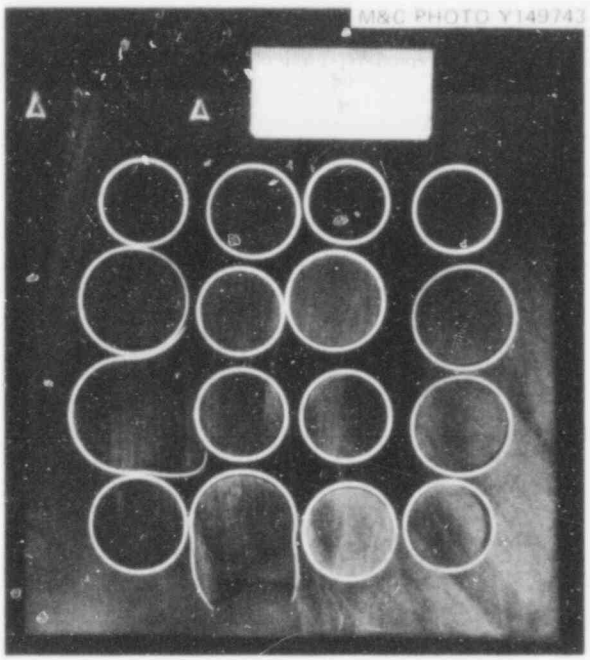

Fig. 78. Section of B-1 at 46.7-cm elevation.

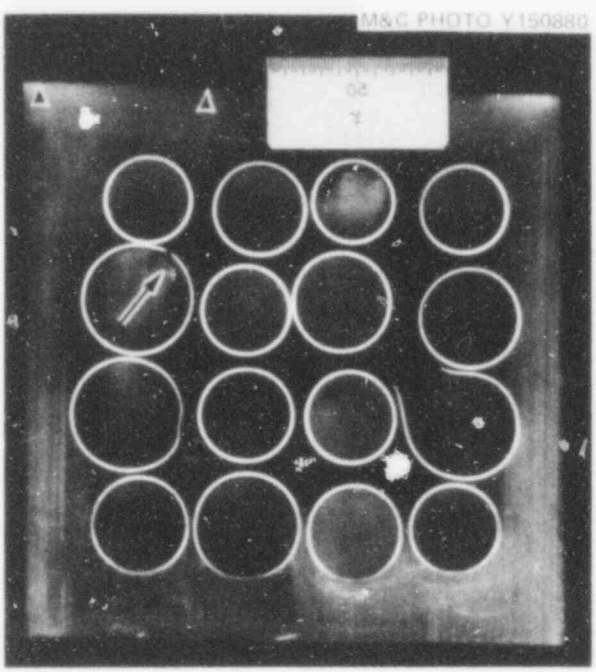

Fig. 79. Section of B-1 at 47.5-cm elevation. (Printed in reverse to show cross section in proper position.)

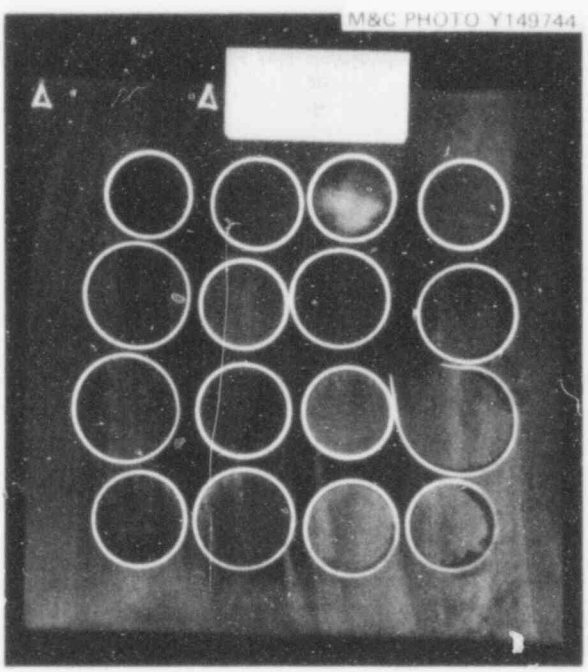

Fig. 80. Section of B-1 at 48.6-cm elevation.

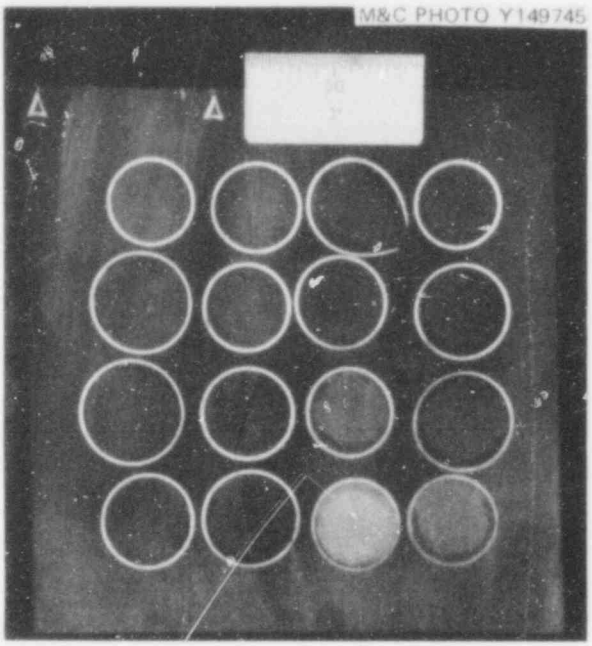

Fig. 81. Section of B-1 at 50.4-cm elevation.

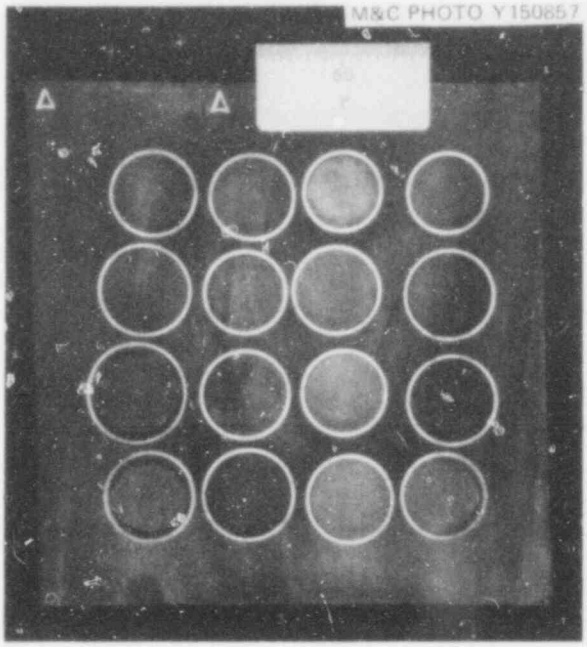

Fig. 82. Section of B-1 at 52.4-cm elevation.

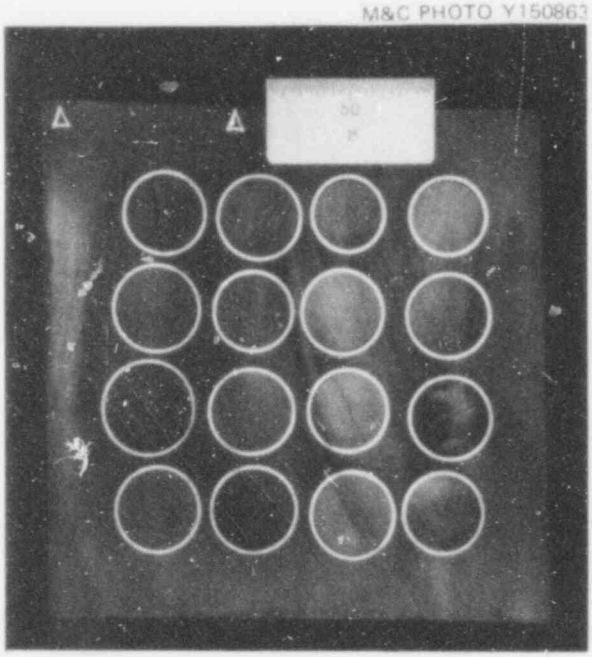

Fig. 83. Section of B-1 at 54.0-cm elevation.

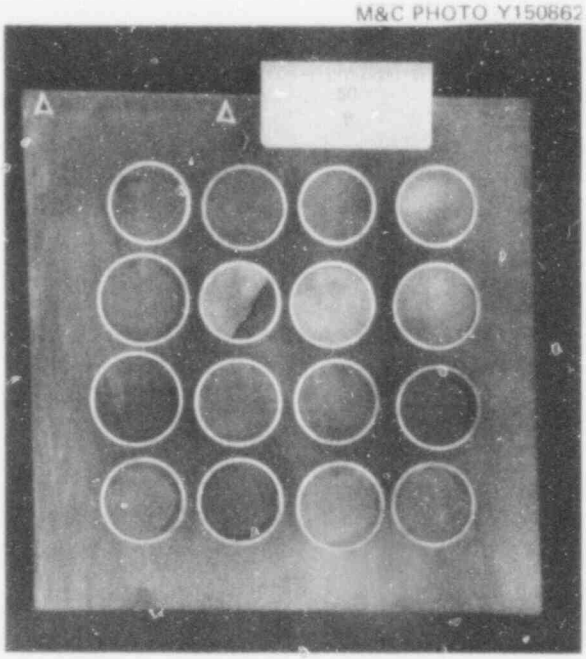

Fig. 84. Section of B-1 at 55.6-cm elevation.

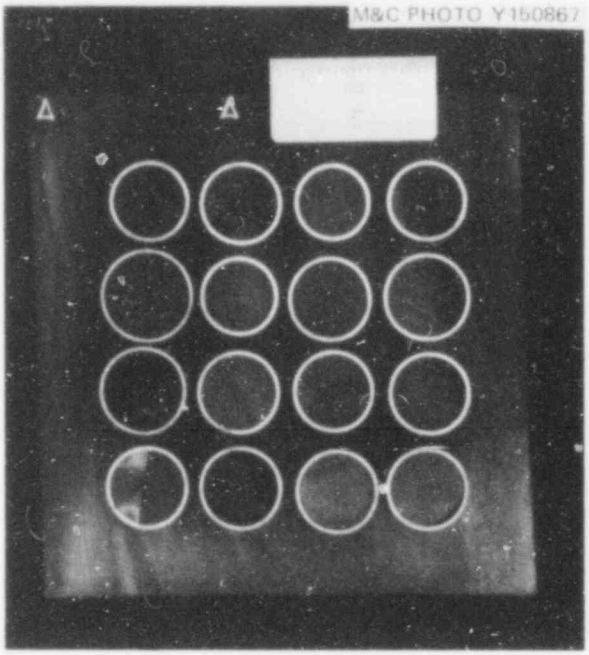

Fig. 85. Section of B-1 at 57.8-cm elevation.

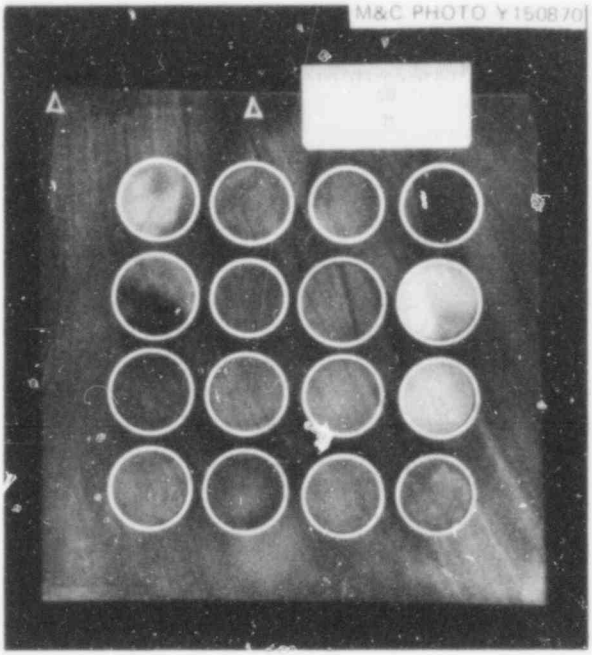

Fig. 86. Section of B-1 at 60.1-cm elevation.

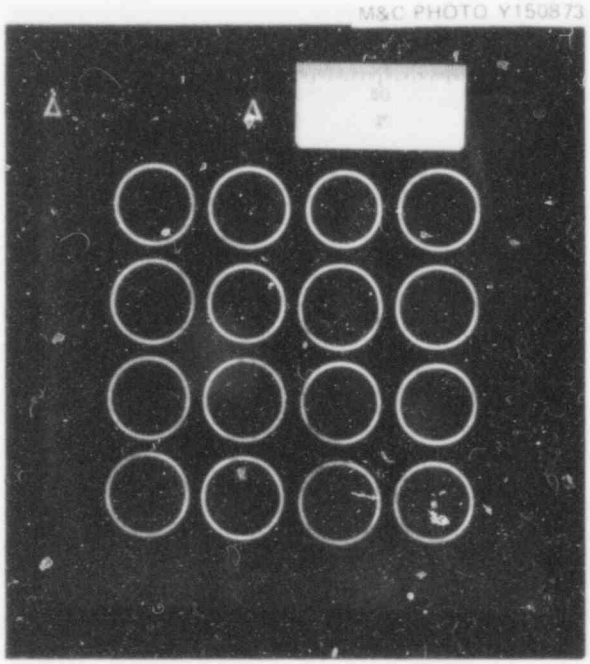

Fig. 87. Section of B-1 at 61.7-cm elevation.

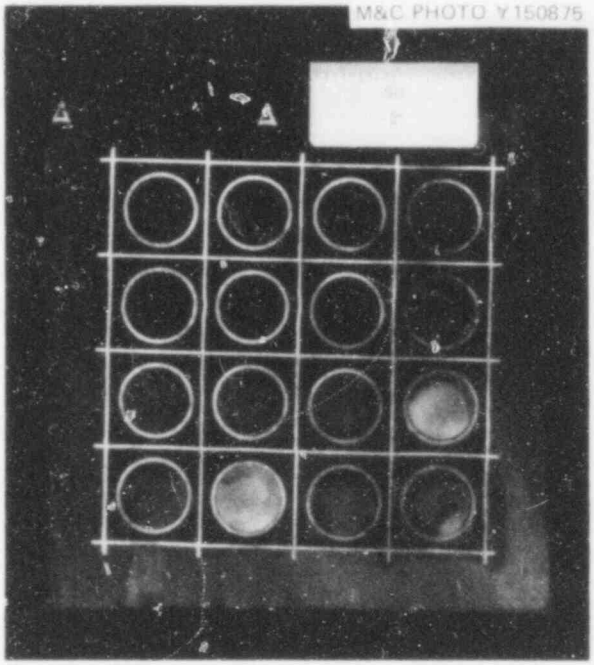

Fig. 88. Section through upper grid of B-1 at 64.1-cm elevation.

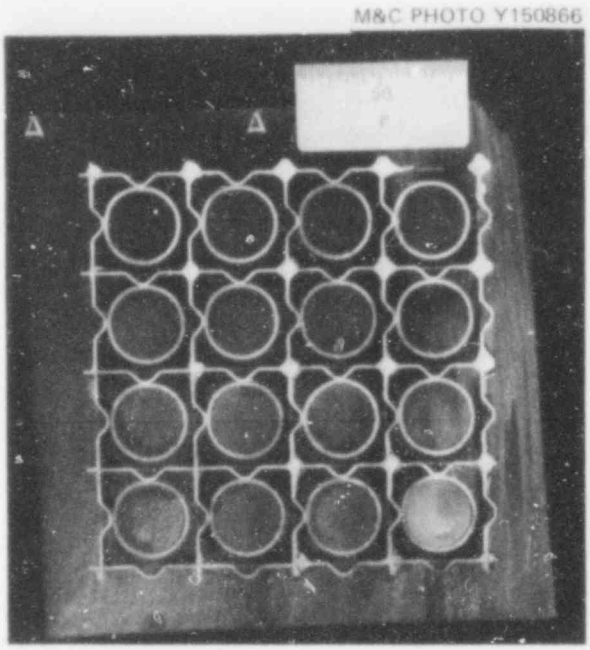

Fig. 89. Section through upper grid of B-1 at 66.9-cm elevation.

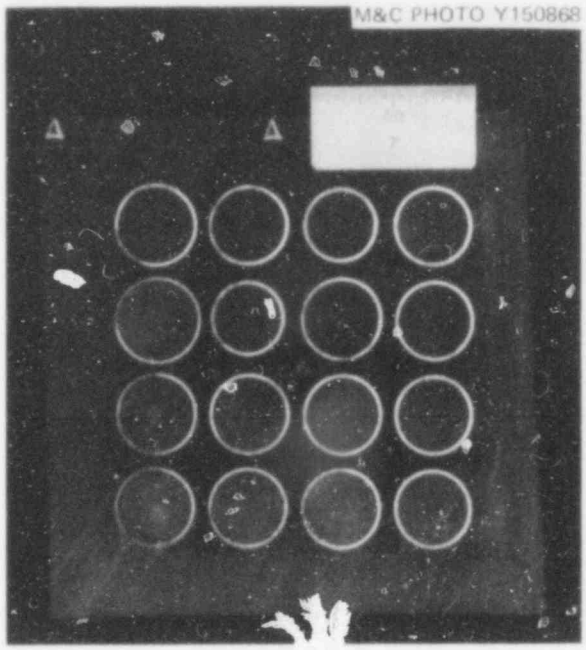

Fig. 90. Section of B-1 at 68.8-cm elevation.

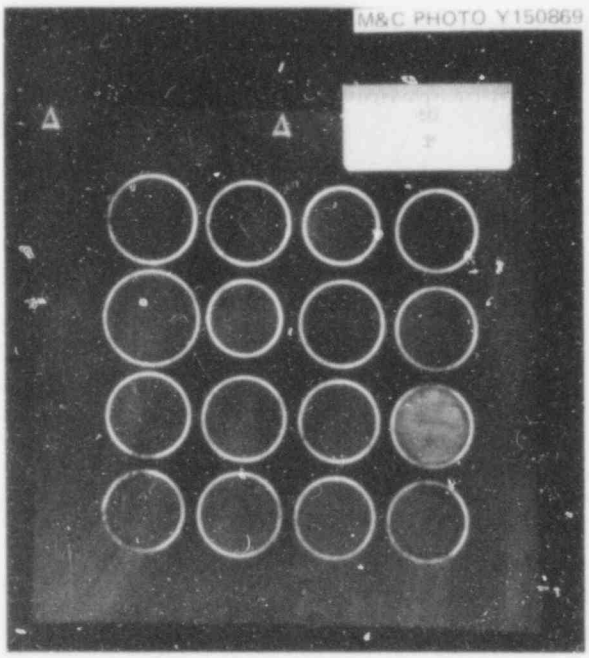

Fig. 91. Section of B-1 at 70.3-cm elevation.

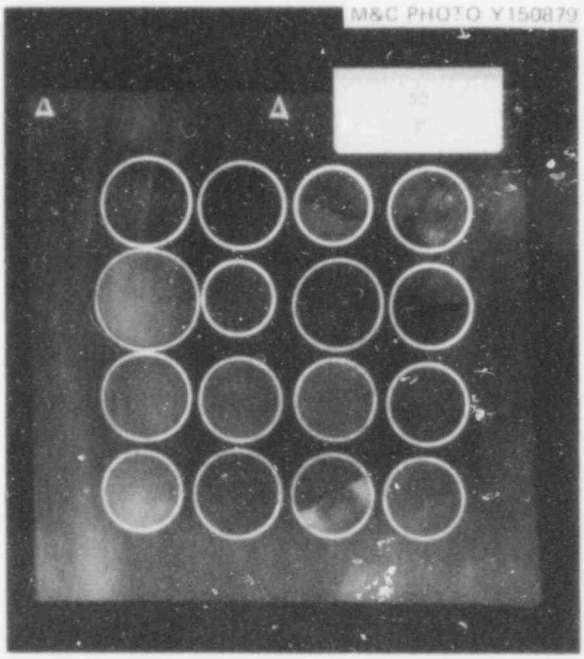

Fig. 92. Section of B-1 at 72.7-cm elevation.

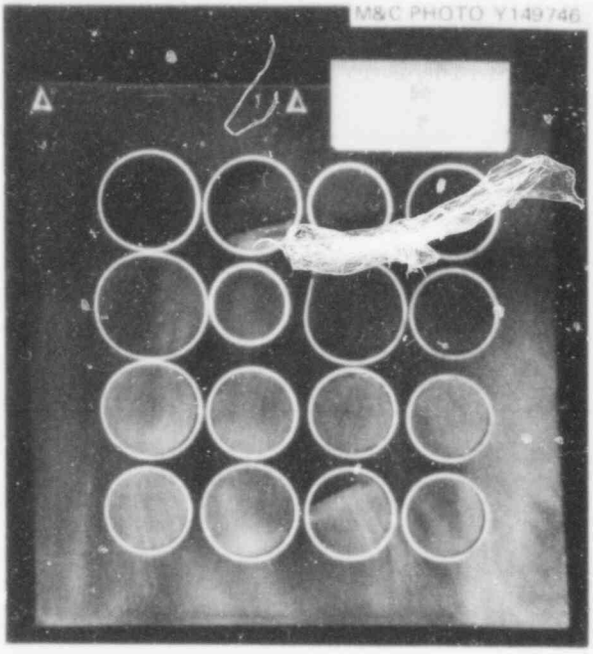

Fig. 93. Section of B-1 at 74.2-cm elevation.

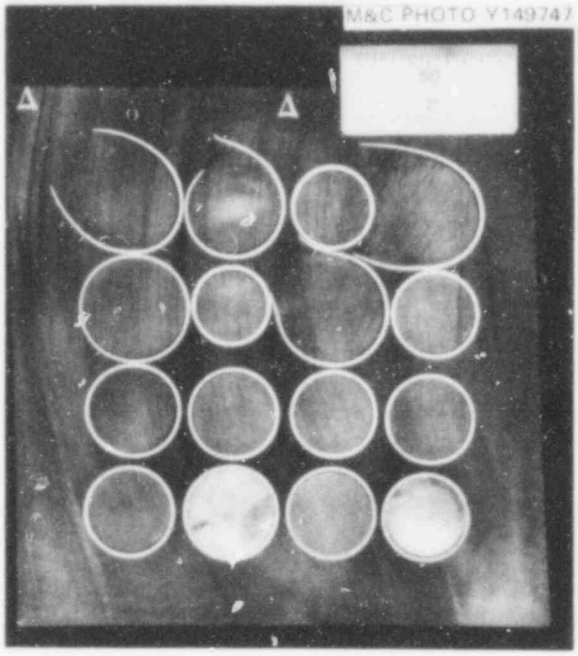

Fig. 94. Section of B-1 at 76.5-cm elevation.

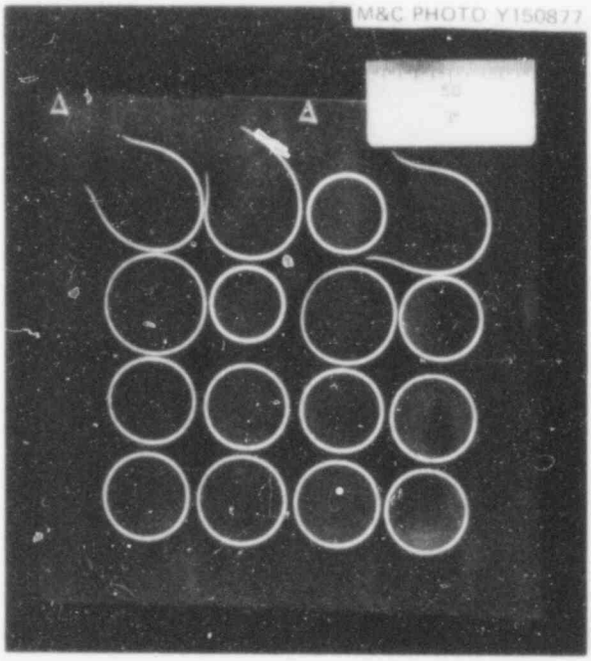

Fig. 95. Section of B-1 at 77.3-cm elevation.

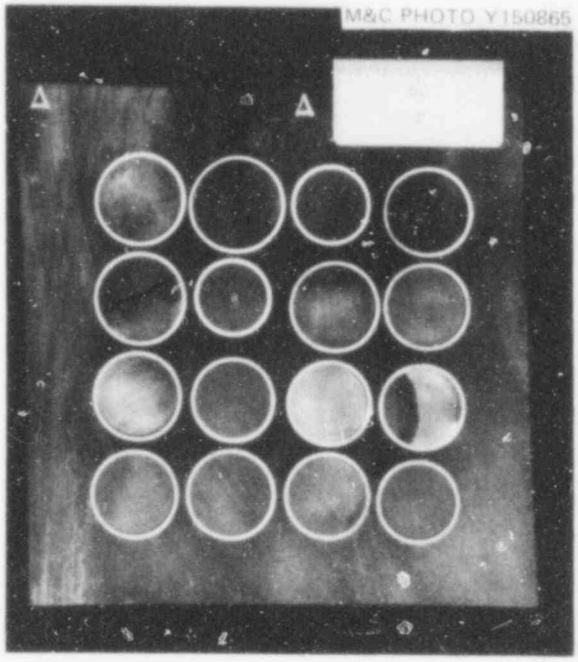

Fig. 96. Section of B-1 at 80.2-cm elevation.

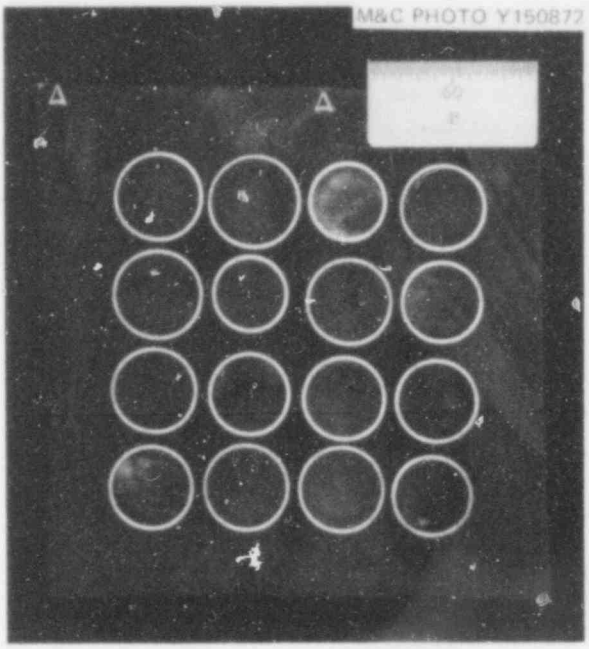

Fig. 97. Section of B-1 at 81.6-cm elevation.

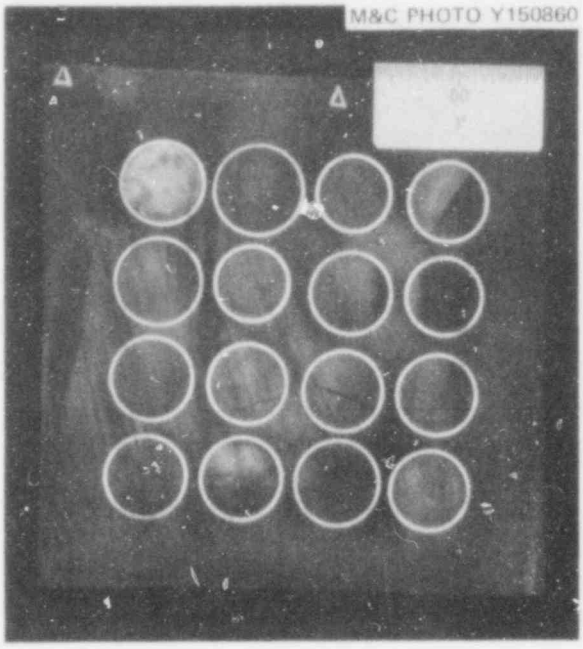

Fig. 98. Section of B-1 at 83.5-cm elevation.

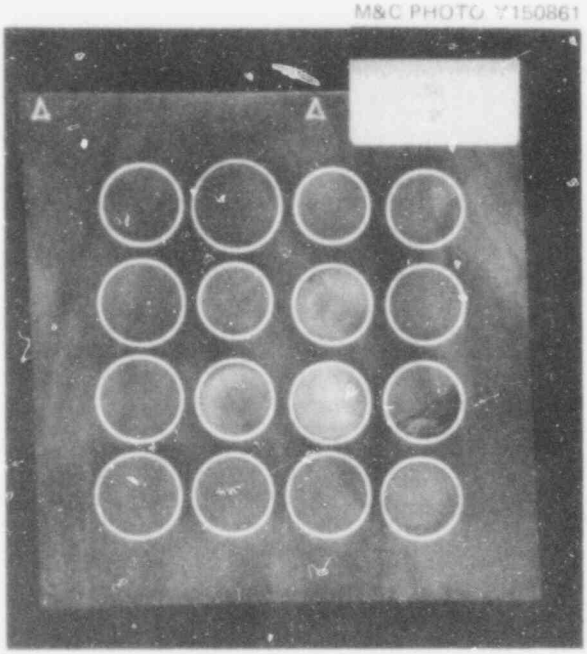

Fig. 99. Section of B-1 at 85.1-cm elevation.

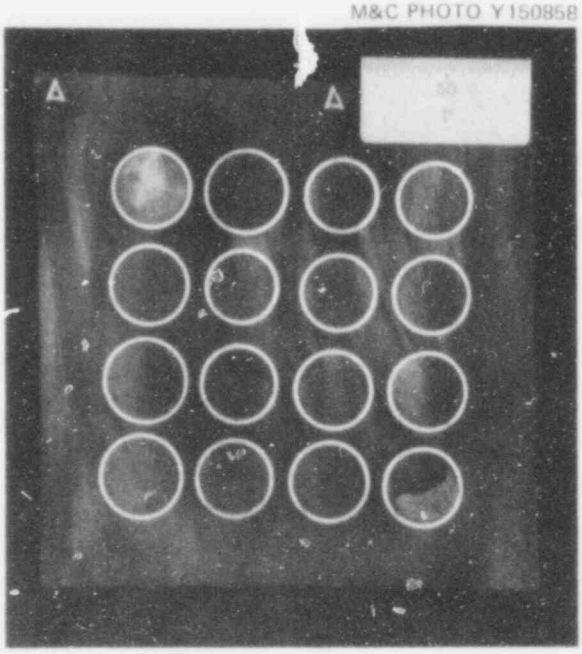

Fig. 100. Section of B-1 at 86.5-cm elevation.

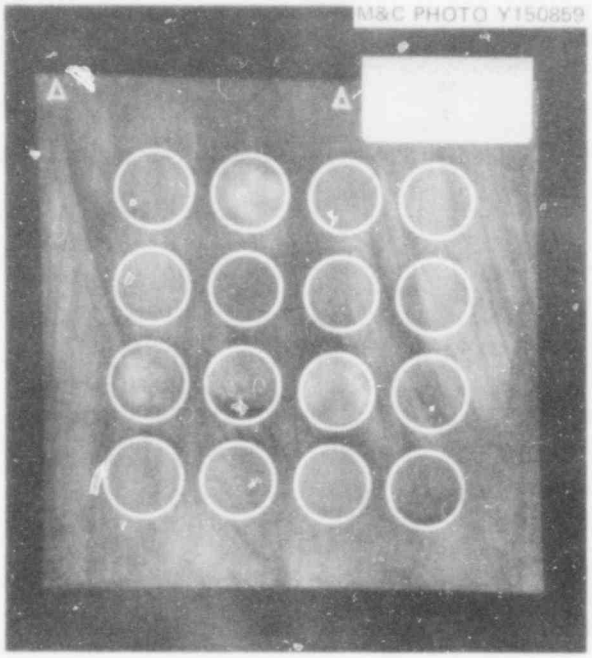

Fig. 101. Section of B-1 at 87.9-cm elevation.

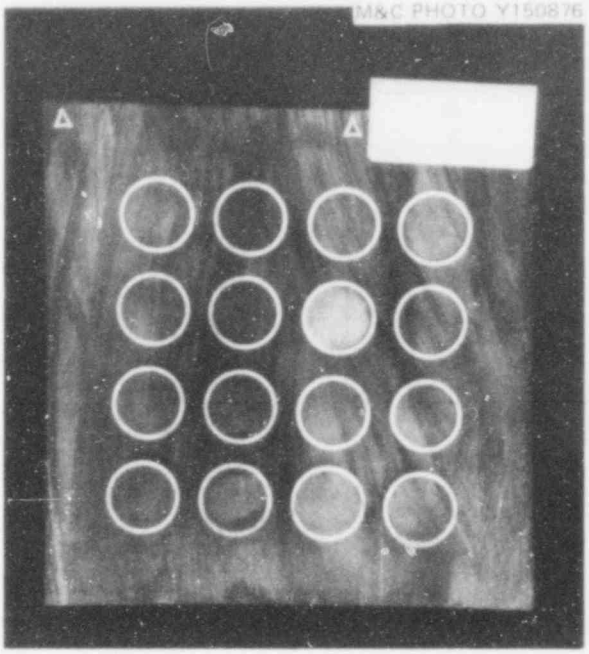

Fig. 102. Section of B-1 at 90.0-cm elevation.

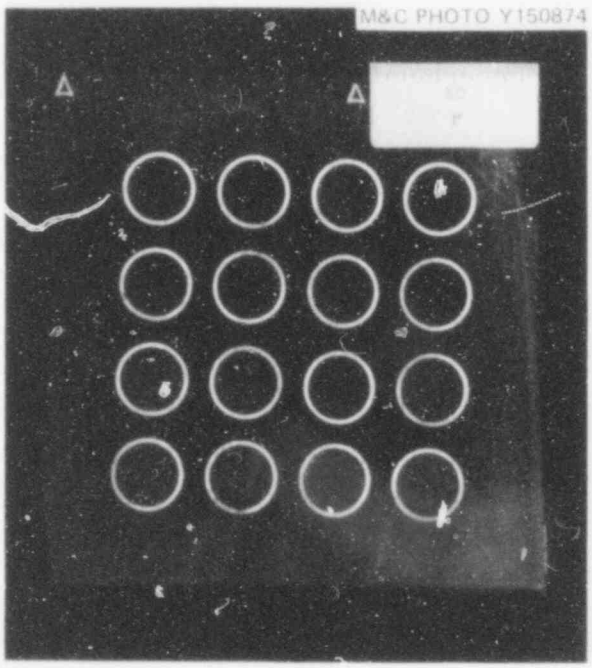

Fig. 103. Section of B-1 at 92.5-cm elevation.

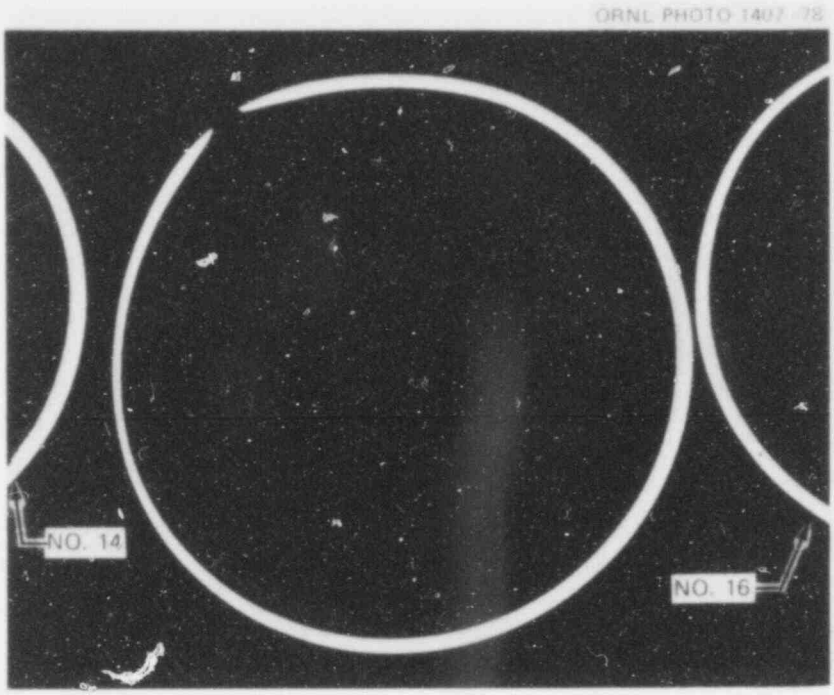

Fig. 104. Enlarged view of tube No. 15 at 20.1-cm elevation showing pinhole burst.

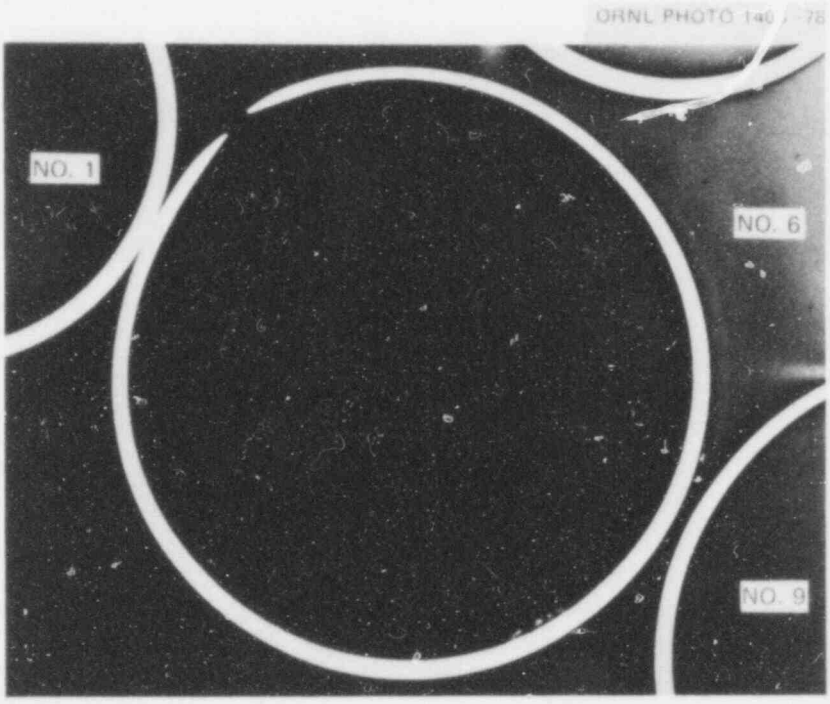

Fig. 105. Enlarged view of tube No. 5 at 47.5-cm elevation showing pinhole burst.

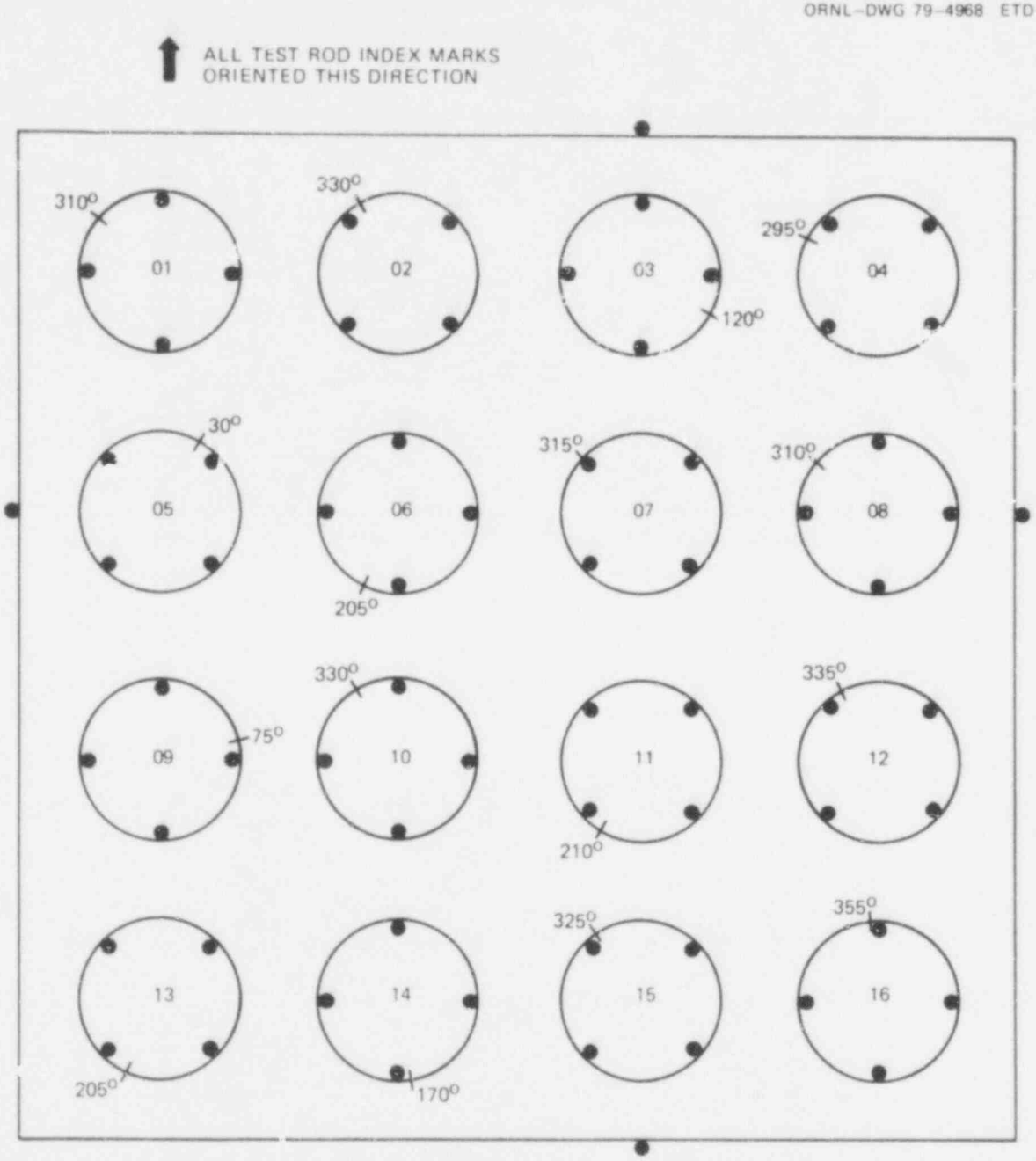

Fig. 106. Approximate burst orientations in B-1 test.

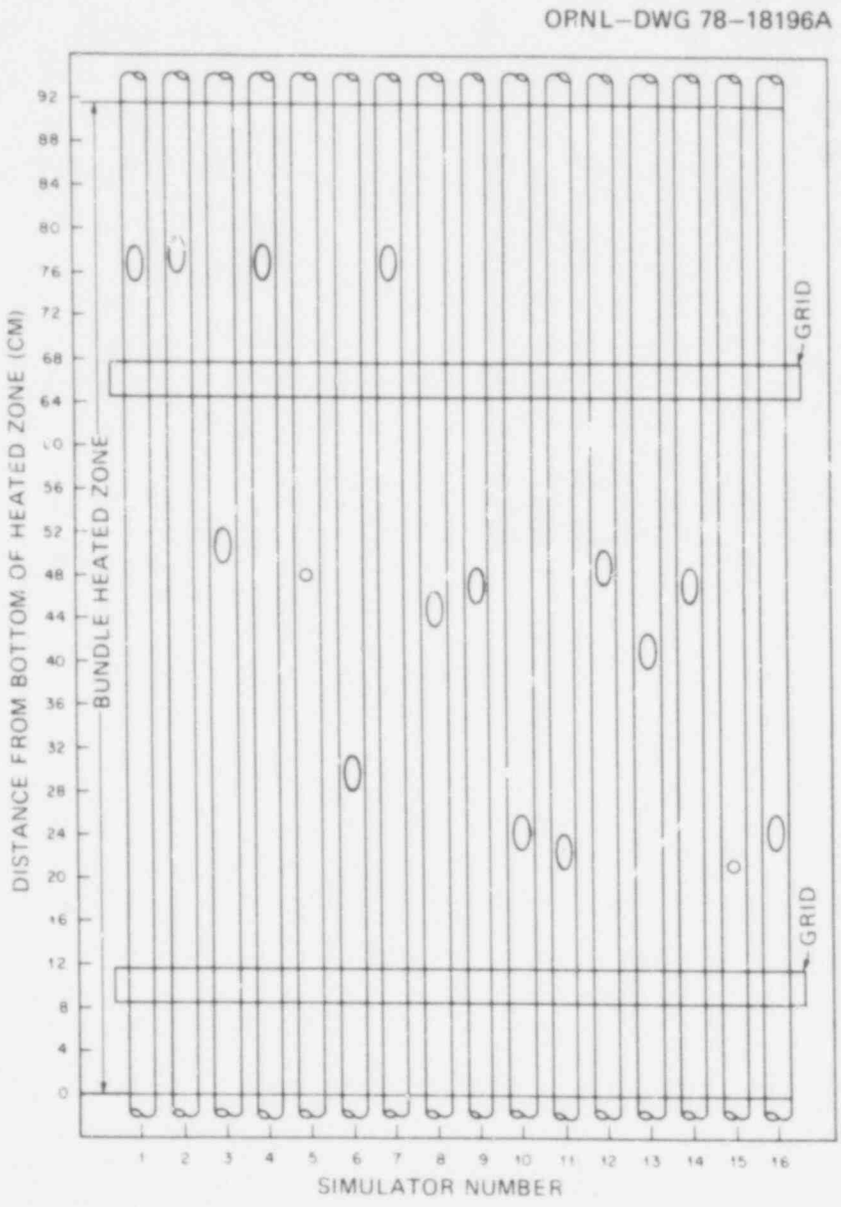

Fig. 107. Axial distribution of bursts in B-1 test.

ORNL-DWG 78-18194A

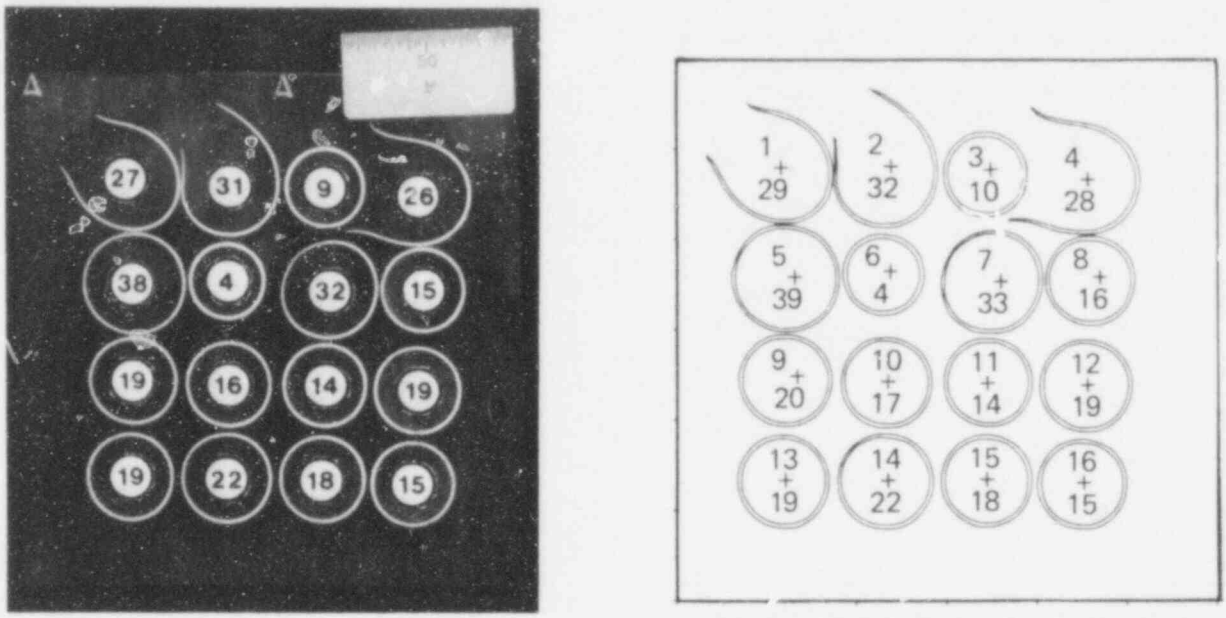

PHOTOGRAPH OF B-1 SECTION AT 77.3-CM ELEVATION

COMPUTER SIMULATION OF B-1 SECTION AT 77.3-CM ELEVATION

Fig. 108. Comparison of computer simulation of cross section with actual cross section.

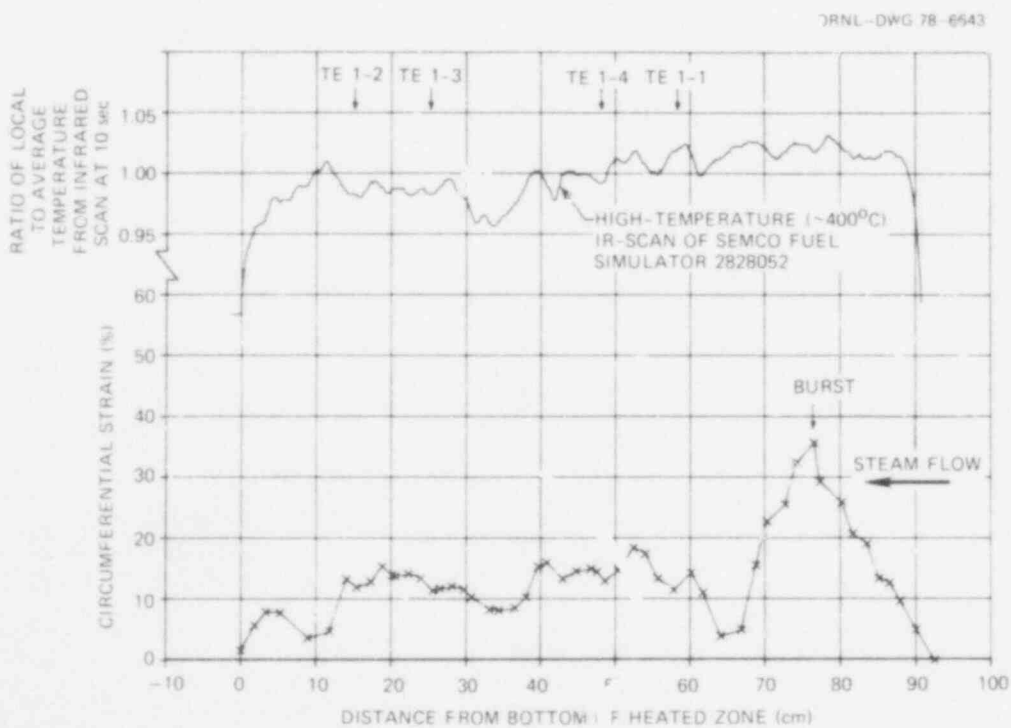

Fig. 109. Deformation profile of tube 1 in B-1 test.

518

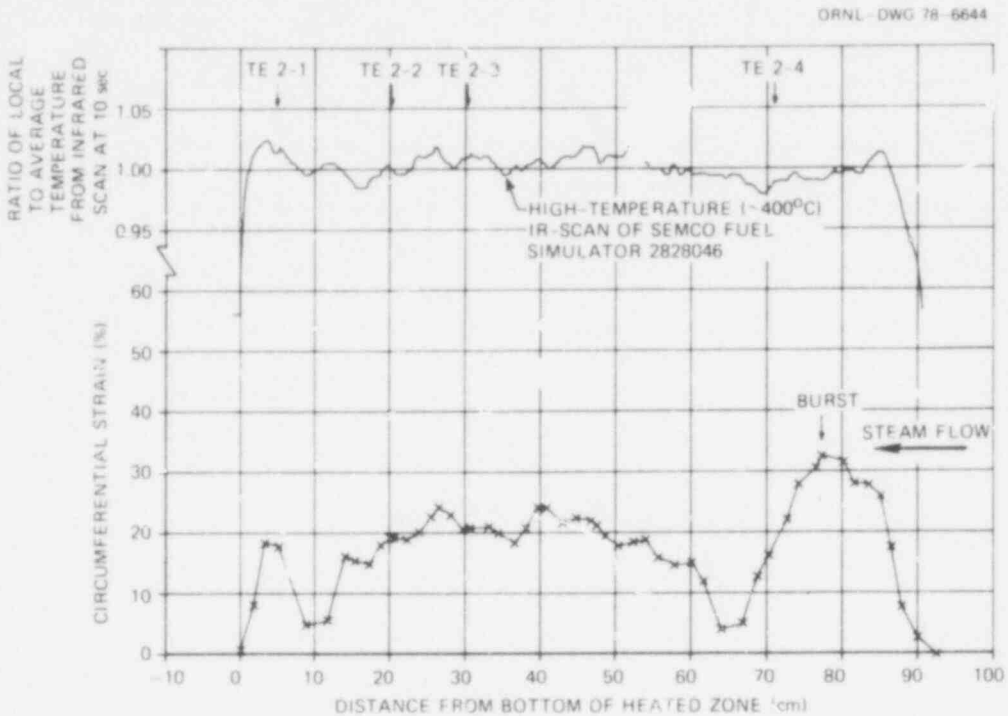

Fig. 110. Deformation profile of tube 2 in B-1 test.

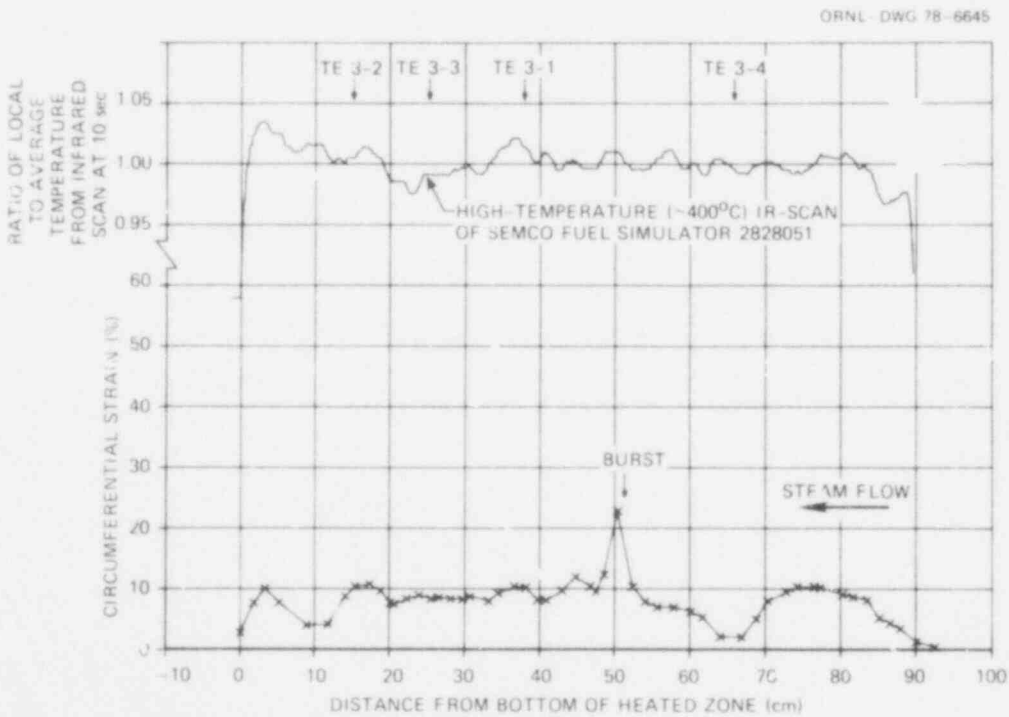

Fig. 111. Deformation profile of tube 3 in B-1 test.

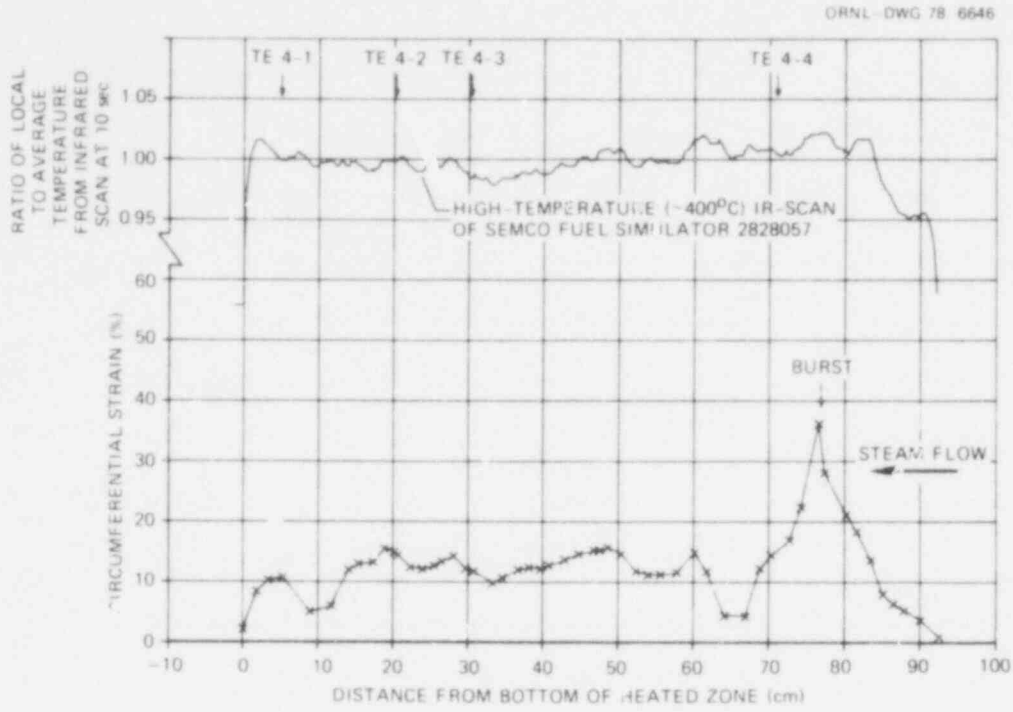

Fig. 112. Deformation profile of tube 4 in B-1 test.

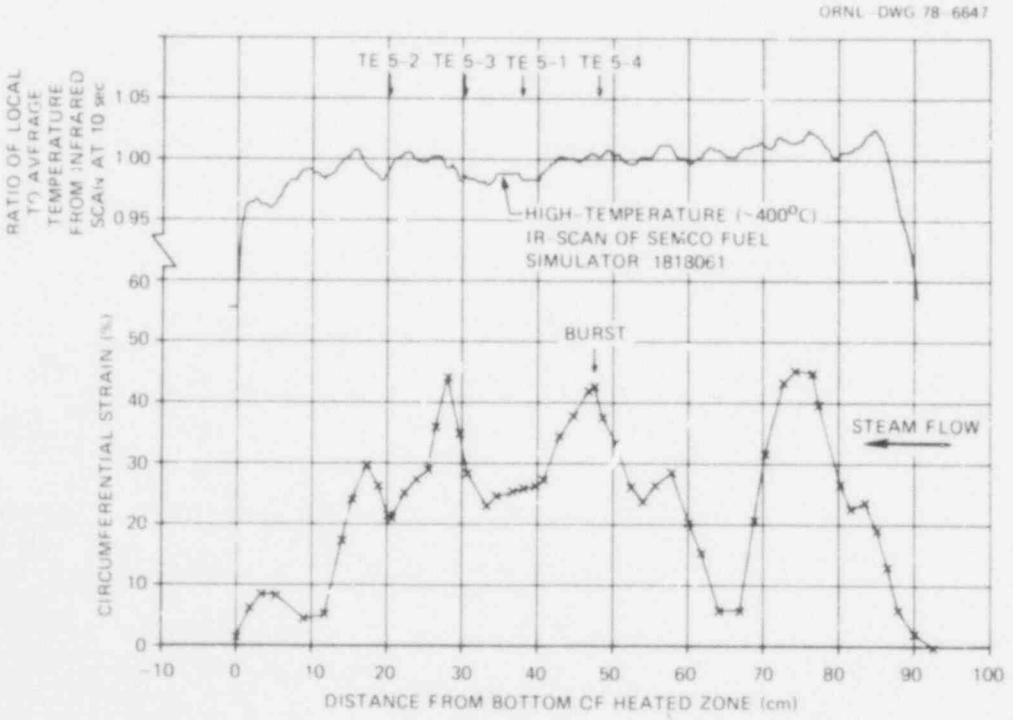

Fig. 113. Deformation profile of tube 5 in B-1 test.

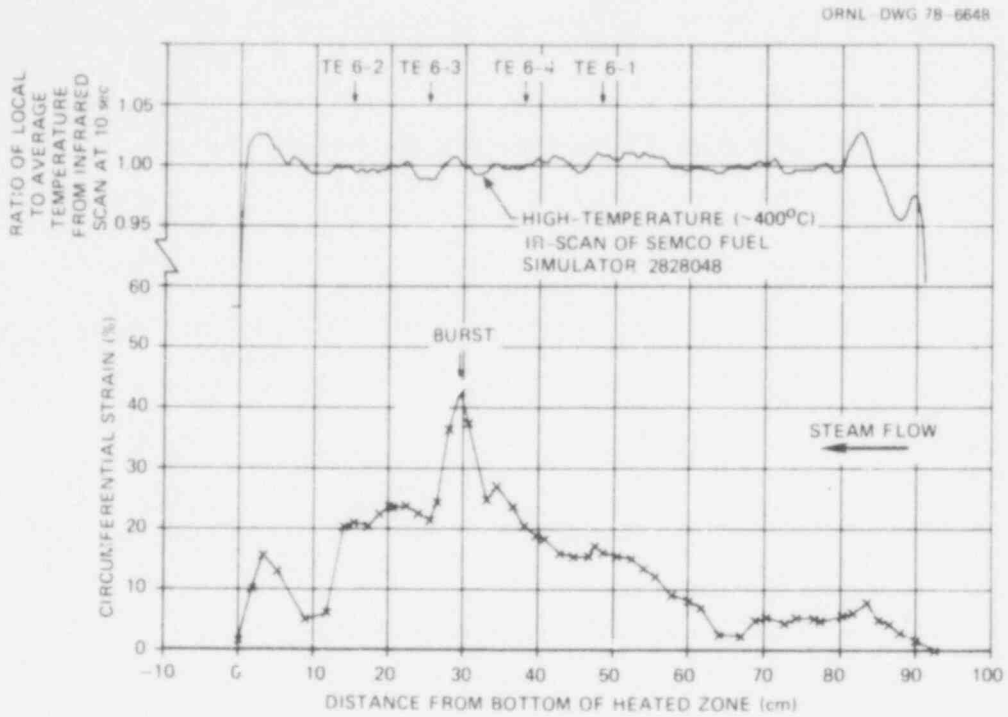

Fig. 114. Deformation profile of tube 6 in B-1 test.

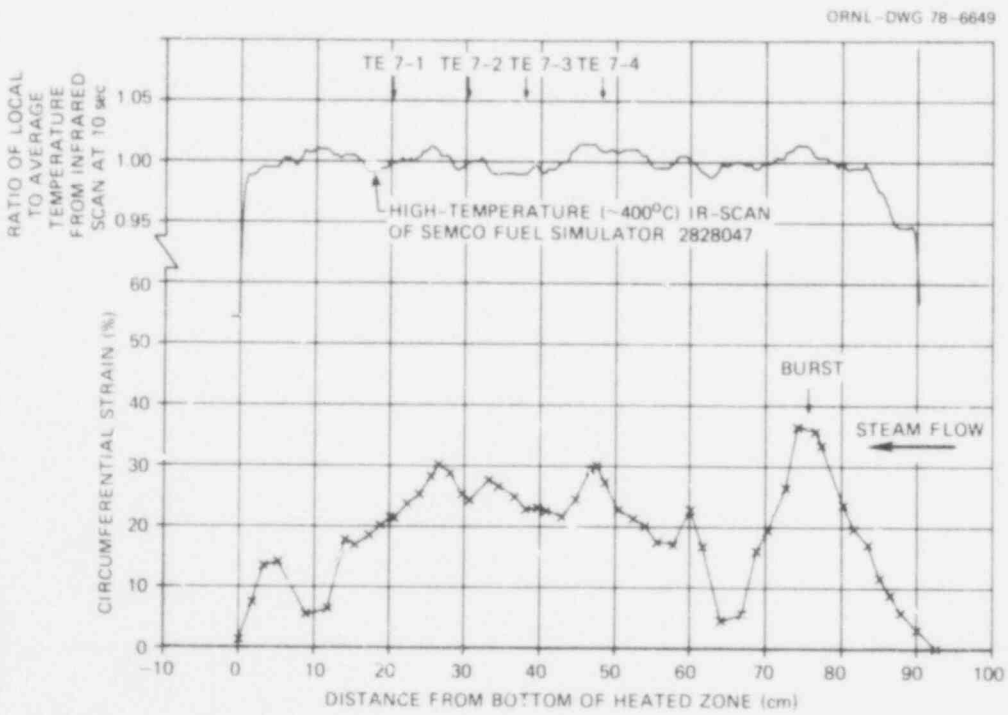

Fig. 115. Deformation profile of tube 7 in B-1 test.

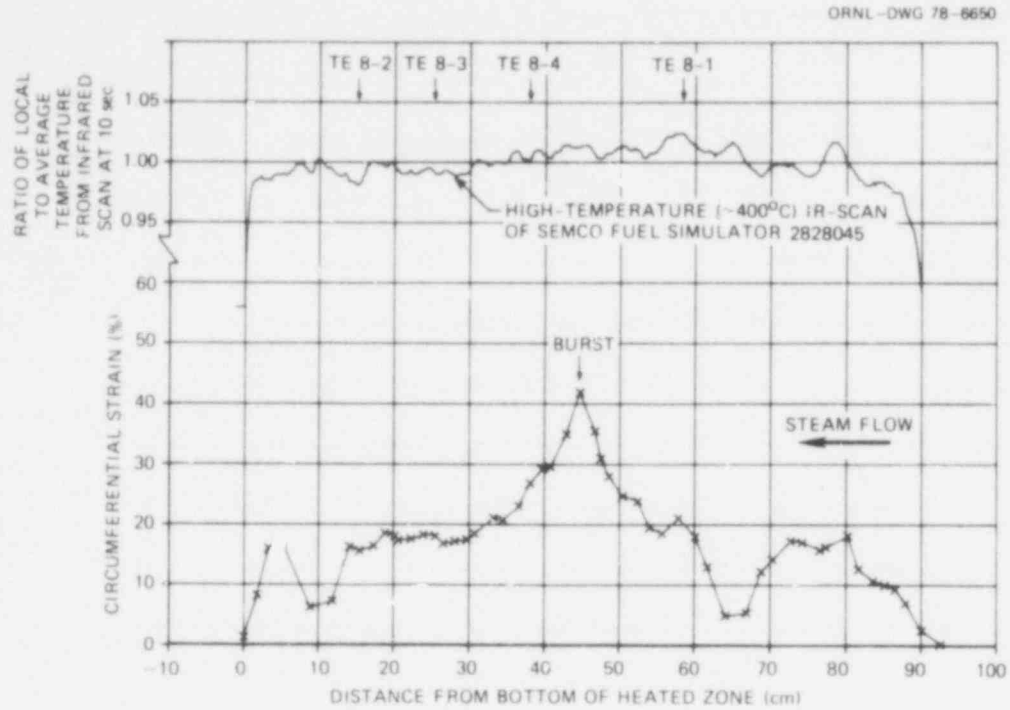

Fig. 116. Deformation profile of tube 8 in B-1 test.

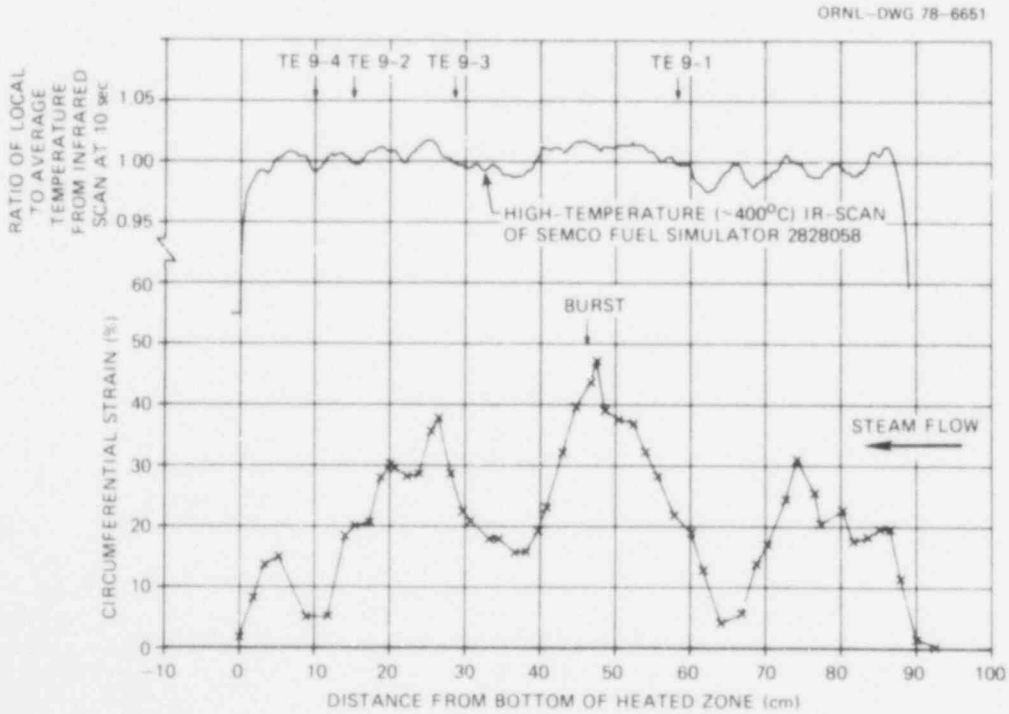

Fig. 117. Deformation profile of tube 9 in B-1 test.

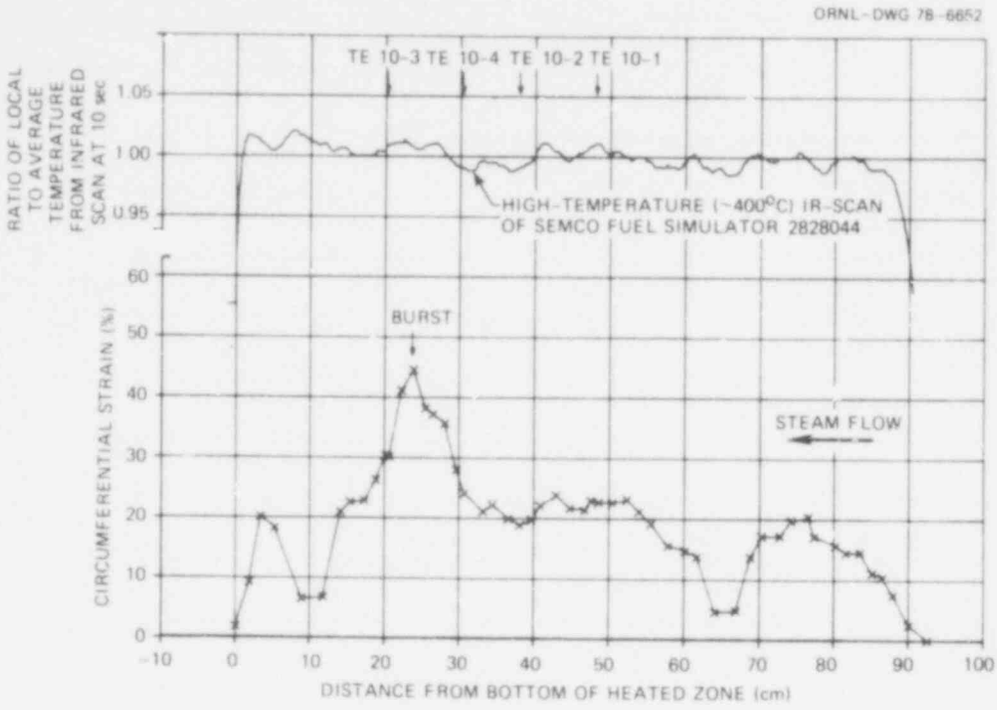

Fig. 118. Deformation profile of tube 10 in B-1 test.

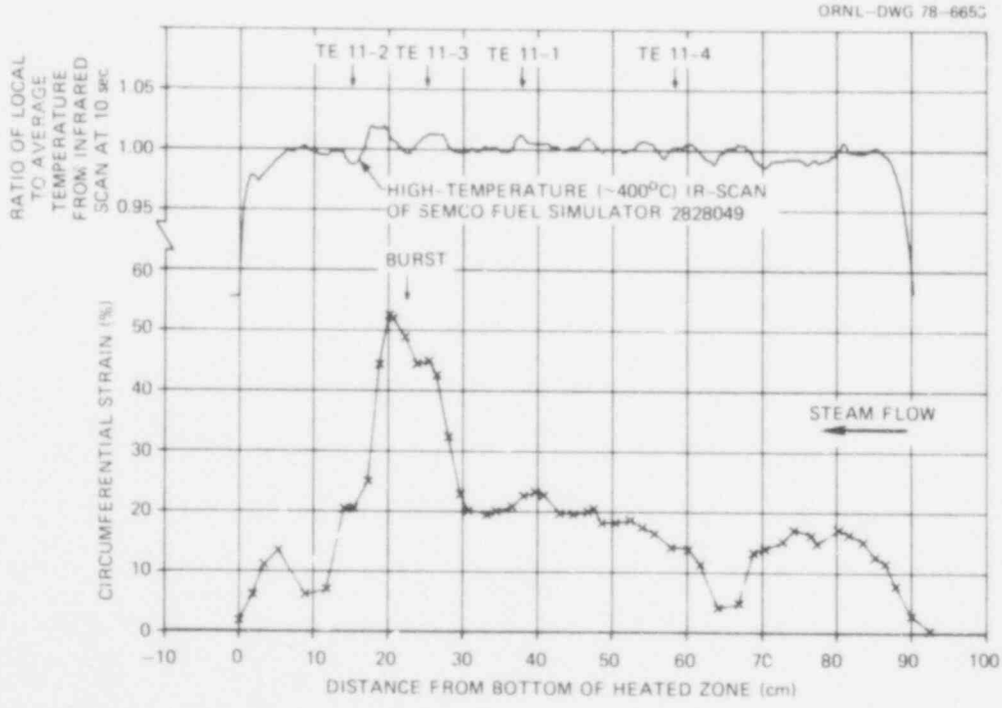

Fig. 119. Deformation profile of tube 11 in B-1 test.

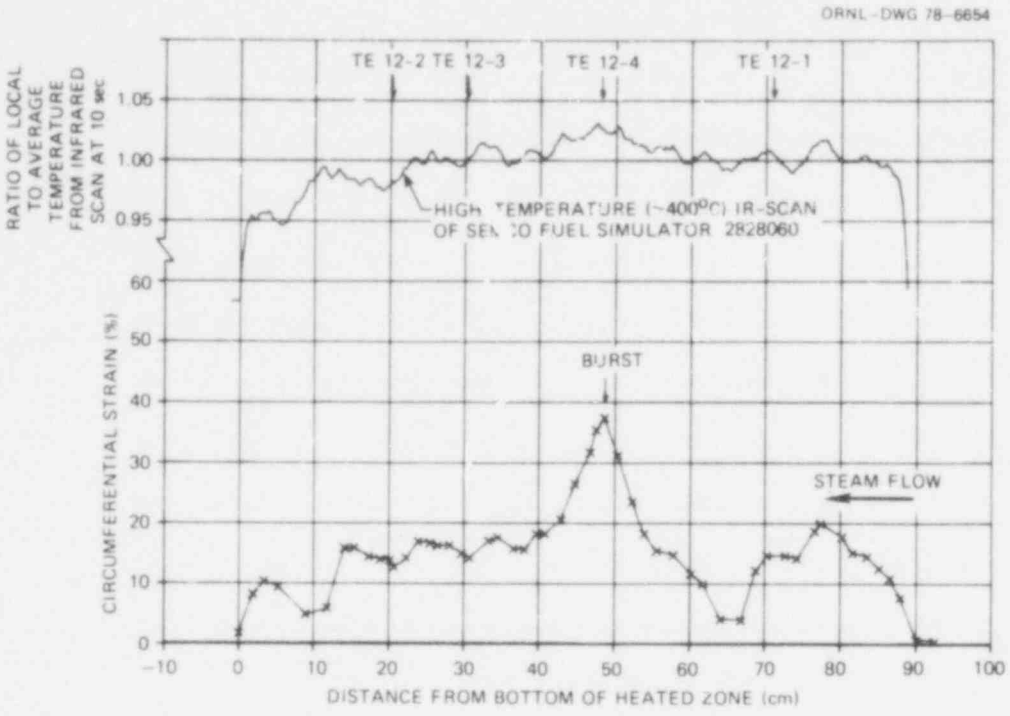

Fig. 120. Deformation profile of tube 12 in B-1 test.

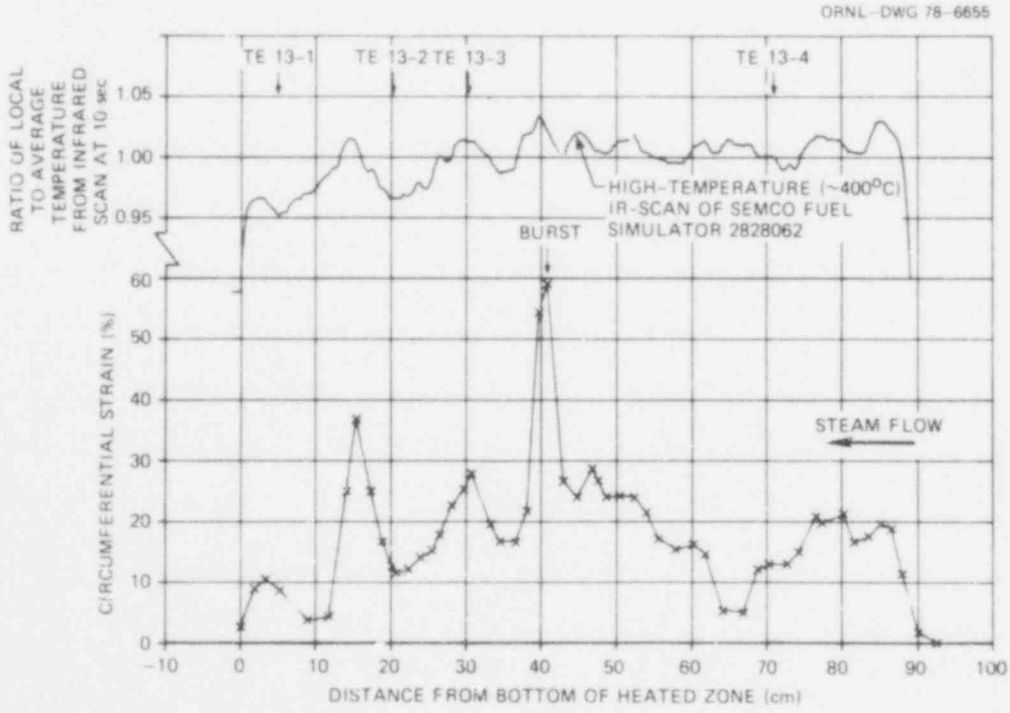

Fig. 121. Deformation profile of tube 13 in B-1 test.

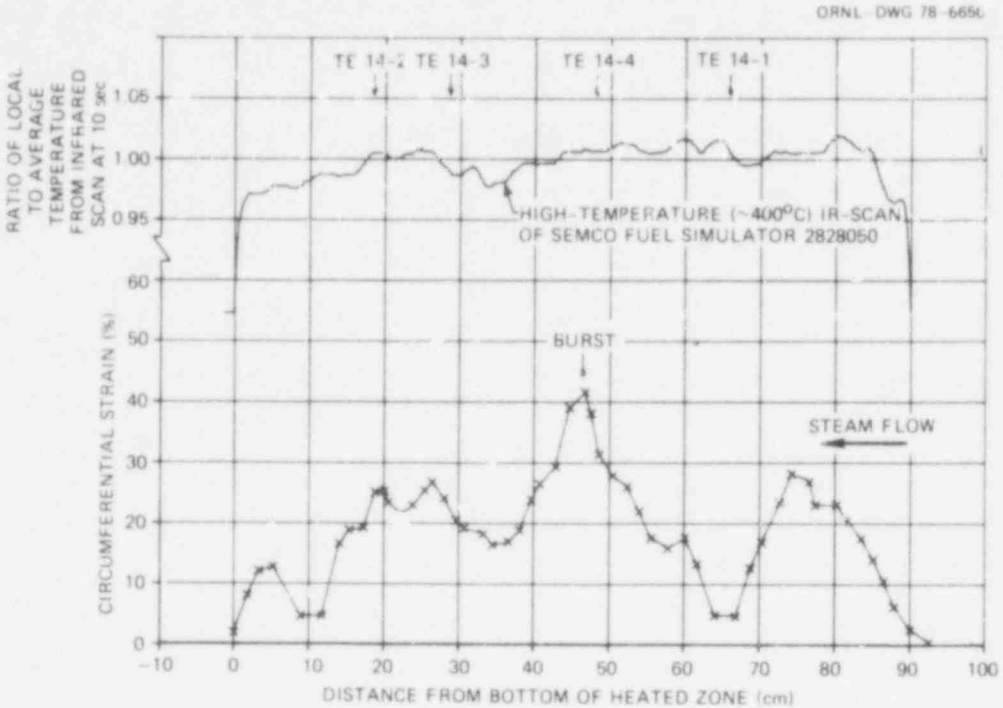

Fig. 122. Deformation profile of tube 14 in B-1 test.

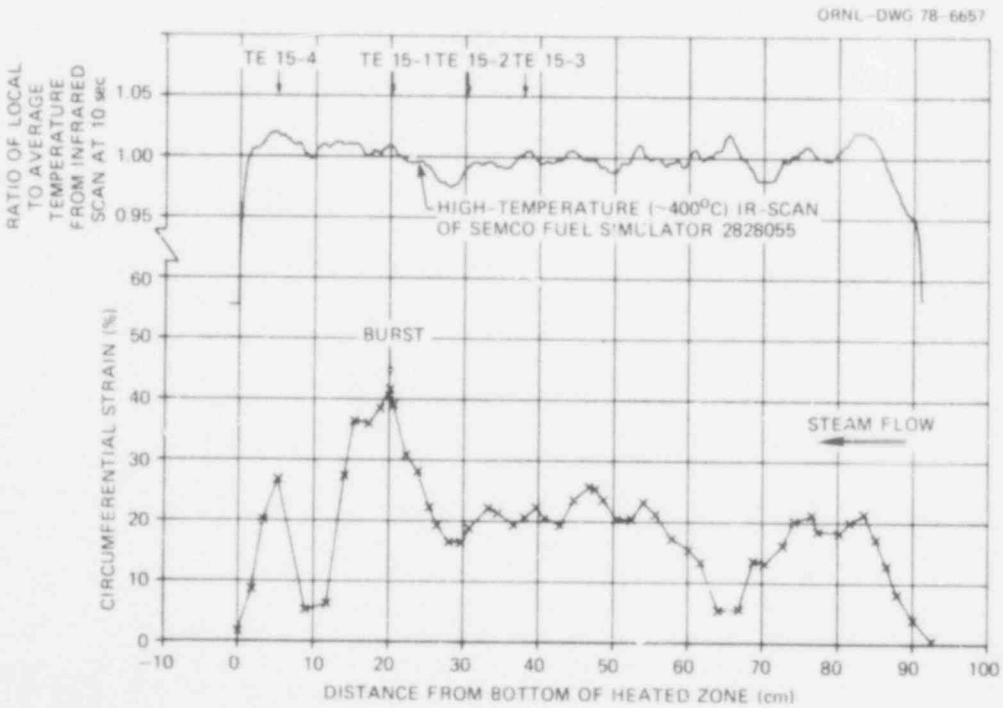

Fig. 123. Deformation profile of tube 15 in B-1 test.

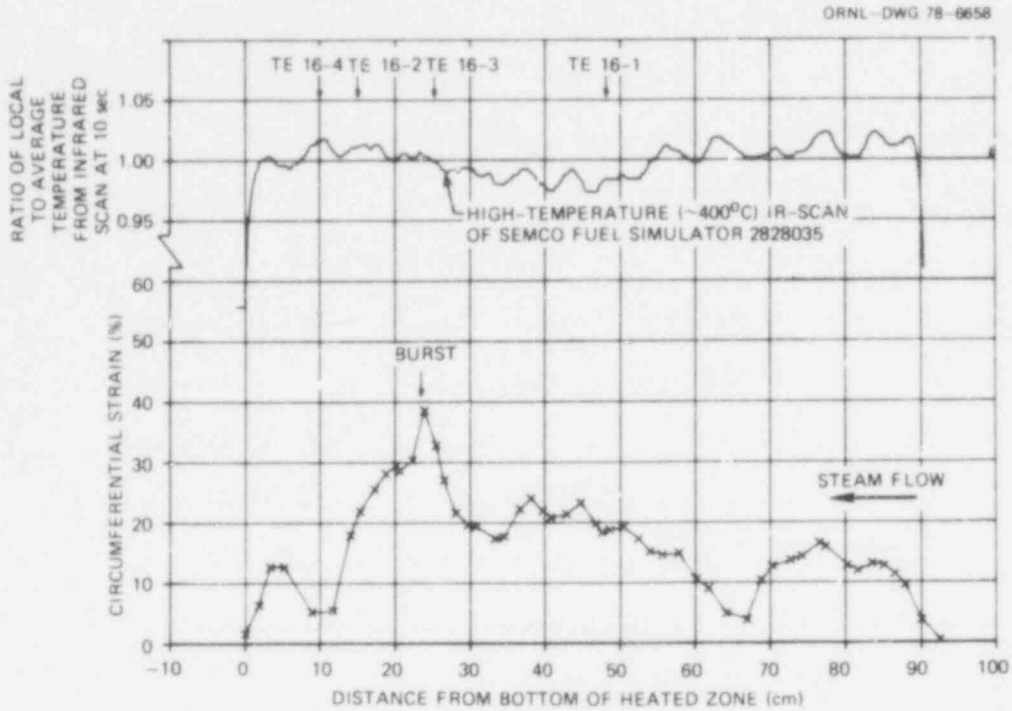

Fig. 124. Deformation profile of tube 16 in B-1 test.

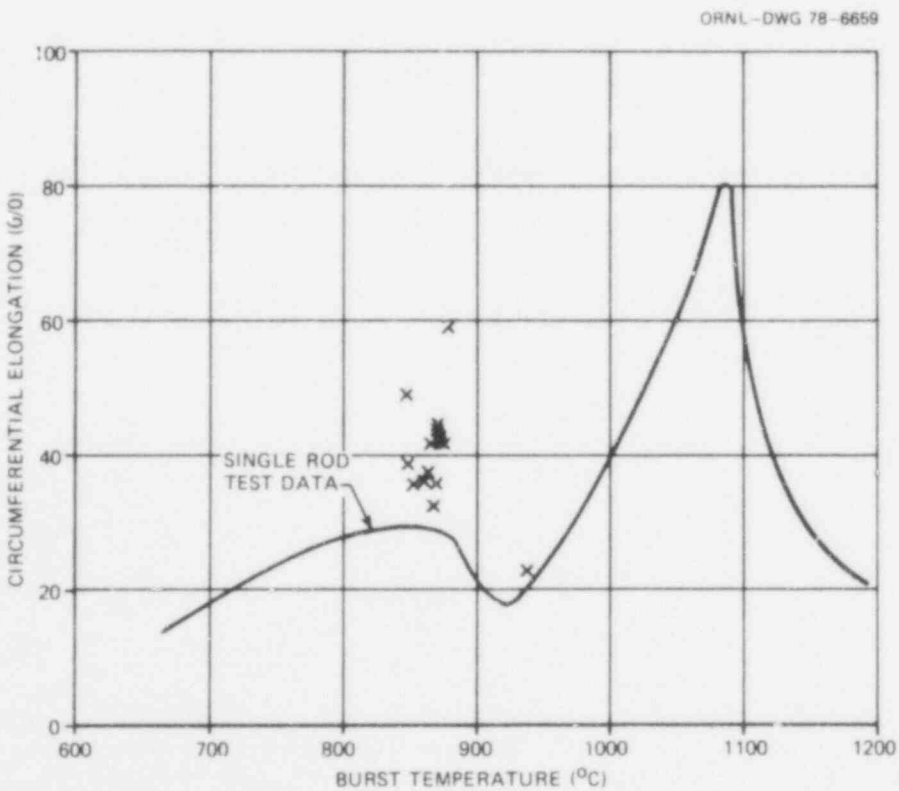

Fig. 125. Comparison of burst strains in B-1 test with single-rod test data.

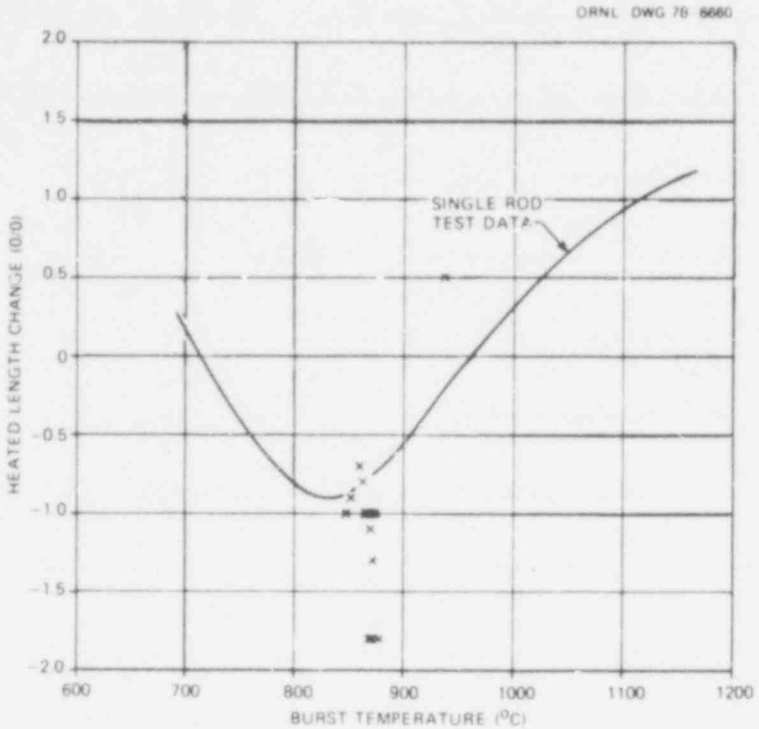

Fig. 126. Comparison of tube axial shrinkage in B-1 test with single-rod test data.

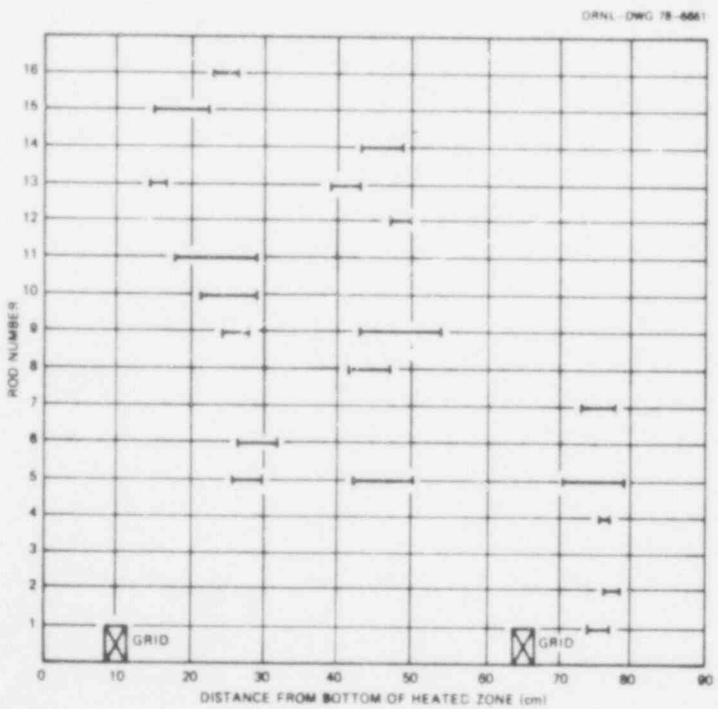

Fig. 127. Portions of tubes with greater than 32% strain in B-1 test.

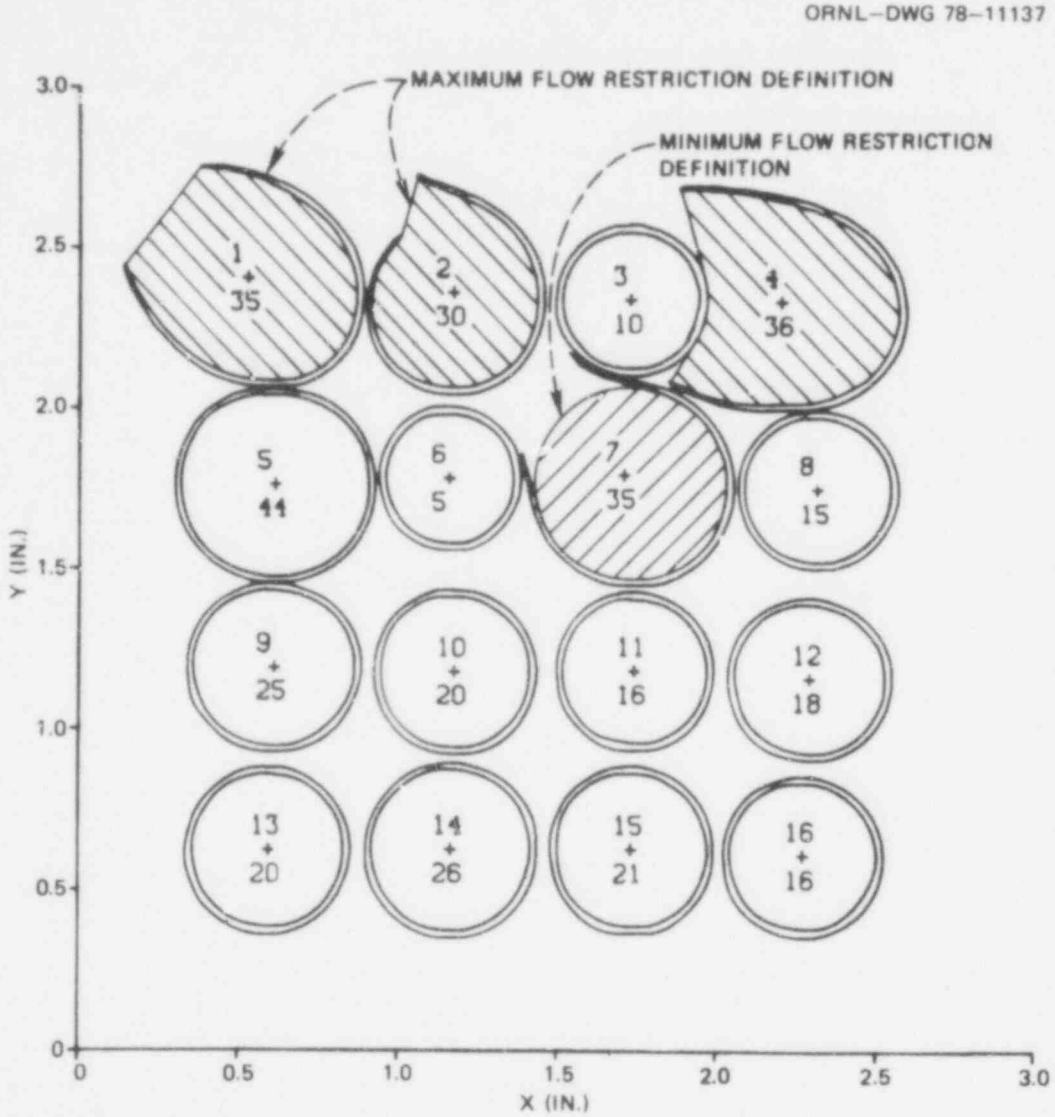

Fig. 128. Computer simulation of B-1 section of 76.5-cm elevation showing maximum and minimum flow restriction definitions.

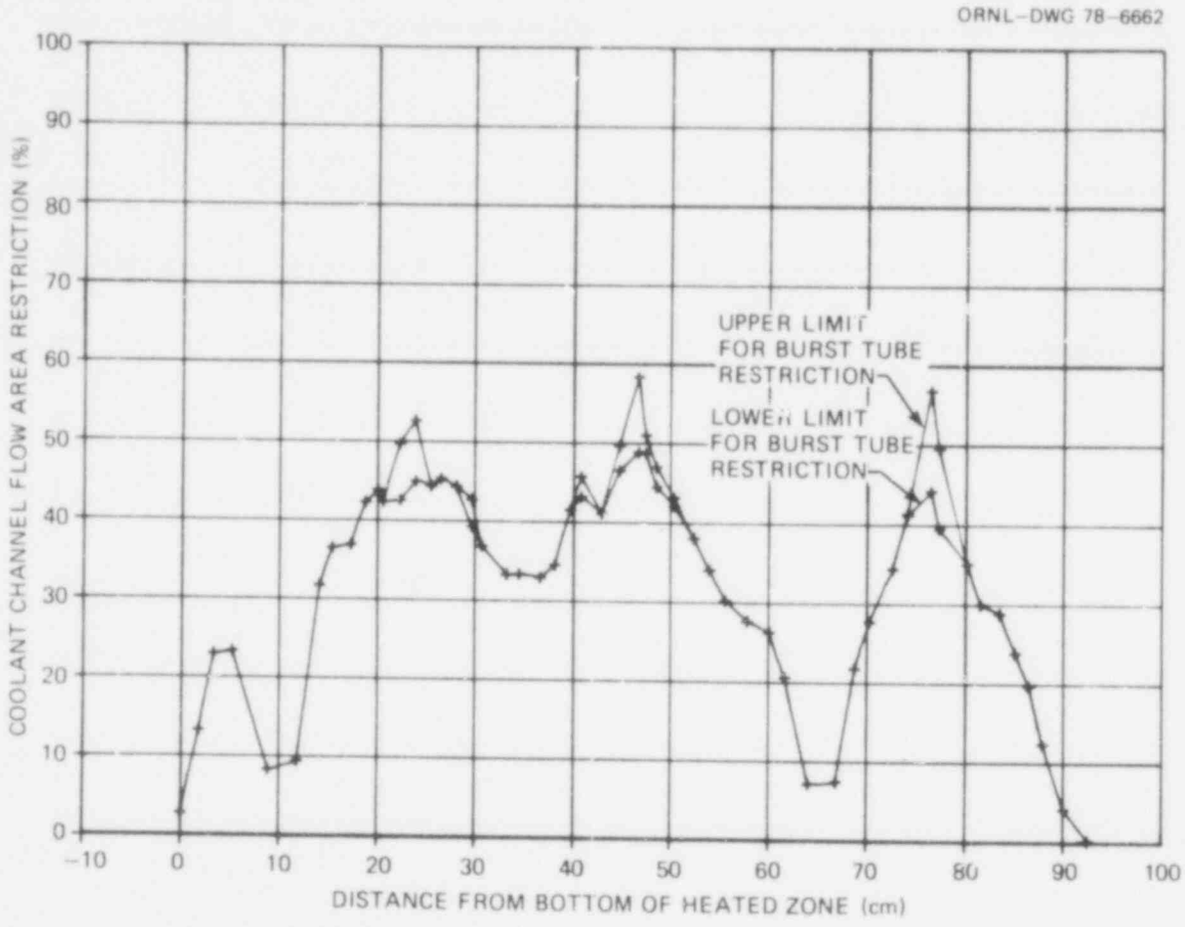

Fig. 129. Coolant channel flow area restriction in B-1 based on a rod-centered unit cell and estimated upper and lower limits of burst flow restriction.

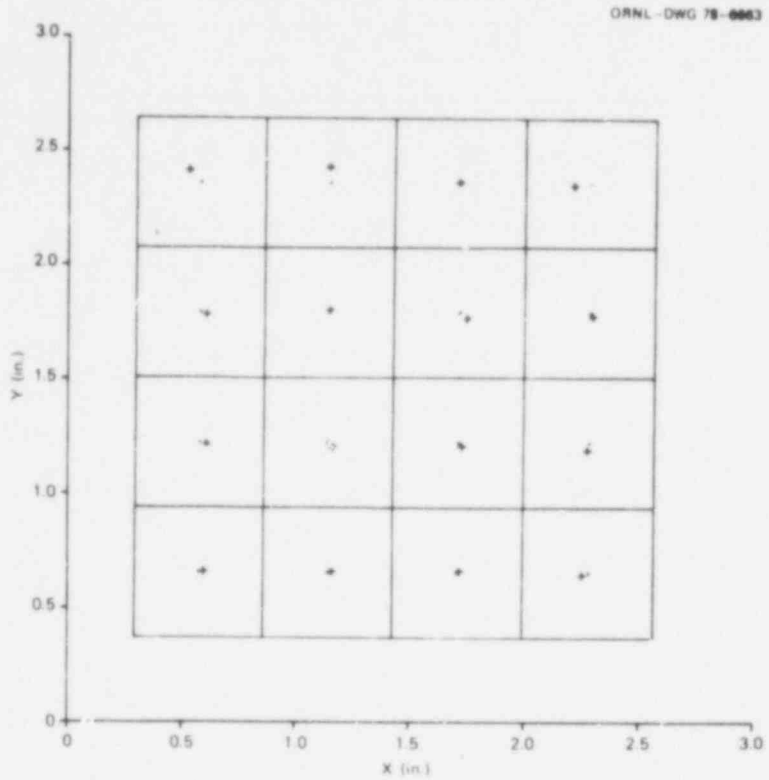

Fig. 130. Posttest locations (+) of tubes in B-1 test superimposed on the original layout.

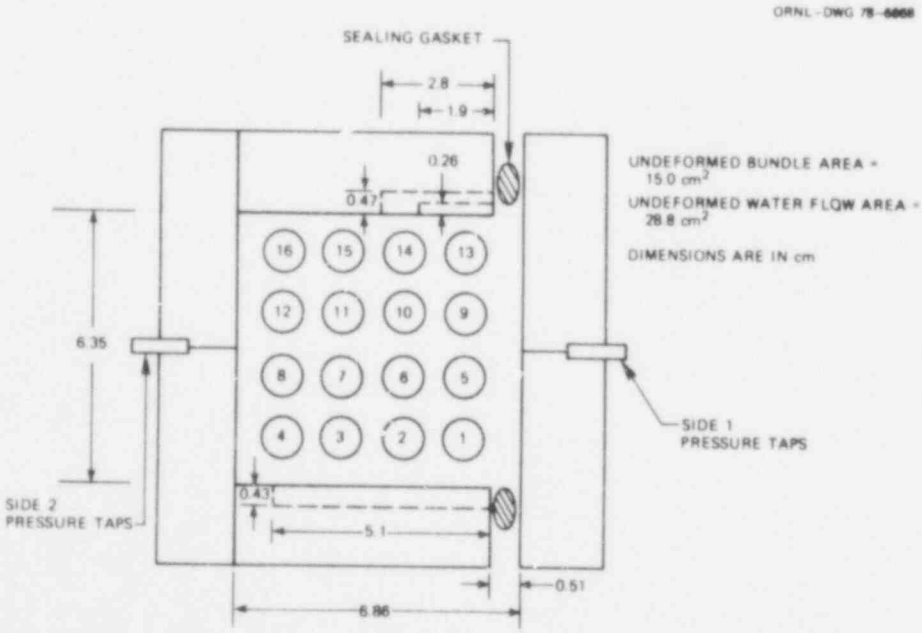

Fig. 131. Flow test configuration of B-1.

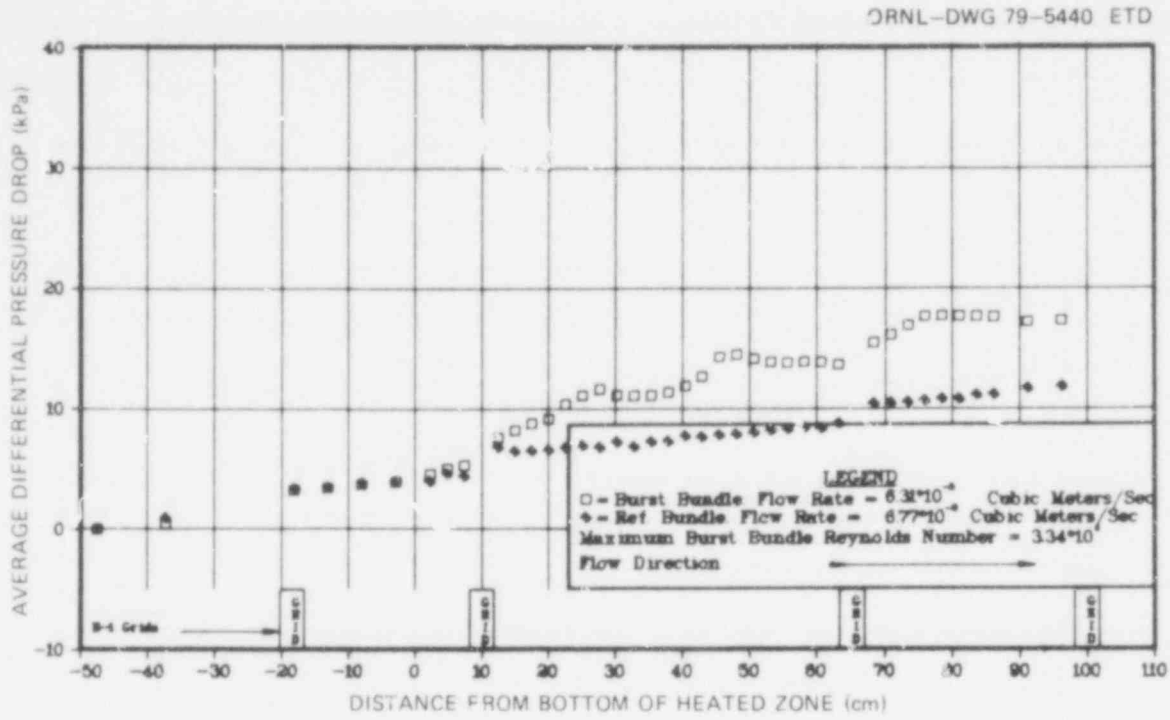

Fig. 132. B-1 and reference bundle axial pressure drop profiles at a flow rate of approximately 0.0065 m^3/sec.

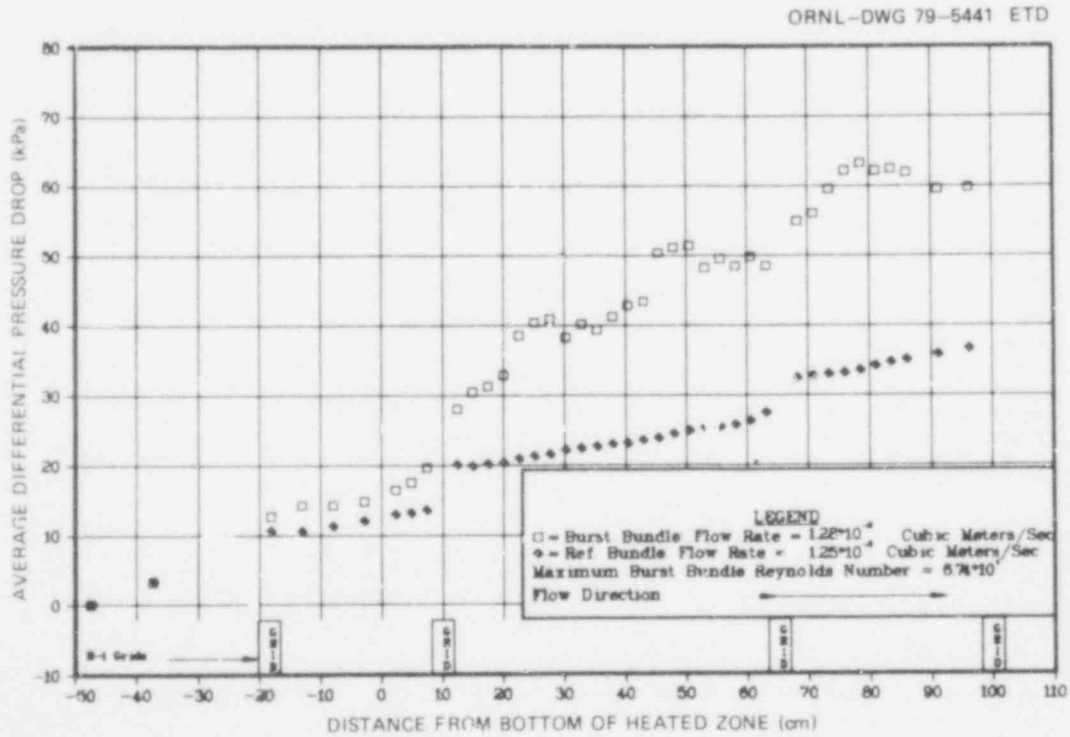

Fig. 133. B-1 and reference bundle axial pressure drop profiles at a flow rate of approximately 0.013 m^3/sec.

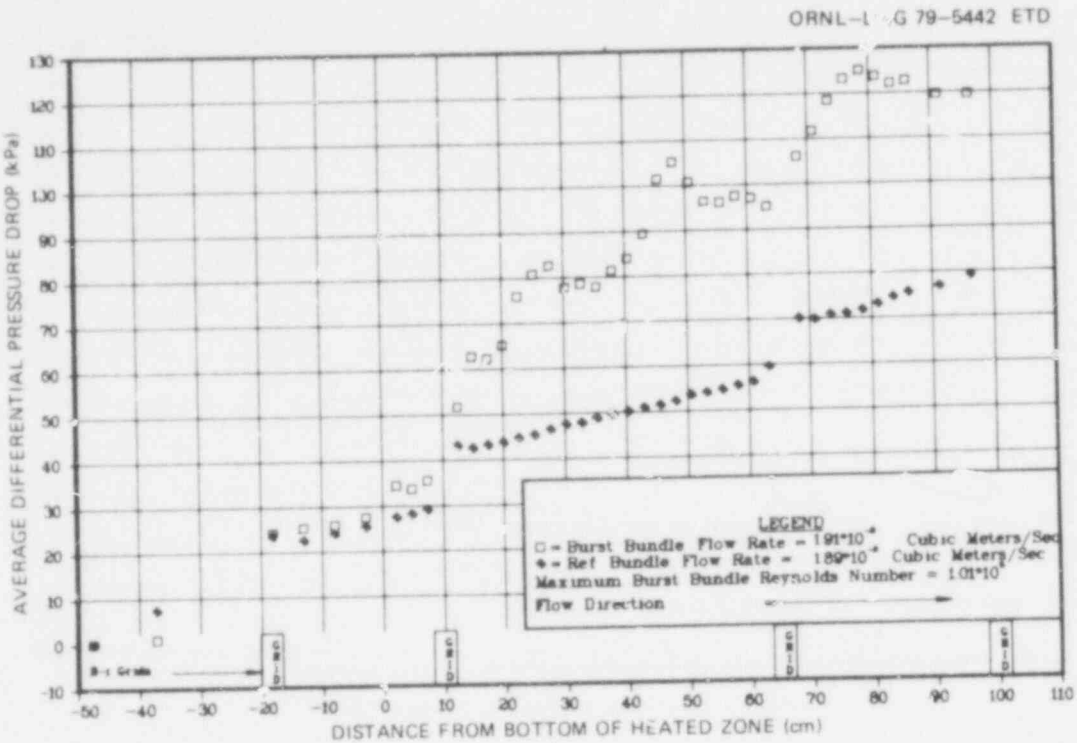

Fig. 134. B-1 and reference bundle axial pressure drop profiles at a flow rate of approximately 0.019 m^3/sec.

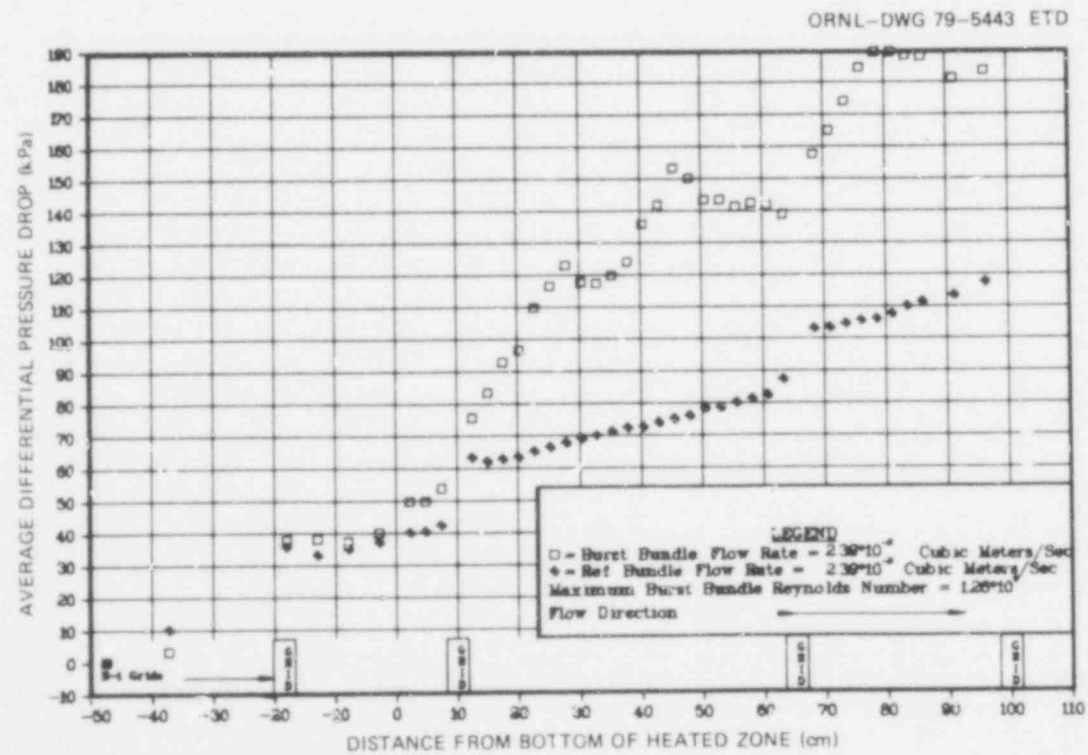

Fig. 135. B-1 and reference bundle axial pressure drop profiles at a flow rate of approximately 0.024 m^3/sec.

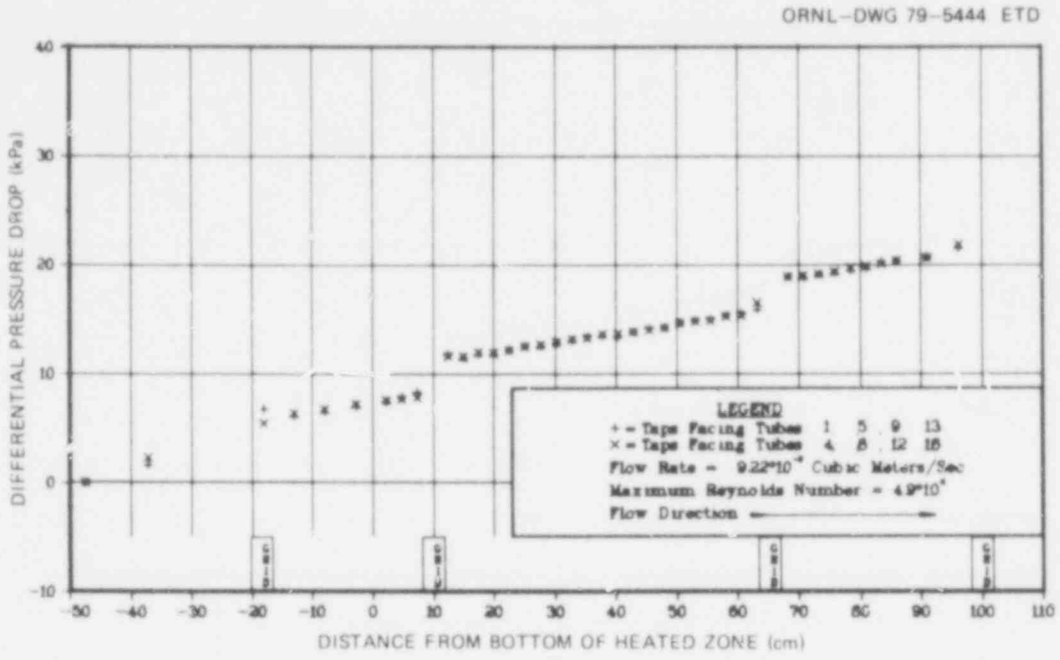

Fig. 136. Reference bundle axial pressure drop profile for a flow rate of 0.0092 m^3/sec.

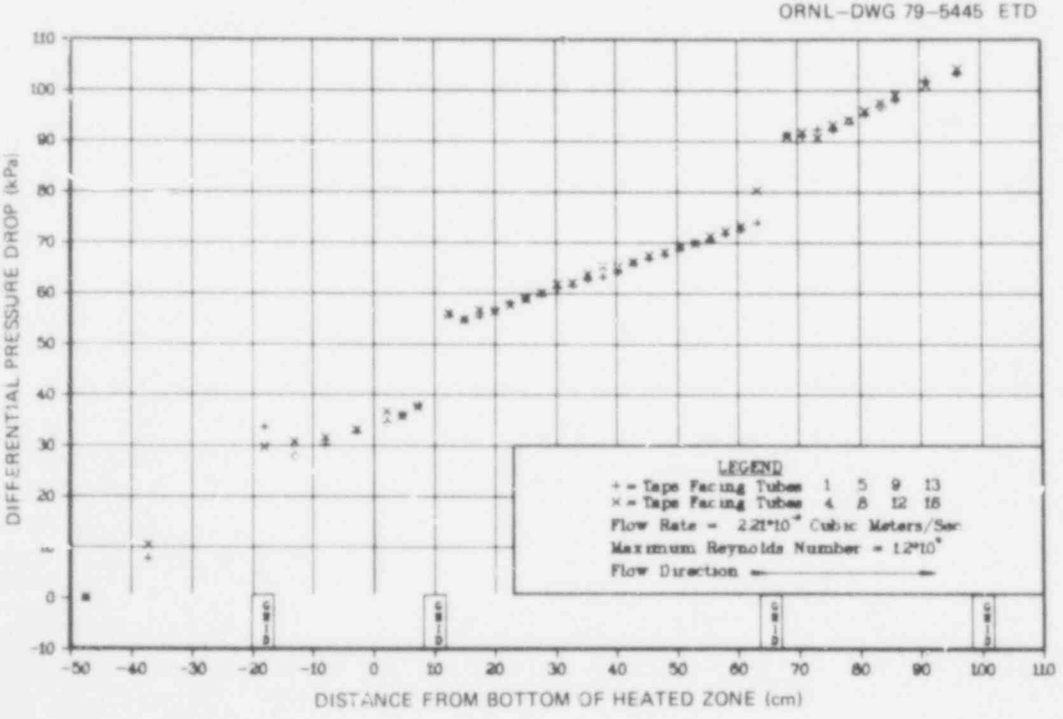

Fig. 137. Reference bundle axial pressure drop profile for a flow rate of 0.022 m^3/sec.

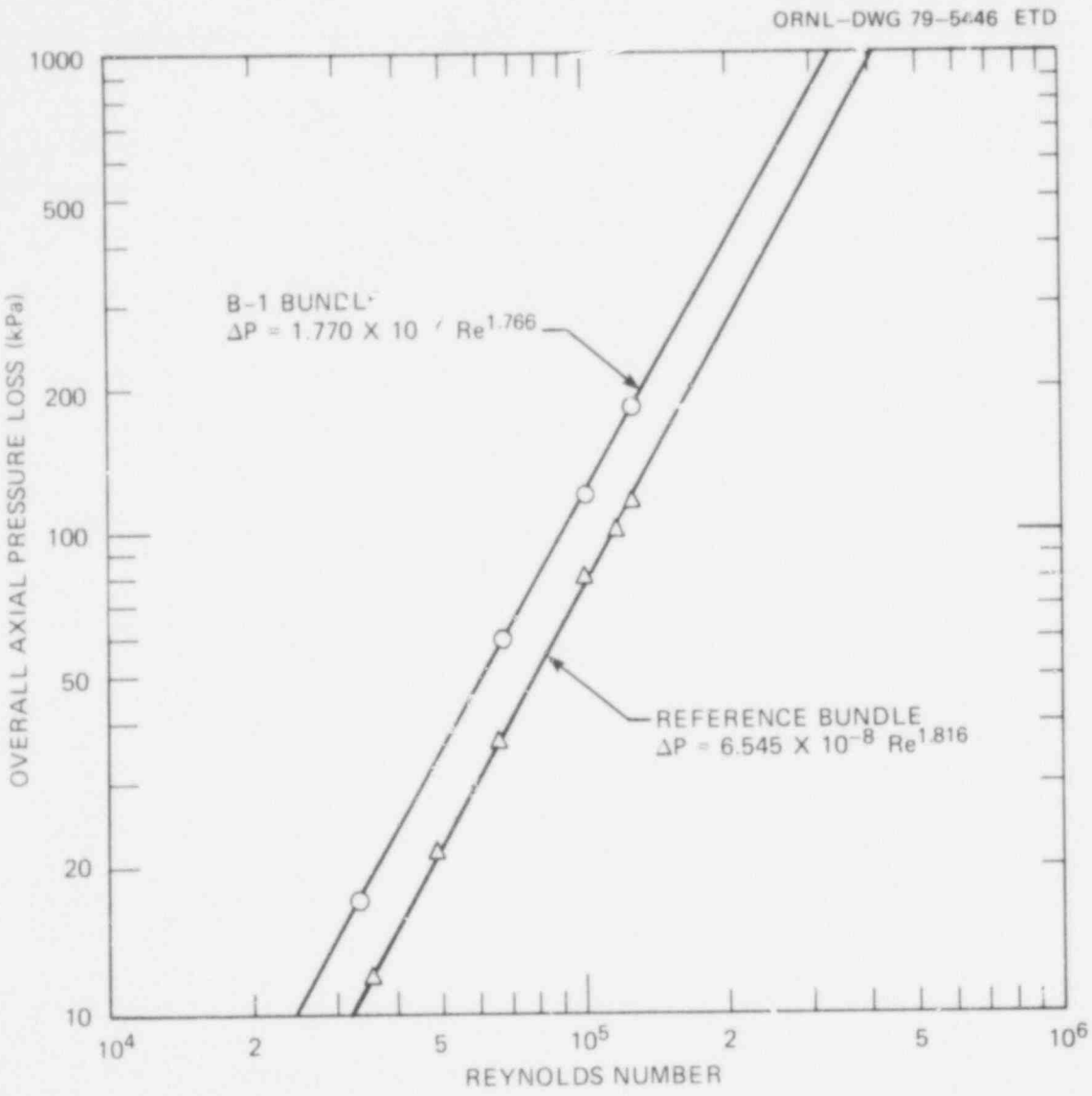

Fig. 138. Overall axial pressure loss vs Reynolds number for the B-1 and reference bundle flow tests.

Internal Distribution

1-10. R. H. Chapman
11. J. L. Crowley
12. D. O. Hobson
13. A. W. Longest
14. J. F. Mincey
15. F. R. Mynatt
16. J. L. Rich
17. Patent Office
18. Nuclear Safety Information Center
19-20. Central Research Library
21. Document Reference Section
22-24. Laboratory Records Department
25. Laboratory Records (RC)

External Distribution

26. R. A. Adamson, Mail Code V-03, General Electric Company, Vallecitos Atomic Laboratory, P.O. Box 846, Pleasanton, Calif. 94566
27. D. L. Bauman, Westinghouse Nuclear Fuel Division, P.O. Box 355, Pittsburgh, Pa. 15230
28. C. E. Crouthamel, Exxon Nuclear, Inc., 2955 George Washington Way, Richland, Wash. 99352
29. D. L. Hagrman, EG&G Idaho, Inc., INEL, Idaho Falls, Idaho 83401
30. A. L. Lowe, Babcock and Wilcox Company, P.O. Box 1260, Lynchburg, Va. 24505
31. P. A. Smerd, Combustion Engineering, Inc., 1000 Prospect Road, Windsor, Conn. 06093
32. M. Fischer, Projekt Nukleare Sicherheit, Kernforschungszentrum Karlsruhe, 75 Karlsruhe, Federal Republic of Germany
33. S. Kawasaki, Fuel Reliability Laboratory III, JAERI Tokai Research Establishment, Takai-mura, Naka-gun, Ibaraki-ken, Japan
34. D. O. Pickman, UKAEA Springfields Nuclear Power Development Laboratories, Springfields, Preston (Lancs) PP4 ORR, England
35. Chief, Fuel Behavior Branch, Office of Nuclear Regulatory Research, Nuclear Regulatory Commission, Washington, D.C. 20555
36. R. O. Meyer, Core Performance Branch, Office of Nuclear Reactor Regulation, Nuclear Regulatory Commission, Washington, D.C. 20555
37. M. L. Picklesimer, Fuel Behavior Branch, Office of Nuclear Regulatory Research, Nuclear Regulatory Commission, Washington, D.C. 20555
38. Director, Office of Assistant Manager, Energy Research and Development, DOE, ORO
39. Director, Reactor Division, DOE, ORO
40-41. NRC Public Document Room, Nuclear Regulatory Commission, Washington, D.C. 20555
42-43. Technical Information Center, Oak Ridge TN 37830